

©2009

Xue Jiang

ALL RIGHTS RESERVED

ENGINEER CELL GROWTH USING A DNA CROSSLINKED HYDROGEL WITH STATIC AND DYNAMIC STIFFNESSES

by

XUE JIANG

A Dissertation submitted to the

Graduate School-New Brunswick

Rutgers, The State University of New Jersey

and

The Graduate School of Biomedical Sciences

University of Medicine and Dentistry of New Jersey

In partial fulfillment of the requirements

For the degree of

Doctor of Philosophy

Graduate Program in Biomedical Engineering

Written under the direction of

Professor Noshir A. Langrana

And approved by

New Brunswick, New Jersey

May 2009

ABSTRACT OF THE DISSERTATION

ENGINEER CELL GROWTH USING A DNA CROSSLINKED HYDROGEL WITH STATIC AND DYNAMIC STIFFNESSES

by XUE JIANG

Dissertation Director:

Dr. Noshir A. Langrana

Elucidation of the interactions between cells and extracellular matrices (ECM) is critical to not only the understanding of the basic biology of development, tissue functioning and pathological conditions, but also successful design and implementation of bioscaffolds in tissue engineering applications. Mechanical characteristics, including mechanical stiffness, of the local microenvironment play an important role in cell decision making processes. Aiming at the neural tissue engineering applications, we examined the mechano-sensing of neural cells in the context of neuron-astroglia interactions, and differentiated between dendrites and axons by deploying bis- and DNA-crosslinked hydrogels. These studies revealed the complexity in the neural cell mechano-sensing which is coupled with cell-cell interactions and possesses specificity towards cellular property, cell type and stiffness range.

The dynamic and changing nature of cells' local physiological environment particularly of its mechanical characteristics makes it desirable to develop a cell culture system or bioscaffold whose mechanical properties can be modulated in a controlled and temporal fashion. DNA crosslinked hydrogels offer unique opportunities for modifying mechanical properties of the substrates or scaffolds via DNA delivery during cell culture without changing environmental factors. Two types of fibroblasts, L929 and GFP fibroblasts, and spinal cord cells were subjected to the dynamic alterations in the mechanical stiffness of the DNA gels. It was found that both fibroblasts and neurons are able to sense the mechanical stiffness change. Fibroblasts respond mainly by altering morphology, focal adhesion or cytoskeletal structures whereas neurons respond largely by adjusting neurite outgrowth and adhesion properties.

The significance of the current thesis work includes the following:

1. It highlights the importance of the mechanical aspects of cell-ECM interactions, particularly cellular response to static and dynamic mechanical stiffnesses.
2. It reveals the complexity in the mechano-sensing with specificity towards or dependence on cell type, cellular property and stiffness range. It can be further coupled with cell-cell interactions, and other factors including dimensionality and biological cues.
3. It adds a new dimension, *Time*, to the mechanical compliance of the substrate in understanding cell-ECM events.
4. It provides design guidelines for the choice of the mechanical stiffness of the bio-scaffold in tissue engineering applications.

PREFACE

A man can be destroyed but not defeated.

*There isn't any symbolism. The sea is the sea. The old man is an old man.
The boy is a boy and the fish is a fish. The shark are all sharks no better
and no worse. All the symbolism that people say is shit. What goes beyond is
what you see beyond when you know.*

-- Ernest Hemingway

This is not the end.

It is not even the beginning of the end.

But it is, perhaps, the end of the beginning.

-- Winston Churchill

ACKNOWLEDGMENTS

Towards the end of this long journey and close to another milestone in my life, I am convinced it would have been absolutely impossible for me to walk through the ocean of challenges and obstacles without the support and guidance from a great number of individuals and groups.

My appreciation goes first to my family, my parents, brothers, sister-in-laws, and my little nephew, for their encouragement and unconditional support across the barrier of space, from Texas and China, especially at some of the most difficult times in my graduate pursuit. Grandfather, aunts, uncles and their families have been great support.

Next and foremost, I owe my deepest debt to my advisor, Dr. Noshir A. Langrana, who not only offered his incredible patience, superior guidance and inspiring insight and vision, but also exposed me to an array of valuable opportunities, to work in an interdisciplinary team, to get enriched in a unique multi-cultural environment, and to get engaged in various research projects. I am fortunate and grateful to have him as mentor, supervisor, and friend, if I may say. The rest of the committee, Drs. Bonnie Firestein, Rene Schloss, David Shreiber, and Bernard Yurke, has been with me throughout my PhD pursuit starting from the very first meeting on 12/14/2004. Working with these wonderful individuals and having their advice was such an enjoyment and I am truly honored and humbled to be surrounded by these wonderful researchers. Many other faculty members kindly offered help and advice, and contributed to my completion of the degree requirements, and special thanks go to Drs. Boustany, Androulakis, and Metaxas in my research rotation, Drs. Uhrich and Buettner for help in my application for

fellowship and classes; Drs, Moghe, Chabal, Shoane, Dunn, Cai, Zahn, Shinbrot, Li, Roth, Kim, Semlow, Russotti, Anthony and Scarbrough for classes and interactions in many occasions. The financial support from BME, NJCSCR and NIH is acknowledged.

In addition, I need to express my sincere gratitudes to my fellow group members and members from the laboratories of Drs. Shreiber, Firestein, and Schloss for various assistance they offered: David Lin, Uday Chippada, Lulu Li, Sarah Dubowsky, Penelope Georges, and Devendra Verma from our group; Margaret, Gary, Harini, Shirley, Ian, Jason, Hailing and Chris from Shreiber group; Yangzhou, Baogang, Hongxin, Erick, Kenyatta, Maxine, Jose, Damien, Chia-Yi, Sweet, Melinda, Michelle, Munjin, Chris, and Norell from Firestein group; Arnold, Mike, Ramya, Loreto, Eric, Jeff, Sharon, Tiffany, Er, Nilay, and Aaron from the the first year study group; Alex, Mercedes, and Larry from Zahn group; Jeremy and Leilani from Uhrich group; John and Mindy from Kohn group; Tim, Eric N., Kevin, and Eric W. from Yarmush group; Ram, Jing, Julia, Aaron, Jocie, Vanesa, Nicole I., Nicole P., Tamar, and Mat from Moghe group; Mohemad and Sai from MAE; Nuria, Kerri-Ann, and Norman from BME. Assistance from John Petrowski, Bill, Joe, Joyce and Tannie is also appreciated. I also benefited in working with undergraduate and high-school researchers: Kevin H., Sagar, Kevin T., Daeun, Alexandra and Reema.

The kindness and care from Ursula, Mary, Larry, Linda, Stratos and Robin has been an important part of my experience at Rutgers, and I am grateful to it. The friendship from Feng, Xiahua, Peter, Polo, Xinquan, Howard, Christine, Glen, Vivi, Sandeep, Keren, and other friends has helped me in maintaining sanity. There are also many individuals that I owe gratitudes for various help I received, which made my life much easier and more enjoyable. I also value the lives of the lab animals used in the study.

DEDICATION

To my grandparents on both sides of the Taiwan Strait, and

To the democratization and unification of China

TABLE OF CONTENTS

ABSTRACT OF THE DISSERTATION.....	ii
PREFACE.....	iv
ACKNOWLEDGMENTS	v
DEDICATION..	vii
TABLE OF CONTENTS	viii
LIST OF TABLES	xv
LIST OF ILLUSTRATIONS	xviii
LIST OF ACRONYMS	xxiv
CHAPTER 1 INTRODUCTION.....	1
1.1 Problem Statement	1
1.2 Objective of the Dissertation Research.....	4
1.3 Dissertation Organization	6
References.....	8
CHAPTER 2..... BACKGROUND	10
2.1 DNA crosslinked hydrogels	10
2.1.1 Polymer hydrogels	10
2.1.2 Natural vs. synthetic materials	11
2.1.3 Biodegradable vs. non-biodegradable materials	11
2.1.4 The properties of DNA	12
2.1.5 DNA as structural materials.....	13
2.1.6 Using DNA to crosslink a polymer network.....	14

2.1.7	Mechanical characterization of hydrogels and soft materials.....	18
2.2	Choice of cell types.....	19
2.2.1	Fibroblasts.....	19
2.2.2	Neurons and other cells in central nervous system.....	19
2.2.3	Spinal cord injuries and therapeutic strategies.....	21
2.3	Cell-ECM interactions	26
2.3.1	Cell-ECM interplay.....	26
2.3.2	Major determinants in cell responses and physical cues	27
2.3.3	Cell mechano-sensing	30
2.3.4	Effect of substrate mechanical stiffness on cells	31
	References.....	34
CHAPTER 3 GELS WITH STATIC STIFFNESS		42
CHAPTER 3A . EFFECT OF NEURON-ASTROGLIA INTERACTIONS.....		43
3A.1	Background.....	43
3A.1.1	Bis-crosslinked polyacrylamide gel culture system.....	43
3A.1.2	Neuron-astroglia interactions.....	46
3A.1.3	Mechanical stiffness range under study.....	46
3A.2	MATERIALS AND METHODS.....	49
3A.2.1	Mechanical characterization of bis-gels.....	49
3A.2.2	Bis-gel preparation.....	50
3A.2.3	Mixed spinal cord cell culture.....	50
3A.2.4	Pure spinal cord neuron culture	53
3A.2.5	Pure astroglial culture	53

3A.2.6	Immunostaining and cell counting.....	54
3A.2.7	Assessment of dendrite number and neurite length	56
3A.3	Results.....	56
3A.3.1	Mechanical stiffness of bis-gels.....	56
3A.3.2	Gel functionalization for spinal cord cell attachment	58
3A.3.3	Mixed spinal cord cell culture on bis-gels	58
3A.3.4	Effect of gel stiffness on spinal cord cell in mixed cultures	61
3A.3.5	Effect of gel stiffness on pure spinal cord neuron culture	62
3A.3.6	Effect of gel stiffness on pure astroglia culture	65
3A.4	Discussion.....	68
	References.....	72
CHAPTER 3B .. SPINAL CORD NEURONS ON DNA GELS		76
3B.1	Background.....	76
3B.1.1	Significance of the substrate mechanical stiffness.....	77
3B.1.2	Contrast between bis-gel and DNA-gel systems	77
3B.2	Materials and methods	79
3B.2.1	DNA gel design and preparation.....	79
3B.2.2	Mechanical characterization of DNA gels.....	80
3B.2.3	DNA gel functionalization and assessment of ligand density	83
3B.2.4	Rat spinal cord cell culture	83
3B.2.5	Immunocytochemistry and cell counting.....	84
3B.2.6	Characterization of neurite outgrowth and statistical analysis	85
3B.3	Results.....	86

3B.3.1	DNA sequence and DNA gel design	86
3B.3.2	Viscosity and stiffness of DNA-crosslinked gels	89
3B.3.3	Assessment of gel surface ligand density	91
3B.3.4	Spinal cord cell growth on DNA crosslinked gels.....	93
3B.3.5	Neurite outgrowth on DNA crosslinked gels.....	98
3B.3.6	FAK expression in neurons on DNA gels.....	99
3B.4	Discussion	104
3B.4.1	Mechanical sensitivity of neurite outgrowth.....	104
3B.4.2	Mechanical stimuli provided by DNA gels	108
3B.4.3	FAK expression in neurons in response to stiffness	110
	References.....	113
CHAPTER 4 ... GELS WITH DYNAMIC STIFFNESS.....		118
CHAPTER 4A .. ACELLULAR STUDIES		119
4A.1	Background.....	119
4A.1.1	DNA diffusion	119
4A.1.2	Previous DNA gel study with DNA delivery	120
4A.1.3	Hydrogel property change upon DNA delivery.....	120
4A.1.4	Gel preparation using DNA without purification	121
4A.1.5	The purpose of the acellular study.....	121
4A.2	DNA incorporation into the gel network	122
4A.2.1	Rationale	122
4A.2.2	Materials and Methods.....	122
4A.2.3	Results.....	124

4A.2.4	Summary	125
4A.3	Discussion	126
	References	130
CHAPTER 4B .. FIBROBLAST GROWTH ON A DYNAMIC SUBSTRATE.....		131
4B.1	Background	131
4B.1.1	Fibroblast mechano-sensing	131
4B.1.2	Dynamic stimuli	132
4B.1.3	Dynamic stiffness of the substrate	133
4B.2	Materials and Methods	135
4B.2.1	DNA sequence design and DNA gel preparation	135
4B.2.2	DNA and bis gel functionalization	135
4B.2.3	Mechanical characterization	136
4B.2.4	Fibroblast cell culture and DNA delivery	136
4B.2.5	Cell growth characterization and statistical analysis	137
4B.3	Results	142
4B.3.1	Effect of substrate mechanical stiffness on fibroblast growth	142
4B.3.2	DNA sequence screening and similarity analysis	142
4B.3.3	Mechanical stiffness of the substrates	145
4B.3.4	Effect of DNA delivery on L929 and GFP fibroblast growth	145
4B.3.5	Effect of dynamic stiffness on L929 fibroblasts	146
4B.3.6	Effect of dynamic stiffness on GFP fibroblasts	154
4B.4	Discussion	158
4B.4.1	Mechanically dynamic cues applied to fibroblasts	158

4B.4.2	Expression of FAK and F-actin in L929 fibroblasts	159
4B.4.3	Distribution of FAK and F-actin in GFP fibroblasts	161
4B.4.4	FAK expression and actin structure of cells on dynamic gels	162
4B.4.5	Cell growth in response to mechanically dynamic cues	171
4B.4.6	Factors in fibroblast mechanosensing of dynamic stiffness	176
References		184
CHAPTER 4C .. SPINAL CORD NEURONS ON A DYNAMIC SUBSTRATES. 189		
4C.1	Background	189
4C.1.1	Neuronal mechano-sensing	189
4C.1.2	Mechanically dynamic stimuli	192
4C.2	Materials and methods	193
4C.2.1	DNA sequence design and DNA gel preparation	193
4C.2.2	DNA gel functionalization	194
4C.2.3	Neuronal cell culture and DNA delivery	194
4C.2.4	Cell growth characterization and statistical analysis	195
4C.3	Results	198
4C.3.1	DNA sequence screening and similarity analysis	198
4C.3.2	Effect of DNA delivery on neurite outgrowth	200
4C.3.3	Effect of DNA -induced stiffness change on neurite outgrowth....	200
4C.3.4	FAK expression in neurons on dynamic DNA gels	203
4C.3.5	N-CAM expression of spinal cord cells on dynamic substrate	203
4C.4	Discussion	212
4C.4.1	Mechanically dynamic cues applied to neurons	212

4C.4.2	Neurite outgrowth in response to mechanically dynamic cues.....	214
4C.4.3	FAK and N-CAM expression in response to dynamic substrate ...	217
4C.4.4	Factors in neuronal sensing and response to dynamic stiffness.....	220
	References.....	228
Chapter 5	CONCLUSIONS AND SUMMARY	232
5.1	Summary of the dissertation work	232
5.1.1	Summary of motivation and key observations.....	232
5.1.2	Significance.....	234
5.1.3	Novelty.....	235
5.2	Limitations and discretion.....	237
5.3	Future work.....	240
	References.....	241
APPENDICES..	243
Appe 1	Mechanical characterization with microbeads.....	243
Appe 2	DNA sequence design used in this dissertation research.....	254
Appe 3	AFM testing of spinal cord neurons on hydrogels.....	255
Appe 4	BLAST search results	257
CURRICULUM VITA	261

LIST OF TABLES

CHAPTER 2

Table 2-1	Examples of potential DNA crosslinked hydrogels.....	17
------------------	--	----

CHAPTER 3A

Table 3A-1	Partial list of the previous mechano-biology studies using bis-crosslinked PAM gels.	45
Table 3A-2	Partial list of the stiffness of CNS tissues of different species	48
Table 3A-3	Primary and secondary antibodies used in the dissertation research.	55
Table 3A-4	Neurite length of spinal cord neurons in mixed cultures on different bis-crosslinked polyacrylamide gels.	63

CHAPTER 3B

Table 3B-1	DNA sequence of Designs A and B used in the study of spinal cord cells on DNA gels with static stiffness.....	88
Table 3B-2	Mechanical stiffness of the DNA crosslinked polyacrylamide hydrogels used in the study of spinal cord cells on DNA gels with static stiffness. .	90
Table 3B-3	Summary of the observations of spinal cord cellular behavior as DNA gel mechanical stiffness increases from 6 kPa to 30 kPa	106

CHAPTER 4A

Table 4A-1	The initial and final crosslinking density of different schemes of crosslinker DNA delivery.	127
-------------------	---	-----

CHAPTER 4B

Table 4B-1	The initial and final crosslinking density of different schemes of crosslinker DNA delivery.	143
Table 4B-2	DNA sequence design for the study of fibroblasts on DNA gels with dynamic stiffness.	143
Table 4B-3	Mechanical stiffness of the DNA crosslinked polyacrylamide hydrogels used in this study.	149
Table 4B-4	Comparisons between L929 cell behavior on starting stiffness and that on dynamic stiffness (A), and between cell behavior on dynamic stiffness and that on static gels with same ending stiffness (B).....	174
Table 4B-5	Comparisons between GFP fibroblast behavior on starting stiffness and that on dynamic stiffness, and between cell behavior on dynamic stiffness and that on static gels with same ending stiffness.	175
Table 4B-6	Important factors influencing the cellular response to mechanically dynamic cues.....	181

CHAPTER 4C

Table 4C-1	Partial list of the previous reports of neuronal responses to the rigidity of the substrate and ECM.	191
-------------------	---	-----

Table 4C-2	DNA sequences used in the study of neurite outgrowth on DNA gels with dynamic stiffness.	199
Table 4C-3	The initial and final crosslinking density of different schemes of crosslinker DNA delivery.	199
Table 4C-4	Comparisons of neurite outgrowth between static and dynamic gels with the same starting stiffness and between dynamic and static gels with the same ending stiffness.	224
Table 4C-5	Important factors affecting the response in neuronal growth and neurite outgrowth to dynamic stiffnesses.	224

LIST OF ILLUSTRATIONS

CHAPTER 2

Figure 2-1	Schematic depicting the reverse process of DNA crosslinking.	16
Figure 2-2	Examples of the major approaches in altering mechanical properties of the DNA crosslinked hydrogels.	16
Figure 2-3	Schematic of the typical morphology of a neuron.	24
Figure 2-4	Summary of the major challenges in finding a cure for spinal cord injuries and the strategies proposed to tackle the problem.	25
Figure 2-5	Tissue engineering approaches adopted in the current research	25
Figure 2-6	Schematic depicting the interactions between cells and the local micro-environment at the molecular level.	29

CHAPTER 3A

Figure 3A-1	Experimental setup for non-intrusive measurement of mechanical properties of hydrogel materials.	52
Figure 3A-2	Stiffness of the bis-crosslinked polyacrylamide hydrogel with respect to the monomer concentration at fixed monomer/crosslink ratio of 29:1.....	57
Figure 3A-3	Rat spinal cord neurons grown on functionalized (upper panel) and un-functionalized (lower panel) bis-crosslinked polyacrylamide gels.....	59
Figure 3A-4	Mixed culture of rat spinal cord cells on bis-crosslinked gels.....	60
Figure 3A-5	Change of total cell number of rat spinal cord cells on bis-gels with different stiffnesses.	63

Figure 3A-6	Effects of gel stiffnesses on spinal cord cell growth.....	64
Figure 3A-7	Effects of gel stiffness on pure spinal cord neuron culture.....	66
Figure 3A-8	Effects of gel stiffness on pure astrocyte culture.	67

CHAPTER 3B

Figure 3B-1	Chemical structures of DNA- and bis-crosslinked hydrogels, and DNA gel design schemes.....	81
Figure 3B-2	Schematic of DNA gel synthesis.	82
Figure 3B-3	A DNA crosslinked hydrogel was immobilized on a circular cover glass (12mm in diameter) with thickness of approximately 100~300 μ m.....	88
Figure 3B-4	Changes in viscosity of DNA gels of Design B with respect to the temperature at various levels of crosslinking.....	90
Figure 3B-5	Fluorescent density of collagen on DNA gels assessed with increased (left to right) percentage of fluorescent collagen replacement of regular collagen.	92
Figure 3B-6	Fluorescence intensity (in arbitrary units, A.U.) of bound type-I collagen, when 0%, 5% and 10% of total collagen is fluorescent, to the surface of the DNA gels.....	92
Figure 3B-7	Attachment and growth of rat spinal cord cells on DNA crosslinked gels.	95
Figure 3B-8	Rat spinal cord cells extended processes on DNA crosslinked poly-acrylamide hydrogels, with visible length of approximately 1 mm.....	96

Figure 3B-9	Changes of MAP2+ neuron, GFAP+ astroglia, and total cell numbers in response to the stiffness of the DNA crosslinked gels.....	97
Figure 3B-10	Morphology of rat spinal cord neurons on DNA crosslinked hydrogels.	100
Figure 3B-11	Neurite outgrowth on DNA gels with different levels of crosslinking or with crosslinkers of different length and monomer concentration.	101
Figure 3B-12	Frequency plots of mean primary dendrite length (A), Primary dendrite number (B), and axonal length (C) per neuron on DNA gels of two designs.....	102
Figure 3B-13	Double immunolabeling and DAPI staining of spinal cord cells on DNA crosslinked gels of Designs A (A-C) and B (D-F) using monoclonal antibodies against MAP2 and focal adhesion kinase (FAK).	103

CHAPTER 4A

Figure 4A-1	Change of DNA purity with the length of the ssDNA used in DNA gel designs of A, B, and C (Appendix 2).....	128
Figure 4A-2	Calibration for spectrophotometric determination of the DNA concentration.....	128
Figure 4A-3	The concentration of residual DNA in the buffer solution rinsing DNA gels, as determined by spectrophotometric measurement two days after the DNA delivery to the DNA gel groups	129
Figure 4A-4	Adjusted DNA concentration determined by spectrophotometric measurement two days after the DNA delivery to the DNA gel groups	129

CHAPTER 4B

Figure 4B-1	Schemes of DNA delivery to the fibroblast culture on DNA crosslinked hydrogels.....	140
Figure 4B-2	Schematic illustrating the alteration of the mechanical properties of the DNA crosslinked hydrogels via DNA delivery.	141
Figure 4B-3	The survival and proliferation of L929 cells correlate strongly with the substrate mechanical stiffness.....	144
Figure 4B-4	The growth of L929 fibroblasts on tissue culture plates, with (DNA+) and without (DNA-) DNA delivery.....	149
Figure 4B-5	The growth of GFP fibroblasts on tissue culture plates, with (DNA+) and without (DNA-) DNA delivery.....	150
Figure 4B-6	Projection area and aspect ratio of L929 fibroblasts on DNA crosslinked hydrogels of Designs A (▲) and B (■) (Table 4B-2) on Day 2, before DNA delivery.....	151
Figure 4B-7	L929 fibroblasts growth on dynamic DNA substrates.....	152
Figure 4B-8	Frequency plots of projection area (A) and aspect ratio (B) of L929 fibroblasts grown on dynamic DNA crosslinked hydrogels.	153
Figure 4B-9	GFP fibroblasts growth on dynamic DNA substrates.....	156
Figure 4B-10	Frequency plots of projection area (A) and aspect ratio (B) of GFP fibroblasts grown on dynamic DNA crosslinked hydrogels.	157
Figure 4B-11	Study of the ‘bleeding-over’ of the fluorescence channels.	166
Figure 4B-12	FAK expression and actin staining of L929 fibroblasts on four groups of DNA gel samples: D50, D50_100, D80_100 and D100.....	167

Figure 4B-13	Quantification of the fluorescence intensity (in arbitrary unit, A.U.) of focal adhesion kinase (FAK) of L929 fibroblast grown on DNA gels. ..	168
Figure 4B-14	Actin staining of GFP fibroblasts grown on DNA crosslinked gels.....	169
Figure 4B-15	FAK immunostaining of GFP fibroblasts grown on DNA crosslinked gels.	170
Figure 4B-16	Schematic for the cell-ECM interface with the emphasis on cell mechanosensing and responses to the stiffness change in the ECM or gel substrate.	182
Figure 4B-17	Illustration showing that on the gels with static stiffness, the cells are subject to much greater rate of change in the mechanical stiffness upon plating than that on the gels of dynamic stiffnesses.	183
Figure 4B-18	Schematic of the modifications of the mechanical compliance of the substrate upon the delivery of crosslinker DNA or its complements ('Removal DNA').	183

CHAPTER 4C

Figure 4C-1	Schematic of procedures in the preparation of DNA crosslinked polyacrylamide hydrogel.....	197
Figure 4C-2	Schematic of the DNA delivery to the DNA gel groups for spinal cord cell culture.	197
Figure 4C-3	Neurite outgrowth on tissue culture plates with (DNA+) and without (DNA-) DNA delivery.	205

Figure 4C-4	Typical image of spinal cord neurons grown on DNA crosslinked hydrogels with both static (D100 and D50) and dynamic (D100_80 and D100_50) stiffnesses.....	206
Figure 4C-5	Neurite outgrowth on DNA gels with dynamic stiffnesses.	207
Figure 4C-6	Frequency plots of mean primary dendrite length (A), primary dendrite number (B) and axonal length (C) per neuron on DNA gels with dynamic stiffnesses.....	208
Figure 4C-7	Typical images of focal adhesion kinase (FAK) and neural-cell adhesion molecules (N-CAM) in the spinal cord neurons grown on DNA gels with dynamic stiffnesses.	209
Figure 4C-8	Typical images of focal adhesion kinase (FAK) and actin in the spinal cord neurons grown on DNA gels with dynamic stiffnesses.....	210
Figure 4C-9	Focal adhesion kinase (FAK) expression in the spinal cord neurons grown on DNA gels with dynamic stiffnesses.....	211
Figure 4C-10	Schematic for the cell-ECM interface events with the emphasis on neuronal mechanosensing and responses to the stiffness change in the ECM or gel substrate	225
Figure 4C-11	Nestin immunostaining of the spinal cord cells showing neural progenitor cells on culture plates during the course of the culture.....	226
Figure 4C-12	Tau-1 and MAP2 immunostaining of the spinal cord cells showing dendrites and axons, respectively, on culture plates during the course of the culture.....	227

LIST OF ACRONYMS

A.U.	<i>Arbitrary unit</i>
AFM	<i>Atomic force microscopy</i>
ANOVA	<i>Analysis of variance</i>
APS	<i>Ammonium Persulfate</i>
BDNF	<i>Brain-derived neurotrophic factor</i>
BLAST	<i>Basic local alignment search tool</i>
CNS	<i>Central nervous system</i>
DIV	<i>Days in vitro</i>
DMEM	<i>Dulbecco's Modified Eagle's Medium</i>
DPBS	<i>Dulbecco's Phosphate Buffered Saline</i>
dsDNA	<i>Double-stranded DNA</i>
ECM	<i>Extracellular matrix/ matrices</i>
FA	<i>Focal adhesion</i>
FAK	<i>Focal adhesion kinase</i>
FBS	<i>Fetal bovine serum</i>
FDA	<i>US Food and Drug Administration</i>
GFAP	<i>Glial fibrillary acidic protein</i>
HCT/P(s)	<i>Human cell, tissue and cellular and tissue-based product(s)</i>
HEMA	<i>Hydroxyethyl methacrylate</i>
HPLC	<i>High performance liquid chromatography</i>
HPMA	<i>Hydroxy-propyl-methacrylamide</i>

IF	<i>Immunofluorescence</i>
IgG	<i>Immunoglobulin G</i>
MAP2	<i>Microtubule associated protein 2</i>
MEM	<i>Minimum Essential Medium</i>
N-CAM	<i>Neural cell adhesion molecule</i>
NB	<i>Neurobasal (medium)</i>
NIH	<i>National Institute of Health</i>
PAGE	<i>Polyacrylamide gel electrophoresis</i>
PAM	<i>Polyacrylamide</i>
PBS	<i>Phosphate buffer saline</i>
PDL	<i>Poly-D-lysine</i>
PFA	<i>Paraformaldehyde</i>
PNS	<i>Peripheral nervous system</i>
RT	<i>Room temperature</i>
SCI	<i>Spinal cord injury</i>
SCM	<i>Serum containing medium</i>
SEM	<i>Standard error of mean</i>
ssDNA	<i>Single-stranded DNA</i>
TGF	<i>Transforming growth factor</i>
TE	<i>Tissue engineering</i>

CHAPTER 1 INTRODUCTION

1.1 Problem Statement

The physical world was here first and, no matter what animals and plants do to it, it will be here last. We are no more than a cause of temporary discontinuities in a formless web of time and space.

— Vicent, J.F.V. 'Life among the formulae of physics' (Science, 2004)

The 'collision or synergy' between physics and biology has yielded many fascinating fields of knowledge and technologies, among which are biomechanics, biophysics, and mechanobiology, and they contributed to the emergence of tissue engineering.

Tissue engineering, often times referred to as regenerative medicine, has emerged as a vibrant and exciting field during the last few decades fueled by advancement in biotechnology, medicine and materials sciences and engineering¹⁹. It has the potential in repairing or replacing damaged tissues to restore and maintain normal tissue or cell functions and holds the promise of meeting the great demand for organ transplantation and repair that far surpasses the current availability or affordability^{10, 24}. An investment of US\$0.86 billion to research and development was made and the total sales of TE related products reached US\$1.5 billion in 2007 alone²². The regulatory concerns have been raised and regulations have been formulated in the manufacturing of tissue engineered products in conjunction with regulation of medical devices, pharmaceuticals

and biotechnology, as reflected in the latest guidance for human cell, tissues and cellular and tissue-based products (HCT/P)⁵⁻⁷ released by FDA.

Tissue engineering generally involves repair, regeneration or replacement of tissues and organs. In almost all cases, successful implementation of tissue engineering strategies requires a good understanding of the interface between cells or tissues and the bio-scaffolds (e.g., implants), the cell harvesting systems (e.g., stem cell harvesting platform), or extracellular matrix in the host tissue and organs (e.g., in the preparation of xeno-transplant). This understanding is also important in basic biology and medicine as it is involved in a myriad of subjects including development, tissue/organ structure and function, pathology and physiology.

The effect of cell-ECM interactions on cellular regulation, development and general cell behavior is well recognized and is being subjected to intensive research effort. Various aspects of this effect have been investigated and major determinants of the cell decision making process have been identified, which include dimensionality, chemical and biochemical composition as well as physical characteristics of the substrates. Echoing the ever-increasing recognition of the significance of the mechanical and physical side of the cell-ECM interactions,³ **we directed our effort to the study of the effect of the mechanical stiffness on neurons and associated astroglia and the effect of the neuron-astroglia interactions on their respective mechanosensing,** aiming at neural tissue engineering applications including spinal cord injury repair. This has been the motivation for the static study part of this dissertation research.

The majority of the published studies were performed using substrates that remained unchanged or ‘static’ in their physical characteristics throughout the process.

Even though a number of studies of the ‘fourth dimension’ or temporal alterations in the cellular morphology and function have been conducted, **little attention and effort has been given to the physical or mechanical dynamics of the microenvironment that cells are subject to.** That the dynamics of the microenvironment deserves consideration stems from, first of all, the fact that in actualities cells do reside in a constantly changing micro-environment, composed of extracellular matrices and other cells. The ECM undergoes degradation and synthesis, which may lead to the alterations in the mechanical stiffness. Its mechanical compliance could also be modified with ageing^{1, 2, 16, 21, 23}, upon external assault, or through pathological processes^{8, 9, 11, 14, 17, 18, 20, 21, 25}. Moreover, dynamics in both cells and implants at the tissue-implant interface could give rise to the alterations in the cellular microenvironment^{15, 19, 24}. Thirdly, recent studies showed that the mechano-response is cell type specific, and also cellular property specific¹², which shed light to the engineering potential of temporally changing mechanical stiffness, in achieving optimal combination of cell groups or cell properties at different time point. Lastly, controlling stem cell differentiation and harvest also desires the feasibility of modifying substrate compliance temporally in a controlled fashion⁴.

We directed our effort to the study of the cellular responses to the changes in the mechanical compliances of the extracellular microenvironment, and do so in a quantitative manner. This is a key part of our effort in addressing the inability of current biomimetic materials in going through defined temporal remodeling¹⁵. In a word, the need to better understand the actualities of the cell behavior in a changing environment (e.g., normal tissue, development and pathological conditions, cell-implants interface), the capability of mimicking such changes in the substrates (i.e., DNA delivery

induced hydrogel modification) and the desirability of having such changes (e.g., engineering potential and stem cell therapy) motivate the part of this dissertation research involving dynamic substrates.

1.2 Objective of the Dissertation Research

For the scientist or engineer, the important questions he/she must find answers to are:

How shall I formulate the problem?

How shall I choose the alternate hypothesis?

What kind of experiments would justify or deny or improve my hypotheses?

How exhaustive should the investigation be?

Where might errors appear?

How much time is required to obtain a reasonable solution? At what cost?

These are the questions which concern active investigators and are question of synthesis, which employ analyses as tools.

—Y.C. Fung (*Preface of A First Course in Continuum Mechanics*)

The research in our laboratory, in a broad sense and in the long run, is aimed at obtaining a better understanding of tissue-scaffold and cell-biomaterial interfacial events and at facilitating the design of implantable bio-scaffolds for various tissue engineering applications including spinal cord injury repair, liver tissue engineering and stem cell engineering.

This Dissertation research examines the effect of the static and dynamic mechanical characteristics of a substrate or scaffold on the cell growth of two distinctive cell types, fibroblasts and neurons, and it explores the potential of engineering the

fibroblast growth and neurite (a collective term for axons and dendrites of neurons) outgrowth with mechanically dynamic cues. The hypotheses we formulated for the study include,

- Like other mechano-sensitive cells, neurons are able to sense and respond to the difference in the mechanical stiffness of the substrates, and the neuron-astroglia interactions impact their respective mechanosensing.
- Cells are able to sense the dynamic alterations in the mechanical stiffness of the substrates, and respond by changing morphology, adhesion or neurite outgrowth.

This dissertation research was conducted to address the following questions,

- Do spinal cord neurons and astroglia respond to mechanical stiffness, and if so, do they respond differently with and without the presence of the other party, or their interactions? Is there any possibility of engineering the neurite outgrowth?
- Do cellular properties respond differently to the mechanical stiffness? Do they respond differently to distinctive ranges of stiffness?
- Do cells respond to the changes of the mechanical stiffness of the substrate? If so, do they respond differently from one cell type to another, from one cellular property to another?
- Is there a correlation between phenotype or morphological changes and cellular adhesion and cell-cell interactions amidst these mechano-responses?

We utilized bis and DNA-crosslinked hydrogel systems in this pursuit, since these systems allow the controlled alterations of mechanical stiffness.

1.3 Dissertation Organization

At the onset, following Chapter 1 is background information on cells and substrates as well as the rationale for the choice of the specific cell types and biomaterials. The overview of the research on the cell-ECM interactions and the specific mechanical aspect concludes Chapter 2 which provides readers a general idea of the context of this dissertation research.

In Chapter 3, the research conducted on hydrogels with static mechanical stiffness is described. To delineate the effect of the cell-cell interactions on cell-substrate mechano-responses particularly for neural cells, the mixed and pure cultures of spinal cord cells were investigated on bis-crosslinked hydrogels and results on the effect of neuron-astroglia interactions on mechano-sensing are presented first (Chapter 3A). Portions of this chapter were published in *The Open Neuroscience Journal*¹³,

As a prelude to the dynamic study, the second half of the chapter 3 (Chapter 3B) is devoted to a discussion of the detailed responses of each cell property of the neuronal primary structures. The responses were assessed on DNA crosslinked hydrogels whose design was also expanded. This part is preceded by the discussion on the advantages of DNA gels over their bis-crosslinked counterparts. The results of studies on both of these types of gels are presented in Chapter 3. Portions of this chapter appeared in *Annals of Biomedical Engineering*¹².

Presented in Chapter 4 is the research using DNA-crosslinked hydrogels whose mechanical stiffnesses can be dynamically changed. The chapter is divided into three parts, addressing issues regarding characterization of DNA incorporation into gel network upon delivery (Chapter 4A), fibroblast mechano-responses (Chapter 4B) and

neuronal mechano-responses (Chapter 4C) to the mechanical dynamics in the DNA gels. Two manuscripts are in preparation for the work reported in this portion of the dissertation.

Chapter 5 concludes the dissertation with a summary of the observations and a discussion of the significance and novelty of the static and dynamic studies. Then a discussion on the limitations and discretions is followed by comments on the potential direction of future research.

In this dissertation, we refer to ‘static gels’ as the gels whose stiffness is not altered and ‘static study’ as the investigation conducted using these ‘static gels’; and ‘dynamic gels’ are referred to as gels whose mechanical stiffness is modified due to the changes in the crosslinking density via DNA delivery and ‘dynamic study’ as the study performed using these ‘dynamic gels’.

References

1. Badylak, S. F. The extracellular matrix as a biologic scaffold material. *Biomaterials*. 28:3587-3593, 2007.
2. Chen, C. S., X. Jiang, and G. M. Whitesides. Microengineering the environment of mammalian cells in culture. *MRS BULLETIN*. 30:194-201, 2005.
3. Discher, D. E., P. Janmey, and Y. L. Wang. Tissue cells feel and respond to the stiffness of their substrate. *Science*. 310:1139-1143, 2005.
4. Engler, A. J., S. Sen, H. L. Sweeney, and D. E. Discher. Matrix elasticity directs stem cell lineage specification. *Cell*. 126:677-689, 2006.
5. FDA. Human cells, tissues, and cellular and tissue-based products; establishment registration and listing. Food and drug administration, hhs. Final rule. *Fed Regist*. 66:5447-5469, 2001.
6. FDA. Eligibility determination for donors of human cells, tissues, and cellular and tissue-based products. Final rule. *Fed Regist*. 69:29785-29834, 2004.
7. FDA. Current good tissue practice for human cell, tissue, and cellular and tissue-based product establishments; inspection and enforcement. Final rule. *Fed Regist*. 69:68611-68688, 2004.
8. Freed, L. E., R. Langer, I. Martin, N. R. Pellis, and G. Vunjak-Novakovic. Tissue engineering of cartilage in space. *Proc Natl Acad Sci U S A*. 94:13885-13890, 1997.
9. Georges, P. C., J. J. Hui, Z. Gombos, M. E. McCormick, A. Y. Wang, M. Uemura, R. Mick, P. A. Janmey, E. E. Furth, and R. G. Wells. Increased stiffness of the rat liver precedes matrix deposition: Implications for fibrosis. *Am J Physiol Gastrointest Liver Physiol*. 293:G1147-1154, 2007.
10. Griffith, L. G., and G. Naughton. Tissue engineering--current challenges and expanding opportunities. *Science*. 295:1009-1014, 2002.
11. Huang, S., and D. E. Ingber. Cell tension, matrix mechanics, and cancer development. *Cancer Cell*. 8:175-176, 2005.
12. Jiang, F. X., B. Yurke, B. L. Firestein, and N. A. Langrana. Neurite outgrowth on a DNA crosslinked hydrogel with tunable stiffnesses. *Ann Biomed Eng*. 36:1565-1579, 2008.
13. Jiang, X., P. C. Georges, B. Li, Y. Du, M. K. Kutzinger, M. L. Previtera, N. A. Langrana, and B. L. Firestein. Cell growth in response to mechanical stiffness is affected by neuron-astroglia interactions. *Open Neuroscience Journal*. 1:7-14, 2007.
14. Jungbauer, S., H. Gao, J. P. Spatz, and R. Kemkemer. Two characteristic regimes in frequency-dependent dynamic reorientation of fibroblasts on cyclically stretched substrates. *Biophys J*. 95:3470-3478, 2008.
15. Lahann, J., and R. Langer. Smart materials with dynamically controllable surfaces. *MRS BULLETIN*. 30:185-188, 2005.
16. Marquez, J. P., G. M. Genin, K. M. Pryse, and E. L. Elson. Cellular and matrix contributions to tissue construct stiffness increase with cellular concentration. *Ann Biomed Eng*. 34:1475-1482, 2006.

17. McElhaney, J. H., J. W. Melvin, V. L. Roberts, and H. D. Portnoy. Dynamic characteristics of the tissues of the head,. In: R. M. Kenedi, editor. Perspectives in biomedical engineering,, MacMillan Press: London, 1973; pp 215–222.
18. Meiss, R. A. Dynamic stiffness of rabbit mesotubarium smooth muscle: Effect of isometric length. *Am J Physiol.* 234:C14-26, 1978.
19. Park, D. H., C. V. Borlongan, D. J. Eve, and P. R. Sanberg. The emerging field of cell and tissue engineering. *Med Sci Monit.* 14:RA206-220, 2008.
20. Paszek, M. J., and V. M. Weaver. The tension mounts: Mechanics meets morphogenesis and malignancy. *J Mammary Gland Biol Neoplasia.* 9:325-342, 2004.
21. Petroll, W. M., and L. Ma. Direct, dynamic assessment of cell-matrix interactions inside fibrillar collagen lattices. *Cell Motil Cytoskeleton.* 55:254-264, 2003.
22. Polak, J., S. Mantalaris, and S. E. Harding. *Advances in tissue engineering*, Imperial College Press: London, UK, 2008.
23. Silver, F. H., D. DeVore, and L. M. Siperko. Invited review: Role of mechanophysiology in aging of ecm: Effects of changes in mechanochemical transduction. *J Appl Physiol.* 95:2134-2141, 2003.
24. Sipe, J. D. Tissue engineering and reparative medicine. *Ann N Y Acad Sci.* 961:1-9, 2002.
25. Sumura, M., K. Shigeno, T. Hyuga, T. Yoneda, H. Shiina, and M. Igawa. Initial evaluation of prostate cancer with real-time elastography based on step-section pathologic analysis after radical prostatectomy: A preliminary study. *Int J Urol.* 14:811-816, 2007.

CHAPTER 2 BACKGROUND

2.1 DNA crosslinked hydrogels

2.1.1 Polymer hydrogels

Hydrogels are a class of hydrophilic polymers that possess both solid- and liquid-like properties. They have attracted great interest and have become ever-increasingly popular for many applications, including biomedical ones, since the development of a crosslinked HEMA hydrogels in the sixties of the last century^{4, 23, 57, 58, 85, 91, 114, 115, 121}. A hydrogel typically consists of an insoluble network of crosslinked polymer chains immersed in solvent which can be 10-20% to many times of its dry weight after swelling^{57, 66}. Due to its hydrated nature, a hydrogel can better mimic the properties of the natural tissues and neural micro-environment that cells reside in. This has also fueled the interest and development of hydrogels-based tissue engineering scaffolds. In addition, hydrogels generally respond to the environmental factors such as temperature and pH, and thus are among the candidates for the development of drug delivery systems³¹.

Based on the types of crosslinker, hydrogels can be categorized into two classes; gels with covalent junctions and gels with physical junctions (weak forces, physical entanglement or others), or more simply stated, chemical and physical gels.

Natural polymers are synthesized by living organisms mostly through enzymatic processes, while synthetic polymers generally involve either condensation or addition

approaches⁵⁷. Crosslinking yields a polymer network where polymer chains are interconnected, many of which possess sol-gel transition characteristics.

2.1.2 Natural vs. synthetic materials

The materials that are used to construct scaffolds can be generally divided into three categories: natural and synthetic materials, and hybrid materials consisting of both natural and synthetic components. Natural polymers such as alginate gels and collagen gels were among those whose use in tissue engineering applications were attempted earlier due to their inherent biocompatibility⁵⁷. However, they also possess a number of inherent disadvantages that include, but are not limited to, difficulties in fully characterizing bioactivities, batch-to-batch variations, potential transplant rejection or adverse host response³. Synthetic polymers offer an alternative with relative abundance, availability and ease in characterization, which brings controllability and reproducibility where natural materials suffer^{3, 37}.

2.1.3 Biodegradable vs. non-biodegradable materials

Bio-degradable, bio-erodable or bio-absorbable materials have the advantages over their counterpart of non-biodegradable materials in that they are relatively better characterized and have been used in the previous tissue engineering applications. Although biodegradable materials have these apparent attractions, they are not without problems which include insufficient support caused by premature degradation and possible harmful intermediates *in vivo*^{5, 24}. Alternatively, non-absorbable polymers or their copolymers have also shown potential utility in tissue engineering applications, and have attracted

considerable interest^{38, 93}. For instance, in a recent study, Bakshi et al.⁵ found in animal studies, mild inflammatory responses, little scarring, significant angiogenesis, and axonal penetration in a scaffold made from poly-hydroxyethyl methacrylate (pHEMA), a non-degradable hydrogel.

2.1.4 The properties of DNA

DNA (deoxyribonucleic acid) is a biopolymer of fundamental importance to living organisms and serves as the carrier of genetic information. Since its discovery over half a century ago, more and more unique properties and functions have been identified. It is now recognized that it is not only an ideal media for preserving hereditary codes, but also a good candidate as a structural component for materials and serves as building blocks for nanotechnology^{8, 42, 109, 119, 134}. Among these properties are molecular recognition (specificity), stable structure held by stacking H-bonds and other weak forces (stability), and flexibility in separation of the base-pairing allowing, for instance, DNA replication and recombination¹²⁶.

The hybridization reaction occurs between two complementary DNA strands, and is affected by temperature and strand length. Branch migration takes place when a single-stranded DNA (ssDNA) competitively hybridizes with one strand of the DNA duplex, and extends the hybridization until that strand is displaced entirely from the original DNA duplex¹²⁶. The process has a low rate constant several orders of magnitude less than the hybridization reaction¹⁰³, and by designing a toehold, the process has been shown to increase dramatically¹³⁵ (Figure 2-1). Yurke and Mills have determined that for a toehold length of eight bases, the exchange rate increases by six orders of magnitude¹³⁵.

DNA re-association or re-annealing kinetics

Upon being heated above its melting temperature (T_m), duplex DNA will separate into complimentary strands of ssDNA since the hydrogen bonds in between the two strands and other stabilizing forces in the duplex can not withstand the separating forces. This process is also called thermal denaturation of the DNA, and can be reversed if the melted DNA is cooled slowly, for which the term ‘re-association’, ‘re-naturation’, or ‘re-annealing’ is used^{7, 34, 74, 112}. Four major factors dictate the rate of re-association: temperature, salt concentration, DNA concentration, and the length of DNA strand⁷⁴. The optimal re-association temperature is approximately 20°C below melting temperature, and the presence of adequate amount of cations is necessary for re-annealing⁷⁴.

2.1.5 DNA as structural materials

Although DNA primarily serves as a carrier of genetic information in biological organisms, it has proven useful in various applications^{42, 109}, particularly in the construction of DNA nano-assemblies⁸ and DNA linked microstructures¹¹⁹. The inherent advantages of using DNA over other macromolecules as a structural component include the predictability of DNA strand interaction due to the simplicity (only four distinct bases: A/T/G/C) and specificity of Watson-Crick base pairing. With a persistence length of 50 nm, duplex DNA has a structural rigidity suitable for the construction of nanodevices. The flexibility of single stranded DNA and the relatively weak bonding in duplex DNA allows interacting DNA strands to seek thermodynamically favored configurations, making possible programmed self assembly of complex structures. This also allows DNA to be used as a fuel to drive DNA nanomachines⁴². DNA sliding, if

tailored through the choice of base sequence, may be useful in imparting unique properties to these materials⁹⁰. DNA containing hydrogels have also been constructed^{27, 118}.

2.1.6 Using DNA to crosslink a polymer network

DNA has been proven a useful material to give bulk materials added functionality. In particular, by using DNA hybridization instead of covalent bonding to form crosslinks between polymer strands, hydrogel polymers have been given a temperature-dependent rigidity and thermal reversibility in crosslinking and gelation^{78, 88}. This has generated interests in using DNA as crosslinking agent for various applications^{2, 76, 87, 104, 128}.

Polyacrylamide (PAM) gels have wide applications as biomaterials due to a number of advantages⁹. By incorporating AcryditeTM modified oligonucleotides in PAM gels, in our laboratory, Lin and colleagues⁷⁸ illustrated and characterized reversible gelation and achieved a range of stiffness from a few hundred Pa to 10 kPa by varying crosslinker DNA density⁷⁷. The ease with which the mechanical properties of DNA crosslinked gels can be changed suggests that they would be useful in tissue engineering applications.

In these gels, AcryditeTM modified oligonucleotides co-polymerize with acrylamide monomers to form polymer long chains with DNA side chains of specific length and sequence designated as SA1 and SA2. “Crosslinker” oligonucleotides (L2) with a ‘toehold’ assume the functions of a crosslinker by hybridizing with SA1 and SA2 at the same time. By carefully designing another single-stranded DNA (ssDNA), also called “removal” DNA, that is complementary to L2, one is able to reverse the crosslinking process (Figure 2-1).

Replacing the covalently bound bis-crosslinks with paired DNA strands results in a gel possessing quite a few potentially useful properties, such as thermal reversibility with a tunable melting temperature, reversibility of gelation without heating and without the need of initiator-catalyst system for re-gelation^{78, 79}. More interestingly, by modifying the DNA crosslinking (i.e., oligonucleotide length or concentration), the mechanical properties of the gels can be engineered to take on particular values. Specifically, via delivery of more crosslinks, the DNA association/dissociation ratio could increase, resulting in a stiffened gel; in contrast, gels could be softened by lowering the crosslink density with removal DNA strands (designated as CL2, Figure 2-1) that are complementary to L2. CL2 strands competitively base-pair with L2 strands and remove them from the gel network. Examples of the major approaches used to alter DNA gel nano-scale structures and hence the gel's physical properties are illustrated in Figure 2-2.

Besides polyacrylamide, poly-hydroxyethyl methacrylate (pHEMA), poly-hydroxy-propyl-methacrylamide(pHPMA), polymethyl methacrylate (pMMA), and copolymers (e.g. pHEMA-co-MMA and pHEMA-co-AEMA) are among the most studied non-biodegradable polymers for tissue engineering applications, including SCI research^{38, 45, 71, 93} owing in part to their resemblance to highly hydrated natural tissues¹⁰². The design of these polymers can benefit from the DNA crosslinking mechanism due to the presence of the vinyl group in their monomers (Table 2-1). They have been engineered to carry neuro-trophic factors and present communicating porous structures^{5, 16}, and to facilitate necrosis reduction, vasculature formation and axonal outgrowth across the graft-tissue interface^{30, 71, 133}.

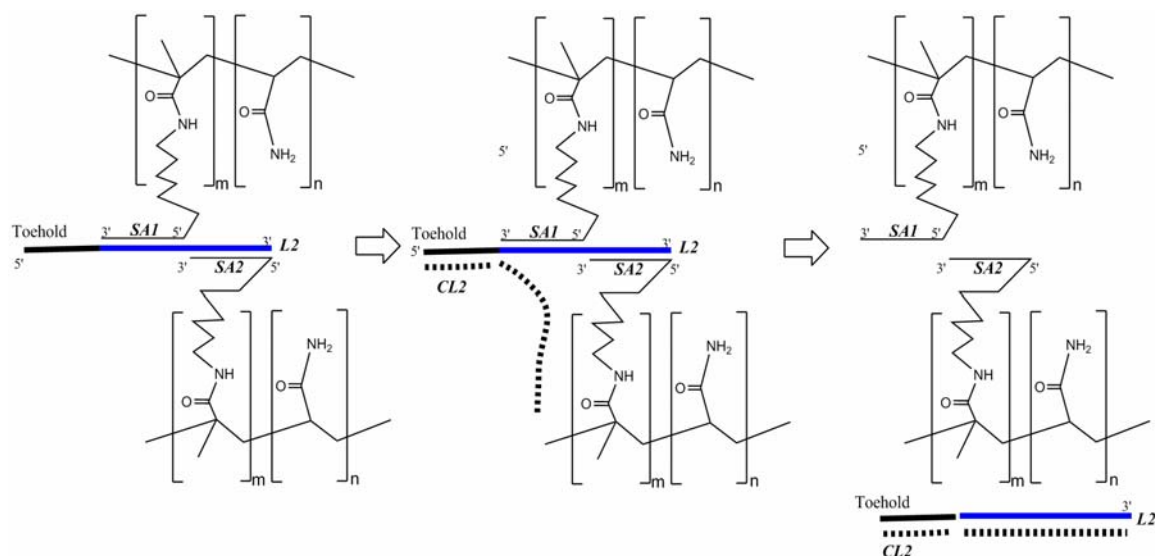


Figure 2-1 Schematic depicting the reverse process of DNA crosslinking. By adding a toehold to the end of the L2 strand, the crosslinker can be displaced via delivery of CL2 (dotted line) complementary to L2, thus reducing the crosslinking level.

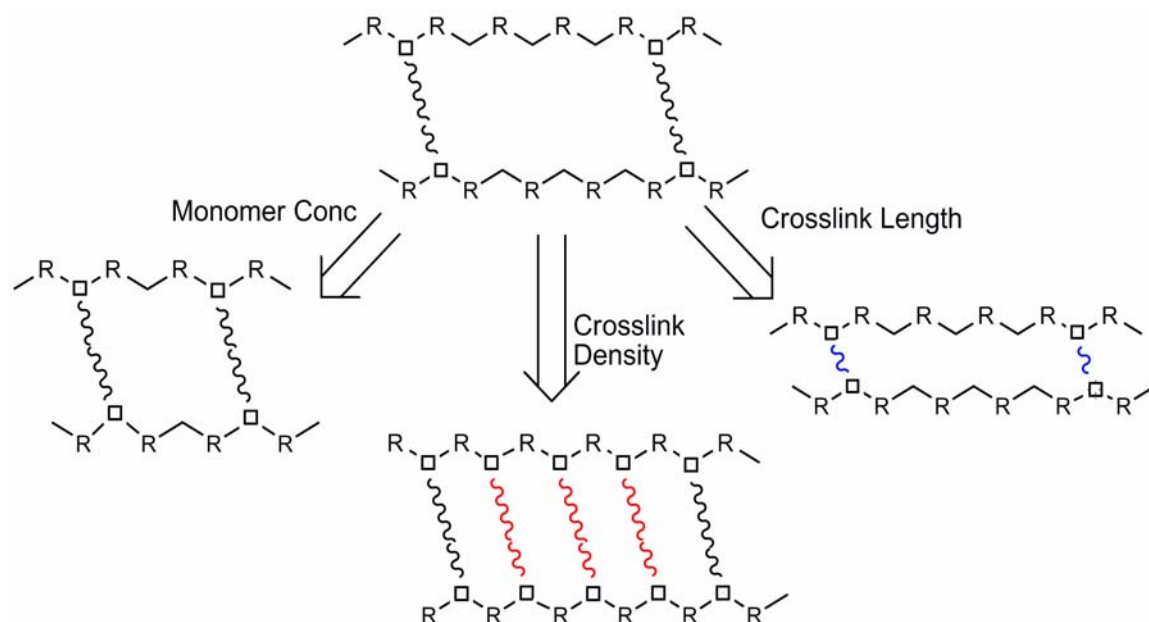
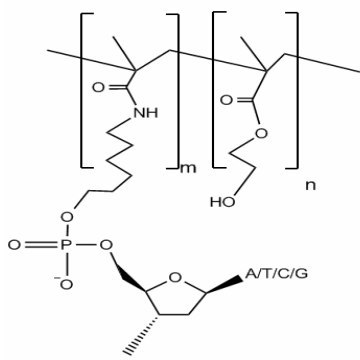
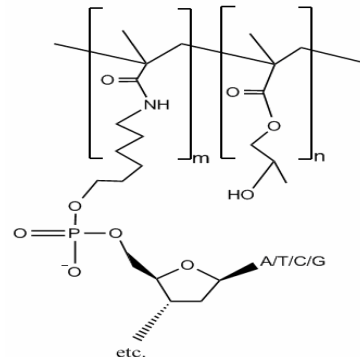


Figure 2-2 Examples of the major approaches in altering mechanical properties of the DNA crosslinked hydrogels. Approaches include change in crosslinker length (i.e., number of bases), crosslink density, or monomer concentration. R: polymer monomer.

Table 2-1 Examples of potential DNA crosslinked hydrogels.
L2: crosslinker DNA.

DNA X-linked polymer	Gel preparation	Chemical structure	Notes
pHEMA, poly-(hydroxyethyl methacrylate) ^{5, 22, 45}	Crosslink: L2 (replacing EGDMA) HEMA (Aldrich, St. Louis, MO) (20%-60%) Initiator-catalyst (APS-TEMED)		Pore size: 10 μm to 20 μm
pHPMA, poly-(hydroxypropyl-methacrylamide) ^{38, 113}	Crosslink: L2 (replacing DMHA) HPMA monomer Initiator (AIBN)		Pore size: 10 μm to 50 μm

2.1.7 Mechanical characterization of hydrogels and soft materials

The mechanical properties of hydrogels need to be characterized prior to their application, with respect to crosslink concentration, crosslink length, acrylamide monomer concentration and other parameters. Previously, Pelham and Wang⁹⁸ used a rather crude and simple way to measure the Young's modulus where they applied weight (e.g. hanging binder clip) to the strips of gel sample and recorded deformation following conventional approach for materials like metals. Later on, they made the samples in a 'dog-bone' shape like that used in conventional mechanical measurements^{98, 129}. Because the viscoelastic nature of the hydrogels and loading conditions (i.e. clip hanging) complicate these testing procedures, better testing procedures are desired. Wong et al¹²⁹ also pointed out that measurements performed on the surface of a gel or on a thin gel did not yield values that are identical to those obtained from bulk gels. A micro-needle measurement technique was designed, and the researchers established the correlation between the deflection of the needle tip perpendicular to the gels and the forces that were generated^{70, 98}. This method has an inherent drawback that a highly localized force is generated and could induce stress concentration which renders the results unreliable.

Another approach, known as the Hertz cone method, is to drop a steel ball on the gel and calculate the compliance using the known force (weight of the ball) and measured indentation with the help of Hertz theory^{81, 129}. Particle image velocimetry (PIV) has been utilized to study the local deformation of the hydrogels⁶³. Recently, rheometry was employed to quantify the visco-elasticity of hydrogels^{44, 132}. Although the mechanical properties of gels can be characterized before their use in cell culture or tissue engineering experiments, *in situ* measurements during the course of the experiment and

under physiological conditions would be ideal. Very recently, an atomic force microscopy (AFM) technique has been implemented^{35, 40, 94}, to probe the surface physical properties of the hydrogels in the aqueous conditions, with refined theoretical framework for interpretation of the data⁸⁰.

2.2 Choice of cell types

2.2.1 Fibroblasts

Fibroblast cells are among the most abundant cell types in various tissues and in almost every organ in human body^{55, 130}, especially in the connective tissues. They assume the role of ‘scaffold support’ maintaining the integrity of the tissue structures by synthesizing and remodeling extracellular matrices (ECM). Fibroblast cells produce most of the ECM components⁸². Additionally, they have been shown to play roles in wound-healing, organ development, inflammation, among other things⁵⁵. Great progress has been made during the past few decades in engineering fibroblasts for various applications, including, vascular tissue engineering⁸⁶, skin tissue engineering⁹², and neural tissue engineering¹⁰⁷.

The response and sensitivity of fibroblasts to mechanical cues is well documented. (See, for instance, references^{20, 26, 59, 100}). These cues consist of mechanical forces^{12, 36, 122}, mechanical stress/strain³², as well as mechanical stiffness^{98, 123} of the ECM.

2.2.2 Neurons and other cells in central nervous system

The nervous system consists mainly of two groups of cells, the neurons and glia, with the former one classified based mainly on dendritic morphology^{21, 72} and the latter composed

of a number of subclasses (e.g., astrocyte, microglia, oligodendrocyte) differentiated based on their morphology and functions. Unlike fibroblasts, neurons, the functional unit in the neural circuitry, are relatively specialized and exist mostly in the nervous system. Their role in transferring and processing information via intercellular signaling lays the foundation for the functioning of the nervous system. The major disparity between neurons and other cell types lies in neurons' inability to undergo mitosis. Distinction in their functions also stems from their structures which differ greatly to those of the fibroblasts. Typically, a neuron has three distinctive structural elements, the axon, usually only one, from which the information is transferred to the next neuron, the dendrite where the information is received, and the cell body, or soma, which is capable of firing the action potential and releasing neurotransmitters¹⁹ (Figure 2-3). Within the neuronal populations in the nervous system, subpopulations of neurons can also differ significantly from one another depending on the tissue types and functional roles, which adds greatly to the complexity in the identification, characterization, and engineering of the neurons⁷².

Glial cells have long been thought to act as a 'glue', keeping neurons together, as indicated by how its name was coined^{19, 72}. More and more evidence has pointed to their active participation in the proper functioning of nerve cell and the nervous system^{15, 43}. Unlike neurons, glial cells are capable of dividing and multiplying via mitosis.

2.2.3 Spinal cord injuries and therapeutic strategies

2.2.3.1 Neural tissues

The nervous system, composed of central and peripheral nervous systems (CNS/PNS), senses and responds to external stimuli, and contributes to the maintenance of homeostasis of the living organisms. The CNS includes the brain and the spinal cord whose major function is the transmission of information between brain and the periphery of the body. The spinal cord can be further subdivided into segments, and it is composed of two primary regions, the white matter and the gray matter. The spinal cord is covered by meninges consisting of three layers, the outer dura mater, the arachnoid mater, and the pia mater¹³.

2.2.3.2 Significance and challenges

Each year, there are 10,000 new cases of traumatic SCI, with a prevalence of 200,000 in the general population. These injuries bring about tremendous economic and emotional costs to the inflicted individuals and the society^{48, 84}. Once described as ‘a disease that cannot be treated’ by ancient Egyptians⁸⁴, SCI has received great attention. It is always accompanied by loss of functions such as breathing, bladder and bowel control, motility, and sexual functions. Considerable effort has been made in the recent decade in attempts to repair and regenerate neural tissues for patients with neurodegenerative diseases or traumatic injuries to the nervous system^{64, 107}. Researchers have been searching for cures and have primarily identified axonal regeneration, synaptogenesis and formation of the neuronal circuitry among the key steps in gaining functional recovery after SCI.

Microscopically, spinal cord injury (SCI) often results in damage to axons in the white matter of the spinal cord and subsequent interruption of neuronal communication.

2.2.3.3 Major approaches in finding the cure

Unlike the major problems associated with a myriad of types of injuries and also distinct from injuries to the periphery nervous system (PNS), the challenges accompanying central nervous system (CNS) are many fold and unique (Figure 2-4). They include, but are not limited to, the existence of regeneration-inhibiting glycoproteins, a much slower functioning of macrophages, unappreciable upregulation of cell adhesion molecules, glial scar formation, and the existence of the blood-spine barrier¹⁰⁷. Thinking in terms of the level of functional recovery required, the task of complete recovery might seem unachievable—not only would the axons have to be able to regenerate in a controlled fashion, but synapse formation also needs to occur to reestablish neural communication. Additionally PNS-CNS interfacial zone would also have to be functionally restored^{41, 101}.

Encouraged by the progress in the basic research on neuroscience and the development in tissue engineering, various approaches (Fig. 2-4) have been attempted, to promote neuronal growth and protect neurons from further insults^{41, 107}, which include designing bio-scaffolds, delivering trophic factors and other biological reagents, and cellular therapies utilizing cells such as olfactory ensheathing cells and stem cells.

2.2.3.4 Tissue engineering approach and biomaterial design

The re-establishment of neural circuitry via regeneration of axons is a critical step in reversing the effects of SCI. While numerous biological and cellular therapies (i.e. stem

cell, olfactory ensheathing cell, pharmacological) are being pursued to enhance spinal cord nerve regeneration in searching for cures of spinal cord injuries (SCI)^{41, 68, 107}, nerve grafts or scaffolds providing physical support and guidance in addition to enabling biomolecule delivery hold great promise and are under aggressive development^{3, 47, 51, 93, 107}. These grafts or scaffolds are desired to not only establish a bridge or channel allowing growth of regenerating axons from the proximal to the injury site and further to the distal target, but also provide a multitude of stimuli including physical ones to enhance and direct the regeneration of the neurites.

In a recent study, Bakshi et al.⁵ found in animal studies, mild inflammatory responses, little scarring, significant angiogenesis, and axonal penetration occur in a hydrogel scaffold made from poly-hydroxyethyl methacrylate (pHEMA). DNA crosslinking also can be applied to those polymers with demonstrated biocompatibility, and consequently confer on these polymers the versatility (e.g., tunable flexibility and non-chemical and non-thermal reversibility) to achieve significant axonal growth in addition to those aforementioned benefits.

In the current work, we aim to design a DNA crosslinked hydrogel that can offer a conducive environment for axonal regeneration and neuritogenesis and at the same time enable the application of the external stimuli, such as dynamic mechanical stiffness, to the neuron and astroglia, in a manner that will facilitate and promote neurite regeneration (Figure 2-5).

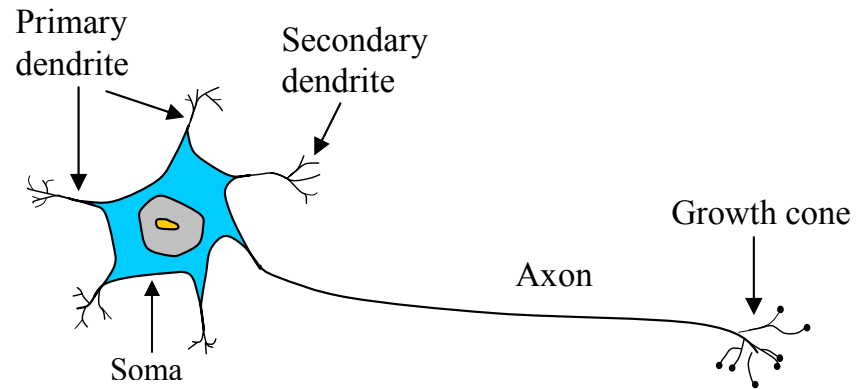


Figure 2-3 Schematic of the typical morphology of a neuron. The neuron is composed of dendrite, axon, and neuronal soma. Stemming from primary dendrites are secondary dendrites.

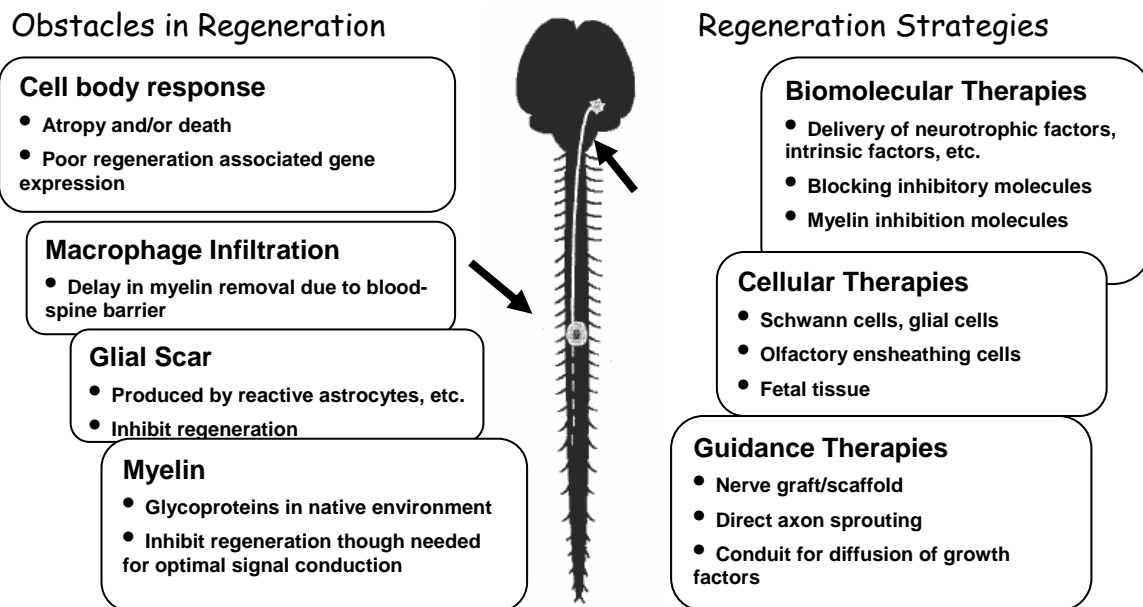


Figure 2-4 Summary of the major challenges in finding a cure for spinal cord injuries and the strategies proposed to tackle the problem. Extracted and modified from⁶⁷.

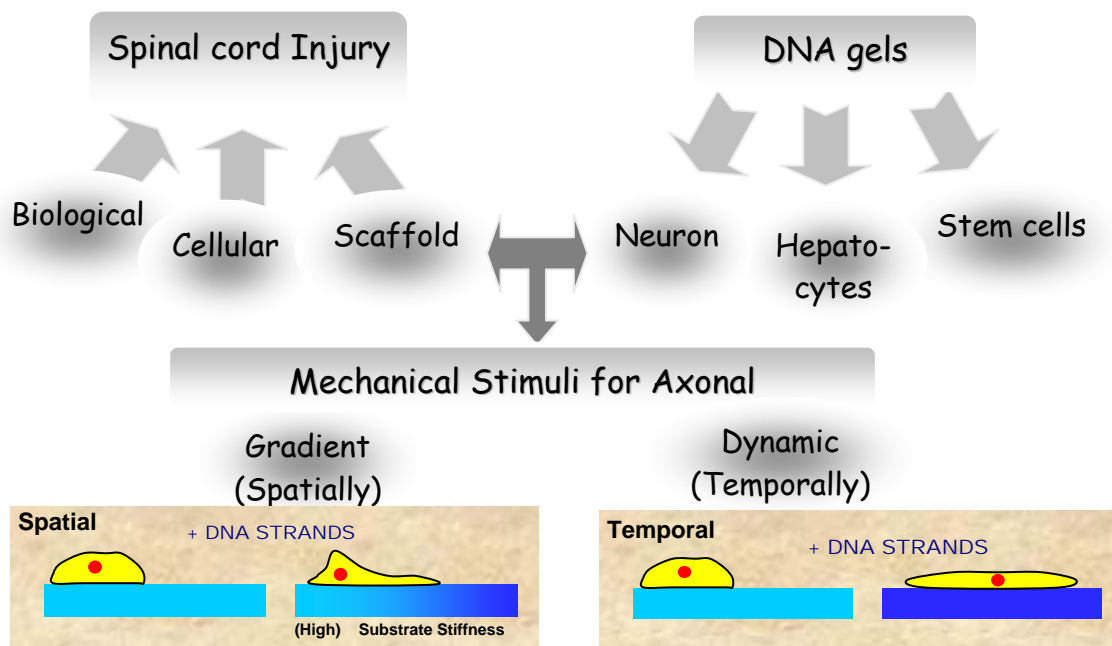


Figure 2-5 Tissue engineering approaches adopted in the current research

2.3 Cell-ECM interactions

2.3.1 Cell-ECM interplay

Interactions between cells and extracellular matrix (ECM) are subject to intensive research effort both experimentally and numerically in recent years^{17, 26}. These interactions, coupled with the cell-cell crosstalk, constitute the external factors that affect cell behavior. There is an increasing awareness that mechanical interactions are an integral part of the cell-ECM interactions, in addition to the chemical interplays^{6, 28}.

On the one hand, various chemical, biological, and mechanical information in ECM is gathered and processed for cellular decision making¹⁰⁸, resulting in distinct cellular behaviors (e.g.,^{39, 54}). Perhaps one of the most interesting reports about this is that responses of the collagen matrix to external loading are not brought about by changes in mechanical properties of the gels but mediated by cells²⁰. On the other hand, cells alter the surrounding environment by, e.g., secreting ECM components so as to adhere, proliferate, and locomote⁸³; cells also induce the reorganization of ECM by exerting forces⁶⁰. The force generation is a very important capability of cells in, for example, wound closure mediation⁸⁹ and tissue component alignment⁵³. As another example, it is generally believed that fibroblasts apply mechanical pulling forces to collagen fibers in maintaining the integrity of connective tissue⁸³. Moreover, it has long been reported that cells react to reorganization of the ECM resulting from tractions by other cells⁵⁶ and that cells incorporate feedback from ECM to adjust shape and function⁶⁰. Furthermore, dynamic analysis is inevitable in characterizing many cellular behaviors such as cellular motility and migration¹¹⁰. As a result, this cell-cell interaction via ECM plus the possible

control mechanism and dynamic behavior in addition to aforementioned interaction between cells and ECM complicates the whole picture of cell-ECM events.

2.3.2 Major determinants in cell responses and physical cues

Recent studies^{28, 50} showed that in investigating cellular behavior under the influence of extracellular matrix (ECM) *in vitro*, one would less likely achieve an accurate representation of *in vivo* events without taking in account any of the following three factors: three-dimensionality, chemical composition and mechanical properties of the ECM. These factors can be sensed following intracellular pathways and trigger a series of events leading to the alterations in gene expression, which is manifested in the phenotype (Figure 2-6). Ever since the finding of Bissell's group¹²⁷, more and more proof has been presented from various studies for the importance of 3D cell culture in that a few observations made in 3D culture were quite different, if not opposite, to those in 2D culture and that 3D culture systems more closely resemble the cell environment *in vivo*¹. Spatial arrangement of the cells is important and cells on planar structure do not function in the same way as those in real tissues. There are mainly three ways of creating a 3D culture system: simple gels incorporating collagen, customized gels form ECM of proper tissues and a basement membrane matrix—Matrigel¹⁴. It was suggested that 3-D scaffolds and 3-D cultures might be fabricated in the same fashion⁴⁶.

The effects of chemical cues provided by the ECM have also received considerable attention. In particular, chemical composition in site of injury and molecular mechanism of repair has been intensively studied although this research is far from complete. In contrast, mechanical stimuli provided by the ECM have attracted

substantial attention only relatively recently, despite the critical role played by mechanical stimuli including stiffness or compliance and viscosity of ECM on cellular behavior such as adhesion, migration, and signal transduction in development. For instance, mechanical tension has been shown to determine the axonal fate in hippocampal neurons⁶⁹.

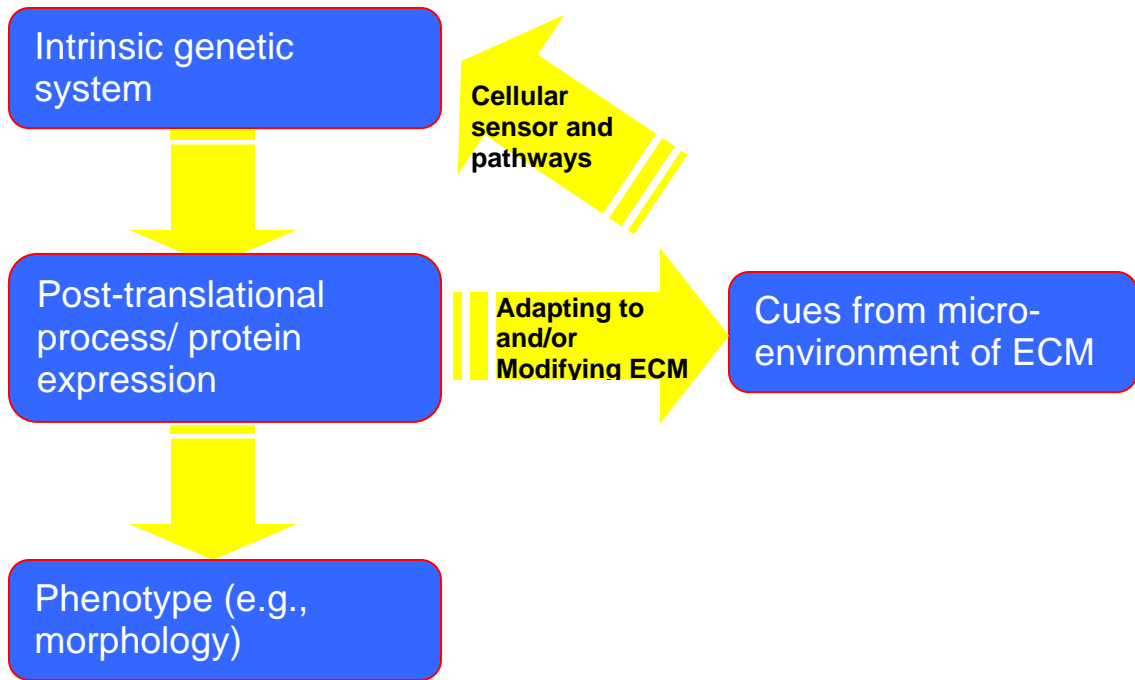


Figure 2-6 Schematic depicting the interactions between cells and the local micro-environment at the molecular level.

The principle holds that ‘Gene is the gun, ‘micro-environment’ pulls the trigger’.

2.3.3 Cell mechano-sensing

In contrast to the long history of efforts directed to elucidate the roles of various biological molecules in cellular events, it has been about only a decade since physical cues, especially externally applied forces or tension^{18, 111, 136} and mechanical properties of the substrates or scaffolds^{10, 81, 98}, started to draw ever-increasing attention. However, external force or traction application remains a problem *in vivo* that could pose a great challenge for efforts to take advantage of cellular responses to mechanical cues for medical applications. In contrast, much more control could be gained in synthetic media, over the physical properties of the substrate as a subset of mechanical cues provided to cells. It can be achieved by carefully selecting materials and designing the substrates (2D) or the scaffolds (3D). Among all of the physical properties that can be controlled are surface topography, surface pore size, and surface geometric patterns including those produced by micro-posts²⁵.

To better understand cell-ECM interactions, particularly, the coupling between mechanical responses and biological functions, much effort has been made in the qualitative or quantitative study of tissue and cell mechanics⁶. For these studies, the elucidation of direction and magnitude of cellular forces acting on the ECM is of prime importance^{33, 81, 106, 120}. In light of this, many experimental methods have been developed for the mechanical studies. Elastic micropatterned substrates were designed by Schwarz et al.¹¹⁶ to monitor the cellular forces in the cell-ECM interface at the focal adhesion (FA) sites. Comparing cellular forces measured on silicon elastomers by imaging their surfaces, Wroble et al.¹³¹ were able to study the differential behavior in force exertion of fibroblasts and myofibroblasts. With the help of optical sectioning microscopy which

excludes the need of extrinsic marker, Vanni et al.¹²⁰ investigated 3T3 fibroblast behavior with displacement measured in collagen gels and they found that the gel anisotropy due to cellular forces can be sensed by others cells even a relatively long distance away. For a comprehensive review of ways of measuring cellular traction forces, one is referred to Beningo and Wang¹¹ and Roy et al.¹⁰⁶.

As an example of a cell for which mechanical interaction with the ECM is crucial to its function, consider myofibroblasts, also referred to as fibroblastic cells within granulation tissue. They typically exert mechanical forces in normal tissue and under pathological conditions, e.g. Dupuytren's disease⁴⁹. These cells play a critical role in wound healing but have a transitory existence in connective tissue injury¹¹⁷. An underlying molecular mechanism has been proposed for the force generation as well as ECM synthesis of these cells that causes the reorganization of the ECM^{49, 117}. The mechanical interaction of myofibroblasts with the ECM is apparent: it is the mechanical loads that activate cardiac fibroblasts and initiate their differentiation towards myofibroblasts¹²⁴. Fibroblastic cells on collagen gels exhibit a morphology that is distinct from that observed in common culture dishes, and such gels are contracted by cells and exhibit realignment of the collagen fibrils⁵⁴.

2.3.4 Effect of substrate mechanical stiffness on cells

Among critical extracellular cues, the effect of physical stimuli, including traction force, mechanical strain, surface topography^{39, 81, 95, 98, 99, 125, 129, 132} and particularly substrate stiffness, have been found to affect cellular behavior in a cell-type specific manner^{29, 44, 52, 65, 75, 96, 97}. Mechanical stiffness, sometimes also referred to as mechanical rigidity or the

inverse of the compliance, is an inherent property of a specific material. It reflects the resistance of a structure to externally applied forces, and can be characterized by the force acted on a unit area over the deformation of a unit length resulting from the applied force. In living tissues, these signals originate in the ECM which functions as a natural cell substrate and is characterized by tissue-specific protein compositions and cell-ECM interactions.

In *in vitro* conditions, researchers have subjected cultured cells to various substrates composed of natural and synthetic hydrogels, such as collagen¹⁰⁵ and pHEMA⁵, which mimic intrinsic ECM properties. These hydrogels better represent cells' natural fluidic environment than *in vitro* culture plate systems do. Wang and co-workers popularized bis-acrylamide crosslinked hydrogels ('bis-gels', hereafter) as substrates to study cell-substrate interaction¹²⁵. This model system has been utilized in studies involving a variety of cell types, including rat kidney epithelial cells⁹⁷, 3T3 fibroblasts⁹⁷, non-neuronal PNS (peripheral nervous system) cells¹⁰⁵, hepatocytes⁷³ and recently, CNS (central nervous system) cells^{44, 52, 61, 95}.

Flanagan and colleagues⁴⁴ investigated the response of neurons to gels with two different mechanical stiffnesses and found that mouse spinal cord neurons have more dendritic branches on softer gels (E~150 Pa) than on stiffer gels (E~1500 Pa). Their study was extended to rat cortical neurons⁵², and the researchers showed that astrocytes spread less and had poor adhesion on softer gels with a shear modulus of 200 Pa (E~600 Pa), while neurite elongation and attachment of neurons co-cultured with glia were not dramatically different from those on stiffer gels (E~27 kPa). Our group very recently demonstrated that, due to the presence of neuron-astroglia interactions, the responses of

neurons and astroglia to the mechanical stiffness of the ECM could be different than those in their respective pure cultures⁶¹. With a DNA crosslinked hydrogel, we also showed that different neuronal properties, including primary dendrite length and number and axonal length, respond in a distinctive fashion to the range of stiffness explored⁶². It suggests that the neuronal cell body and neurites might have more than one way of detecting and responding to ECM stiffness.

References

1. Abbott, A. Cell culture: Biology's new dimension. *Nature*. 424:870-872, 2003.
2. Alemdaroglu, F. E., and A. Herrmann. DNA meets synthetic polymers--highly versatile hybrid materials. *Org Biomol Chem*. 5:1311-1320, 2007.
3. Angelova, N., and D. Hunkeler. Rationalizing the design of polymeric biomaterials. *Trends Biotechnol*. 17:409-421, 1999.
4. Badylak, S. F. Regenerative medicine and developmental biology: The role of the extracellular matrix. *Anat Rec B New Anat*. 287:36-41, 2005.
5. Bakshi, A., O. Fisher, T. Dagci, B. T. Himes, I. Fischer, and A. Lowman. Mechanically engineered hydrogel scaffolds for axonal growth and angiogenesis after transplantation in spinal cord injury. *J Neurosurg Spine*. 1:322-329, 2004.
6. Bao, G., and S. Suresh. Cell and molecular mechanics of biological materials. *Nat Mater*. 2:715-725, 2003.
7. Bart Haegeman, D. V. J.-J. G. J. H. DNA reassociation kinetics and diversity indices: Richness is not rich enough. *Oikos*. 117:177-181, 2008.
8. Beissenhirtz, M. K., and I. Willner. DNA-based machines. *Org Biomol Chem*. 4:3392-3401, 2006.
9. Benedetto, F., A. Biasco, D. Pisignano, and R. Cingolani. Patterning polyacrylamide hydrogels by soft lithography. *Nanotechnology*. 16:S165-S170, 2005.
10. Beningo, K. A., C. M. Lo, and Y. L. Wang. Flexible polyacrylamide substrata for the analysis of mechanical interactions at cell-substratum adhesions. *Methods Cell Biol*. 69:325-339, 2002.
11. Beningo, K. A., and Y. L. Wang. Flexible substrata for the detection of cellular traction forces. *Trends Cell Biol*. 12:79-84, 2002.
12. Benjamin, M., and B. Hillen. Mechanical influences on cells, tissues and organs - 'mechanical morphogenesis'. *Eur J Morphol*. 41:3-7, 2003.
13. Berne, R. M., M. N. Levy, B. M. Koeppen, and B. A. Stanton. *Physiology*, C.V. Mosby, 2003.
14. Bessea, L., B. Coulomb, C. Lebreton-Decoster, and M. M. Giraud-Guille. Production of ordered collagen matrices for three-dimensional cell culture. *Biomaterials*. 23:27-36, 2002.
15. Bezzi, P., and A. Volterra. A neuron-glia signalling network in the active brain. *Curr Opin Neurobiol*. 11:387-394, 2001.
16. Bilston, L. E., and L. E. Thibault. The mechanical properties of the human cervical spinal cord in vitro. *Ann Biomed Eng*. 24:67-74, 1996.
17. Bischofs, I. B., S. A. Safran, and U. S. Schwarz. Elastic interactions of active cells with soft materials. *Phys Rev E Stat Nonlin Soft Matter Phys*. 69:021911, 2004.
18. Bray, D. Axonal growth in response to experimentally applied mechanical tension. *Dev Biol*. 102:379-389, 1984.
19. Brodal, P. *The central nervous system: Structure and function*, Oxford University Press, 2004.

20. Brown, R. A., R. Prajapati, D. A. McGrouther, I. V. Yannas, and M. Eastwood. Tensional homeostasis in dermal fibroblasts: Mechanical responses to mechanical loading in three-dimensional substrates. *J Cell Physiol.* 175:323-332, 1998.
21. Cajal, R. Y. *Histologie du système nerveux de l'homme et des vertébrés* Maloine: Paris, 1911.
22. Carone, T. W., and J. M. Hasenwinkel. Mechanical and morphological characterization of homogeneous and bilayered poly(2-hydroxyethyl methacrylate) scaffolds for use in cns nerve regeneration. *J Biomed Mater Res B Appl Biomater.* 2006.
23. Chaikof, E. L., H. Matthew, J. Kohn, A. G. Mikos, G. D. Prestwich, and C. M. Yip. Biomaterials and scaffolds in reparative medicine. *Ann N Y Acad Sci.* 961:96-105, 2002.
24. Chapekar, M. S. Tissue engineering: Challenges and opportunities. *J Biomed Mater Res.* 53:617-620, 2000.
25. Chen, C. S., M. Mrksich, S. Huang, G. M. Whitesides, and D. E. Ingber. Geometric control of cell life and death. *Science.* 276:1425-1428, 1997.
26. Chen, C. S., J. Tan, and J. Tien. Mechanotransduction at cell-matrix and cell-cell contacts. *Annu Rev Biomed Eng.* 6:275-302, 2004.
27. Costa, D., M. G. Miguel, and B. Lindman. Responsive polymer gels: Double-stranded versus single-stranded DNA. *J Phys Chem B.* 111:10886-10896, 2007.
28. Cukierman, E., R. Pankov, D. R. Stevens, and K. M. Yamada. Taking cell-matrix adhesions to the third dimension. *Science.* 294:1708-1712, 2001.
29. Curtis, A., and M. Riehle. Tissue engineering: The biophysical background. *Phys Med Biol.* 46:R47-65, 2001.
30. Dalton, P. D., L. Flynn, and M. S. Shoichet. Manufacture of poly(2-hydroxyethyl methacrylate-co-methyl methacrylate) hydrogel tubes for use as nerve guidance channels. *Biomaterials.* 23:3843-3851, 2002.
31. de Las Heras Alarcon, C., S. Pennadam, and C. Alexander. Stimuli responsive polymers for biomedical applications. *Chem Soc Rev.* 34:276-285, 2005.
32. De, R., A. Zemel, and S. A. Safran. Do cells sense stress or strain? Measurement of cellular orientation can provide a clue. *Biophys J.* 94:L29-31, 2008.
33. Dembo, M., and Y. L. Wang. Stresses at the cell-to-substrate interface during locomotion of fibroblasts. *Biophys J.* 76:2307-2316, 1999.
34. Dhillon, S. S., A. V. Rake, and J. P. Miksche. Reassociation kinetics and cytophotometric characterization of peanut (*arachis hypogaea* l.) DNA. *Plant Physiol.* 65:1121-1127, 1980.
35. Dimitriadis, E. K., F. Horkay, J. Maresca, B. Kachar, and R. S. Chadwick. Determination of elastic moduli of thin layers of soft material using the atomic force microscope. *Biophys J.* 82:2798-2810, 2002.
36. Dobereiner, H. G., B. J. Dubin-Thaler, G. Giannone, and M. P. Sheetz. Force sensing and generation in cell phases: Analyses of complex functions. *J Appl Physiol.* 98:1542-1546, 2005.
37. Drury, J. L., and D. J. Mooney. Hydrogels for tissue engineering: Scaffold design variables and applications. *Biomaterials.* 24:4337-4351, 2003.

38. Duconseille, E., S. Woerly, C. Kelche, B. Will, and J. C. Cassel. Polymeric hydrogels placed into a fimbria-fornix lesion cavity promote fiber (re)growth: A morphological study in the rat. *Restor Neurol Neurosci.* 13:193-203, 1998.
39. Engler, A., L. Bacakova, C. Newman, A. Hategan, M. Griffin, and D. Discher. Substrate compliance versus ligand density in cell on gel responses. *Biophys J.* 86:617-628, 2004.
40. Engler, A. J., L. Richert, J. Y. Wong, C. Picart, and D. E. Discher. Surface probe measurements of the elasticity of sectioned tissue, thin gels and polyelectrolyte multilayer films: Correlations between substrate stiffness and cell adhesion. *Surface Science.* 570:142-154, 2004.
41. Fawcett, J. Repair of spinal cord injuries: Where are we, where are we going? *Spinal Cord.* 40:615-623, 2002.
42. Feldkamp, U., and C. M. Niemeyer. Rational design of DNA nanoarchitectures. *Angew Chem Int Ed Engl.* 45:1856-1876, 2006.
43. Fields, R. D., and B. Stevens-Graham. New insights into neuron-glia communication. *Science.* 298:556-562, 2002.
44. Flanagan, L. A., Y. E. Ju, B. Marg, M. Osterfield, and P. A. Janmey. Neurite branching on deformable substrates. *Neuroreport.* 13:2411-2415, 2002.
45. Flynn, L., P. D. Dalton, and M. S. Shoichet. Fiber templating of poly(2-hydroxyethyl methacrylate) for neural tissue engineering. *Biomaterials.* 24:4265-4272, 2003.
46. Folch, A., and M. Toner. Microengineering of cellular interactions. *Annu Rev Biomed Eng.* 2:227-256, 2000.
47. Friedman, J. A., A. J. Windebank, M. J. Moore, R. J. Spinner, B. L. Currier, and M. J. Yaszemski. Biodegradable polymer grafts for surgical repair of the injured spinal cord. *Neurosurgery.* 51:742-751; discussion 751-742, 2002.
48. Fu, E. S., and R. P. Tummala. Neuroprotection in brain and spinal cord trauma. *Curr Opin Anaesthesiol.* 18:181-187, 2005.
49. Gabbiani, G. The myofibroblast in wound healing and fibrocontractive diseases. *J Pathol.* 200:500-503, 2003.
50. Geiger, B. Cell biology. Encounters in space. *Science.* 294:1661-1663, 2001.
51. Geller, H. M., and J. W. Fawcett. Building a bridge: Engineering spinal cord repair. *Exp Neurol.* 174:125-136, 2002.
52. Georges, P. C., W. J. Miller, D. F. Meaney, E. S. Sawyer, and P. A. Janmey. Matrices with compliance comparable to that of brain tissue select neuronal over glial growth in mixed cortical cultures. *Biophys J.* 90:3012-3018, 2006.
53. Grenier, G., M. Remy-Zolghadri, D. Larouche, R. Gauvin, K. Baker, F. Bergeron, D. Dupuis, E. Langelier, D. Rancourt, F. A. Auger, and L. Germain. Tissue reorganization in response to mechanical load increases functionality. *Tissue Eng.* 11:90-100, 2005.
54. Guidry, C., and F. Grinnell. Heparin modulates the organization of hydrated collagen gels and inhibits gel contraction by fibroblasts. *J Cell Biol.* 104:1097-1103, 1987.
55. Haniffa, M. A., M. P. Collin, C. D. Buckley, and F. Dazzi. Mesenchymal stem cells: The fibroblasts' new clothes? *Haematologica.* 2008.

56. Harris, A. K., P. Wild, and D. Stopak. Silicone rubber substrata: A new wrinkle in the study of cell locomotion. *Science*. 208:177-179, 1980.
57. Hoffman, A. S. Hydrogels for biomedical applications. *Adv Drug Deliv Rev*. 54:3-12, 2002.
58. Horkay, F., and G. McKenna. Polymer networks and gels. In: J. E. Mark, editor. *Physical properties of polymers handbook* (hardcover), Springer, 2006.
59. Ingber, D. E. Mechanical signaling and the cellular response to extracellular matrix in angiogenesis and cardiovascular physiology. *Circ Res*. 91:877-887, 2002.
60. Ingber, D. E. Mechanosensation through integrins: Cells act locally but think globally. *Proc Natl Acad Sci U S A*. 100:1472-1474, 2003.
61. Jiang, X., P. C. Georges, B. Li, Y. Du, M. K. Kutzinger, M. L. Previtera, N. A. Langrana, and B. L. Firestein. Cell growth in response to mechanical stiffness is affected by neuron-astroglia interactions. *Open Neuroscience Journal*. 1:7-14, 2007.
62. Jiang, X., B. Yurke, B. L. Firestein, and N. A. Langrana. Neurite outgrowth on a DNA crosslinked hydrogel with tunable stiffnesses. *Ann Biomed Eng*. (Accepted for publication):2008.
63. Johnson, B., J. M. Bauer, D. J. Niedermaier, W. C. Crone, and D. J. Beebe. Experimental techniques for mechanical characterization of hydrogels at the microscale *Experimental Mechanics*. 44:21-28, 2003.
64. Kerschensteiner, M., C. Stadelmann, G. Dechant, H. Wekerle, and R. Hohlfeld. Neurotrophic cross-talk between the nervous and immune systems: Implications for neurological diseases. *Ann Neurol*. 53:292-304, 2003.
65. Khatiwala, C. B., S. R. Peyton, and A. J. Putnam. Intrinsic mechanical properties of the extracellular matrix affect the behavior of pre-osteoblastic mc3t3-e1 cells. *Am J Physiol Cell Physiol*. 290:C1640-1650, 2006.
66. Kopecek, J. Polymer chemistry: Swell gels. *Nature*. 417:388-389, 391, 2002.
67. Kwon, B. K., and W. Tetzlaff. Spinal cord regeneration: From gene to transplants. *Spine*. 26:S13-22, 2001.
68. Kwon, B. K., Dvorak, M. F., Fisher, C. G., Tetzlaff, W. Spinal cord injury regenerative strategies and obstacles. *Curr. Opin. Orthop*. 15:196-201, 2004.
69. Lamoureux, P., G. Ruthel, R. E. Buxbaum, and S. R. Heidemann. Mechanical tension can specify axonal fate in hippocampal neurons. *J Cell Biol*. 159:499-508, 2002.
70. Lee, J., M. Leonard, T. Oliver, A. Ishihara, and K. Jacobson. Traction forces generated by locomoting keratocytes. *J Cell Biol*. 127:1957-1964, 1994.
71. Lesny, P., J. De Croos, M. Pradny, J. Vacik, J. Michalek, S. Woerly, and E. Sykova. Polymer hydrogels usable for nervous tissue repair. *J Chem Neuroanat*. 23:243-247, 2002.
72. Levitan, I. B., and L. K. Kaczmarek. *The neuron: Cell and molecular biology* Oxford University Press: New York, 1997.
73. Li, L., N. Sharma, U. Chippada, X. Jiang, R. Schloss, M. L. Yarmush, and N. A. Langrana. Functional modulation of es-derived hepatocyte lineage cells via substrate compliance alteration. *Ann Biomed Eng*. 36:865-876, 2008.

74. Li, Y., J. White, D. Stokes, G. Sayler, and M. Sepaniak. Capillary electrophoresis as a method to study DNA reassociation. *Biotechnol Prog.* 17:348-354, 2001.
75. Lichter, J. A., M. T. Thompson, M. Delgadillo, T. Nishikawa, M. F. Rubner, and K. J. Van Vliet. Substrata mechanical stiffness can regulate adhesion of viable bacteria. *Biomacromolecules.* 9:1571-1578, 2008.
76. Liedl, T., H. Dietz, and B. Yurke. Controlled trapping and release of quantum dots in a DNA-linked hydrogel. *SMALL.* 3:1688, 2007.
77. Lin, D., N. Langrana, and B. Yurke. Inducing reversible stiffness changes in DNA-crosslinked gels. *Journal of Materials Research.* 20:1456-1464, 2006.
78. Lin, D. C., B. Yurke, and N. A. Langrana. Mechanical properties of a reversible, DNA-crosslinked polyacrylamide hydrogel. *J Biomech Eng.* 126:104-110, 2004.
79. Lin, D. C. (2005). Design and properties of a new dna-crosslinked polymer hydrogel, Mechanical and Aerospace Engineering Piscataway, NJ: Rutgers University.
80. Lin, D. C., and F. Horkay. Nanomechanics of polymer gels and biological tissues: A critical review of analytical approaches in the hertzian regime and beyond. *Soft Matter.* 4:669-682, 2008.
81. Lo, C. M., H. B. Wang, M. Dembo, and Y. L. Wang. Cell movement is guided by the rigidity of the substrate. *Biophys J.* 79:144-152, 2000.
82. Lodish, H., A. Berk, P. Matsudaira, C. A. Kaiser, M. Krieger, M. P. Scott, S. L. Zipursky, and J. Darnell. *Molecular cell biology*, , W.H. Freeman and Company: New York, 2004.
83. Lodish, H., A. Berk, P. Matsudaira, C. A. Kaiser, M. Krieger, M. P. Scott, S. L. Zipursky, and J. Darnell. *Molecular cell biology*, W.H. Freeman and Company: New York, 2004.
84. Luba, V. In search of the lost cord: Solving the mystery of spinal cord regeneration, Joseph Henry Press: Washington, D.C, 2001.
85. Mironov, V., R. P. Visconti, and R. R. Markwald. What is regenerative medicine? Emergence of applied stem cell and developmental biology. *Expert Opin Biol Ther.* 4:773-781, 2004.
86. Munoz, V., K. Campbell, and J. Shibayama. Fibroblasts: Modulating the rhythm of the heart. *J Physiol.* 586:2423-2424, 2008.
87. Murakami, Y., and M. Maeda. DNA-responsive hydrogels that can shrink or swell. *Biomacromolecules.* 6:2927-2929, 2005.
88. Nagahara, S., and T. Matsuda. Hydrogel formation via hybridization of oligonucleotides derivatized in water-soluble vinyl polymersd in water-soluble vinyl polymers. *Polymer Gels Networks.* 4:111-127, 1996.
89. Nedelec, B., A. Ghahary, P. G. Scott, and E. E. Tredget. Control of wound contraction. Basic and clinical features. *Hand Clin.* 16:289-302, 2000.
90. Neher, R. A., and U. Gerland. DNA as a programmable viscoelastic nanoelement. *Biophys J.* 89:3846-3855, 2005.
91. Nisbet, D. R., K. E. Crompton, M. K. Horne, D. I. Finkelstein, and J. S. Forsythe. Neural tissue engineering of the cns using hydrogels. *J Biomed Mater Res B Appl Biomater.* 87:251-263, 2008.

92. Nolte, S. V., W. Xu, H. O. Rennekampff, and H. P. Rodemann. Diversity of fibroblasts--a review on implications for skin tissue engineering. *Cells Tissues Organs*. 187:165-176, 2008.
93. Novikova, L. N., L. N. Novikov, and J. O. Kellerth. Biopolymers and biodegradable smart implants for tissue regeneration after spinal cord injury. *Curr Opin Neurol*. 16:711-715, 2003.
94. Opdahl AK, T. S., E. Amitay-Sadovsky, J. Kim, and G. A. Somorjai. Topical review: Characterization of polymer surface structure and surface mechanical behaviour by sum frequency generation surface vibrational spectroscopy and atomic force microscopy. *Journal of Physics: Condensed Matter*. 16:R659-R677, 2004.
95. Patel, S., R. G. Thakar, J. Wong, S. D. McLeod, and S. Li. Control of cell adhesion on poly(methyl methacrylate). *Biomaterials*. 27:2890-2897, 2006.
96. Pedersen, J. A., and M. A. Swartz. Mechanobiology in the third dimension. *Ann Biomed Eng*. 33:1469-1490, 2005.
97. Pelham, R. J., and Y.-L. Wang. Cell locomotion and focal adhesions are regulated by substrate flexibility. *Proc. Natl. Acad. Sci USA*. 94:13661-13665, 1997.
98. Pelham, R. J., Jr., and Y. Wang. Cell locomotion and focal adhesions are regulated by substrate flexibility. *Proc Natl Acad Sci U S A*. 94:13661-13665, 1997.
99. Peyton, S. R., and A. J. Putnam. Extracellular matrix rigidity governs smooth muscle cell motility in a biphasic fashion. *J Cell Physiol*. 204:198-209, 2005.
100. Prajapati, R. T., B. Chavally-Mis, D. Herbage, M. Eastwood, and R. A. Brown. Mechanical loading regulates protease production by fibroblasts in three-dimensional collagen substrates. *Wound Repair Regen*. 8:226-237, 2000.
101. Ramer, L. M., M. S. Ramer, and J. D. Steeves. Setting the stage for functional repair of spinal cord injuries: A cast of thousands. *Spinal Cord*. 43:134-161, 2005.
102. Ratner, B. D., and S. J. Bryant. Biomaterials: Where we have been and where we are going. *Annu Rev Biomed Eng*. 6:41-75, 2004.
103. Reynaldo, L. P., A. V. Vologodskii, B. P. Neri, and V. I. Lyamichev. The kinetics of oligonucleotide replacements. *J Mol Biol*. 297:511-520, 2000.
104. Roberts, M. C., M. C. Hanson, A. P. M. , E. A. Karren, and P. F. Kiser. Dynamically restructuring hydrogel networks formed with reversible covalent crosslinks. *Advanced Materials*. 19:2503-2507, 2007.
105. Rosner, B. I., T. Hang, and R. T. Tranquillo. Schwann cell behavior in three-dimensional collagen gels: Evidence for differential mechano-transduction and the influence of tgfbeta 1 in morphological polarization and differentiation. *Exp Neurol*. 195:81-91, 2005.
106. Roy, P., Z. Rajfur, P. Pomorski, and K. Jacobson. Microscope-based techniques to study cell adhesion and migration. *Nat Cell Biol*. 4:E91-96, 2002.
107. Schmidt, C. E., and J. B. Leach. Neural tissue engineering: Strategies for repair and regeneration. *Annu Rev Biomed Eng*. 5:293-347, 2003.
108. Schwarz, U. S., N. Q. Balaban, D. Riveline, L. Addadi, A. Bershadsky, S. A. Safran, and B. Geiger. Measurement of cellular forces at focal adhesions using elastic micro-patterned substrates. *Materials Science & Engineering C-Biomimetic and Supramolecular Systems*. 23:387-394, 2003.

109. Seeman, N. C. From genes to machines: DNA nanomechanical devices. *Trends Biochem Sci.* 30:119-125, 2005.
110. Shreiber, D. I., V. H. Barocas, and R. T. Tranquillo. Temporal variations in cell migration and traction during fibroblast-mediated gel compaction. *Biophys J.* 84:4102-4114, 2003.
111. Smith, D. H., J. A. Wolf, and D. F. Meaney. A new strategy to produce sustained growth of central nervous system axons: Continuous mechanical tension. *Tissue Eng.* 7:131-139, 2001.
112. Smith, M. J., R. J. Britten, and E. H. Davidson. Studies on nucleic acid reassociation kinetics: Reactivity of single-stranded tails in DNA-DNA renaturation. *Proc Natl Acad Sci U S A.* 72:4805-4809, 1975.
113. St'astny, M., D. Plocova, T. Etrych, M. Kovar, K. Ulbrich, and B. Rihova. Hpma-hydrogels containing cytostatic drugs. Kinetics of the drug release and in vivo efficacy. *J Control Release.* 81:101-111, 2002.
114. Stocum, D. L. Regenerative biology and medicine. *J Musculoskelet Neuronal Interact.* 2:270-273, 2002.
115. Stocum, D. L. Tissue restoration through regenerative biology and medicine. *Adv Anat Embryol Cell Biol.* 176:III-VIII, 1-101, back cover, 2004.
116. Swartz, M. A., D. J. Tschumperlin, R. D. Kamm, and J. M. Drazen. Mechanical stress is communicated between different cell types to elicit matrix remodeling. *Proc Natl Acad Sci U S A.* 98:6180-6185, 2001.
117. Tomasek, J. J., G. Gabbiani, B. Hinz, C. Chaponnier, and R. A. Brown. Myofibroblasts and mechano-regulation of connective tissue remodelling. *Nat Rev Mol Cell Biol.* 3:349-363, 2002.
118. Um, S. H., J. B. Lee, N. Park, S. Y. Kwon, C. C. Umbach, and D. Luo. Enzyme-catalysed assembly of DNA hydrogel. *Nat Mater.* 5:797-801, 2006.
119. Valignat, M. P., O. Theodoly, J. C. Crocker, W. B. Russel, and P. M. Chaikin. Reversible self-assembly and directed assembly of DNA-linked micrometer-sized colloids. *Proc Natl Acad Sci U S A.* 102:4225-4229, 2005.
120. Vanni, S., B. C. Lagerholm, C. A. Otey, D. Velegol, D. L. Taylor, and F. Lanni. Fibroblast mechanics in a model extracellular matrix—an application of optical sectional microscopy. *Euro. Cells Materials.* 2:21-22, 2001.
121. Vats, A., N. S. Tolley, J. M. Polak, and J. E. Gough. Scaffolds and biomaterials for tissue engineering: A review of clinical applications. *Clin Otolaryngol Allied Sci.* 28:165-172, 2003.
122. Vogel, V., and M. Sheetz. Local force and geometry sensing regulate cell functions. *Nat Rev Mol Cell Biol.* 7:265-275, 2006.
123. Wang, H. B., M. Dembo, and Y. L. Wang. Substrate flexibility regulates growth and apoptosis of normal but not transformed cells. *Am J Physiol Cell Physiol.* 279:C1345-1350, 2000.
124. Wang, J., H. Chen, A. Seth, and C. A. McCulloch. Mechanical force regulation of myofibroblast differentiation in cardiac fibroblasts. *Am J Physiol Heart Circ Physiol.* 285:H1871-1881, 2003.
125. Wang, Y. L., and R. J. Pelham, Jr. Preparation of a flexible, porous polyacrylamide substrate for mechanical studies of cultured cells. *Methods Enzymol.* 298:489-496, 1998.

126. Watson, J. D., T. A. Baker, S. P. Bell, A. L. Gann, Michael (Author), , and R. Losick. *Molecular biology of the gene*, Benjamin Cummings, 2003.
127. Weaver, V. M., O. W. Petersen, F. Wang, C. A. Larabell, P. Briand, C. Damsky, and M. J. Bissell. Reversion of the malignant phenotype of human breast cells in three-dimensional culture and in vivo by integrin blocking antibodies. *J Cell Biol.* 137:231-245, 1997.
128. Wei, B., I. Cheng, K. Q. Luo, and Y. Mi. Capture and release of protein by a reversible DNA-induced sol-gel transition system. *Angew Chem Int Ed Engl.* 47:331-333, 2008.
129. Wong, J. Y., A. Velasco, P. Rajagopalan, and Q. Pham. Directed movement of vascular smooth muscle cells on gradient-compliant hydrogels. *Langmuir.* 19:1908-1913, 2003.
130. Wong, T., J. A. McGrath, and H. Navsaria. The role of fibroblasts in tissue engineering and regeneration. *Br J Dermatol.* 156:1149-1155, 2007.
131. Wrobel, L. K., T. R. Fray, J. E. Molloy, J. J. Adams, M. P. Armitage, and J. C. Sparrow. Contractility of single human dermal myofibroblasts and fibroblasts. *Cell Motil Cytoskeleton.* 52:82-90, 2002.
132. Yeung, T., P. C. Georges, L. A. Flanagan, B. Marg, M. Ortiz, M. Funaki, N. Zahir, W. Ming, V. Weaver, and P. A. Janmey. Effects of substrate stiffness on cell morphology, cytoskeletal structure, and adhesion. *Cell Motil Cytoskeleton.* 60:24-34, 2005.
133. Yu, T. T., and M. S. Shoichet. Guided cell adhesion and outgrowth in peptide-modified channels for neural tissue engineering. *Biomaterials.* 26:1507-1514, 2005.
134. Yurke, B., A. J. Turberfield, A. P. Mills, Jr., F. C. Simmel, and J. L. Neumann. A DNA-fuelled molecular machine made of DNA. *Nature.* 406:605-608, 2000.
135. Yurke, B., and A. P. J. Mills. Using DNA to power nanostructures *Genetic Programming and Evolvable Machines.* 4:111-122, 2003.
136. Zheng, J., P. Lamoureux, V. Santiago, T. Dennerll, R. E. Buxbaum, and S. R. Heidemann. Tensile regulation of axonal elongation and initiation. *J Neurosci.* 11:1117-1125, 1991.

CHAPTER 3 GELS WITH STATIC STIFFNESS

CHAPTER 3A EFFECT OF NEURON-ASTROGLIA INTERACTIONS

3A.1 Background

Recent studies have suggested that cells can integrate and respond to biological and chemical information as well as the physical properties of their extracellular matrix (ECM)^{23, 26, 53}. This integration contributes to the inherent complexity of cellular-ECM interactions. Among the physical stimuli, traction force, mechanical strain, surface topography, and particularly substrate stiffness have been identified and found to affect cellular behavior in a cell-type specific manner^{9, 14, 20, 24, 28, 29, 44}. Researchers have subjected cultured cells to various substrates composed of natural and synthetic hydrogels such as collagen⁵⁰ and pHEMA(poly-hydroxy-ethyl methacrylate)³, which mimic intrinsic ECM properties and better represent cells' natural fluidic environment than the non-physiological *in vitro* culture plate systems do.

3A.1.1 Bis-crosslinked polyacrylamide gel culture system

Wang and co-workers popularized bis-acrylamide crosslinked hydrogels ('bis-gels', hereafter) as substrates to study cell-substrate interaction⁵⁶. This model system and their protocol has been utilized for a variety of cell types, including rat kidney epithelial cells⁴⁵, 3T3 fibroblasts⁴⁵, non-neuronal PNS (peripheral nervous system) cells⁵⁰, and recently, mouse spinal cord²⁰ and rat cortical neurons²⁴. Table 3A-1 shows a partial list of previous studies that have utilized this gel system. The cells were subjected to mechanical cues alone or stimuli with a coupling of mechanical and biological cues¹⁷.

Cellular properties, including differentiation, proliferation, adhesion, spreading, and motility, have been investigated^{45, 46, 48, 51, 61}.

There is also a growing interest in extending this gel system to additional systems such as agarose⁴ and collagen⁵⁰ gels, for the study of neurons in an attempt to provide information for the mechanical design of bio-scaffolds for tissue engineering applications. Currently, there are few studies on neuronal cell types, and fewer on cells of the central nervous system. Flanagan and colleagues²⁰ investigated the response of neurons to gels with two different mechanical stiffnesses and found that mouse spinal cord neurons have more dendritic branches on softer gels ($E \sim 150$ Pa) than on stiffer gels ($E \sim 1500$ Pa). Furthermore, they did not observe glial cells on these gels. Recently, Flanagan's study was extended to rat cortical neurons²⁴, showing that astrocytes spread less and had poor adhesion on softer gels with a shear modulus of 200 Pa ($E \sim 600$ Pa), while neurite elongation and attachment of neurons co-cultured with glia were not dramatically different from those on stiffer gels ($E \sim 27$ kPa).

Table 3A-1 Partial list of the previous mechano-biology studies using bis-crosslinked PAM gels.

(↓ significant decrease, ↑ significant increase, when the stiffness becomes higher);
VSMC: Vascular smooth muscle cell.

Gel stiffness (Pa)		Cell Type	Major Observations
Low	High		
20,000	80,000	Rat kidney epithelial/3T3	Cell spreading ↓ and migration rate ↑ on softer gels ^{45, 55}
5,000	35,000	Bovine VSMC	Directional migration from soft to stiff area ⁵⁸
2,000	10,000	Hepatocyte	Cell compaction ↓ on soft gels; Liver-specific albumin secretion ↓ on soft gels; Less spreading on soft gels ⁵¹
150	1650	Mouse spinal cord	No glia grew on any of the gels; Neuron branch points ↑ on soft gels ²⁰
600	27,000	Cortical cells	Astrocyte spreading ↓ organized F-actin ↓ on soft gels; Neurons extended long neurites and polymerize actin filaments on both soft and stiff gels ²⁴
21	60, 000	PC-12 neuronal like	Threshold responses ³²

Note: Shear modulus has been converted to Young's modulus by assuming Poisson's ratio of 0.5, purely elasticity and isotropy.

3A.1.2 Neuron-astroglia interactions

It is not yet clear whether and how astroglia and neurons affect each other's growth on biomaterials of different stiffnesses. The question remains open for previous studies using neural cells as to what extent their respective responses can be attributed solely to their own mechano-sensing mechanism. The answers to this question are especially relevant in the applications where a differential effect of mechanical cues on cellular properties of neurons and astroglia is desired. For instance, scaffolds that supply mechanical cues inhibiting astroglia growth while promoting neurite regeneration could be used to cope with the scar formation following spinal cord injuries

Considerable effort has been directed towards delineating neuronal-glial interactions²². It has been demonstrated that cellular crosstalk plays a critical role in development, plasticity, response to injury, and normal and disease states, both in general⁵ and in specific processes such as neuronal cell migration^{15, 36}, synaptogenesis and synaptic plasticity^{2, 57}, and growth cone pathfinding⁷. However, the role of neuron-astroglia interactions in the mechano-sensing by neurons and glia has not yet been studied.

3A.1.3 Mechanical stiffness range under study

The majority of previous studies have been performed on bio-gel stiffness lower than 80 kPa (Table 3A-1). Mechanical testing results for various CNS (central nervous system) tissues of a number of different species provide the incentive for performing studies on stiffer gels. These studies have shown a relatively broad range of stiffnesses from a few Pa to hundreds of kPa or higher and different moduli for the same tissue type from the

same species^{3, 19, 20, 47} (Table 3A-2). In addition, many polymers, such as pHEMA and PLGA (poly-lactic-co-glycolic acid), used as implant materials in CNS tissue repair, have mechanical stiffnesses in the 100 kPa to MPa range^{10, 54}. Also, although close resemblance to the natural cell environment (e.g., fluidic and soft ECM) in designing biomaterials is of great significance, it is not without benefits to examine other possibilities (e.g., high stiffness), considering better neuronal growth on plastic culture plates that have a stiffness of GPa magnitude. Consequently, from an engineering perspective, it is important to examine cell behavior on these higher stiffnesses.

Thus, the objective of the research presented in this chapter was to investigate spinal cord cell adhesion and morphology on bis-gels whose stiffnesses span a large range, varying from ~300 Pa (soft gel) to ~230 kPa (hard gel). In this research, the number and morphological properties of spinal cord neurons and astroglia in mixed and pure cultures were evaluated and contrasted. The results of this study will aid in our understanding of the effects of neuron-astroglia interactions on each cell type's response to mechanical stiffness and guide us in devising a biomaterial that will achieve desired outcome of both neuronal and astroglial growth as well as neurite outgrowth.

Table 3A-2 Partial list of the stiffness of CNS tissues of different species.
(SC = spinal cord; BR = brain)

Specie	Tissue	Stiffness	Techniques	Ref
Rat	SC	0.1MPa~MPa (0.08MPa/0.12=0.67MPa) (1.88MPa)	Uniaxial tensile tests (at different rate: 0.002 to 0.2 s ⁻¹)	19
Rat	BR	330Pa (shear modulus)	Rheology	24
Cat	SC	0.2~0.3MPa	Uniaxial tensile tests	6
Cattle	SC	0.6 or 0.365MPa (gray matter) 0.277 or 0.154MPa (white matter)	Uniaxial tensile tests (at rate of 0.5 to 0.005 mm/second	27
Cattle	SC	50Pa (shear modulus)	Shear tests	20
Rabbit	SC	N/A	Compression (circular and dynamic manner)	38
Rabbit	SC	3.4 kPa (for both gray and white matter)	Aspiration using glass pipette	42
Rabbit	SC	2.3MPa (for pia mater) w/ pia mater: 16kPa w/o pia mater: 5kPa	Uniaxial tensile tests	43
Pig	BR	200Pa (shear modulus) Ogden coefficient	Shear/ compression tests	47
Human	BR	275Pa (shear modulus)	MRI	62
Human	SC	N/A		
Human	BR dura mater	2.75MPa	Tensile test; tearing strength tests	60

3A.2 MATERIALS AND METHODS

3A.2.1 Mechanical characterization of bis-gels

Bis-gels with monomer concentrations of 3% and 5% and fixed acrylamide/bis-acrylamide ratio (29:1) were prepared in micro-centrifuge tubes with initiator and catalyst (0.1% ammonium persulfate and 0.1% TEMED). A steel bead (0.79 mm in diameter; Small Parts, Miami Lakes, FL) was embedded in the gel during polymerization, and a customized fixture was utilized to measure the mechanical properties of the gels (Fig. 3A-1)³³. The measurements were performed at room temperature (RT).

The bulk elasticity modulus of the hydrogel is a function of the monomer concentration and crosslinker density³³⁻³⁵. A calibrated magnetic force was applied to the bead and the displacement was measured with a video microscope. The experimental method is non-intrusive and was used to monitor gel compliance changes. Classical linear elasticity theory was used to model the test conditions as a problem of a rigid spherical inclusion in an isotropic, elastic medium. Under the influence of an externally applied known magnetic load F , the sphere is displaced by a distance δ , which depends on the elastic modulus, Poisson's ratio, and the boundary conditions. Assuming gels are incompressible as they essentially are, the modulus computed, E_a , was expressed in the form:

$$E_a = \frac{\rho}{2\pi R_0} \left(\frac{F}{\delta} \right).$$

where R_0 is the radius of the sphere and ρ is a geometrical factor to account for the effect of finite boundary. In this study, ρ is determined to be 0.967.

Stiffnesses of bis-gels with monomer concentration higher than 10% (including 10%, 15% and 20%) were evaluated by standard tensile tests (sample cross section diameter 15 mm, and length varying from 38.1 to 66.0 mm). Each test has been repeated at least twice.

3A.2.2 Bis-gel preparation

Round glass coverslips (12 mm) were used for gel preparation according to the protocol of Pelham and Wang^{45, 56}. Briefly, the glass surface was activated by treatment with 3-aminopropyltrimethoxysilane and 0.5% glutaraldehyde (Sigma). A series of gels was prepared by pipetting 12 μ l of gel solutions, containing 3-20% acrylamide monomer (acrylamide:bis of 29:1, EMD Chemicals, Gibbstown, NJ), 0.1% ammonium persulfate, and 0.1% TEMED, on the glass coverslip and covering it with another siliconized glass coverslip. After polymerization was completed, the top coverslip was removed, and the gel bound to the bottom coverslip was transferred into a 24-well culture plate. Gels were washed and functionalized with Sulfo-SANPAH (Pierce, Rockford, IL). The gels were then coated with poly-D-lysine (1 mg/ml solution in water). Care has been taken to maintain flatness of the gel surface to minimize the effect of surface topography. The average thickness of the prepared gels is approximately 100 μ m.

3A.2.3 Mixed spinal cord cell culture

Spinal cords were dissected from embryonic day 16 (E16) Sprague Dawley rats (Taconic, Hudson, NY), and cells were dissociated and plated on gels in 24-well plates at a cell density of 25,000 cells/cm². They were also plated to the control wells without gels and

treated with poly-D-lysine. Cells were cultured in serum-containing medium (SCM; MEM containing 10% horse serum, 1% penicillin/streptomycin, 0.6% glucose) at 37 °C for 1 day. At 2 DIV (days *in vitro*) SCM was changed to Neurobasal (NB) medium (Gibco) containing 2% B27 supplement (Gibco), 69 µg/ml L-glutamine, 25 µM beta-mercaptoethanol, and 1% penicillin/streptomycin and grown for 6 days, after which the cells were fixed with 4% paraformaldehyde in PBS.

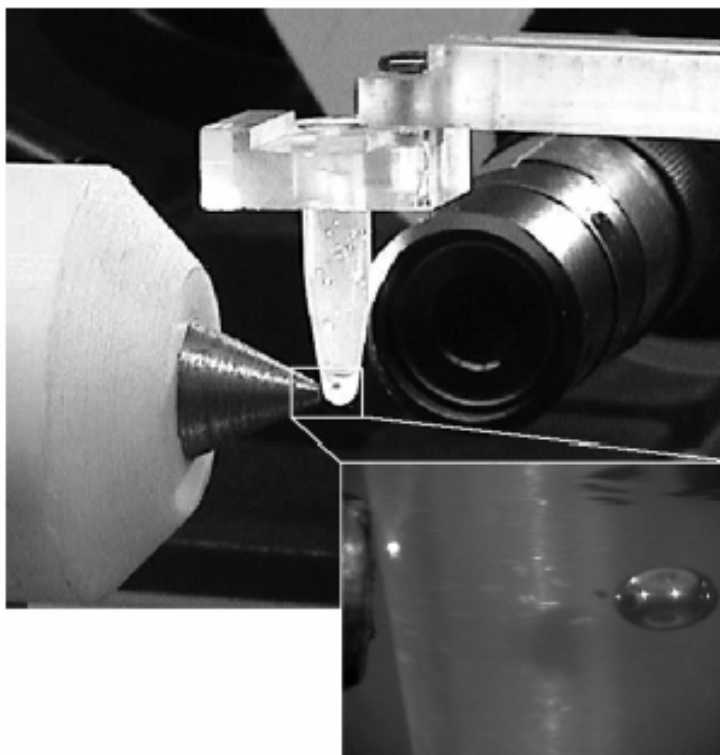


Figure 3A-1 Experimental setup for non-intrusive measurement of mechanical properties of hydrogel materials.

A magnet is used to apply a magnetic force on the steel bead embedded in the gel in a micro-centrifuge tube (shown in insert). Displacement of the bead under applied magnetic fields is measured with video microscopy and the corresponding mechanical stiffness is calculated.

3A.2.4 Pure spinal cord neuron culture

To grow pure spinal neuron cultures, we followed the same steps (including cell seeding) in culturing mixed culture except that, after changing SCM to NB medium and allowing cells to grow for additional 24 hours, cytosine arabinoside (Ara-C, 5 μ M) was added to these cultures to remove proliferating cells by inhibiting DNA synthesis. The cell culture was then maintained for 3 days after which the Ara-C-containing media was changed to fresh NB media without Ara-C. The neurons were grown for another 3 days and were fixed with 4% paraformaldehyde in PBS.

3A.2.5 Pure astroglial culture

Spinal cord astroglial cultures were derived from postnatal day 1 (P1) rats using a modified approach from McCarthy and de Vellis³⁹. Spinal cords were dissected and dissociated with trituration. Cells were plated in tissue culture flasks at density of 1000 cells/mm². Cultures were grown in NM-15 medium (84.4% MEM, 15% Fetal Bovine Serum, 0.6% glucose, supplemented with penicillin/streptomycin) for 9 days. The medium was changed every 3 days. The flasks were then shaken at 400 x rpm for 20 minutes before the medium was changed and the floating cells (mostly microglia) were washed away. The flasks were again shaken overnight at 250 x rpm to remove attached oligodendrocytes and remaining microglia. Following shaking, floating cells were washed away and medium was changed. Ara-C was added to final concentration of 10 μ M to reduce the number of undifferentiated cells. Cultures were grown for 3 additional days before being trypsinized and re-plated on gels in 24-well plates with a cell density of 25,000 cells/cm².

3A.2.6 Immunostaining and cell counting

Cells were blocked with PBS containing 2% normal goat serum, 0.1% Tween, and 0.02% sodium azide for 2 hr, and incubated with primary antibody overnight at 4° C. Primary antibodies were as follows: mouse anti-MAP2 antibody to label neurons (1:500, BD PharMingen, San Diego, CA); rabbit anti-GFAP antibody to label mature astroglia (1:200, Abcam, Cambridge, MA); mouse anti-vimentin antibody to identify immature astroglia (1:500, Chemicon Inc., Temecula, CA). Cells were washed three times with PBS and incubated with secondary antibodies (Cy3-conjugated anti-mouse IgG (1:200); Cy2-conjugated anti-rabbit IgG (1:200), Jackson ImmunoResearch, West Grove, PA) for 1 hr at RT. DAPI nuclear staining was performed to identify all intact cells in the culture. Cells were observed using fluorescence microscopy (Olympus IX50 microscope with a Cooke Sensicam CCD cooled camera fluorescence imaging system and Image Pro software (MediaCybernetics)) and MAP2+, GFAP+, or vimentin+ cells were counted from eight randomly selected areas of each well, aided with the corresponding images of DAPI staining. Each experiment was repeated at least three times, and there were at least three gel samples for each group in every experiment.

The primary and secondary antibodies that were used in this study are summarized in Table 3A-3.

Table 3A-3 Primary and secondary antibodies used in the dissertation research.

(Ms = mouse; Ck = chick; Rb = rabbit)

Antibody	Host	Target	Dilution	Vendor
Anti-MAP2, monoclonal (mouse)	Ms	Neuronal cell body and dendrite	1:1000	BD Pharmingen, San Diego, CA
Anti-MAP2, polyclonal (chicken)	Ck	Neuronal cell body and dendrite	1:5000	Chemicon, Temecula, CA
Anti-GFAP, polyclonal	Ms/Rb	Mature astroglia	1:200	Abcam, Cambridge, MA
Anti-Tau-1, monoclonal	Ms	Axon	1:1000	Chemicon
Anti-Vimentin, monoclonal	Ms	Astrocyte Progenitor	1: 1000	Chemicon
Anti-FAK, monoclonal	Ms	FAK, cell adhesion	1:300	Chemicon
Anti-NCAM, polyclonal	Rb	NCAM, cell adhesion	1: 1000	Chemicon
Anti-CNPase, monoclonal	Ms	Oligodendrocytes	1:2000	Abcam
Anti-Nestin, monoclonal	Ms	Neuroepithelial stem/progenitor cells	1:200	Chemicon
Anti-A2B5, monoclonal	Ms	Stem cell marker, oligodendrocytes precursor cells	1:500	Chemicon

Secondary Antibody	Specificity	Dilution	Vendor
Cy2	Rb/Ms	1: 500	Jackson ImmonoResearch,
Cy3	Ms	1: 200	Jackson ImmonoResearch,
Cy5	Ck	1:300	Jackson ImmonoResearch,

3A.2.7 Assessment of dendrite number and neurite length

Neurons were fixed and immunostained for MAP2 as described above. Primary dendrites were counted as described previously¹. Neurite length was measured by using Scion Image software (Scion Corp., Frederick, MD). Only those neurites with a clear end-point were measured and when the neurite connects two neurons, half of the neurite length was counted for both neurons. Dendrites of those neurons that overlap each other, which prevented origin determination, were not measured. Cell numbers in control and treated groups were compared with one-way analysis of variance (ANOVA) followed by Tukey's tests for multiple comparisons.

3A.3 Results

3A.3.1 Mechanical stiffness of bis-gels

The elastic moduli of bis-gels with different monomer concentrations were either computed based on the formula described in the Materials and Methods section with the experimental measurements of applied magnetic forces and displacements, or measured by standard tensile tests (for gels with stiffness over ~50 kPa). Mechanical stiffnesses of gels with acrylamide concentration ranging from 3 to 20% span three orders of magnitude (Fig. 3A-2). It is noticed that the stiffness increases almost in a linear fashion with monomer concentration higher than 5% (Fig. 3A-2 in linear scale). Note that mechanical stiffness and elastic modulus were used interchangeably in this work. Finally, it has been previously reported²⁰ and confirmed in this study that functionalization and protein conjugation do not significantly alter the mechanical stiffness of the gels.

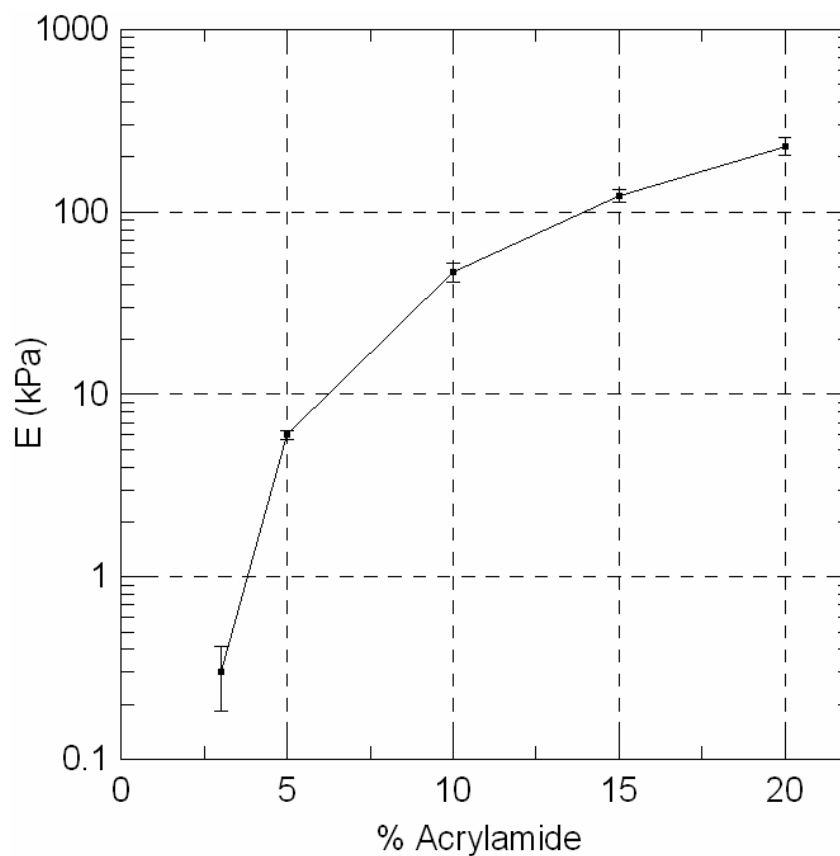


Figure 3A-2 Stiffness of the bis-crosslinked polyacrylamide hydrogel with respect to the monomer concentration at fixed monomer/crosslink ratio of 29:1.

The stiffness increases with acrylamide monomer concentration. Single magnet set-up was used to acquire the first two data points, and Instron testing was used for the last three. Error bars indicate standard error of mean. $n > 3$, i.e., more than 3 samples were used to acquire each single data point.

3A.3.2 Gel functionalization for spinal cord cell attachment

Without functionalization and subsequent protein conjugation, rat spinal cord neurons demonstrated low cell number or survivor rate, and large clumps and aggregations, suggesting that the substrates without functionalization or protein conjugation were less conducive for attachment and neurite elongation (Figure 3A-3).

3A.3.3 Mixed spinal cord cell culture on bis-gels

Typical morphology of neurons, mature (GFAP+) astroglia, and immature (vimentin+) astroglia in their co-culture on gels of three out of five different mechanical stiffnesses is shown in Figure 3A-4. On all stiffnesses tested, rat spinal cord neurons extended processes from cell bodies, exhibiting no distinct difference from their counterparts on culture plates. Mature astroglia (GFAP+) assumed a variety of morphologies: an extended string-shape, a star shape, or a small, round irregular shape, whereas vimentin+ immature astroglia displayed only the round (on softest gels) and polygonal morphologies. We also examined the growth of oligodendrocytes on gels by CNPase staining, and we found no detectable CNPase positive cells.

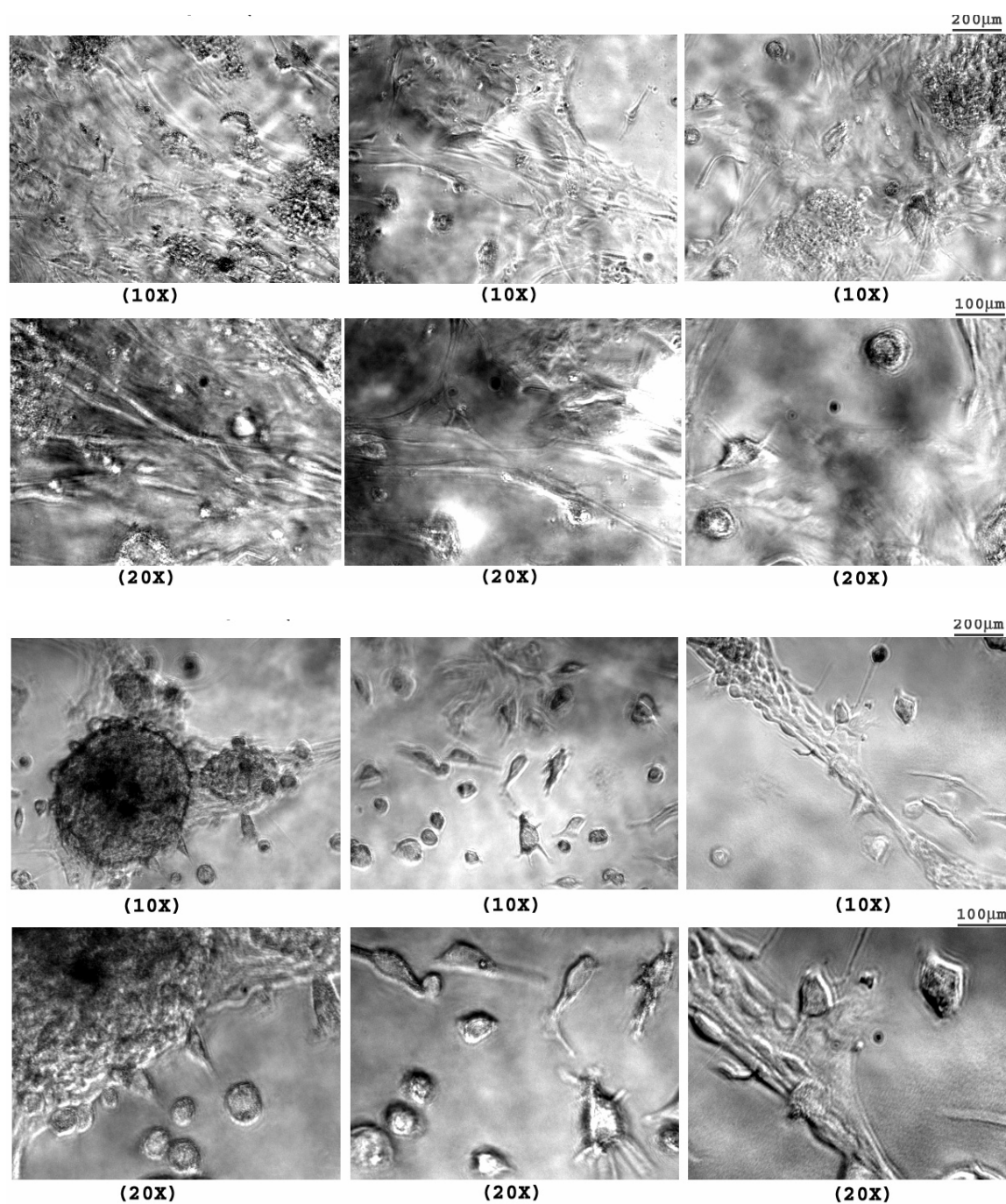


Figure 3A-3 Rat spinal cord neurons grown on functionalized (upper panel) and unfunctionalized (lower panel) bis-crosslinked polyacrylamide gels.

Three different spots were imaged and the lower (10×) and higher (20×) magnification images showed that without functionalization, the survival rate is low and the cell growth is poor.

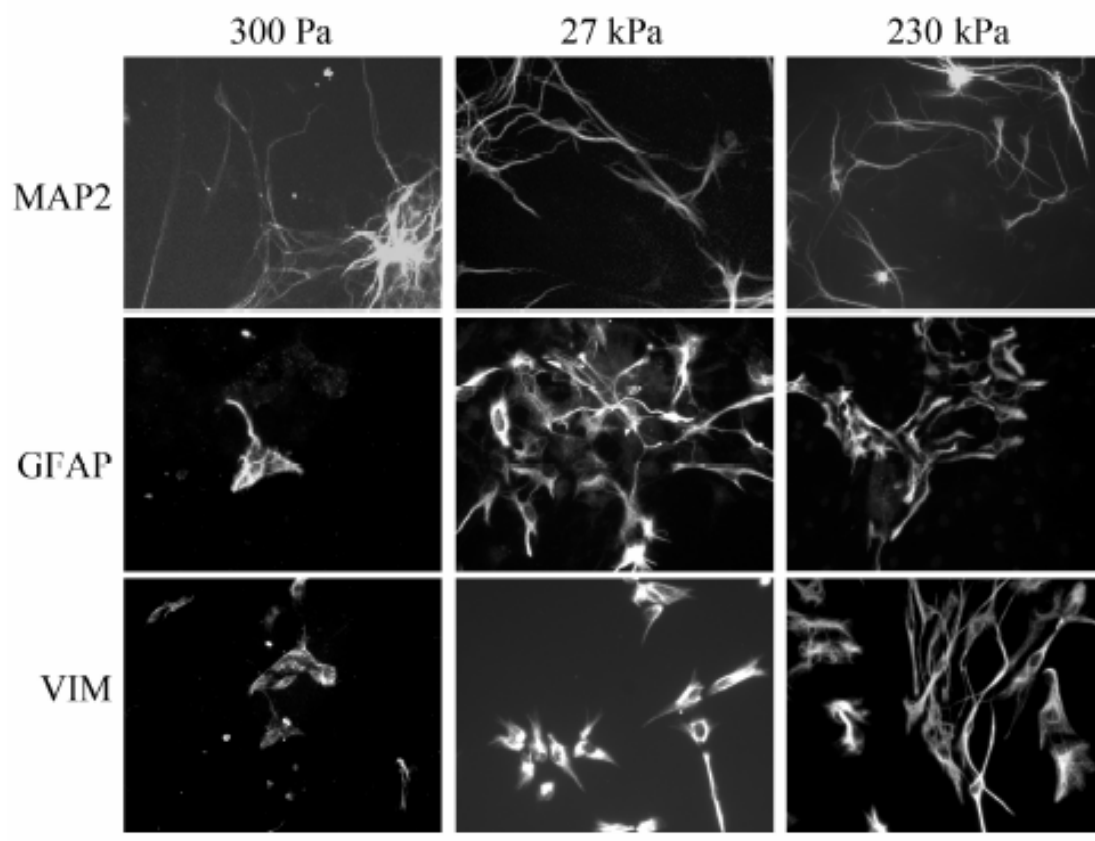


Figure 3A-4 Mixed culture of rat spinal cord cells on bis-crosslinked gels. Upper panel: MAP2 immunocytochemistry shows typical morphology of spinal cord neurons on three of five gels tested (300 Pa, 27 kPa, and 230 kPa). Middle: GFAP immunocytochemistry shows the growth of mature astroglia on bis-crosslinked gels. Lower panel: Vimentin immunocytochemistry shows the growth of immature astroglia. Scale bar: 100 μm .

3A.3.4 Effect of gel stiffness on spinal cord cell in mixed cultures

There is a slight increase in the total cell number determined by nuclear staining when cells were cultured on gels of higher stiffness (Figure 3A-5). Figure 3A-6 summarizes the alterations in number of neurons, mature (GFAP+) and immature (vimentin+) astroglia along with neurite numbers on gels with five different monomer concentrations. According to MAP2 immunostaining used to specifically visualize neurons, we found that neuronal adhesion in mixed cultures does not significantly change as gel stiffness increases (Fig. 3A-6A). The number of neurons on gels ranging in stiffness from 300 Pa to 230 kPa was not significantly different.

Immature astroglial cells (indicated by positive staining for vimentin, but not GFAP) increased in number as gel stiffness increased (Fig. 3A-6B). All stiffnesses greater than 300 Pa had significantly more adherent immature astroglia. On the other hand, the response of mature astroglia (visualized with GFAP immunostaining) to this range of stiffnesses exhibits a somewhat biphasic trend, that is, at different stiffness ranges the trend (decrease or increase) is different. Mature astroglia are least adhesive to softest (300 Pa) gels. There were a significantly higher number of adherent astrocytes on intermediate 27 kPa gels compared to 300 Pa gels. Furthermore, while the average number of cells on 230 kPa gels was lower than intermediate stiffnesses, these differences were not significant (Fig. 3A-6C). These data suggest a possible optimal range of stiffness that best supports mature astroglia adhesion.

In addition to cell counting, we also examined neurite length and numbers in MAP2+ neurons. We found that there was no significant difference in neurite length (Table 3A-4) with an average of approximately 50 μm . Dendrite number, however, was

at a minimum when cells were plated on intermediate stiffnesses in mixed culture (Figure 3A-6D). Neurite numbers were significantly lower on 27 kPa and 47 kPa gels than on 300 Pa gels.

3A.3.5 Effect of gel stiffness on pure spinal cord neuron culture

Based on GFAP and MAP2 immunostaining as well as nuclear staining, we confirmed that 95% of the total cell population is neuronal and that no mature astroglia can be detected in pure neuronal cultures (Fig. 3A-7A).

Typical neuronal morphology can be seen on all gel samples. Unlike their counterparts in the mixed culture (Fig. 3A-6), there are more spinal cord neurons in pure culture as the substrate becomes more rigid (Figure 3A-7B). Moreover, examination of neurite length and number at three unique stiffnesses revealed that neurite number was significantly lower on 47 kPa gels than the other two gel groups tested (Figure 3A-7C). In pure cultures, neurite number was examined on three of the five stiffnesses. Stiffnesses were chosen based on experimental data from mixed cultures, including one stiffness which yielded significantly fewer dendrites (47 kPa) as well as two others with non-significant lower (6 kPa) and higher (230 kPa) dendrite numbers (Figure 3A-7C). Examination of the neurite length revealed no appreciable differences among gels groups (Figure 3A-7D).

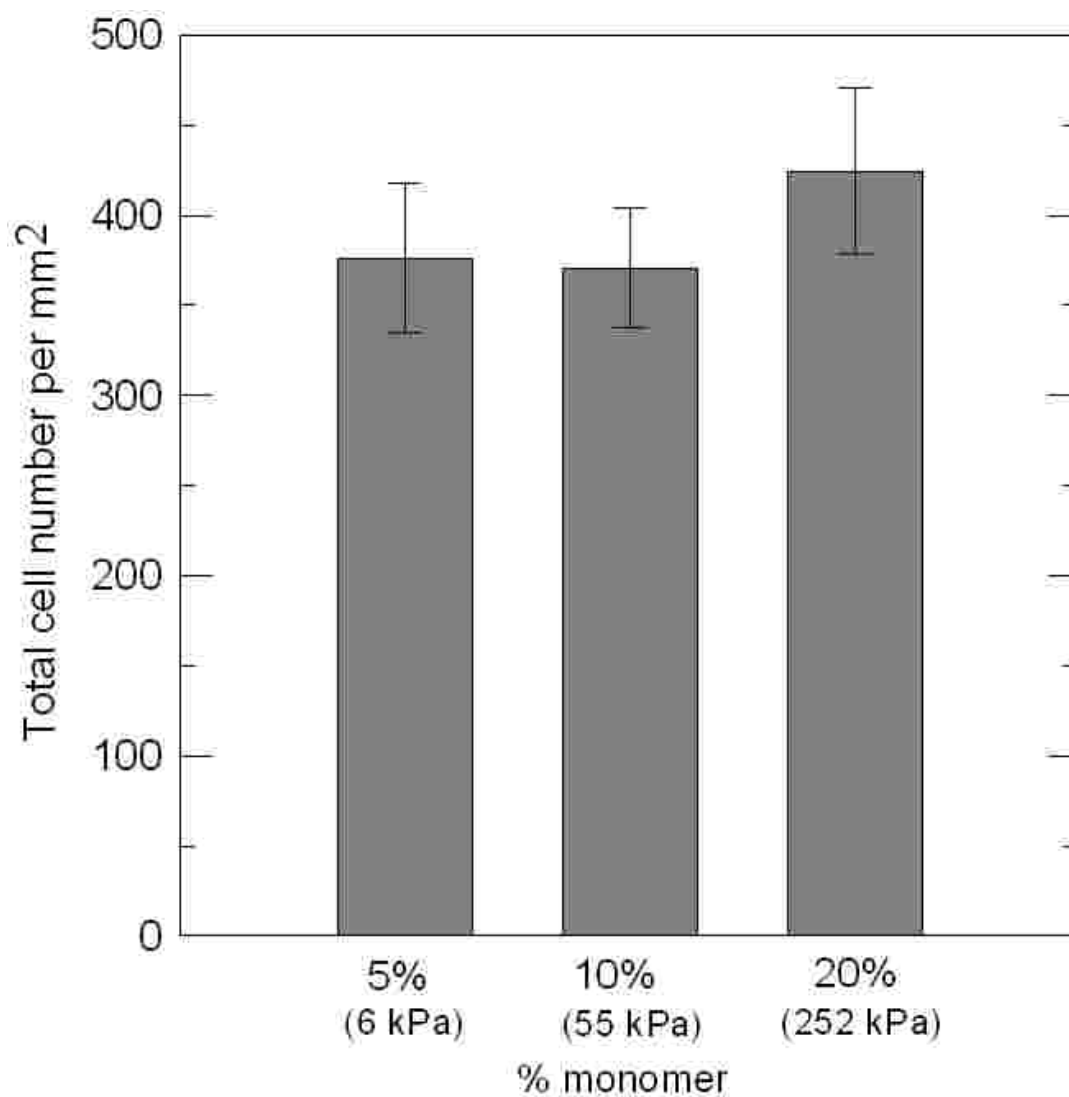


Figure 3A-5 Change of total cell number of rat spinal cord cells on bis-gels with different stiffnesses.
 $n > 33$ (views).

Table 3A-4 Neurite length of spinal cord neurons in mixed cultures on different bis-crosslinked polyacrylamide gels.

There is no significant difference in neurite length between gel groups.

Monomer Concentration	5%	10%	20%
Neurite length (μm)	50.1 ± 2.3	48.6 ± 2.5	50.3 ± 3.0

Note: value in mean \pm SEM.

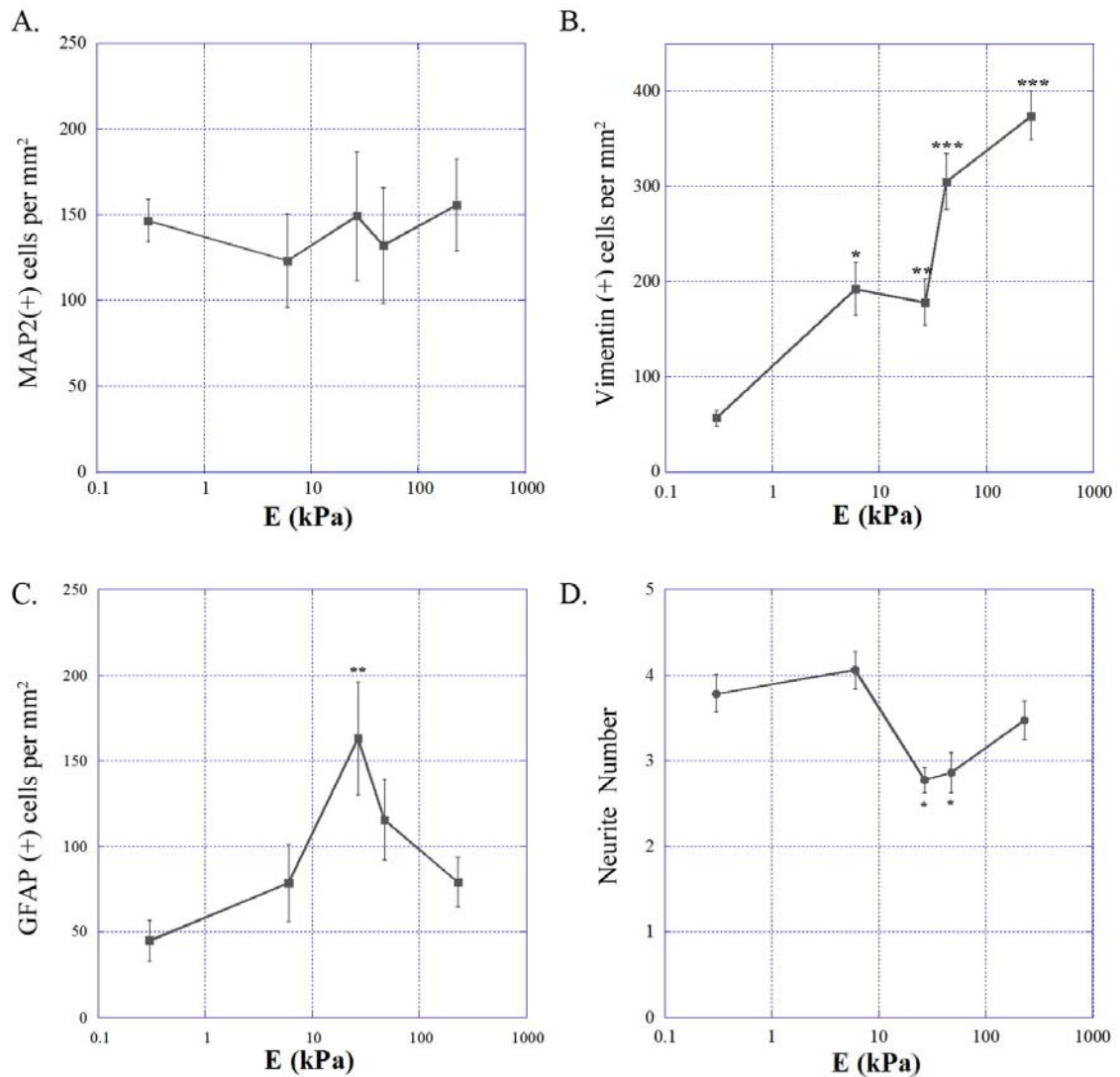


Figure 3A-6 Effects of gel stiffnesses on spinal cord cell growth.

A: Quantification of MAP2+ neurons grown on bis-gels. The results indicate that neuronal cell number does not significantly change with gel stiffness. B: Quantification of vimentin+ cells identifies immature astroglia grown on bis-gels. Immature astroglia adhesion increases with gel stiffness ($p_{6\text{kPa}} = 0.04$, $p_{27\text{kPa}} = 0.02$, $p_{47\text{kPa}} < 0.001$, $p_{230\text{kPa}} < 0.001$). C: Quantification of GFAP+ cells to identify mature astroglia grown on bis-gels. Mature astroglia preferentially adhere to 27 kPa (** $p < 0.01$). D: Neurite number is lowest on 27 ($p < 0.001$) and 47 kPa ($p = 0.04$) gels compared to 300 Pa gels. * $p < 0.05$, ** $p < 0.01$, *** $p < 0.001$ by ANOVA followed by Tukey HSD test for multiple comparisons versus 300 Pa gel.

3A.3.6 Effect of gel stiffness on pure astroglia culture

Representative images of pure astroglia immunostained for either GFAP or vimentin on three of the five stiffnesses tested are shown in Figure 3A-8A. The adhesion of GFAP+ cells in pure astroglial cultures was similar to that in mixed culture (Fig. 3A-8B). Specifically, adhesion was very low on 300 Pa gels and cells preferentially adhered to gels with intermediate stiffness (27 kPa). In contrast to the adhesion trend observed for immature astroglia in mixed cultures (Figure 3A-6B), cell number for vimentin+ immature astroglia in pure culture was not significantly affected (Fig. 3A-8C).

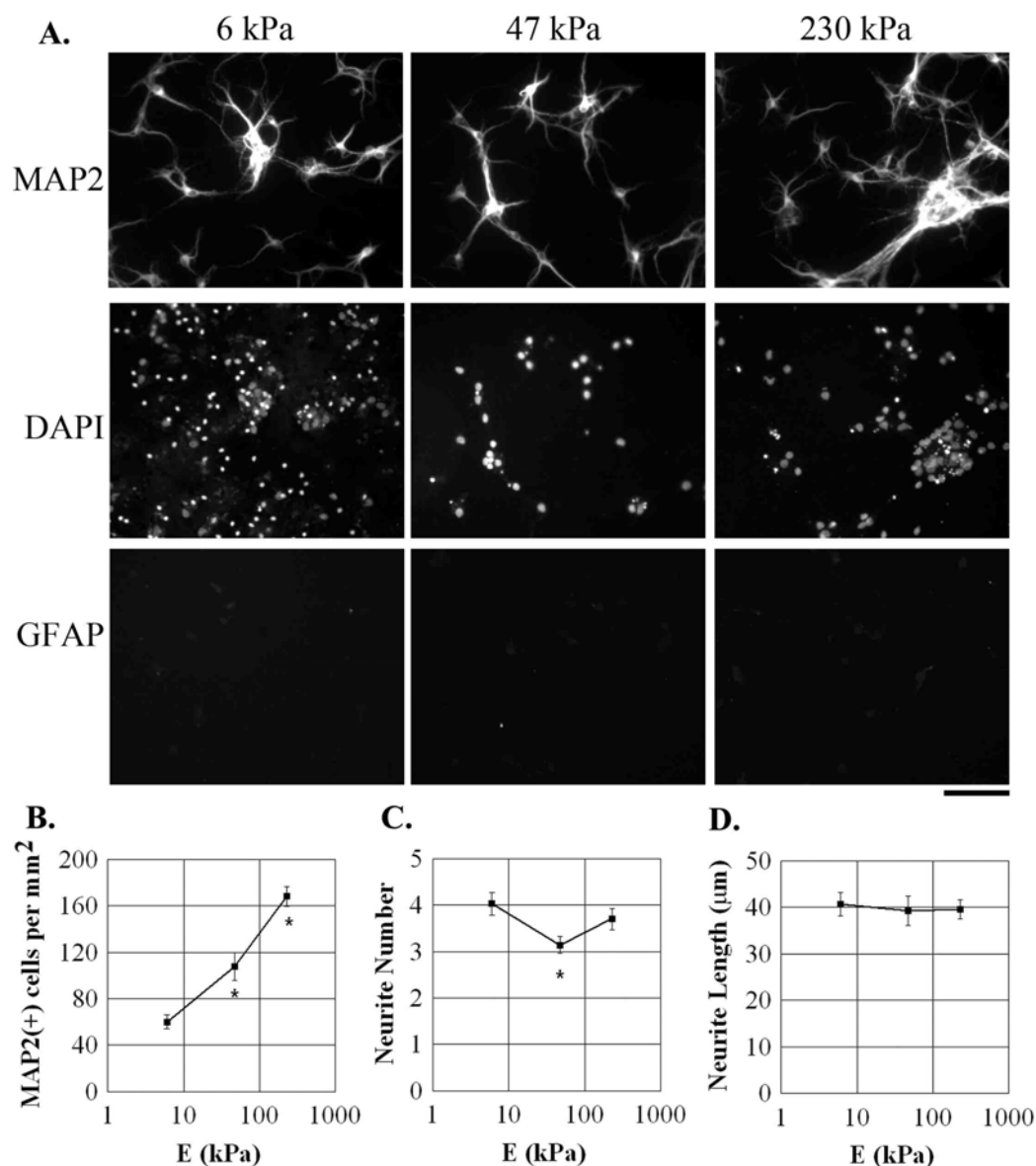


Figure 3A-7 Effects of gel stiffness on pure spinal cord neuron culture.

A: MAP2 immunostaining shows that neurons grow on gels; DAPI staining shows that each intact nucleus corresponds to one MAP2+ cell (notice the condensed, bright nuclear staining indicating non-viable cells); GFAP staining shows that there are no mature astroglia surviving in the culture. Scale bar: 100 μm. B: There is a significant increase in MAP2+ neuron numbers as gel stiffness increases from 6 to 230 kPa. * $p < 0.05$ by ANOVA followed by Tukey HSD test versus 6 kPa gel. C: Neurons grown on 47 kPa gel have the lowest number of primary dendrites compared to 6 or 230 kPa gels, while the neurite numbers between 6 and 230 kPa groups did not significantly differ. D: Neurite length is not significantly different among different gel groups. * $p < 0.05$ by ANOVA followed by Tukey HSD test for multiple comparisons versus 6 kPa gel.

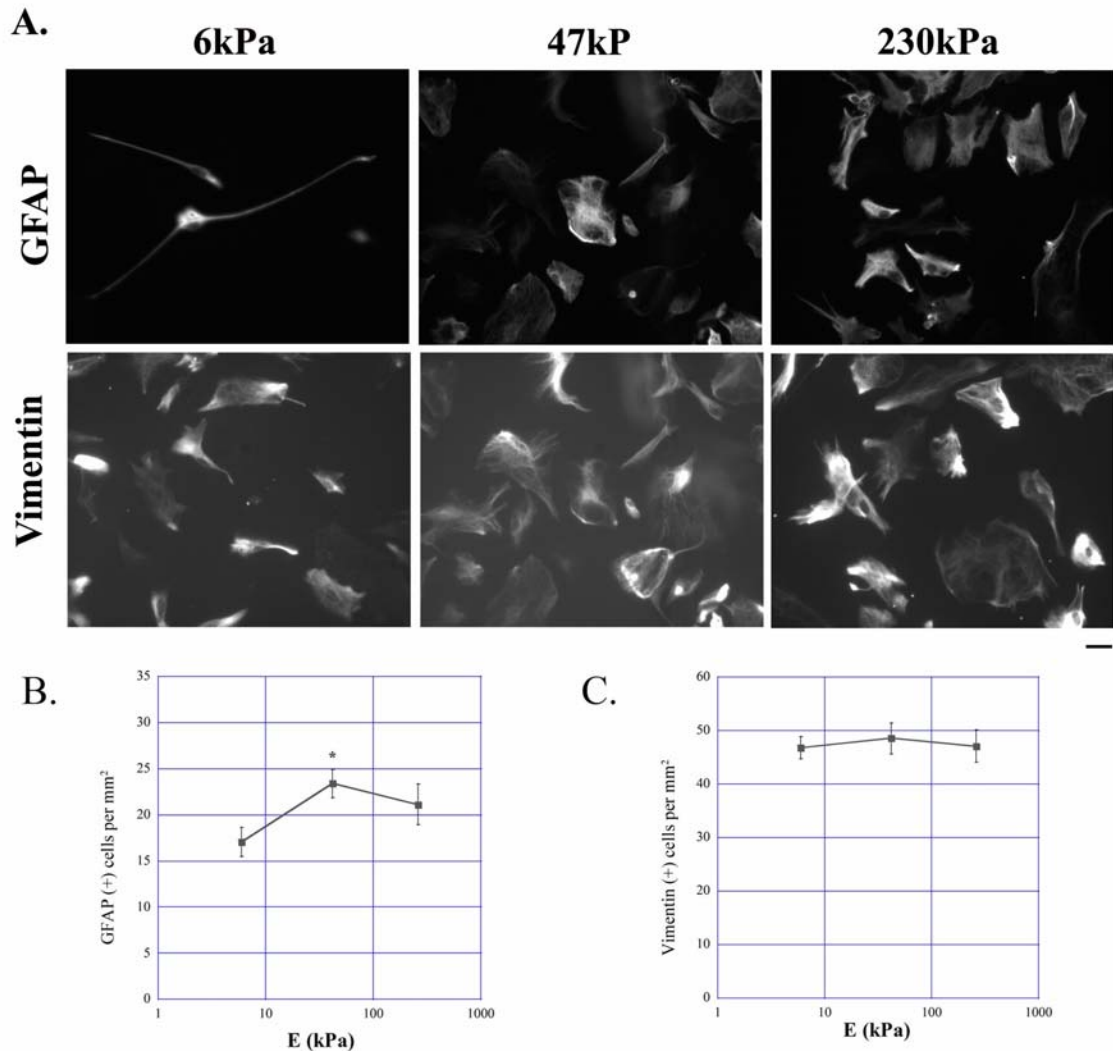


Figure 3A-8 Effects of gel stiffness on pure astrocyte culture.

A: Representative images of pure astrocytes cultured on 6, 47 and 230 kPa gels immunostained for either GFAP or vimentin. Scale bar: 30 μ m. B: Adhesion of GFAP+ cells increases with stiffness to a maximum at 47 kPa. C: Vimentin+ cell counting shows that adhesion of immature astroglia is not significantly affected. * $p < 0.05$ by ANOVA followed by Tukey HSD test for multiple comparisons versus 6 kPa gel.

3A.4 Discussion

Our current work asks whether or not differences in neuronal behavior induced by substrate rigidity can be fully attributed to mechanosensing of neurons alone or whether interactions between neurons and glia cells can affect their respective responses to mechanical stimuli. We employed a well-developed polyacrylamide gel system, and by exposing cells to substrates with different mechanical stiffnesses but identical surface adhesion properties, we evaluated cell number, neurite length and number, either in co-culture or in pure cultures. Neuronal adhesion increased with increasing elastic modulus of the substrate in pure, but not mixed cultures (Figs. 3A-6A and 3A-7B). Interactions between neurons and astroglia may contribute to this difference. The differences in neuron numbers in pure cultures among gel stiffness groups may have occurred due to the difference in neuronal precursor cell proliferating rates, since the precursor cells are present in the mixed cultures at the time of plating and will proliferate for several days¹², all of which are under the influence of mechanical properties of the substrates. A limited number of neurons were also found in aggregation with astroglia, which leads to the possibility that some neurons grew on top of astrocytes³⁷. AraC, a mitotic inhibitor, used in the pure neuronal culture might also be part of reason underlying the distinction. Average neurite length was not sensitive to the range of stiffness we investigated; however, average neurite number was lowest on gels with intermediate stiffness (27kPa or 47kPa) (Figs. 3A-6D and 3A-7C) in both mixed and pure cultures.

We have also found that the number of GFAP+ mature astroglia in co-culture (Fig. 3A-6C) as well as pure astroglial culture (Fig. 3A-8B) was affected by gel stiffness. In the presence of neurons, gels of 27 kPa stiffness showed the highest number of

GFAP+ cells. A similar trend was also found in pure neuronal culture (Fig. 3A-7C). Based on these observations, the possibility exists that neuronal cells could have intrinsic mechano-sensing mechanism to substrate stiffness, part of which will not be affected by the presence of astroglia and will lead to consistent behavior such as neurite outgrowth, although their attachment (cell number) to the substrate may apparently be altered. The observation that neuronal number follows the same trend in mixed and pure cultures on the stiffness range explored contrasts with the report that astrocytes, particularly reactive astrocytes, release a number of pro-inflammatory cytokines that are implicated in neurite branching⁴¹. Different than neurons whose average neurite number does not appear to be affected by the presence of astroglia, in the mixed culture, vimentin+ cells exhibited sensitivity to mechanical compliance in the range of 300 Pa to 230 kPa, as indicated by the increased cell number on stiffer gels (Fig. 3A-6B), and this sensitivity was not observed in pure astroglia culture (Fig. 3A-8C).

The differential effect of the mechanical characteristics of the hydrogel materials was observed in co-culture of neurons and astroglia (Fig. 3A-6A and 3A-6C). These data will aid in the development of biomaterial scaffold designs, which support and promote neuronal growth while inhibiting astrocyte proliferation, differentiation, or growth. This is important for inhibition of a glial scar when regeneration of neurites after spinal cord injury is an issue. Our current data are also consistent with previous studies reporting that surface adhesion properties are not greatly altered by the stiffness of the substrate^{17, 20, 24} and that variations in cell response can be primarily attributed to changes in the mechanical properties of the underlying gel.

Previous studies of mouse spinal cord and rat cortical neurons suggest softer gels are preferential for neuronal cells to grow based on a marked increase in branching number²⁰. We found that neuronal number does not differ significantly in the mixed culture to the range of stiffnesses under study. Glial cells were also observed on the softest gels in our study, different than what was reported previously²⁰. Moreover, there are proportionally more neurons on soft gels in mixed culture, possibly due to inhibition of astroglial attachment²⁴. Differences between our study and those of Flanagan and colleagues²⁰ and Georges and colleagues²⁴ include the following: First, we examined gels with a range of stiffnesses (300 Pa~230 kPa) that differs from those used in other studies (150 Pa ~ 1600 Pa in²⁰ and 600 Pa ~ 27 kPa in²⁴). We chose the gel stiffnesses at these different magnitudes in such a way that they span a range from that of natural CNS material (300 Pa) to that of relatively stiff gel (20%, 230 kPa), which is close to the stiffness reported for implant materials and also other CNS tissues (e.g., hundreds of kPa for rat spinal cord in¹⁹, Table 3A-2). This selection is also based on the possibility that the physiological stiffness condition is not necessarily the optimal condition for spinal cord nerve regeneration *in vitro*. Secondly, the species difference (mouse vs. rat) and tissue type (cortex vs. spinal cord) could contribute to differences as well as culture medium conditions, for which we used serum-free medium with added supplements (e.g., B27). Moreover, there is also variation in the cell plating density used in cell culture. For E16 rat spinal cord cells, we found that too high a density can cause aggregation, while too low a density results in poor survival of cells. Therefore, our work is not necessarily in conflict with previous work, but may complement the previous studies.

There is an ever-increasing recognition of the complex nature of neuron-astroglia interactions. On one hand, glial cells, predominantly astrocytes, release soluble factors or secrete ECM components to regulate neuronal functioning, including synaptic transmission⁸ and synapse formation^{7, 40}, axonal guidance⁷, and neuroprotection^{13, 16, 30, 59}, especially after injury^{18, 52}. For example, in astrocyte-poor cultures, glutamate toxicity of cortical neurons is higher than that of neurons grown in astrocyte-rich culture⁴⁹. On the other hand, neurons also actively participate in the regulation of glial activities such as migration and positioning⁷, by releasing TGF- β 1¹¹, steroids²¹, and BDNF^{25, 31}. Neurons, due to the nature of their role in the nervous system, normally communicate with each other, and thus, it is likely that neuron-neuron interactions play a role in the regulation of cellular responses to mechanical cues. It might be meaningful to be able to reseed glia cells back to the pure neuronal culture to see if the responses of neurons to the mechanical stiffnesses will be the same as those in the mixed culture.

Finally, although the mechanical characterization of bis-gels has also been carried out by many other investigators^{17, 20, 24, 45, 56, 58}; Table 3A-1), our study has several distinctions. First, a non-intrusive method was used to measure the stiffness *in situ*. Second, other investigators altered the stiffness of the gels by keeping monomer concentration constant while varying crosslink concentration. In our study, monomer-to-crosslink ratio remained constant and the amounts of both were changed simultaneously.

In summary, our study not only confirms that the mechanical stiffness of the substrate impacts neuron and astrocyte survival and growth, but also reveals that the way in which these individual cell types respond to mechanical stimuli is altered in the presence and absence of interaction with each other. The results from this study provide

important information for our understanding of the mechanical aspects of cellular-ECM interactions. Further studies must be carried out before our *in vitro* data can be applied to developing cures for traumatic CNS injuries.

References

1. Akum, B. F., M. Chen, S. I. Gunderson, G. M. Riefler, M. M. Scerri-Hansen, and B. L. Firestein. Cypin regulates dendrite patterning in hippocampal neurons by promoting microtubule assembly. *Nat Neurosci.* 7:145-152, 2004.
2. Allen, N. J., and B. A. Barres. Signaling between glia and neurons: Focus on synaptic plasticity. *Curr Opin Neurobiol.* 15:542-548, 2005.
3. Bakshi, A., O. Fisher, T. Dagci, B. T. Himes, I. Fischer, and A. Lowman. Mechanically engineered hydrogel scaffolds for axonal growth and angiogenesis after transplantation in spinal cord injury. *J Neurosurg Spine.* 1:322-329, 2004.
4. Balgude, A. P., X. Yu, A. Szymanski, and R. V. Bellamkonda. Agarose gel stiffness determines rate of drg neurite extension in 3d cultures. *Biomaterials.* 22:1077-1084, 2001.
5. Benarroch, E. E. Neuron-astrocyte interactions: Partnership for normal function and disease in the central nervous system. *Mayo Clin Proc.* 80:1326-1338, 2005.
6. Chang, G. L., T. K. Hung, and W. W. Feng. An in-vivo measurement and analysis of viscoelastic properties of the spinal cord of cats. *J Biomech Eng.* 110:115-122, 1988.
7. Chotard, C., and I. Salecker. Neurons and glia: Team players in axon guidance. *Trends Neurosci.* 27:655-661, 2004.
8. Cuevas, M. E., M. A. Carrasco, Y. Fuentes, P. Castro, F. Nualart, J. Roa, and L. G. Aguayo. The presence of glia stimulates the appearance of glycinergic synaptic transmission in spinal cord neurons. *Mol Cell Neurosci.* 28:770-778, 2005.
9. Curtis, A., and M. Riehle. Tissue engineering: The biophysical background. *Phys Med Biol.* 46:R47-65, 2001.
10. Dalton, P. D., L. Flynn, and M. S. Shoichet. Manufacture of poly(2-hydroxyethyl methacrylate-co-methyl methacrylate) hydrogel tubes for use as nerve guidance channels. *Biomaterials.* 23:3843-3851, 2002.
11. de Sampaio e Spohr, T. C., R. Martinez, E. F. da Silva, V. M. Neto, and F. C. Gomes. Neuro-glia interaction effects on gfap gene: A novel role for transforming growth factor-beta1. *Eur J Neurosci.* 16:2059-2069, 2002.
12. Deloulme, J. C., J. Baudier, and M. Sensenbrenner. Establishment of pure neuronal cultures from fetal rat spinal cord and proliferation of the neuronal precursor cells in the presence of fibroblast growth factor. *J Neurosci Res.* 29:499-509, 1991.
13. Dhandapani, K., and D. Brann. Neuroprotective effects of estrogen and tamoxifen in vitro: A facilitative role for glia? *Endocrine.* 21:59-66, 2003.
14. Discher, D. E., P. Janmey, and Y. L. Wang. Tissue cells feel and respond to the stiffness of their substrate. *Science.* 310:1139-1143, 2005.

15. Donnelly, B. R., and J. Medige. Shear properties of human brain tissue. *J Biomech Eng.* 119:423-432, 1997.
16. Dougherty, K. D., C. F. Dreyfus, and I. B. Black. Brain-derived neurotrophic factor in astrocytes, oligodendrocytes, and microglia/macrophages after spinal cord injury. *Neurobiol Dis.* 7:574-585, 2000.
17. Engler, A., L. Bacakova, C. Newman, A. Hategan, M. Griffin, and D. Discher. Substrate compliance versus ligand density in cell on gel responses. *Biophys J.* 86:617-628, 2004.
18. Faulkner, J. R., J. E. Herrmann, M. J. Woo, K. E. Tansey, N. B. Doan, and M. V. Sofroniew. Reactive astrocytes protect tissue and preserve function after spinal cord injury. *J Neurosci.* 24:2143-2155, 2004.
19. Fiford, R. J., and L. E. Bilston. The mechanical properties of rat spinal cord in vitro. *J Biomech.* 38:1509-1515, 2005.
20. Flanagan, L. A., Y. E. Ju, B. Marg, M. Osterfield, and P. A. Janmey. Neurite branching on deformable substrates. *Neuroreport.* 13:2411-2415, 2002.
21. Garcia-Ovejero, D., I. Azcoitia, L. L. DonCarlos, R. C. Melcangi, and L. M. Garcia-Segura. Glia-neuron crosstalk in the neuroprotective mechanisms of sex steroid hormones. *Brain Res Brain Res Rev.* 48:273-286, 2005.
22. Gasser, U. E., and M. E. Hatten. Neuron-glia interactions of rat hippocampal cells in vitro: Glial-guided neuronal migration and neuronal regulation of glial differentiation. *J Neurosci.* 10:1276-1285, 1990.
23. Geiger, B. Cell biology. Encounters in space. *Science.* 294:1661-1663, 2001.
24. Georges, P. C., W. J. Miller, D. F. Meaney, E. S. Sawyer, and P. A. Janmey. Matrices with compliance comparable to that of brain tissue select neuronal over glial growth in mixed cortical cultures. *Biophys J.* 90:3012-3018, 2006.
25. Ghosh, A., J. Carnahan, and M. E. Greenberg. Requirement for bdnf in activity-dependent survival of cortical neurons. *Science.* 263:1618-1623, 1994.
26. Griffith, L. G., and M. A. Swartz. Capturing complex 3d tissue physiology in vitro. *Nat Rev Mol Cell Biol.* 7:211-224, 2006.
27. Ichihara, K., T. Taguchi, I. Sakuramoto, S. Kawano, and S. Kawai. Mechanism of the spinal cord injury and the cervical spondylotic myelopathy: New approach based on the mechanical features of the spinal cord white and gray matter. *J Neurosurg.* 99:278-285, 2003.
28. Ingber, D. E. Mechanical signaling and the cellular response to extracellular matrix in angiogenesis and cardiovascular physiology. *Circ Res.* 91:877-887, 2002.
29. Khatiwala, C. B., S. R. Peyton, and A. J. Putnam. Intrinsic mechanical properties of the extracellular matrix affect the behavior of pre-osteoblastic mc3t3-e1 cells. *Am J Physiol Cell Physiol.* 290:C1640-1650, 2006.
30. Kirchhoff, F., R. Dringen, and C. Giaume. Pathways of neuron-astrocyte interactions and their possible role in neuroprotection. *Eur Arch Psychiatry Clin Neurosci.* 251:159-169, 2001.
31. Kohara, K., A. Kitamura, M. Morishima, and T. Tsumoto. Activity-dependent transfer of brain-derived neurotrophic factor to postsynaptic neurons. *Science.* 291:2419-2423, 2001.

32. Leach, J. B., X. Q. Brown, J. G. Jacot, P. A. Dimilla, and J. Y. Wong. Neurite outgrowth and branching of pc12 cells on very soft substrates sharply decreases below a threshold of substrate rigidity. *J Neural Eng.* 4:26-34, 2007.
33. Lin, D. C., B. Yurke, and N. A. Langrana. Mechanical properties of a reversible, DNA-crosslinked polyacrylamide hydrogel. *J Biomech Eng.* 126:104-110, 2004.
34. Lin, D. C. (2005). Design and properties of a new dna-crosslinked polymer hydrogel, Mechanical and Aerospace Engineering Piscataway, NJ: Rutgers University.
35. Lin, D. C., B. Yurke, and N. A. Langrana. Use of rigid spherical inclusions in young's moduli determination: Application to DNA-crosslinked gels. *J Biomech Eng.* 127:571-579, 2005.
36. Liu, Z., and L. E. Bilston. Large deformation shear properties of liver tissue. *Biorheology.* 39:735-742, 2002.
37. Lu, Y. B., K. Franze, G. Seifert, C. Steinhäuser, F. Kirchhoff, H. Wolburg, J. Guck, P. Janmey, E. Q. Wei, J. Kas, and A. Reichenbach. Viscoelastic properties of individual glial cells and neurons in the cns. *Proc Natl Acad Sci U S A.* 103:17759-17764, 2006.
38. Marquardt, G., M. Setzer, A. Theisen, E. Dettmann, and V. Seifert. A novel dynamic model for experimental spinal cord compression. *J Neurosurg Spine.* 2:466-471, 2005.
39. McCarthy, K. D., and J. de Vellis. Preparation of separate astroglial and oligodendroglial cell cultures from rat cerebral tissue. *J Cell Biol.* 85:890-902, 1980.
40. Nagler, K., D. H. Mauch, and F. W. Pfrieger. Glia-derived signals induce synapse formation in neurones of the rat central nervous system. *J Physiol.* 533:665-679, 2001.
41. Neumann, H., R. Schweigreiter, T. Yamashita, K. Rosenkranz, H. Wekerle, and Y. A. Barde. Tumor necrosis factor inhibits neurite outgrowth and branching of hippocampal neurons by a rho-dependent mechanism. *J Neurosci.* 22:854-862, 2002.
42. Ozawa, H., T. Matsumoto, T. Ohashi, M. Sato, and S. Kokubun. Comparison of spinal cord gray matter and white matter softness: Measurement by pipette aspiration method. *J Neurosurg.* 95:221-224, 2001.
43. Ozawa, H., T. Matsumoto, T. Ohashi, M. Sato, and S. Kokubun. Mechanical properties and function of the spinal pia mater. *J Neurosurg Spine.* 1:122-127, 2004.
44. Pedersen, J. A., and M. A. Swartz. Mechanobiology in the third dimension. *Ann Biomed Eng.* 33:1469-1490, 2005.
45. Pelham, R. J., and Y.-L. Wang. Cell locomotion and focal adhesions are regulated by substrate flexibility. *Proc. Natl. Acad. Sci USA.* 94:13661-13665, 1997.
46. Peyton, S. R., and A. J. Putnam. Extracellular matrix rigidity governs smooth muscle cell motility in a biphasic fashion. *J Cell Physiol.* 204:198-209, 2005.
47. Prange, M. T., and S. S. Margulies. Regional, directional, and age-dependent properties of the brain undergoing large deformation. *J Biomech Eng.* 124:244-252, 2002.

48. Reinhart-King, C. A., M. Dembo, and D. A. Hammer. The dynamics and mechanics of endothelial cell spreading. *Biophys J.* 89:676-689, 2005.
49. Rosenberg, P. A., S. Amin, and M. Leitner. Glutamate uptake disguises neurotoxic potency of glutamate agonists in cerebral cortex in dissociated cell culture. *J Neurosci.* 12:56-61, 1992.
50. Rosner, B. I., T. Hang, and R. T. Tranquillo. Schwann cell behavior in three-dimensional collagen gels: Evidence for differential mechano-transduction and the influence of tgf-beta 1 in morphological polarization and differentiation. *Exp Neurol.* 195:81-91, 2005.
51. Semler, E. J., C. S. Ranucci, and P. V. Moghe. Tissue assembly guided via substrate biophysics: Applications to hepatocellular engineering. *Adv Biochem Eng Biotechnol.* 102:1-46, 2006.
52. Silver, J., and J. H. Miller. Regeneration beyond the glial scar. *Nat Rev Neurosci.* 5:146-156, 2004.
53. Stegemann, J. P., H. Hong, and R. M. Nerem. Mechanical, biochemical, and extracellular matrix effects on vascular smooth muscle cell phenotype. *J Appl Physiol.* 98:2321-2327, 2005.
54. Teng, Y. D., E. B. Lavik, X. Qu, K. I. Park, J. Ourednik, D. Zurakowski, R. Langer, and E. Y. Snyder. Functional recovery following traumatic spinal cord injury mediated by a unique polymer scaffold seeded with neural stem cells. *Proc Natl Acad Sci U S A.* 99:3024-3029, 2002.
55. Wang, H. B., M. Dembo, and Y. L. Wang. Substrate flexibility regulates growth and apoptosis of normal but not transformed cells. *Am J Physiol Cell Physiol.* 279:C1345-C1350, 2000.
56. Wang, Y. L., and R. J. Pelham, Jr. Preparation of a flexible, porous polyacrylamide substrate for mechanical studies of cultured cells. *Methods Enzymol.* 298:489-496, 1998.
57. Witcher, M. R., S. A. Kirov, and K. M. Harris. Plasticity of perisynaptic astroglia during synaptogenesis in the mature rat hippocampus. *Glia.* 55:13-23, 2007.
58. Wong, J. Y., A. Velasco, P. Rajagopalan, and Q. Pham. Directed movement of vascular smooth muscle cells on gradient-compliant hydrogels. *Langmuir.* 19:1908-1913, 2003.
59. Wu, H., W. J. Friedman, and C. F. Dreyfus. Differential regulation of neurotrophin expression in basal forebrain astrocytes by neuronal signals. *J Neurosci Res.* 76:76-85, 2004.
60. Yamada, K., S. Miyamoto, I. Nagata, H. Kikuchi, Y. Ikada, H. Iwata, and K. Yamamoto. Development of a dural substitute from synthetic bioabsorbable polymers. *J Neurosurg.* 86:1012-1017, 1997.
61. Yeung, T., P. C. Georges, L. A. Flanagan, B. Marg, M. Ortiz, M. Funaki, N. Zahir, W. Ming, V. Weaver, and P. A. Janmey. Effects of substrate stiffness on cell morphology, cytoskeletal structure, and adhesion. *Cell Motil Cytoskeleton.* 60:24-34, 2005.
62. Yuan, Q., L. Dougherty, and S. S. Margulies. *In vivo* human cervical spinal cord deformation and displacement in flexion. *Spine.* 23:1677-1683, 1998.

CHAPTER 3B SPINAL CORD NEURONS ON DNA GELS

3B.1 Background

Understanding the interplay between cells and the extracellular matrix (ECM) is fundamental for the successful design of biomaterials for tissue engineering applications. It provides insight into biomaterial-tissue interactions since these biomaterials essentially serve as analogs of the ECM^{2, 58}. Specific cellular properties have been found to be sensitive to substrate compliance for a number of cell types in various culture systems^{14, 40, 44, 54}. Among these systems, the bis-acrylamide crosslinked polyacrylamide hydrogel ('bis-gel', hereafter) has been gaining popularity in probing cell mechanosensing and cell-substrate interactions, and it has recently been used for the study of CNS (central nervous system) cells^{22, 27, 39, 43}. For instance, for the range of stiffness of tens of Pa to a few kPa, neurite branching number (i.e., secondary dendritic number) is significantly higher and astroglia are less adherent to softer gels^{22, 27}. When grown on bis-gels and other hydrogels, PC12 cells showed changes in neurite outgrowth with changes in substrate compliance^{30, 43}. Furthermore, it has been recently shown that neuron-astroglial interactions are among the key factors in cell decision-making in response to substrate rigidities³⁹. These studies shed light upon the potential for promoting neurite elongation, neurite branching, axonal regeneration, and the possibility of differentially controlling neuronal and astroglial populations (e.g. for overcoming glial scar formation) by modulating the mechanical properties of substrates.

3B.1.1 Significance of the substrate mechanical stiffness

In addition to the long-established recognition that biomechanical interactions are critical to bioscaffold design for major load-bearing tissues^{18, 29, 61}, there is an increasing awareness that mechanical properties also play a key role in successful utilization of scaffolds for those tissues whose major functions are not load-bearing⁶³, such as the spinal cord³. This is partly based on the knowledge gained during recent decades that mechanical interactions are an integral part of cellular/tissue-ECM events in addition to chemical interplay at both molecular and cellular levels^{5, 13}. Moreover, among all of the parameters of biomechanical design, in addition to mechanical compatibility considerations, mechanical stiffness or rigidity of the materials has been drawing increasing attention^{17, 21, 31, 32, 63, 66}. In light of this, there is a growing interest in incorporating mechanical cues in biomaterial design for neural tissue engineering applications, including those for spinal cord injury recovery, where axonal regeneration, synaptogenesis and rewiring of neural circuitry is strongly desired^{20, 35, 53}.

3B.1.2 Contrast between bis-gel and DNA-gel systems

Although the use of bis-gels has yielded interesting results, introducing a DNA crosslinking mechanism into gel formation to replace bis-acrylamide should provide new possibilities due to changes in the nanostructures of the gel network^{1, 47, 48} (e.g. as the design shown in Fig. 3B-1). By incorporating AcryditeTM modified oligonucleotides into polyacrylamide gels, in our laboratory, Lin and colleagues⁴⁷ illustrated and characterized reversible temperature-independent gelation. These DNA-crosslinked hydrogels (referred to as ‘DNA gels’ hereafter) have a range of stiffness from a few hundred Pa to

10 kPa depending on the crosslinker DNA density. Incorporation of DNA crosslinking allows versatility in supplying mechanical cues, which is beneficial in designing hydrogels for various applications. For example, changes in the length and design of crosslinker DNA make it possible for DNA gels to carry molecules, such as growth factors, of different sizes. Liedl and co-workers⁴⁵ found that quantum dots did not move out of DNA gels of certain design. This study provided insight to the nano-level structures of the gels that may lead to their use as a drug delivery vehicle. The ease with which crosslinking density can be changed facilitates the dynamic modulation of mechanical stiffness. Ongoing work in this area is presented in this dissertation.

In the work described in this section, the possibility of modifying gel properties by varying crosslinker length and monomer concentration has been further explored. As a prelude to the study to temporally alter gel stiffness and provide dynamic mechanical cues to cells, the range of the stiffness has been expanded and made available to probe cellular responses. This was motivated by the fact that mechanical stiffnesses of CNS tissues range from a few Pa to hundreds of kPa^{26, 33, 51} and that polymers currently used in CNS tissue repair have rigidities of more than 30 kPa and up to MPa^{15, 64}. Similar to their bis-crosslinked counterparts, DNA gels must be functionalized for protein conjugation and cell attachment. The hypothesis has been tested that DNA gels can be functionalized in a fashion similar to that used with bis-gels by deploying a bi-functional linker and that the different DNA gel designs employed will vary in mechanical stiffness but not in surface ligand density. Cellular behavior of primary rat spinal cord cells has been examined and emphasis was placed on the neurite outgrowth of spinal cord neurons. Finally, the neuronal expression of focal adhesion kinase (FAK), one of the key

regulators of various cell activities at focal adhesions (FAs) or point contacts, has been assessed. The results provide insight into the mechanisms of neuronal cell mechanosensing and will assist in incorporating mechanical cues into the design of biomaterials for neural tissue engineering applications.

3B.2 Materials and methods

3B.2.1 DNA gel design and preparation

Figure 3B-1A depicts the chemical structure of DNA and bis-crosslinked polyacrylamide hydrogels. The base sequences for the DNA strands used in this structure were designed in a manner similar to that reported by Lin and colleagues^{47, 48} from our laboratory. Customized software was utilized to minimize unwanted hybridization, to reduce possibilities of secondary structures, and to reach balanced AT/GC content. These customized DNA strands, a number of which were modified with AcryditeTM, were manufactured and shipped lyophilized by Integrated DNA Technologies, Coralville, IA.

DNA gels were prepared according to a protocol previously published⁴⁷. Briefly, AcryditeTM modified DNA strands SA1 and SA2 were respectively co-polymerized with 4% or 10% acrylamide monomer, initiated by 0.05% ammonium persulfate (APS) and catalyzed by 0.5% TEMED, in TBE (10×) buffer to form polymer solutions (Figure 3B-2). The solutions were de-aerated with nitrogen bubbling before and after addition of APS and TEMED, and formed long polymer chains with SA1 or SA2 as side chains. The SA1 and SA2 polymer solutions were then mixed and stirred, and a solution containing crosslinker L2 (3 mM in TE buffer) was added to the mixture to form gels. During the

process, the mixture was heated to over 70°C, well above the DNA melting temperature, to facilitate mixing, and cooled to allow re-gelation.

3B.2.2 Mechanical characterization of DNA gels

Viscosity tests were performed to determine the gel point, or the critical crosslinker density, of the DNA gels, using a previously reported method⁴⁷ based on the observation of no appreciable movement from a steel bead (0.79mm in diameter, Small Parts, Miami Lakes, FL) for a time period of over 24 hrs at room temperature (RT). For stiffness tests, DNA gels were prepared at the critical crosslinker densities in microcentrifuge tubes mounted to a customized fixture similar to the one used before^{46, 47}, and the measurements were performed as detailed previously⁴⁷. In brief, by applying a calibrated magnetic force to a bead embedded in the gel sample and measuring the resulting displacement of the bead at 14~15°C, one can calculate the stiffness based on a solution previously formulated⁴⁷. An increment of 5% crosslinker was then added to the gels, and measurements were repeated. After reaching 100% crosslinking, additional crosslinker DNA solution was added, and testing was performed to ensure that the gel was fully crosslinked.

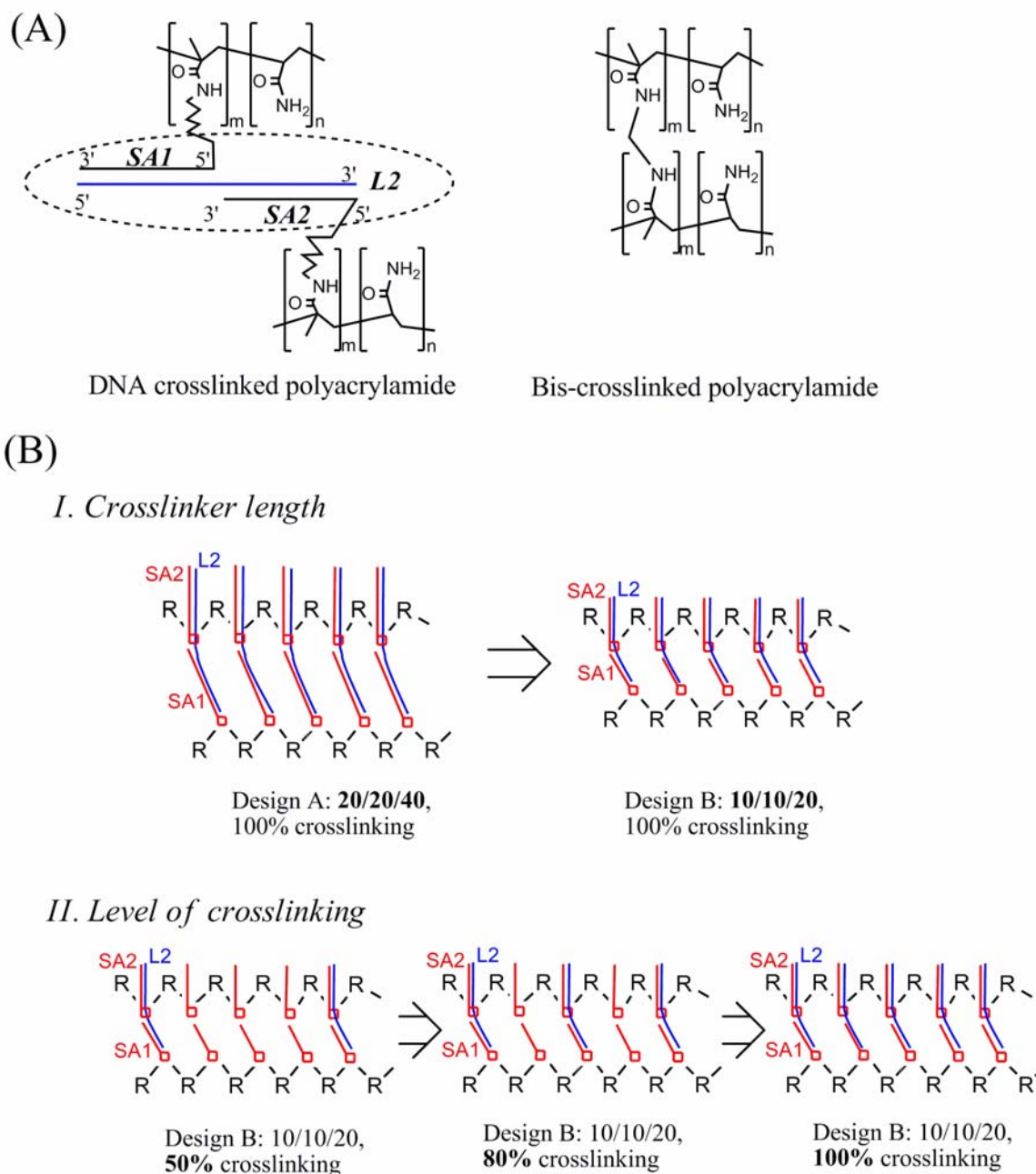


Figure 3B-1 Chemical structures of DNA- and bis-crosslinked hydrogels, and DNA gel design schemes.

(A) Chemical structures of DNA and bis crosslinked polyacrylamide gels. SA1 and SA2 denote the side DNA chains with AcryditeTM modification, and L2 represents crosslinker DNA complimentary to both SA1 and SA2. (B) Two schemes of DNA gel comparisons. I. Changes in the length of crosslinkers at full crosslinking (as detailed in Table 3B-1); II. Changes in the level of crosslinking (50%, 80% and 100%) with the same crosslinker length. *R* indicates the monomer of vinyl polymers, and in this study it represents acrylamide.

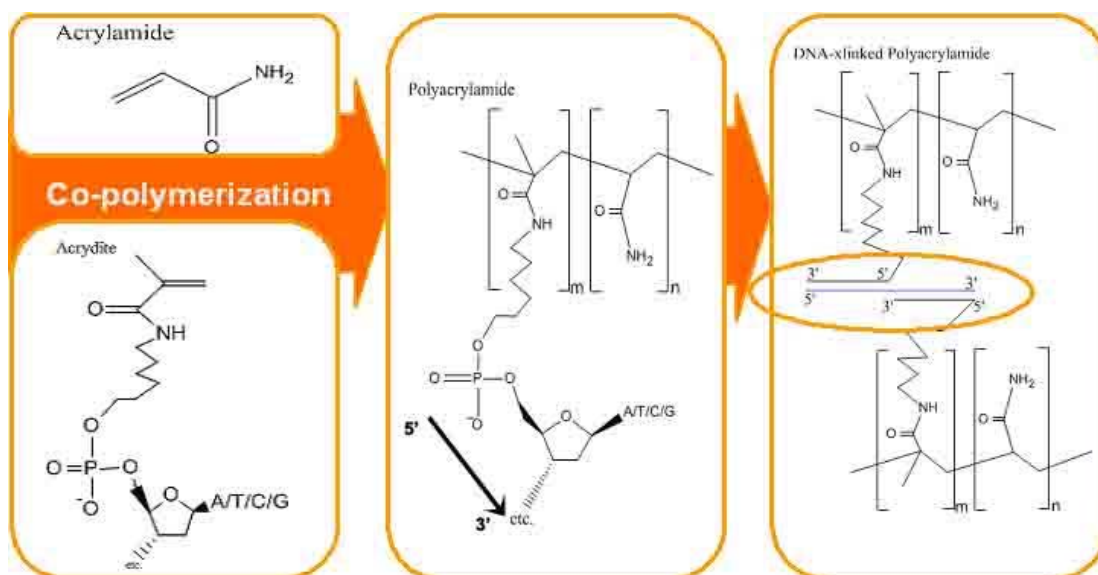


Figure 3B-2 Schematic of DNA gel synthesis.

Co-polymerization of acrylamide monomer and Acrydite (R) modified DNA results in polymer chains with DNA side chain, and upon delivery of crosslinker DNA, a gel can be formed.

3B.2.3 DNA gel functionalization and assessment of ligand density

DNA gels were immobilized onto coverglass by using an optical adhesive (#72, Norland, New Brunswick, NJ) and were kept in PBS at 4°C until usage. To activate the gels for cell attachment, a bifunctional photoactivable crosslinker, Sulfo SANPAH (Pierce, Rockford, IL), in HEPES was applied, allowing conjugation of adhesion-promoting molecules. The functional groups in Sulfo SANPAH covalently bind to both N-H sites on polyacrylamide backbones and amino groups. Poly-D-lysine (PDL, Sigma, St. Louis, MO) at 1 mg/mL was applied in all experiments except that in those for the measurement of gel surface ligand density, a mixture of type I collagen (USB, Cleveland, OH) and collagen fluorescein (Elastin, Owensville, MO) was applied at different ratios for a final concentration of 0.2 mg/mL. PDL is a sufficient adhesive substrate, although other ECM molecules (e.g., fibronectin, laminin) can also be used. After incubation at 4°C overnight, excess PDL or collagen was removed. Images of the surfaces of collagen coated gel samples were taken at a fixed exposure time by using an Olympus IX50 fluorescent microscope system. Eight random fields from each gel sample were imaged, and the mean value of fluorescence intensity was measured.

3B.2.4 Rat spinal cord cell culture

All animal work was carried out with an approved protocol from the Rutgers University Animal Care and Facilities Committee. Cells were obtained from spinal cords dissected from rat embryos at 16 days gestation and dissociated (Sprague Dawley rats, Taconic, Hudson, NY). The cells were then plated on functionalized DNA gels in 24-well culture plates at a density of 5×10^4 cells/cm² in serum-containing medium (minimum essential

medium, 10% horse serum and 0.6% glucose supplemented with antibiotics (penicillin/streptomycin)). Plates were kept in a humidified CO₂ incubator at 37°C. One day after cell plating, the medium was changed to Neurobasal medium (Gibco) supplemented with B-27, antibiotics, and β -mercaptoethanol (1 μ L per 500 mL medium) to promote neuronal growth.

3B.2.5 Immunocytochemistry and cell counting

For immunocytochemistry, cells were grown for 6 days *in vitro* (6 DIV) and fixed using paraformaldehyde (4% in PBS) for 20 min, and incubated in blocking solution (PBS with 0.1% Triton X-100, 2% normal goat serum, 0.02% sodium azide) for 30 min. Cells were incubated with the following antibodies: chicken polyclonal antibody against MAP2 (1:2000, Chemicon, Temecula, CA); rabbit polyclonal antibody against GFAP (1:200, Abcam, Cambridge, MA), monoclonal antibody against Tau-1 (1:1000, Chemicon), or monoclonal antibody against FAK (1:300, Chemicon). Cells were then incubated with the appropriate secondary antibodies (1:200, Jackson Immuno-Research) for 1 hr at RT. Intact cells were identified with DAPI nuclear staining. Labeled cells were visualized with fluorescence microscopy (Olympus IX50 microscope with a Cooke Sensicam charge-coupled device cooled camera fluorescence imaging system and Image Pro (Media Cybernetics, Bethesda, MD) software). On each gel sample, the areas with cell growth were imaged, and MAP2⁺ and GFAP⁺ cells were counted manually, aided with corresponding images of DAPI staining by using ImageJ software (NIH, Bethesda, MD). Total cell counts were also performed based on DAPI staining. Each experiment was repeated at least three times.

The primary and secondary antibodies that were used in this study are summarized in Table 3A-3 in Chapter 3A.

3B.2.6 Characterization of neurite outgrowth and statistical analysis

Axons were identified by immunostaining for Tau-1, whereas dendrites were identified by MAP2 immunostaining. Primary dendrites were identified as processes directly extending from the soma, and the primary dendrite length was determined from the point where the dendrites emanated from soma to the tip of the neurites. Neurite length was measured with Scion Image software (Scion Corp., Frederick, MD) and calibrated to yield absolute distance in metric units. The number of primary dendrites was counted and their length was measured only for those isolated neurons with clear morphology, and axonal length was measured for all Tau-1-positive processes, including those extending from a clump of cells^{28, 42}. The mean primary dendrite length, primary dendrite number, and axonal length were recorded for each neuron and grouped for each gel condition. In assessing FAK expression in the neuronal cell body, the cells were imaged at a fixed exposure time and neurons were identified based on MAP2 immunofluorescence. The level of FAK expression in the cell body of individual neurons was assessed and grouped for each gel condition.

One way ANOVA was carried out to compare the four different gel conditions, followed by Tukey's multiple comparisons test. If only two groups of data were compared, an unpaired two-tailed *t*-test was performed to determine significance. The difference in distribution among distinct groups was assessed by using Chi-square test of goodness of fit. $p < 0.05$ was considered significant.

3B.3 Results

3B.3.1 DNA sequence and DNA gel design

Two crosslinkers of differing length were designed. The base sequences for the DNA strands of these two crosslinkers, arrived at by the optimization procedure, are given in A and B of Table 3B-1. SA1 and SA2 denote the DNA side chains and have a length of 10 nucleotides each in Design A and 20 nucleotides each in Design B. L2 represents crosslinker DNA which can base-pair with both SA1 and SA2 (Fig. 3B-1), hence 20/20/40 (length of SA1/SA2/L2) denotes Design A and 10/10/20 denotes Design B. The molar concentration of SA1 is always equal to that of SA2. If equimolar concentrations of SA1 and L2 are present in the gel network, the gel is referred to as being 100% or fully crosslinked. When the molar concentration of L2 is only 50%, 80%, or 100% of that of SA1, the gel is referred to as being 50%, 80%, and 100% crosslinked, respectively. Observations that there was no increase in the gel stiffness upon adding extra crosslinkers after reaching 100% crosslinking confirmed that the gels were fully crosslinked. It is noticed that it is possible that not all SA1 and SA2 strands contribute to the functional crosslinking of the gel network; and that the actual crosslinking density will be lower than what one can infer from the concentration of SA1 and SA2. Thus, gels were prepared with SA1 and SA2 stoichiometrically, and the degree of crosslinking was inferred from the amount of L2 added; and a ratio of L2 to SA1 or SA2 was used as an approximation for the degree of crosslinking.

In Scheme I (Fig. 3B-1B), the effect of crosslinker length and monomer concentration on the mechanical properties of the gels was studied, and the cells were

plated onto gels of two different designs at full crosslinking. The crosslinker length in Design A is double that of Design B, and the monomer concentration is lower. In contrast, in Scheme II (Fig. 3B-1B), the dependency of mechanical properties on the level of crosslinking for gels with Design B was investigated. It should be noted that the crosslinker between polymer chains is half of the total length of the crosslinker DNA (Fig. 3B-1A). This is due to the fact that only half of the length of the L2 strand is employed in forming the duplex DNA spacer between the two polyacrylamide chains in the crosslink structure (Fig. 3B-1A). The remaining length of the L2 strand is simply employed to hold one of the polyacrylamide strands to the crosslink structure but does not contribute to the spacing between attachment points on the crosslinker structure (Fig. 3B-1A). This configuration was necessitated by the fact that Acrydite modification of DNA is available at only the 5' end from the manufacturer (Integrated DNA Technologies, Coralville, IA.).

An example of DNA crosslinked hydrogel on coverglass in the experiment is shown in Fig. 3B-3.

Table 3B-1 DNA sequence of Designs A and B used in the study of spinal cord cells on DNA gels with static stiffness.

(A)	DNA strand	# of bases	Design A- DNA sequence (5' to 3')
	SA1	20	ACG GAG GTG TAT GCA ATG TC
	SA2	20	CAT GCT TAG GGA CGA CTG GA
	L2	40	TCC AGT CGT CCC TAA GCA TGG ACA TTG CAT ACA CCT CCG T
(B)	DNA strand	# of bases	Design B - DNA sequence (5' to 3')
	SA1	10	GCA CCT TTG C
	SA2	10	GTC AGA ATG A
	L2	20	TCA TTC TGA CGC AAA GGT GC

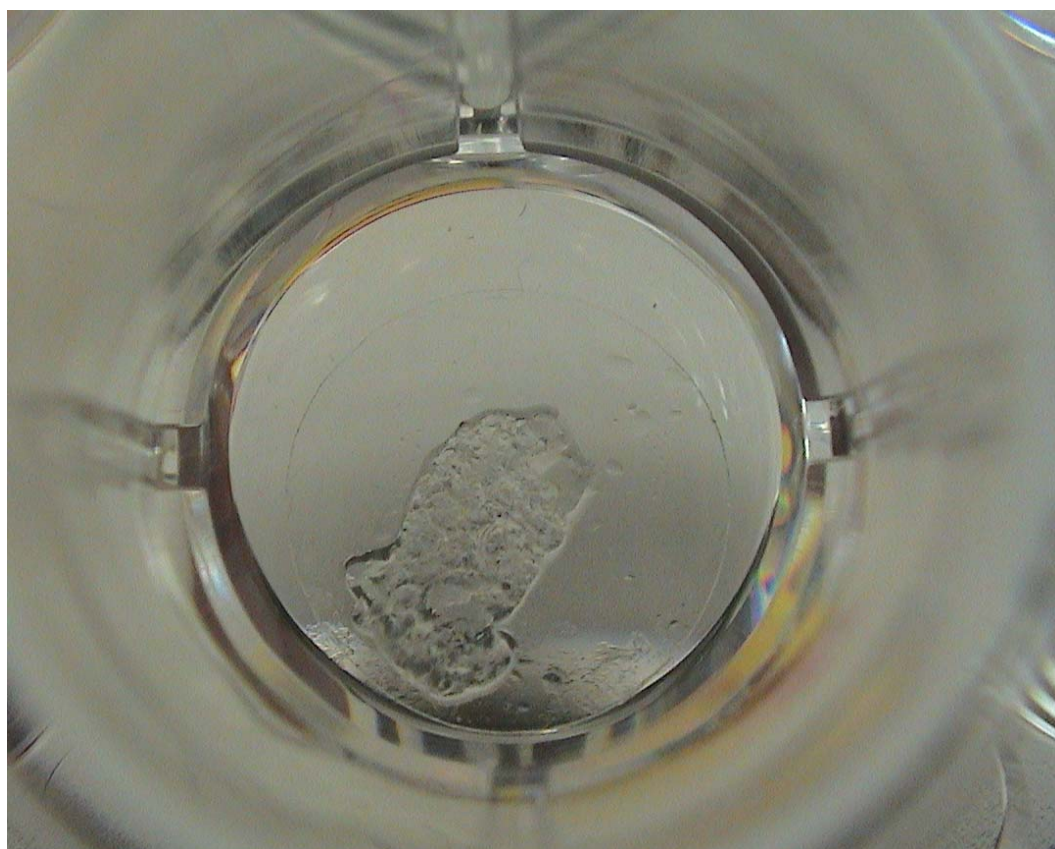


Figure 3B-3 A DNA crosslinked hydrogel was immobilized on a circular cover glass (12mm in diameter) with thickness of approximately 100~300 μ m.

3B.3.2 Viscosity and stiffness of DNA-crosslinked gels

Previously, 25% crosslinking was determined to be critical for DNA gels of Design A at room temperature (RT)⁴⁷, where gelation starts to occur. Viscosity data show that for DNA gels of Design B, the critical crosslinker density is approximately 30% at RT since this is the lowest crosslinking density that we studied for which we did not observe appreciable movement of the bead in the gel over a time period of 24 hrs according to the protocol (Figure 3B-4). Mechanical stiffness values were obtained by measuring the resulting displacement of embedded beads in response to applied calibrated magnetic force. The measurement was repeated for DNA gels at different levels of crosslinking (Table 3B-2). For both designs, as the level of crosslinking approaches 100%, the modulus increases. For Design B, a relatively larger stiffness range (hundreds of Pa to ~30 kPa) was achieved than that of Design A. Note that mechanical stiffness and elastic modulus were used interchangeably in this dissertation. To gels of 100% crosslinking, when excess crosslinker DNA was added, the gel stiffness remained unchanged. We note that the examinations were performed under RT in which gels were not fully swelled, as the first priority was given to probing cellular behavior and activities.

After the available stiffness range (a few hundred Pa to ~30 kPa) was identified, target mechanical stiffnesses of 6.6, 17.1 and 30 kPa were chosen for the study in Scheme II, which include the stiffness of soft substrates (~5 kPa) that have been previously studied^{27, 43}, the largest stiffness available for gels with Design B (30 kPa), and an intermediate stiffness (~15 kPa). Based on the results from mechanical characterization, it was determined that DNA gels with Design B at 50%, 80%, and 100% crosslinking have the desired stiffnesses.

Table 3B-2 Mechanical stiffness of the DNA crosslinked polyacrylamide hydrogels used in the study of spinal cord cells on DNA gels with static stiffness.

	Design B			Design A	
DNA crosslinker length	10/10/20			20/20/40	
Monomer Concentration	10%			10%	4%
DNA crosslinker density	50%	80%	100%	100%	100%
Stiffness (kPa) *	6.6 ± 0.6	17.1 ± 0.8	29.8 ± 2.5	25.2 ± 0.5	10.4 ± 0.6
Designation	B50	B80	B100		A100

* Mean \pm SEM (Standard Error of Mean)

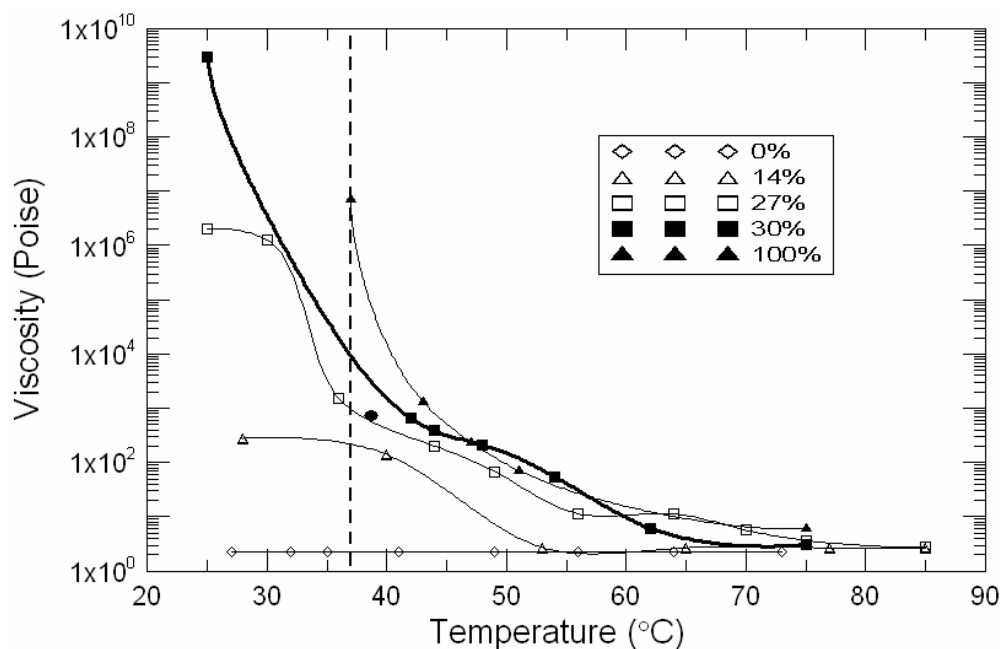


Figure 3B-4 Changes in viscosity of DNA gels of Design B with respect to the temperature at various levels of crosslinking.

Only 0%, 14%, 27%, 30% and 100% are shown for clarity. Note that at 37°C, the DNA gels at 30% crosslinking are effectively solid.

3B.3.3 Assessment of gel surface ligand density

In order to rule out the possible contribution of variation in gel surface ligand density to changes in cellular behavior, fluorescence intensity of collagen was used as an indicator of surface ligand density in a way similar to that in previous studies (e.g., ¹⁹). The initial collagen concentration used ($0.5\sim 1\times 10^5$ ng/cm²) was much higher than that studied previously^{19,25}, ensuring that the amount of collagen was excessive and not limiting, and that all of the possible adhesion sites were occupied (Figure 3B-5). There is no significant difference in the surface fluorescence intensity of labeled collagen among DNA gels of different designs or different levels of crosslinking (Fig. 3B-6). Since the size of bound type I collagen (~300 kD) on the surface is comparable to that of PDL (~150 kDa), the ligand density available on the DNA gel surface for cellular attachment where PDL was used is not significantly different than that probed in fluorescence intensity studies. It is emphasized here that the absolute ligand density is not critical to this work, and that maintaining relative density is sufficient to eliminate the effect of surface ligand density on the differential cellular responses. Based on gel electrophoresis, no noticeable damage to DNA strands was observed after they were exposed to UV light at exposure times and intensities applied in DNA gel immobilization and functionalization.

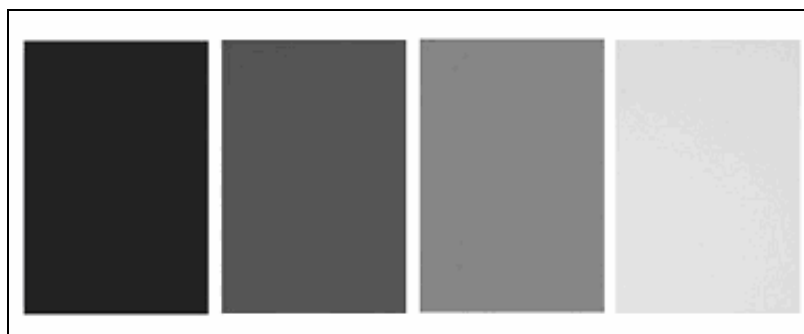


Figure 3B-5 Fluorescent density of collagen on DNA gels assessed with increased (left to right) percentage of fluorescent collagen replacement of regular collagen. 0%, 5%, 10%, and 15% from left to right.

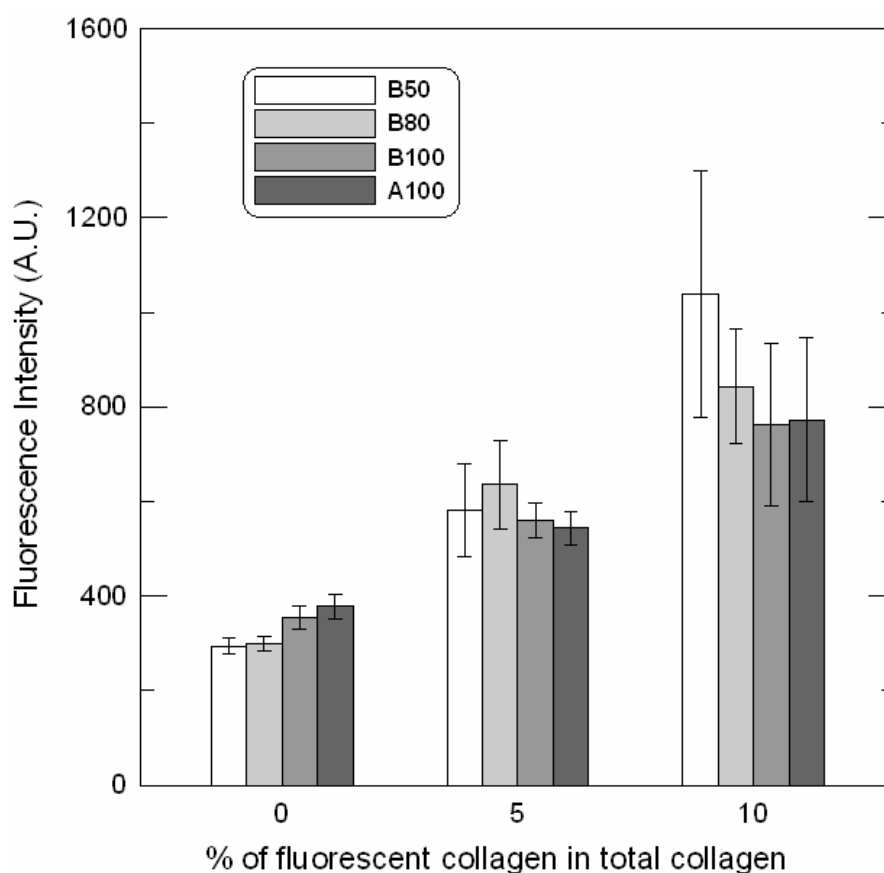


Figure 3B-6 Fluorescence intensity (in arbitrary units, A.U.) of bound type-I collagen, when 0%, 5% and 10% of total collagen is fluorescent, to the surface of the DNA gels. DNA gels are of Designs A and B and of different percentages of crosslinking. Error bars represent standard error of mean. $n \geq 8$.

3B.3.4 Spinal cord cell growth on DNA crosslinked gels

Rat spinal cord cells exhibit typical morphology on DNA gels (Fig. 3B-7). MAP2 and Tau-1 immunostaining (Fig. 3B-7:A-B) demonstrates neurite outgrowth on DNA gels. Neuronal cells extended processes (Fig. 3B-7:A-B and Fig. 3B-10). Only those isolated neurons with clear morphology were chosen for characterization of the primary dendrites. There were a variety of morphologies seen in GFAP+ mature astroglia, such as elongated fibroblastic (upper image in the inserts of Fig. 3B-7D) and process bearing (lower image in the inserts of Fig. 3B-7D) shapes. Among the intact cells (Fig. 3B-7C) on DNA gels, approximately 60% were MAP2+ neurons and GFAP+ mature astroglia, combined although the proportion of each cell type varies from 20% to 40%. The remaining 40% of the total cell population most likely contains immature astroglia, fibroblasts and neural precursor cells. Occasionally, relatively long neurites can be observed as illustrated in Fig. 3B-8.

It has been suggested that neurons might use astroglia as a soft substrate (with modulus of a few hundred Pa⁴⁹). On DNA gels, it was found that although some spinal cord neurons grew together with astroglia in relatively large aggregates (Fig. 3B-7:A-D), a significant proportion of the neurons adhered to DNA gels relatively far away from each other, in close proximity, or cluster in groups (Fig. 3B-7:A-C). Aggregates of spinal cord cells also occur on glass coverslips, although this occurs less often, and are attributable to interactions between cells due to factors, such as release of trophic factors.

The number of neurons, GFAP+ mature astroglia, and total intact cells (indicated by DAPI stain) increase as the gels become stiffer (Fig. 3B-9). The increase in neuronal and total cell number was significant between the stiffest (29.8 kPa) and the softest (6.6

kPa) gels, similar to the growth on bis-gels³⁹. The spinal cord cells rarely adhered to gel surfaces that were not functionalized, and direct incubation of non-functionalized gels with PDL did not improve cell attachment. In other words, functionalization of DNA gels is needed for protein conjugation and hence cell attachment.

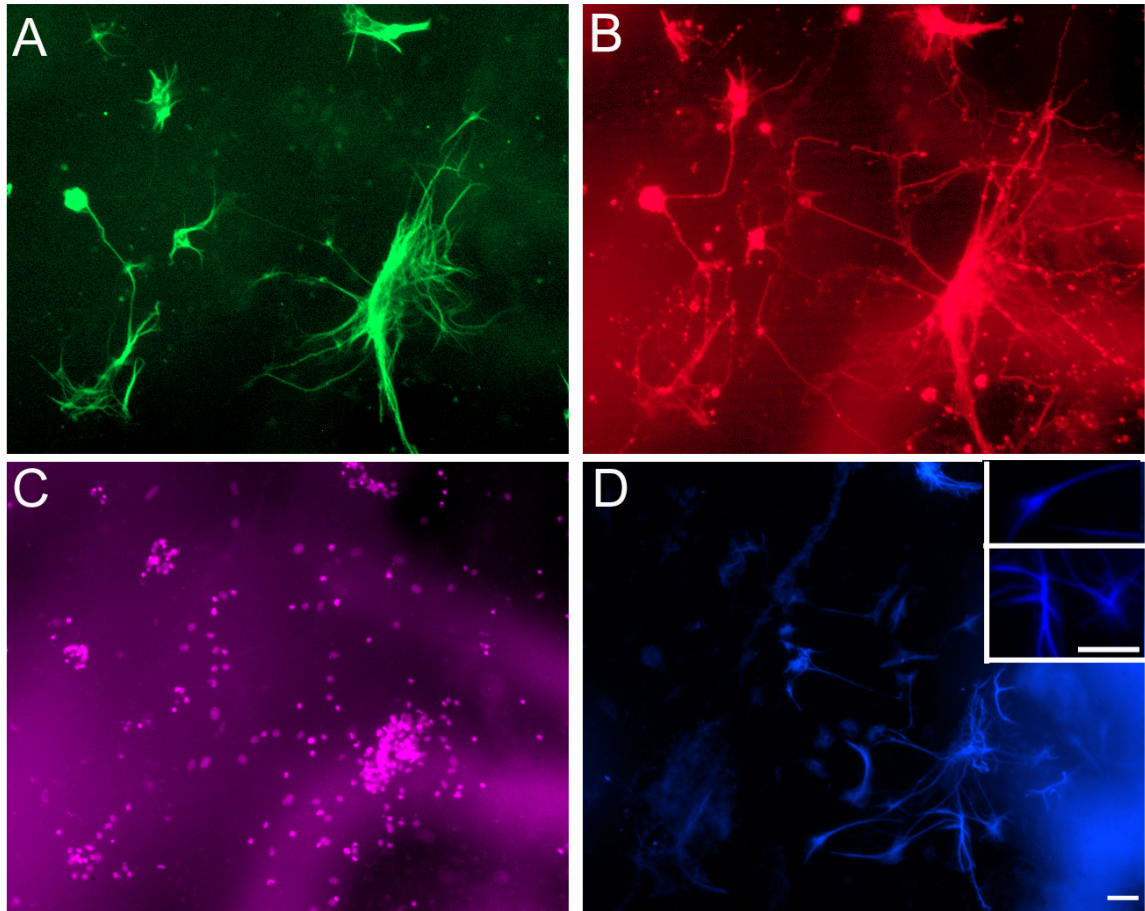


Figure 3B-7 Attachment and growth of rat spinal cord cells on DNA crosslinked gels. Low-power images of immunostaining of (A) MAP2 for dendrite and soma, (B) Tau-1 for axon, (C) DAPI staining for intact nuclei, and (D) GFAP for mature astroglia of the same area on the gel surface. Inserts of (D) illustrate the morphologies of astroglia with upper image showing elongated fibroblastic shape and lower one showing process-bearing shape. **Red: Tau-1** immunostaining; **Green: MAP2** immunostaining; **Blue: GFAP** immunostaining; **Purple: DAPI** staining. Scale bar is 50 μm .

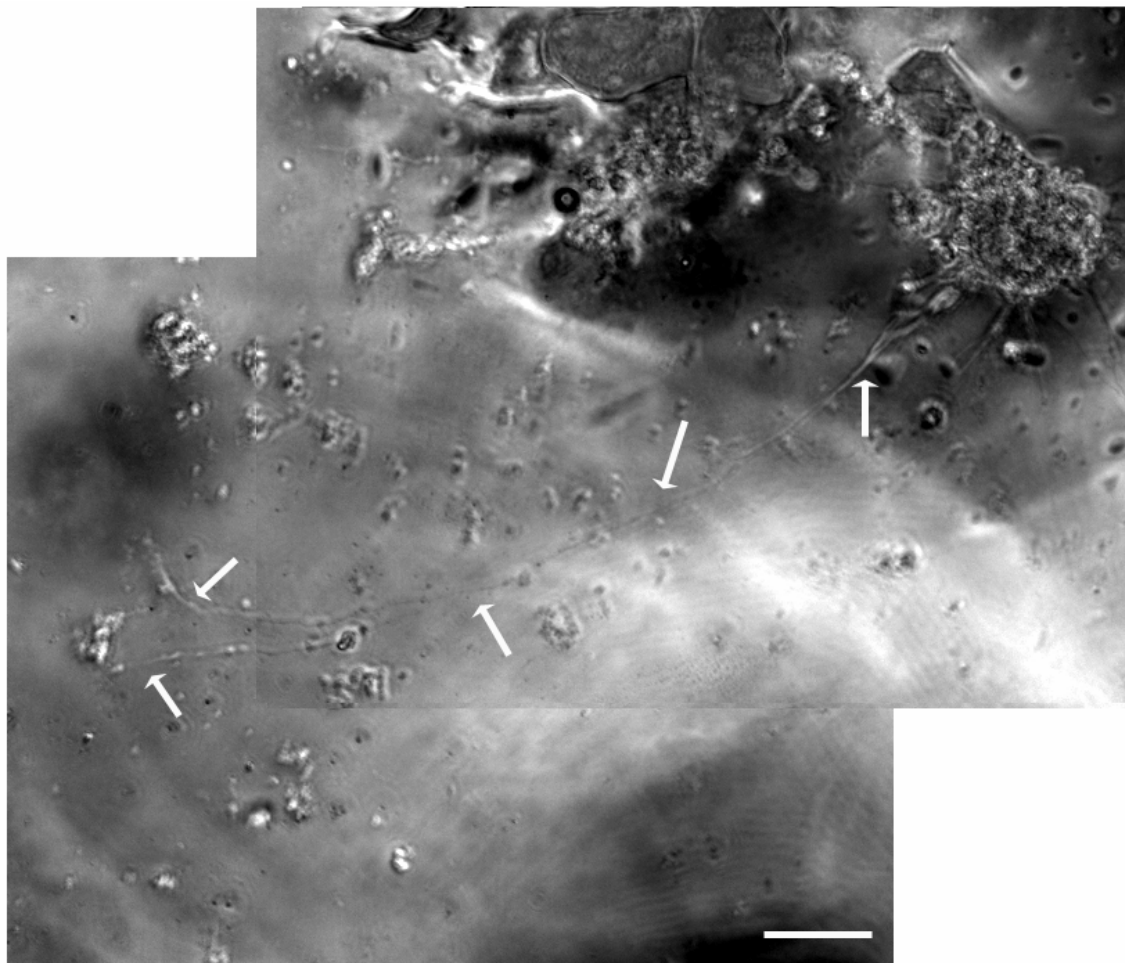


Figure 3B-8 Rat spinal cord cells extended processes on DNA crosslinked polyacrylamide hydrogels, with visible length of approximately 1 mm.
Scale bar: 100 μm .

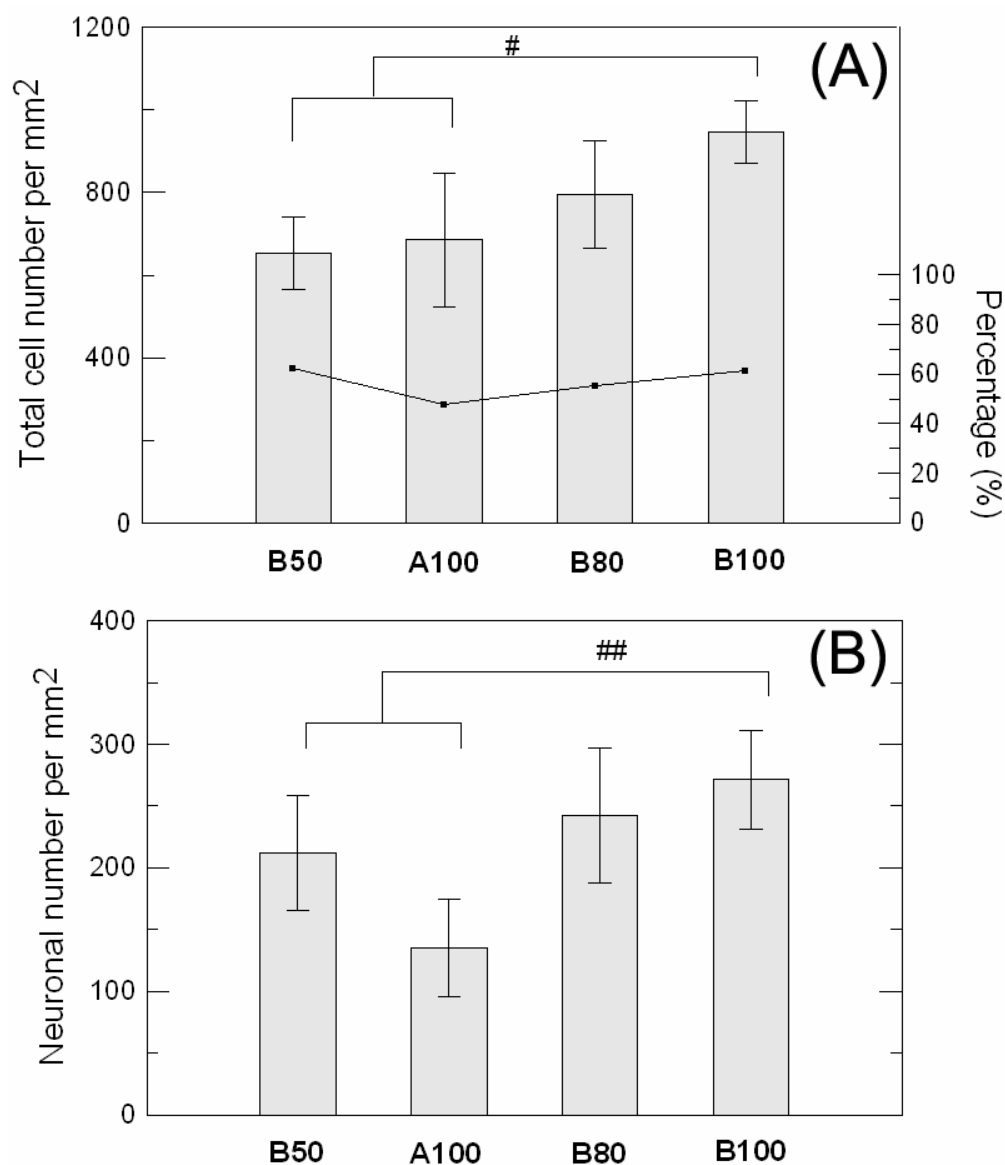


Figure 3B-9 Changes of MAP2+ neuron, GFAP+ astroglia, and total cell numbers in response to the stiffness of the DNA crosslinked gels.

A significant increase was observed in cell numbers when comparing those on the stiffest gels (B100) to those on the softest gels (A100 or B50) as determined by two-tailed unpaired *t*-test. ## $p < 0.005$ for total cell number and # $p < 0.01$ for neurons. No significant difference was found as determined by one-way ANOVA with Tukey's post-test for all four gel conditions. There was no significant difference in GFAP+ mature astroglia number among gel groups. Error bars represent standard error of mean. $n \geq 8$.

3B.3.5 Neurite outgrowth on DNA crosslinked gels

The neurons also extended axons on the DNA gels (arrow and arrowhead in Fig. 3B-10A). Typical multipolar morphology of neurons was observed (Fig. 3B-10B). In addition, it was previously reported that the specificity of Tau-1 staining on axons varies depending on factors such as the state of Tau-1 phosphorylation in hippocampal neuronal culture¹⁶. For spinal cord neurons, axons can be differentiated from dendrites based on Tau-1 staining (Figs. 3B-10 A and C). Tau-1 was also expressed in the soma of a small number of neurons.

To assess the effect of substrate stiffness on outgrowth of the primary dendrites, the number of primary dendrites was counted for each neuron, and the length of each dendrite (according to MAP2+ immunostaining) was measured only for those neurons with clear morphology. No significant differences in mean primary dendrite length per neuron were found for cells on DNA gels with stiffness ranging from 6.6 to 29.8 kPa (Fig. 3B-11A). However, there was a significant difference in primary dendrite number between gels with greatest stiffness (29.8 kPa) and the gels with the other three stiffnesses, and this increase is approximately 10% (Fig. 3B-11B). Comparison of axonal length per neuron on different DNA gel groups revealed a decrease of approximately 25% from gels with stiffnesses less than 10 kPa to those of tens of kPa (Fig. 3B-11C).

Neurite outgrowth of the total neuronal cell population was further examined. Consistent with the observation that changes in rigidity have no significant effect on the mean primary dendrite length, frequency plots showed that the proportion of neurons extending same lengths of neurite is not significantly changed (Figs. 3B-12 A1-A2). A greater proportion of neurons extend more primary dendrites as the substrates become

stiffer (Figs. 3B-12 B1-B2). Interestingly, the trend was the reversed for axonal length (Figs. 3B-12 C1-C2). Furthermore, a larger proportion of neurons have primary dendrites of approximately 40 μm (Figs. 3B-12 A1-A2), suggesting that the net rate of neurite elongation of these CNS neurons (not peripheral nervous system neurons) is approximately 10 μm per day, as neurons were seen to start extending processes on DIV 3 and were analyzed on DIV 6. For axons, the net rate of growth is approximately 25 μm per day, considering the majority of the neurons have axons of approximately 100 μm (Figs. 3B-12 C1-C2).

3B.3.6 FAK expression in neurons on DNA gels

To investigate possible alterations of FAK expression in neurons grown on DNA gels of different sequence designs or levels of crosslinking, double immunolabeling was performed with antibodies against FAK and MAP2. As shown in Fig. 3B-13:A-F, FAK is expressed in the soma, axons, and dendrites of neurons, with especially high abundance at growth cones and the ventral part of the soma where neurites originate^{8, 62, 69}. It was observed that certain MAP2 positive neurites were FAK negative, i.e. there was no detectable FAK expression in these neurites at the time of fixation. Quantification of FAK expression in the neuronal soma shows that as the substrate stiffens there is a significant reduction in FAK expression (Fig. 3B-13G), suggesting a negative correlation between DNA gel stiffness and FAK protein expression in neurons.

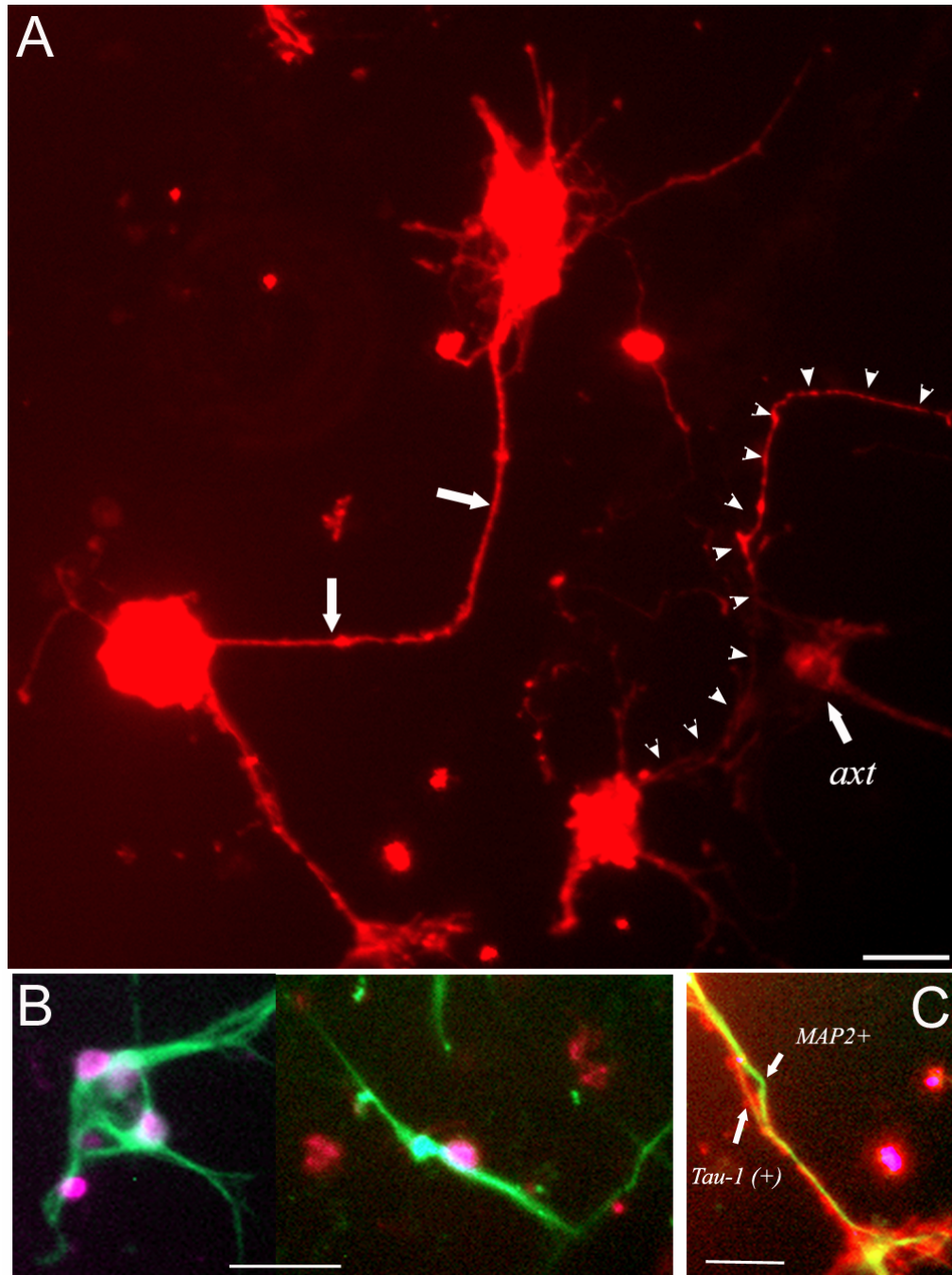


Figure 3B-10 Morphology of rat spinal cord neurons on DNA crosslinked hydrogels. (A) High-power image of Tau-1 staining shows axons (arrow and arrow head). Arrow points to the axon terminal (*axt*). (B) Spinal cord neurons with typical multi-polar morphologies. (C) Overlay of higher power images of MAP2 and Tau-1 stain reveals that axons and dendrites could reside closely in parallel with each other. **Red:** Tau-1 immunostaining; **Green:** MAP2 immunostaining; **Blue:** GFAP immunostaining; **Purple:** DAPI staining. Scale bar is 50 μ m.

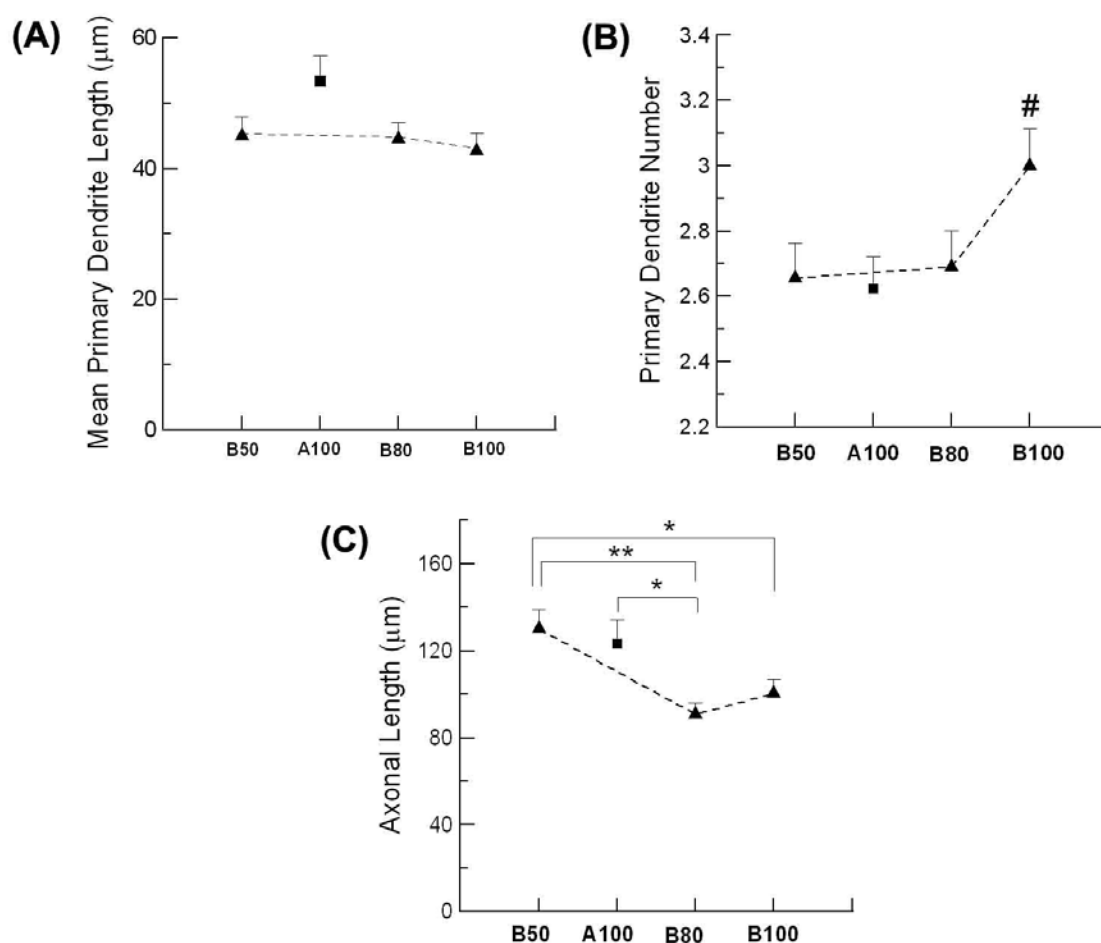


Figure 3B-11. Neurite outgrowth on DNA gels with different levels of crosslinking or with crosslinkers of different length and monomer concentration.

Comparison of neurite outgrowth, including mean primary dendrite length, primary dendrite number, and axonal length per neuron, on DNA gels of Designs A (■) and B (▲) (Table 3B-1). (A) Mean primary dendrite length. No significant difference between groups was observed. (B) Primary dendrite number. A significant difference was observed between stiffest gels (B100) and the rest of the three groups as determined by two-tailed unpaired *t*-test. # $p < 0.01$. No significant difference was found as determined by one-way ANOVA with Tukey's post-test for all four groups. (C) Axonal length. Axons on softer gels are significantly longer than that on stiffer gels as determined by one-way ANOVA followed by Tukey's test. * $p < 0.05$ between B50 and B100 gels and between A100 and B80 gels; ** $p < 0.01$ between B50 and B80 gels. Error bars represent standard error of mean. $n \geq 50$.

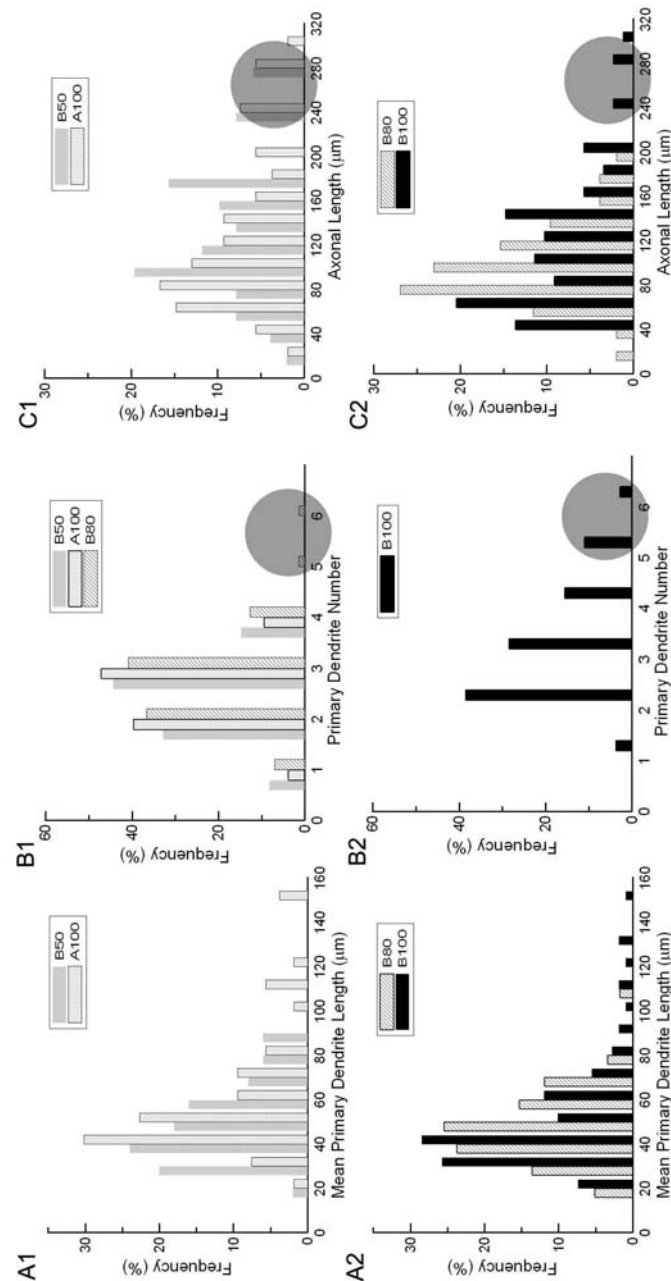


Figure 3B-12 Frequency plots of mean primary dendrite length (A), Primary dendrite number (B), and axonal length (C) per neuron on DNA gels of two designs.

(A) Proportion of neurons having different length of primary dendrites remains unchanged on DNA gels. (B) A larger proportion of neurons have over 4 primary dendrites on the stiffest gels (B100, dark color bar) than the other three groups (light color bars) as determined by Chi-square test ($p < 0.05$). (C) A smaller proportion of neurons have long (over 160 μm) axon on B80 and B100 gels (dark color bars) than those on B50 and A100 gels (light color bar), as determined by Chi-square test ($p < 0.01$). Comparisons were made between groups with bars of light color and those with bars of dark color.

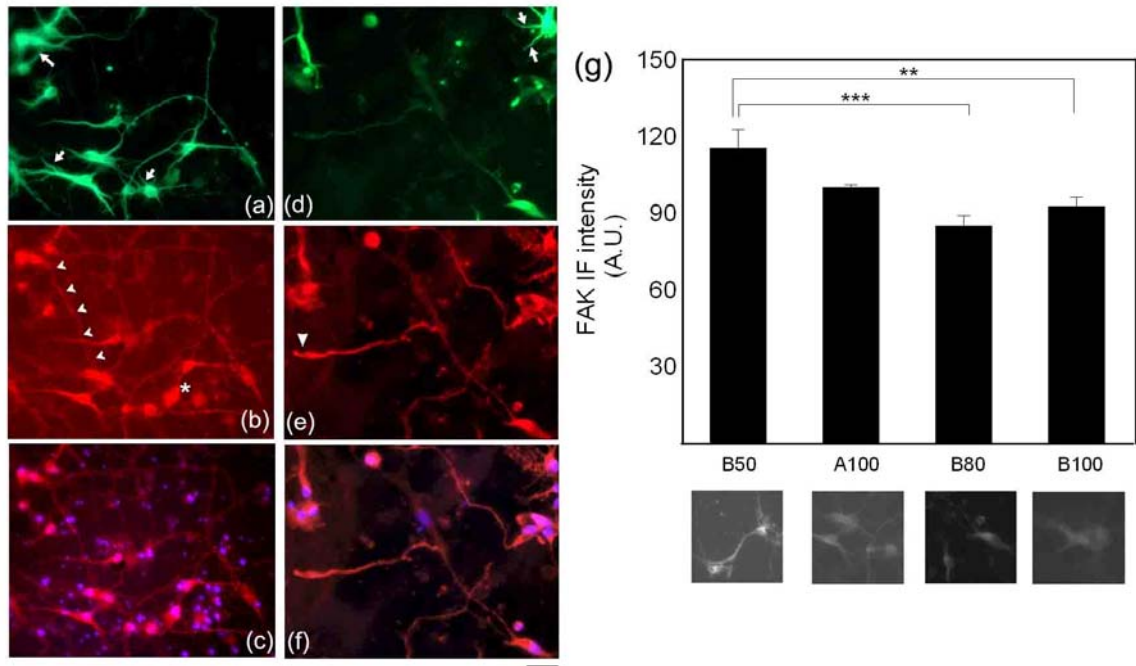


Figure 3B-13 Double immunolabeling and DAPI staining of spinal cord cells on DNA crosslinked gels of Designs A (A-C) and B (D-F) using monoclonal antibodies against MAP2 and focal adhesion kinase (FAK).

MAP2 immunoreactivity is shown in A and D, while FAK immunostaining in B and E. Overlay of FAK immunostaining and DAPI staining indicates that localization of FAK occurs at high levels in the cell body and at low levels in neurites (C and F). On DNA gels of Design A (A-C), FAK staining identifies axons (MAP2 negative, arrowhead in B) and FAK expression is low or absent on some dendrites (arrow in A). Similar observations were made on DNA gels of Design B (D-F). There is elevated expression of FAK at growth cones (arrowhead in E) when compared to the rest of the neurites. G. Quantification of focal adhesion kinase expression in the cell body of neurons grown on DNA gels of different designs or crosslinkers of different lengths. Immunofluorescence (IF) intensity (in arbitrary units, A. U.) on B50 gels is significantly higher than that on B80 gels (** $p < 0.001$) or B100 gels (** $p < 0.01$) as determined by one-way ANOVA followed by Tukey's multiple comparisons test. Representative images of FAK immunostaining are shown below the bar chart for each gel group. Error bars represent standard error of mean. $n \geq 19$. Red: Tau-1 immunostaining; Green: MAP2 immunostaining; Blue: GFAP immunostaining; Purple: DAPI staining. Scale bar is 30 μm .

3B.4 Discussion

3B.4.1 Mechanical sensitivity of neurite outgrowth

In the present work, based on the previous studies⁴⁷, the design parameter space has been expanded by including crosslinker length and monomer concentration. The stiffness range available has been extended from a few hundred Pa to 30 kPa, and it has been demonstrated that by altering the nanoscale structure in the network, gel properties can be modified. These gels were functionalized in a similar fashion to those crosslinked by bis-acrylamide, and the surface ligand density was found to be independent of the design of the DNA crosslinker or gel stiffness. As substrates become more rigid, neuronal and total cell number increase, while the proportion of neurons and astroglia combined in the total cell population remains stable, in line with observations made on bis-gels³⁹. Neurite outgrowth of primary spinal cord neurons was characterized, and it was found that cellular properties such as dendrite length, dendritic number, and axonal length respond differently to the distinct ranges of DNA gel stiffness, guiding design of gel stiffness to achieve specific cellular properties. The potential involvement of FAK, a critical regulator of many cellular activities, in neurite outgrowth in response to mechanical stimuli is suggested. A summary of the observations from this study is provided in Table 3B-3.

Compared to a very recent study⁴³, the current work focused on primary cells from dissociated rat spinal cord including neurons and astroglia, and a more physiologically relevant culture system than cell lines. Similar observations that primary dendrite length is not significantly different on gels of this stiffness range were made also

in reference⁴³, while in this work, it was found that primary dendrite number and axonal length, processes crucial to both development and recovery of the neural circuitry, were significantly affected by gel stiffness. The distinction in the observations between the two studies could be partly attributed to the difference in cell types and the presence of cell-cell interactions in the mixed culture. In comparison to the work by Georges and colleagues²⁷ on rat cortical neurons and Flanagan and co-workers²² on mouse spinal cord neurons, this study concentrated on spinal cord neuronal and astroglial adhesion in mixed culture, and outgrowth of both dendrites and axons, which have rarely been addressed and are of importance for understanding cellular mechano-responses for tailoring specific cellular properties for tissue engineering applications (e.g. axonal elongation for spinal cord injuries). Most of the previous studies on the effect of mechanical stimuli on cellular behavior have focused primarily on the end points, i.e., the lowest and highest stiffnesses. The possibility exists that cellular response to substrate stiffness is not monotonic, and information regarding the sensitivity towards the range of stiffness should also be important, which has been indicated previously⁴³. Therefore, in the current study, intermediate stiffnesses have been incorporated. Additionally, the range of substrate stiffness in our work (6.6 to 30 kPa) is also different than that in reference²² (150 Pa to 1650 Pa).

Table 3B-3 Summary of the observations of spinal cord cellular behavior as DNA gel mechanical stiffness increases from 6 kPa to 30 kPa

(↑ significant increase; ↓ significant decrease; → no significant change)

Parameters	Outcome	
Total cell number	↑	
Neuronal cell #	↑	
Astroglia cell #		→
Mean primary dendrite length per neuron		→
Maximal primary dendrite length per neuron		→
Total primary dendrite length per neuron		→
Primary dendrite number	↑	
Axonal length per neuron		↓
Proportion of neurons bearing longer primary dendrites		→
Proportion of neurons bearing higher primary dendrite number	↑	
Proportion of neurons bearing longer axons		↓
FAK expression in the neuronal cell body		↓

On DNA gels with mechanical stiffness ranging from a few kPa to 30 kPa, it was found that primary dendrite length is not sensitive to changes in rigidity (Fig. 3B-11A) but that primary dendrite number significantly increases. The increase occurs on gel stiffness between stiffnesses of 17.1 kPa and 29.8 kPa (Fig. 3B-11B), whereas a decrease in axonal length is evident before rigidity reaches 17.1 kPa (Fig. 3B-11C). Moreover, a greater proportion of neurons on stiffest gels have more primary dendrites (Fig. 3B-12B) and a higher proportion of neurons on DNA gels of stiffness lower than 17.1 kPa have longer axons (Fig. 3B-12C) than those of other groups. Taken together, these results suggest that there maybe a distinct sensitivity and threshold for specific properties of dendrites and axons (i.e., primary dendrite number, axonal length, secondary dendrite number or branching, etc.). This could be specific to spinal cord neurons, but nevertheless, this property is beneficial for biomaterial design for spinal cord nerve regeneration, i.e. to include mechanical stimuli in the bio-scaffold design. It should also be noted that there is no significant difference in neurite outgrowth on DNA gels with close stiffness of 6.6 kPa (Design B50) and 10 kPa (Design A100) (Fig. 3B-11), suggesting that physical properties other than stiffness do not significantly influence neurite outgrowth behavior (e.g., primary morphology).

Again, although mimicking the natural mechanical environment of the intact spinal cord is of concern, it is not without benefit to study a different range of mechanical properties of biomaterials to understand how to engineer a desired outcome, such as spinal cord nerve regeneration. Previously, it was reported that mechanosensing of neurons and astroglia could be altered by their interaction³⁹. Therefore, it is likely that neurite outgrowth behavior is a result of coupling between cell-substrate interactions and

cell-cell interactions, including neuron-neuron and neuron-astroglia communication. However, our previous study on neuron-glia interactions in a bis-gel system³⁹ has yielded findings that certain neuronal properties might not be changed. For example, when subjected to the same substrate stiffness, neuronal and astroglial survival varies while neurite outgrowth, including primary dendrite length and number remains the same under the absence and the presence of neuron-astroglia interactions. Thus, it is likely that primary morphology of neurons on DNA gels exhibit similar pattern and might not be significantly altered by the presence of astroglia. It is also possible that DNA gel substrate stiffness also affects secondary dendrites (i.e., neurites extending from a primary neurite), which remains to be investigated. For instance, the number, density or length of the secondary neurites could be affected in a way that could assume a pattern that differs from that of the primary ones.

3B.4.2 Mechanical stimuli provided by DNA gels

The correlation between the nano-scale structure in the DNA crosslinker and the mechanical stiffness of the bulk material was investigated. For the DNA gels of both Designs A and B, %T (monomer mass plus crosslinker at equivalent number of moles per 100 μ L of gel), an indicator of the amount of polymer mass, is approximately 7.7%, and %C (proportion of bis-acrylamide in monomer and crosslinker mixture) is approximately 0.06~0.13%, depending on the degree of crosslinking. This indicates that the polymer mass in the gel network of gels of both designs is not significantly different. However, mechanical testing suggested that the stiffness of gels of Design B100 is approximately 20% higher than that of Design A with 10% monomer. Conceptually, as the length of the

crosslinker DNA is reduced, long polymer chains are brought closer making it harder for polymer chains to slide by each other, which was suggested in a previous work⁵⁰ and also demonstrated numerically⁵⁵. It is noted that the energy to bend a DNA strand is inversely correlated to its length⁹, which might contribute to the distinctions between gels of two different crosslinker length. The comparisons between DNA gels of different crosslinker designs indicate that by modifying the nano-structure of the crosslinkers and/or monomer concentration, the physical properties, including mechanical stiffness, can be affected in a way that reflects the chemical structures and physical interactions of the components of the gels.

It is possible that alteration in DNA crosslinking leads to changes in modification of surface physical properties other than stiffness. It is noted that both polyacrylamide and DNA are completely wettable as evidenced by the fact that both are water soluble even at high concentration and high molecular weight. Meanwhile, DNA gels have low polymer density (the percent weight of polymer is approximately 7% for our gels), consisting mostly of water. Hence, the addition of extra crosslinker strands is not expected to significantly change the hydrophilicity or surface energy of the gel surface. Surface pore size has been shown to be important. In our studies, the pore size of the DNA gels might be larger than their bis-crosslinked counter-part whose pore size has been studied before and has been shown to be in the range of a few angstroms, considering that crosslinker DNA is a few nm (10 to 20 bases) and that bis-acrylamide is below 1 nm in length. However, the resulting pore size is most likely still well below the range (a few microns or higher³) that affects neural cell behavior. In addition, no significant neurite in-growth into the gels was noticed.

There are several reasons why polyacrylamide was chosen as the target polymer for DNA crosslinking. First, polyacrylamide hydrogels have long been used in *in vitro* studies as well as in medical applications, such as plastic surgery or soft tissue filler^{36, 70} where the monomer content is less than 1% (medical grade). Second, due to the incorporation of AcryditeTM in polymer formation, DNA crosslinking can also be applied to a number of other vinyl polymers^{10, 23}. One expects that DNA-crosslinked versions of these other polymers will exhibit behavior some, if not all, of which could be similar to DNA-crosslinked polyacrylamide. For instance, the effect of the crosslinker length and density on gel stiffness and the effect of stiffness on neurite growth might be comparable. Therefore, studies using DNA crosslinked polyacrylamide gels should provide general guidance for DNA-crosslinked polymer hydrogel design. Additionally, the results of studies on mechanosensing by neurons can be more meaningful when analyzed in the context of mechanobiology studies using a popular bis-gel system⁶⁸.

3B.4.3 FAK expression in neurons in response to stiffness

As a non-receptor tyrosine kinase, focal adhesion kinase (FAK), plays a critical role in mediating communication between cells and ECM via physical linkage, particularly focal adhesions (FAs) or point contacts⁷, and is heavily involved in various cellular processes, especially cellular mechanosensing and mechanotransduction^{6, 59, 60, 67, 71}. The dependence of formation of FAs on FAK has been reported to be different for neuronal and non-neuronal cells⁵⁷. In the central nervous system (CNS), FAK also plays important roles in the regulation of neuronal activities, ranging from neuronal migration during development and synapse formation to axonal growth, guidance, and branching, and

neurite outgrowth^{8, 41, 52, 56, 57, 59}. Taken together with previous findings that neurite outgrowth is altered as substrate stiffness changes^{22, 30, 39, 43}, it is tempting to speculate that FAK is involved in the neurite outgrowth in response to the mechanical characteristics of the ECM that neurons contact.

Indeed, here it was shown that FAK expression in the cell bodies of spinal cord neurons negatively correlates with mechanical stiffness (Fig. 3B-13G). A few major pathways have been proposed to be important for the mechanical signal transduction, namely mechanically-activated ion channels, transmembrane integrin and its binding to ECM, and cadherins and desmosomes between adjacent cells^{4, 71}. Most of the work has pointed to FAK due to its activation after binding of integrin to the ECM or following depolarization of the plasma membrane. Activation of FAK initiates a cascade of intracellular events in cellular responses to mechanical stimuli^{11, 24, 59}. Also, it was found that both axonal length and FAK expression decrease with increased gel stiffness, whereas primary dendrite number displays an opposite trend. Consequently, the data from this study suggest that decreased FAK expression in response to increased mechanical stiffness of ECM may be involved in the shortening of the axons, most likely by regulating netrin-mediated axonal guidance via activation of FAK and binding to netrin receptors⁷. Some investigators have reported that association of FAK and another tyrosine kinase, Pyk2, with integrin and growth factor receptors at adhesion sites participates in the regulation of neurite extension³⁷. This could contribute to mechanisms underlying outgrowth behavior of primary dendrites observed in the present work. Another possible mechanism is the interaction between FAK and Rho⁷ which has been shown to play an important role in the regulation of dendritic growth⁶⁵. Lastly, there has

been a recognition of the role of FAK in the regulation of F-actin dynamics, cytoskeleton remodeling, and focal adhesion turnover^{7, 59}. This could partly explain why some MAP2+ neurites are FAK negative in the present study, as also suggested in the work by Contestabile, et al.¹².

3B.5 Conclusions

It has been demonstrated that by varying the design parameters of DNA crosslinkers one is able to engineer the mechanical stiffness of hydrogels. Three parameters, namely crosslinker length, monomer concentration and degree of crosslinking, were chosen and the available stiffness from these DNA gels ranges from a few hundred Pa up to 30 kPa. These gels can be functionalized and conjugated with ECM proteins for neuronal cell attachment. Subject to the mechanical cues presented by the DNA gels, spinal cord neurons extend more primary dendrites and shorter axons on stiffer gels, as evidenced by the fact that a greater percentage of neurons have longer primary dendrites and shorter axons on gels of higher stiffness. The length and number of primary dendrites and length of the axons show distinct sensitivities to the range of stiffness. The expression of focal adhesion kinase (FAK) negatively correlates with the increase in gel substrate stiffness, suggesting its involvement in neuritogenesis in response to mechanical stiffness. The findings from this study are useful for incorporating mechanical cues in biomaterial design for neural tissue engineering applications.

References

1. Alemdaroglu, F. E., and A. Herrmann. DNA meets synthetic polymers--highly versatile hybrid materials. *Org Biomol Chem*. 5:1311-1320, 2007.
2. Badylak, S. F. The extracellular matrix as a biologic scaffold material. *Biomaterials*. 28:3587-3593, 2007.
3. Bakshi, A., O. Fisher, T. Dagci, B. T. Himes, I. Fischer, and A. Lowman. Mechanically engineered hydrogel scaffolds for axonal growth and angiogenesis after transplantation in spinal cord injury. *J Neurosurg Spine*. 1:322-329, 2004.
4. Banes, A. J., G. Lee, R. Graff, C. Otey, J. Archambault, M. Tsuzaki, M. Elfervig, and J. Qi. Mechanical forces and signaling in connective tissue cells: Cellular mechanisms of detection, transduction, and responses to mechanical deformation. *Current Opinion in Orthopaedics*. 12:389-396, 2001.
5. Bao, G., and S. Suresh. Cell and molecular mechanics of biological materials. *Nat Mater*. 2:715-725, 2003.
6. Bisht, B., H. L. Goel, and C. S. Dey. Focal adhesion kinase regulates insulin resistance in skeletal muscle. *Diabetologia*. 50:1058-1069, 2007.
7. Bonanomi, D., and F. Valtorta. Focal adhesion kinase in neuritogenesis In: I. de Curtis, editor. *Intracellular mechanisms for neuritogenesis*, Springer US: New York: NY, 2006; pp 155-179.
8. Burgaya, F., A. Menegon, M. Menegoz, F. Valtorta, and J. A. Girault. Focal adhesion kinase in rat central nervous system. *Eur J Neurosci*. 7:1810-1821, 1995.
9. Bustamante, C., Z. Bryant, and S. B. Smith. Ten years of tension: Single-molecule DNA mechanics. *Nature*. 421:423-427, 2003.
10. Carone, T. W., and J. M. Hasenwinkel. Mechanical and morphological characterization of homogeneous and bilayered poly(2-hydroxyethyl methacrylate) scaffolds for use in cns nerve regeneration. *J Biomed Mater Res B Appl Biomater*. 78:274-282, 2006.
11. Chen, L. M., D. Bailey, and C. Fernandez-Valle. Association of beta 1 integrin with focal adhesion kinase and paxillin in differentiating schwann cells. *J Neurosci*. 20:3776-3784, 2000.
12. Contestabile, A., D. Bonanomi, F. Burgaya, J. A. Girault, and F. Valtorta. Localization of focal adhesion kinase isoforms in cells of the central nervous system. *Int J Dev Neurosci*. 21:83-93, 2003.
13. Cukierman, E., R. Pankov, D. R. Stevens, and K. M. Yamada. Taking cell-matrix adhesions to the third dimension. *Science*. 294:1708-1712, 2001.
14. Curtis, A., and M. Riehle. Tissue engineering: The biophysical background. *Phys Med Biol*. 46:R47-65, 2001.
15. Dalton, P. D., L. Flynn, and M. S. Shoichet. Manufacture of poly(2-hydroxyethyl methacrylate-co-methyl methacrylate) hydrogel tubes for use as nerve guidance channels. *Biomaterials*. 23:3843-3851, 2002.
16. Dotti, C. G., G. A. Banker, and L. I. Binder. The expression and distribution of the microtubule-associated proteins tau and microtubule-associated protein 2 in hippocampal neurons in the rat in situ and in cell culture. *Neuroscience*. 23:121-130, 1987.

17. Duan, X., and H. Sheardown. Dendrimer crosslinked collagen as a corneal tissue engineering scaffold: Mechanical properties and corneal epithelial cell interactions. *Biomaterials*. 27:4608-4617, 2006.
18. El Haj, A. Biomechanical interactions in tissue engineering and surgical repair (bites). *Med Biol Eng Comput*. 42:2, 2004.
19. Engler, A., L. Bacakova, C. Newman, A. Hategan, M. Griffin, and D. Discher. Substrate compliance versus ligand density in cell on gel responses. *Biophys J*. 86:617-628, 2004.
20. Fawcett, J. Repair of spinal cord injuries: Where are we, where are we going? *Spinal Cord*. 40:615-623, 2002.
21. Feng, Z., M. Yamato, T. Akutsu, T. Nakamura, T. Okano, and M. Umezu. Investigation on the mechanical properties of contracted collagen gels as a scaffold for tissue engineering. *Artif Organs*. 27:84-91, 2003.
22. Flanagan, L. A., Y. E. Ju, B. Marg, M. Osterfield, and P. A. Janmey. Neurite branching on deformable substrates. *Neuroreport*. 13:2411-2415, 2002.
23. Flynn, L., P. D. Dalton, and M. S. Shoichet. Fiber templating of poly(2-hydroxyethyl methacrylate) for neural tissue engineering. *Biomaterials*. 24:4265-4272, 2003.
24. Garcia, A. J., and D. Boettiger. Integrin-fibronectin interactions at the cell-material interface: Initial integrin binding and signaling. *Biomaterials*. 20:2427-2433, 1999.
25. Gaudet, C., W. A. Marganski, S. Kim, C. T. Brown, V. Gunderia, M. Dembo, and J. Y. Wong. Influence of type I collagen surface density on fibroblast spreading, motility, and contractility. *Biophys J*. 85:3329-3335, 2003.
26. Gefen, A., N. Gefen, Q. Zhu, R. Raghupathi, and S. S. Margulies. Age-dependent changes in material properties of the brain and braincase of the rat. *J Neurotrauma*. 20:1163-1177, 2003.
27. Georges, P. C., W. J. Miller, D. F. Meaney, E. S. Sawyer, and P. A. Janmey. Matrices with compliance comparable to that of brain tissue select neuronal over glial growth in mixed cortical cultures. *Biophys J*. 90:3012-3018, 2006.
28. Greenebaum, B., C. H. Sutton, M. S. Vadula, J. H. Battocletti, T. Swiontek, J. DeKeyser, and B. F. Siskin. Effects of pulsed magnetic fields on neurite outgrowth from chick embryo dorsal root ganglia. *Bioelectromagnetics*. 17:293-302, 1996.
29. Guldberg, R. E. Consideration of mechanical factors. *Ann N Y Acad Sci*. 961:312-314, 2002.
30. Gunn, J. W., S. D. Turner, and B. K. Mann. Adhesive and mechanical properties of hydrogels influence neurite extension. *J Biomed Mater Res A*. 72:91-97, 2005.
31. Haisch, A., G. N. Duda, D. Schroeder, A. Groger, C. Gebert, K. Leder, and M. Sitter. The morphology and biomechanical characteristics of subcutaneously implanted tissue-engineered human septal cartilage. *Eur Arch Otorhinolaryngol*. 262:993-997, 2005.
32. Hidalgo-Bastida, L. A., J. J. Barry, N. M. Everitt, F. R. Rose, L. D. Buttery, I. P. Hall, W. C. Claycomb, and K. M. Shakesheff. Cell adhesion and mechanical properties of a flexible scaffold for cardiac tissue engineering. *Acta Biomater*. 3:457-462, 2007.

33. Hirakawa, K., K. Hashizume, and T. Hayashi. [viscoelastic property of human brain -for the analysis of impact injury (author's transl)]. *No To Shinkei*. 33:1057-1065, 1981.
34. Horkay, F., I. Tasaki, and P. J. Basser. Osmotic swelling of polyacrylate hydrogels in physiological salt solutions. *Biomacromolecules*. 1:84-90, 2000.
35. Horn, E. M., M. Beaumont, X. Z. Shu, A. Harvey, G. D. Prestwich, K. M. Horn, A. R. Gibson, M. C. Preul, and A. Panitch. Influence of cross-linked hyaluronic acid hydrogels on neurite outgrowth and recovery from spinal cord injury. *J Neurosurg Spine*. 6:133-140, 2007.
36. Hruza, G. J. Polyacrylamide hydrogel soft-tissue filler is safe and effective. *Journal Watch Dermatology*. 116:1137-1148 2005.
37. Ivankovic-Dikic, I., E. Gronroos, A. Blaukat, B. U. Barth, and I. Dikic. Pyk2 and fak regulate neurite outgrowth induced by growth factors and integrins. *Nat Cell Biol*. 2:574-581, 2000.
38. Jiang, F. X., B. Yurke, B. L. Firestein, and N. A. Langrana. Neurite outgrowth on a DNA crosslinked hydrogel with tunable stiffnesses. *Ann Biomed Eng*. 36:1565-1579, 2008.
39. Jiang, X., P. C. Georges, B. Li, Y. Du, M. K. Kutting, M. L. Previtera, N. A. Langrana, and B. L. Firestein. Cell growth in response to mechanical stiffness is affected by neuron-astroglia interactions. *Open Neuroscience Journal*. 1:7-14, 2007.
40. Khatiwala, C. B., S. R. Peyton, and A. J. Putnam. Intrinsic mechanical properties of the extracellular matrix affect the behavior of pre-osteoblastic mc3t3-e1 cells. *Am J Physiol Cell Physiol*. 290:C1640-1650, 2006.
41. Kornack, D. R., and R. J. Giger. Probing microtubule +tips: Regulation of axon branching. *Curr Opin Neurobiol*. 15:58-66, 2005.
42. Kuhn, T. B., E. T. Stoeckli, M. A. Condrau, F. G. Rathjen, and P. Sonderegger. Neurite outgrowth on immobilized axonin-1 is mediated by a heterophilic interaction with 11(g4). *J Cell Biol*. 115:1113-1126, 1991.
43. Leach, J. B., X. Q. Brown, J. G. Jacot, P. A. Dimilla, and J. Y. Wong. Neurite outgrowth and branching of pc12 cells on very soft substrates sharply decreases below a threshold of substrate rigidity. *J Neural Eng*. 4:26-34, 2007.
44. Li, L., N. Sharma, U. Chippada, X. Jiang, R. Schloss, M. L. Yarmush, and N. A. Langrana. Functional modulation of es-derived hepatocyte lineage cells via substrate compliance alteration. *Ann Biomed Eng*. 36:865-876, 2008.
45. Liedl, T., H. Dietz, and B. Yurke. Controlled trapping and release of quantum dots in a DNA-linked hydrogel. (accepted). 2007.
46. Lin, D., N. Langrana, and B. Yurke. Inducing reversible stiffness changes in DNA-crosslinked gels. *Journal of Materials Research*. 20:1456-1464, 2006.
47. Lin, D. C., B. Yurke, and N. A. Langrana. Mechanical properties of a reversible, DNA-crosslinked polyacrylamide hydrogel. *J Biomech Eng*. 126:104-110, 2004.
48. Lin, D. C. (2005). Design and properties of a new DNA-crosslinked polymer hydrogel, *Mechanical & Aerospace Engineering*, Piscataway, NJ: Rutgers University.
49. Lu, Y. B., K. Franze, G. Seifert, C. Steinhauser, F. Kirchhoff, H. Wolburg, J. Guck, P. Janmey, E. Q. Wei, J. Kas, and A. Reichenbach. Viscoelastic properties

- of individual glial cells and neurons in the cns. *Proc Natl Acad Sci U S A*. 103:17759-17764, 2006.
50. Mabileau, G., I. C. Stancu, T. Honore, G. Legeay, C. Cincu, M. F. Basle, and D. Chappard. Effects of the length of crosslink chain on poly(2-hydroxyethyl methacrylate) (phema) swelling and biomechanical properties. *J Biomed Mater Res A*. 77:35-42, 2006.
 51. Miller, K., K. Chinzei, G. Orsengo, and P. Bednarz. Mechanical properties of brain tissue in-vivo: Experiment and computer simulation. *J Biomech*. 33:1369-1376, 2000.
 52. Nikolic, M. The molecular mystery of neuronal migration: Fak and cdk5. *Trends Cell Biol*. 14:1-5, 2004.
 53. Novikova, L. N., L. N. Novikov, and J. O. Kellerth. Biopolymers and biodegradable smart implants for tissue regeneration after spinal cord injury. *Curr Opin Neurol*. 16:711-715, 2003.
 54. Pedersen, J. A., and M. A. Swartz. Mechanobiology in the third dimension. *Ann Biomed Eng*. 33:1469-1490, 2005.
 55. Rafaels, K., J. Kerrigan, N. Langrana, and D. Lin. Molecular modeling as a visualization tool in design of DNA crosslinked polyacrylamide, Anaheim, CANovember 2004.
 56. Rico, B., H. E. Beggs, D. Schahin-Reed, N. Kimes, A. Schmidt, and L. F. Reichardt. Control of axonal branching and synapse formation by focal adhesion kinase. *Nat Neurosci*. 7:1059-1069, 2004.
 57. Robles, E., and T. M. Gomez. Focal adhesion kinase signaling at sites of integrin-mediated adhesion controls axon pathfinding. *Nat Neurosci*. 9:1274-1283, 2006.
 58. Rosso, F., A. Giordano, M. Barbarisi, and A. Barbarisi. From cell-ecm interactions to tissue engineering. *J Cell Physiol*. 199:174-180, 2004.
 59. Schober, M., S. Raghavan, M. Nikolova, L. Polak, H. A. Pasolli, H. E. Beggs, L. F. Reichardt, and E. Fuchs. Focal adhesion kinase modulates tension signaling to control actin and focal adhesion dynamics. *J Cell Biol*. 176:667-680, 2007.
 60. Schwarz, U. S., N. Q. Balaban, D. Rivelin, L. Addadi, A. Bershadsky, S. A. Safran, and B. Geiger. Measurement of cellular forces at focal adhesions using elastic micro-patterned substrates. *Materials Science & Engineering C-Biomimetic and Supramolecular Systems*. 23:387-394, 2003.
 61. Spector, M. Novel cell-scaffold interactions encountered in tissue engineering: Contractile behavior of musculoskeletal connective tissue cells. *Tissue Eng*. 8:351-357, 2002.
 62. Stevens, G. R., C. Zhang, M. M. Berg, M. P. Lambert, K. Barber, I. Cantallops, A. Routtenberg, and W. L. Klein. CNS neuronal focal adhesion kinase forms clusters that co-localize with vinculin. *J Neurosci Res*. 46:445-455, 1996.
 63. Taqvi, S., and K. Roy. Influence of scaffold physical properties and stromal cell coculture on hematopoietic differentiation of mouse embryonic stem cells. *Biomaterials*. 27:6024-6031, 2006.
 64. Teng, Y. D., E. B. Lavik, X. Qu, K. I. Park, J. Ourednik, D. Zurakowski, R. Langer, and E. Y. Snyder. Functional recovery following traumatic spinal cord injury mediated by a unique polymer scaffold seeded with neural stem cells. *Proc Natl Acad Sci U S A*. 99:3024-3029, 2002.

65. Threadgill, R., K. Bobb, and A. Ghosh. Regulation of dendritic growth and remodeling by rho, rac, and cdc42. *Neuron*. 19:625-634, 1997.
66. Vickers, S. M., L. S. Squitieri, and M. Spector. Effects of cross-linking type ii collagen-gag scaffolds on chondrogenesis in vitro: Dynamic pore reduction promotes cartilage formation. *Tissue Eng.* 12:1345-1355, 2006.
67. Wang, H. B., M. Dembo, S. K. Hanks, and Y. Wang. Focal adhesion kinase is involved in mechanosensing during fibroblast migration. *Proc Natl Acad Sci U S A*. 98:11295-11300, 2001.
68. Wang, Y. L., and R. J. Pelham, Jr. Preparation of a flexible, porous polyacrylamide substrate for mechanical studies of cultured cells. *Methods Enzymol.* 298:489-496, 1998.
69. Williamson, R., T. Scales, B. R. Clark, G. Gibb, C. H. Reynolds, S. Kellie, I. N. Bird, I. M. Varndell, P. W. Sheppard, I. Everall, and B. H. Anderton. Rapid tyrosine phosphorylation of neuronal proteins including tau and focal adhesion kinase in response to amyloid-beta peptide exposure: Involvement of src family protein kinases. *J Neurosci.* 22:10-20, 2002.
70. Xi, T. F., C. X. Fan, X. M. Feng, Z. Y. Wan, C. R. Wang, and L. L. Chou. Cytotoxicity and altered c-myc gene expression by medical polyacrylamide hydrogel. *J Biomed Mater Res A*. 78:283-290, 2006.
71. Zhu, C., G. Bao, and N. Wang. Cell mechanics: Mechanical response, cell adhesion, and molecular deformation. *Annu Rev Biomed Eng.* 2:189-226, 2000.

CHAPTER 4 GELS WITH DYNAMIC STIFFNESS

CHAPTER 4A ACELLULAR STUDIES

4A.1 Background

4A.1.1 DNA diffusion

In the current studies, DNA strands with specific sequence design were delivered to change the crosslinking level of the DNA gels. After DNA is delivered to the solution where DNA gels are immersed, we primarily rely on diffusion to drive the DNA strands into the gel network¹. Although in previous work electrophoretic forces were applied⁵ to drive DNA into DNA gels, this has limited applicability for *in vitro* and *in vivo* studies.

The pore size of the DNA crosslinked polyacrylamide gels in the current work is likely in the range of 10~100 nm, since that of their bis-crosslinked counterparts is in the tens of nanometer range⁸. The diameter of the flexible single-stranded DNA is much smaller than that of double-stranded DNA (approximately 2 nm^{6, 11}). The diffusion of ssDNA into a hydrogel is dependent on the initial DNA concentration, temperature, the relative size of the DNA strand to the average pore diameter, and the surface area for diffusion. The diffusion will continue until equilibrium in the DNA concentration between inside and outside the gel network is established, as it is essentially driven by concentration difference across the gel surface. In addition, once the DNA gets into the gel, it base-pairs with available SA1 and SA2 DNA side chains (Figures 2-1 and 3B-1), driving the equilibrium to the direction to force more ssDNA into the gel network.

4A.1.2 Previous DNA gel study with DNA delivery

The changes in the properties of DNA crosslinked hydrogels have been reported and studied by both our group⁵ and others¹². In our group, Lin and colleagues⁵ found that with the delivery of ‘fuel strands’, the stiffness of the gels increases two-fold from approximately 200 Pa to 640 Pa; with the initial delivery of the exact amount needed to occupy all the binding sites on the DNA crosslinks. The delivery process, driven by application of an electric field, required eight hours⁵. It is thus hypothesized that without the electric field, the time frame for diffusion would be much greater. However, in the preparation of DNA gels for cell culture, the gels were relatively thin (500~1000 μm in thickness) and the surface area is much larger than that in the funnel as used by Lin and colleagues⁵, thus it was expected the time frame for incorporation of DNA in these two systems would be comparable. However, it is important to directly determine the time scale with which the DNA incorporation into gel network occurs; and it is important to monitor the mechanical stiffness change with time.

4A.1.3 Hydrogel property change upon DNA delivery

The incorporation of crosslinker DNA or its complement into the gel network could result in a change in the crosslinking density, which, in turn, leads to stiffness change and a sol-gel transition if the critical gelation point is reached^{5, 12}. An interesting illustration of this is provided by recent work in which de-gelation is induced by adenosine aptamer interactions¹³.

An increase in the level of crosslinking in the hydrogel network could also potentially cause the compaction or shrinking of the substrate that cells are residing on,

since the change in the crosslinking density could lead to the change in swelling equilibrium^{3, 9, 10}. In addition, the increase or decrease in the degree of crosslinking may directly cause volume change as it affects the inner structure of the gel network. This possibility has attracted much interest^{2, 4, 7}. It is, therefore, conceivable that by altering the crosslinking density, two mechanical stimuli could surface, one of which is the mechanical stiffness and the other is the gel compaction or expansion. If the DNA application occurs while cells are growing in place, the volume change in the gels could translate into compressive or tensile forces that cells respond to.

4A.1.4 Gel preparation using DNA without purification

The DNA strands used in this work were primarily acquired from Integrated DNA technologies (Coralville, IA), and the cost for purification (HPLC or PAGE) consists over half of the total cost of the synthesized DNA strands. On the condition that the absence of purification does not significantly change the DNA gel preparation and crosslinking, it is advantageous to consider alternatives to the purification, or to simply avoid applying purification. The estimated purity according to the IDT for DNA gels of three different available sequence designs is shown in Figure 4A-1. For the rest of the dissertation, the DNA strands without HPLC or PAGE purification were used.

4A.1.5 The purpose of the acellular study

As has been discussed, the acellular study mimicking the cellular conditions was designed to confirm DNA incorporation into the gel network under the conditions applied

in cellular testing. The potential local deformation of DNA gel upon DNA strand delivery and after the change in the crosslinking level was also estimated.

4A.2 DNA incorporation into the gel network

4A.2.1 Rationale

By measuring the quantity of DNA residual in the aqueous solution where the DNA gel resides, one should be able to infer the amount of delivered DNA that is incorporated into the gel network. To eliminate the possibility that DNA strands stay in the gel network but do not participate in the crosslinking and thus do not contribute to the mechanical property change of the gels, a negative control is deployed where a DNA strand with the size comparable to that of the intended crosslinker DNA but with non-specific sequence is employed.

4A.2.2 Materials and Methods

4A.2.2.1 Calibration of multi-mode plate reader

Spectrophotometric measurement of DNA concentration is performed by using a microplate reader (DTX 800, Beckman Coulter, Fullerton, CA). A series of dilution of crosslinker DNA solution was used to assess the linearity correlating the optical density reading and the DNA concentration. A DNA sample solution with initial concentration of 1.22 mg/L was used and a series of samples with dilution of 1 to 300, 600, 1200, 2400, 4800, 9600, and 19200 were prepared.

4A.2.2.2 DNA gel preparation

We followed the procedures outlined in Chapter 3B in synthesizing DNA crosslinked hydrogels. Design B of DNA gels (14/14/40, Appendix 2) was adopted to mimic the conditions in fibroblast culture.

Five groups of DNA gels of Design B at 50% crosslinking, two groups of DNA gels at 80% crosslinking, and one group of 100% crosslinking were prepared and immobilized (Table 4A-1), in a manner similar to those used for fibroblast cell culture, except that they did not go through functionalization and protein conjugation. The gel groups were rinsed in DPBS (Dulbecco's Modified Buffer Saline) containing Ca^{2+} and Mg^{2+} (Sigma-Aldrich) at 1 mL/well in a 24 well plate. The samples were also kept in the incubator at 37C for two days in a way mimicking the conditions in cell culture, to allow the gel to swell to equilibrium and to release prestress in the DNA gels⁵.

4A.2.2.3 Spectrophotometric determination of DNA concentration

At the end of the two days (Day 2) of incubation, the buffer in the wells for the previous step was changed and the proper amount of DNA crosslinker solution (according to Table 4A-1) was delivered. Two control groups with no DNA gels were prepared, to which 0% and 50% of crosslinker needed for full crosslinking was delivered. Two days (Day 4) following the incubation of these samples after DNA addition, the buffer rinsing the gels was collected. The concentration of the single-stranded DNA in the medium was evaluated by using aforementioned multi-mode micro-plate reader. The collected solution was transferred to a UV plate (Corning Costar #3635, Sigma Aldrich) to be fed into the microplate reader.

4A.2.3 Results

4A.2.3.1 Calibration of multi-mode plate reader

To substantiate DNA incorporation into the gel network after delivery, we prepared DNA gels exactly the same way they were prepared in cellular experiments including DNA delivery and gel incubation, except for the functionalization and cell plating. DNA concentration measurement was performed on the buffer solution in which DNA gels were kept and stored for duration of two days after delivery. The DNA concentration has been obtained by multiplication of the optical density (O.D.) reading from the microplate reader and the converting factors (33 for ssDNA and 50 for dsDNA) as well as dilution. The results are shown in Figure 4A-2. The linearity between DNA concentration and reading from micro-plate in the range of 0 to 1.3 was confirmed.

4A.2.2.2 DNA concentration measurement

The DNA concentrations in DPBS buffer (with Ca^{++} and Mg^{++} , Sigma Aldrich) were measured and the raw data are as shown in Figure 4A-3. It is apparent that the reading contains the contribution from the auto-fluorescence from the buffer (reading for 0% sample, Figure 4A-3). Moreover, in the gel groups with no DNA delivery (i.e., D50, D80 and D100 groups, Figure 4A-3), there is a significant reading, which most likely is due to both auto-fluorescence of the buffer and small pieces of DNA gel that sheds from the bulk of the DNA gels, or non-specific ssDNA strands owing to the exclusion of DNA purification.

After subtracting the part of the contribution due to auto fluorescence of DPBS buffer, fragmented polymer gel pieces and non-specific DNA strands, the results are shown in Figure 4A-4. From the fact that the DNA concentrations in two sample groups, D50_Non and 50%, were comparable, it is evident that only DNA strands with specific sequence that is complementary to the crosslinker DNA can be taken up by the DNA gels and removed from the solution. There might be some of the DNA strands that entered into the gels do not participate in crosslinking, but their quantity is negligible. Comparison among gel groups of initial 50% crosslinking density (D50, D50_80, and D50_100) demonstrates that the majority of the DNA strands delivered diffused into the gel network and were incorporated (Figure 4A-4). This was also seen for the DNA gel groups with initial 80% crosslinking level.

4A.2.4 Summary

It was confirmed that the majority of the delivered DNA strands were indeed incorporated into the gel network. We assessed DNA strand incorporation by using gels of Design B (14/14/40, Appendix 2). However, we expect DNA gel with Designs A (used in neuronal dynamic study) and B to behave in the same manner in terms of DNA incorporation. The incorporation of the complementary strands to crosslinker DNA into the gel network is also anticipated to behave in the same manner. These strands were used in the study of neuronal responses towards dynamic stiffness (Chapter 4C) where gels of Design A were used.

4A.3 Discussion

In this chapter, by assessing the reduction in the purity of acquired DNA strands, we have determined the use of DNA strand without HPLC or PAGE purification as a way of carrying out experiments while reducing the cost. The incorporation of the crosslinker DNA into the gel network has been confirmed by measuring the residual DNA concentration. This is a way of indirectly probing the incorporation of the delivered DNA strands. In a separate line of research, with the help of micro-beads which serve as location markers inside the DNA gel, we attempted to quantify the local deformation (Appendix 1). We have showed that, based on a limited number of testings and estimation, the DNA delivery induced deformation, under the specific conditions of our cellular studies, including medium volume, quantity of DNA delivered, delivery profile, and time course followed, is most likely not sufficient to induce towed neurite elongation. Much larger strain generation and force application may be feasible with different experimental conditions, and this is being pursued in ongoing investigation.

Therefore, we concluded that the alteration in the elongation of the neurites will be attributed primarily to the stiffness change caused by changes in DNA gel crosslinking level.

Table 4A-1 The initial and final crosslinking density of different schemes of crosslinker DNA delivery.

Designation	D50	D50_80	D50_100	D50_Non	D80	D80_100	D100
Initial crosslinking density	50%	50%	50%	50%	80%	80%	100%
Final crosslinking density	50%	80%	100%	50%	80%	100%	100%
DNA delivery	—	30%	50%	50%*	—	20%	—

*ssDNA strands of non-specific sequence were delivered.

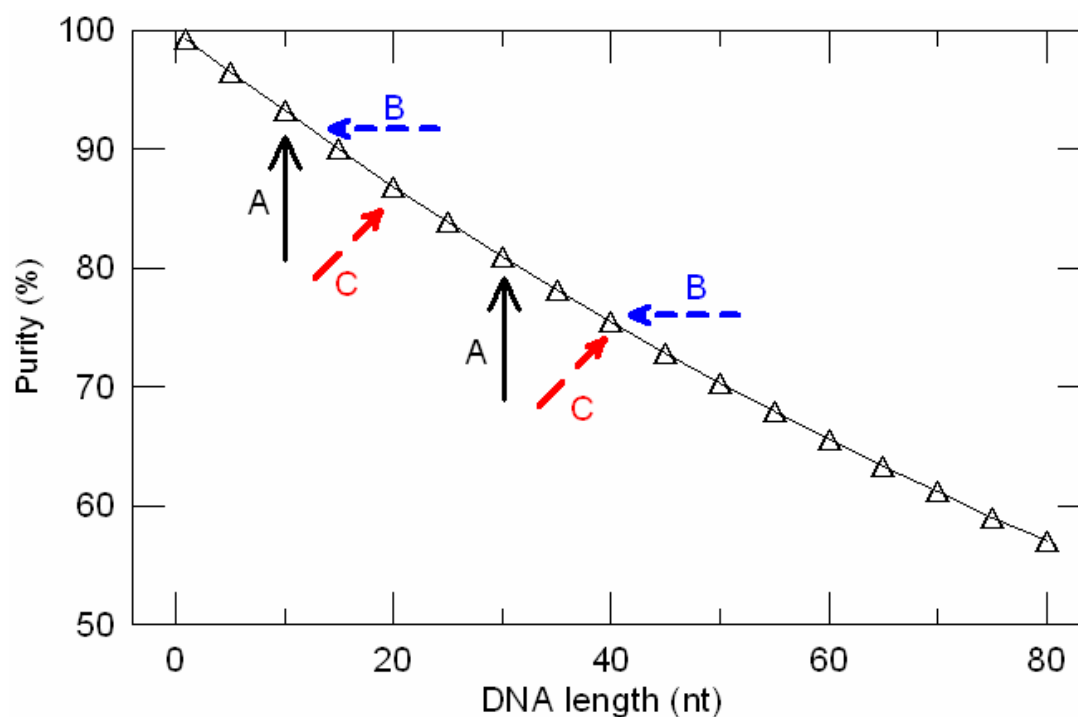


Figure 4A-1 Change of DNA purity with the length of the ssDNA used in DNA gel designs of A, B, and C (Appendix 2).
Estimation made according to IDT specification.

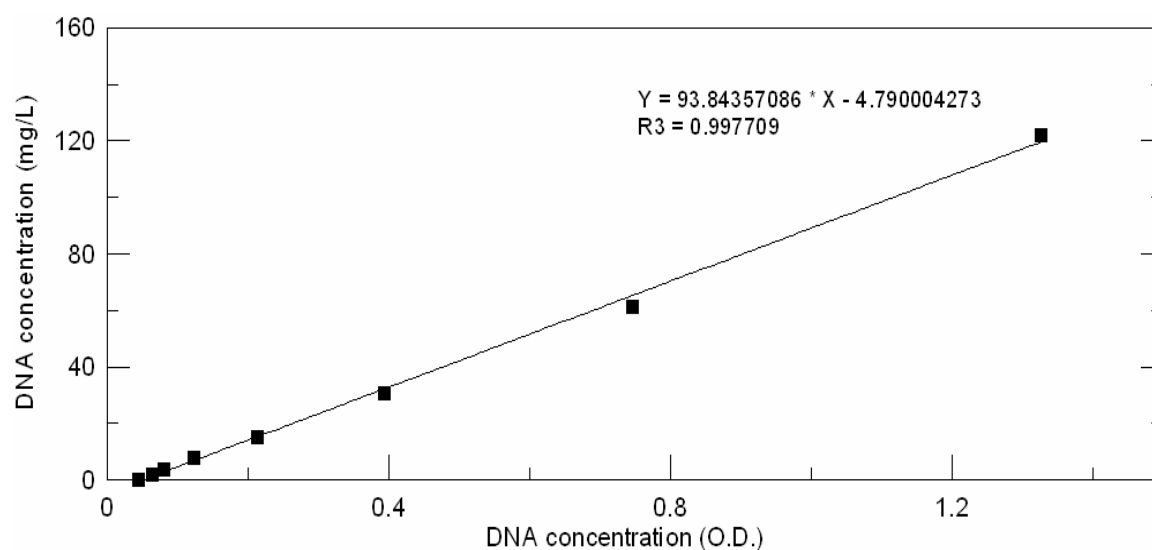


Figure 4A-2 Calibration for spectrophotometric determination of the DNA concentration.

A series of dilutions of the ssDNA solution in DPBS containing Mg^{++} and Ca^{++} was prepared, and their concentration was calculated assuming 100% purity, and concentration (O.D.) was obtained by using UV spectrophotometer. The linearity of DNA concentration is confirmed when the OD reading is smaller than 1.3.

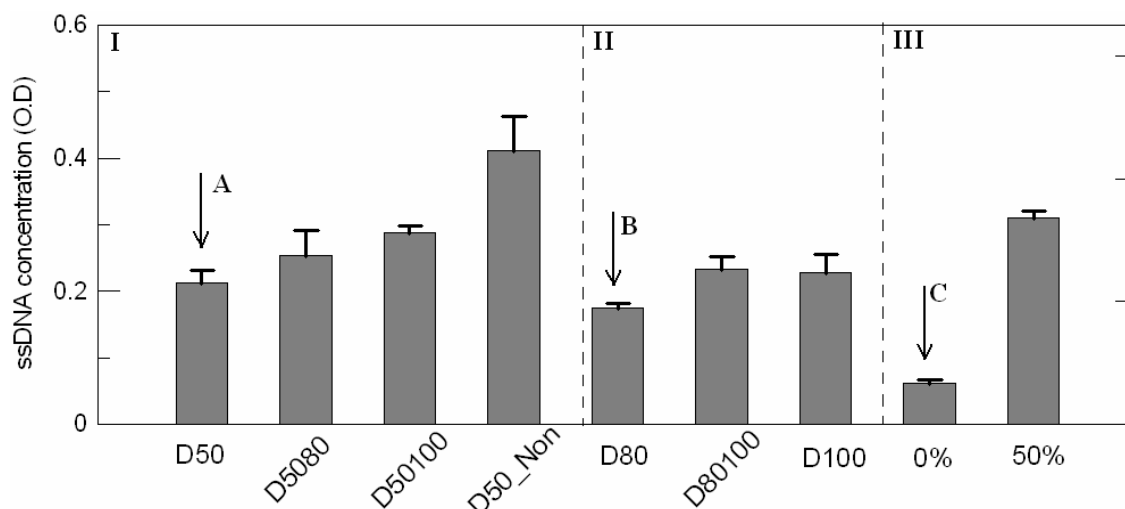


Figure 4A-3 The concentration of residual DNA in the buffer solution rinsing DNA gels, as determined by spectrophotometric measurement two days after the DNA delivery to the DNA gel groups

The significant reading from static gel groups (A and B) mostly likely is due to the DNA gel pieces that shed from bulk DNA gel network and the auto-fluorescence of the buffer used (C). Comparisons in residual ssDNA concentration between gel groups with same 50% initial crosslinking density are made in (I); other three gel groups are in (II); controls for DNA gel quantification are in (III). $n \geq 3$.

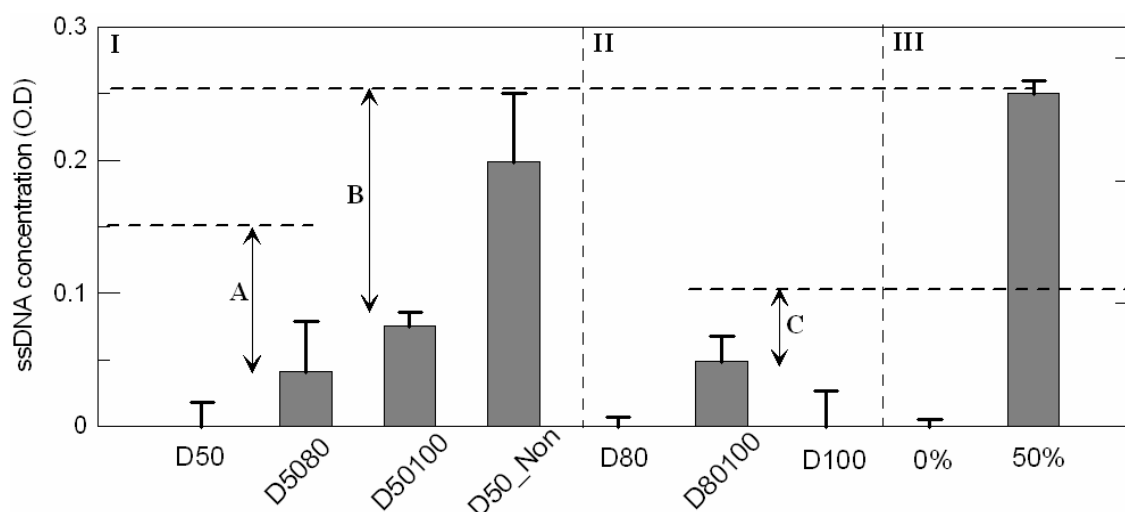


Figure 4A-4 Adjusted DNA concentration determined by spectrophotometric measurement two days after the DNA delivery to the DNA gel groups

Significant proportion of the DNA was incorporated to the gel network as indicated by A, B, C in reference to 30%, 50% and 20% crosslinked density represented by dotted lines, respectively. Comparisons between gel groups with same 50% initial crosslinking density are made in (I) and they are adjusted by subtracting the optical density (OD) value for D50 groups. Other three gel groups are in (II) and are adjusted by subtracting the OD for D80 group to eliminate the contribution from possible free-flowing gel pieces and auto-fluorescence of the buffer. Controls for DNA gel quantification are in (III), and adjusted by subtracting the OD for 0% group in control. $n \geq 3$

References

1. Brahmasandra, S. N., D. T. Burke, C. H. Mastrangelo, and M. A. Burns. Mobility, diffusion and dispersion of single-stranded DNA in sequencing gels. *Electrophoresis*. 22:1046-1062, 2001.
2. Dagani, R. Intelligent gels. *Chem Eng News*. 75:26-37, 1997.
3. Hsu, T., D. S. Ma, and C. Cohen. Effects of inhomogeneities in polyacrylamide gels on thermodynamic and transport properties. *Polymer*. 24:1273-1278, 1983.
4. Kopecek, J. Polymer chemistry: Swell gels. *Nature*. 417:388-389, 391, 2002.
5. Lin, D., N. Langrana, and B. Yurke. Inducing reversible stiffness changes in DNA-crosslinked gels. *Journal of Materials Research*. 20:1456-1464, 2006.
6. Lodish, H., A. Berk, P. Matsudaira, C. A. Kaiser, M. Krieger, M. P. Scott, S. L. Zipursky, and J. Darnell. *Molecular cell biology*, W.H. Freeman and Company: New York, 2004.
7. Osada, Y., and A. Matsuda. Shape memory in hydrogels. *Nature*. 376:219, 1995.
8. Pluen, A., B. Tinland, J. Sturm, and G. Weill. Migration of single-stranded DNA in polyacrylamide gels during electrophoresis. *Electrophoresis*. 19:1548-1559, 1998.
9. Sakurai, S., H. Hayashi, and F. Hamada. Scaling analyses of polyacrylamide gels at swelling equilibrium in water/acetone mixtures by small-angle x-ray scattering. *Polymer*. 34:4625-4628, 1993.
10. Skouri, R., F. Schosseler, J. P. Munch, and S. J. Candau. Swelling and elastic properties of polyelectrolyte gels. *Macromolecules*. 28:197-210, 1995.
11. Watson, J. D., T. A. Baker, S. P. Bell, A. Gann, M. A. Levine, and R. Losick. *Molecular biology of the gene*, Benjamin Cummings, 2003.
12. Wei, B., I. Cheng, K. Q. Luo, and Y. Mi. Capture and release of protein by a reversible DNA-induced sol-gel transition system. *Angew Chem Int Ed Engl*. 47:331-333, 2008.
13. Yang, H., H. Liu, H. Kang, and W. Tan. Engineering target-responsive hydrogels based on aptamer-target interactions. *J Am Chem Soc*. 130:6320-6321, 2008.

CHAPTER 4B FIBROBLAST GROWTH ON A DYNAMIC SUBSTRATE

4B.1 Background

4B.1.1 Fibroblast mechano-sensing

The connective tissue where fibroblasts reside experiences constant external tension, and fibroblasts receive and sense mechanical cues from the ECM, that include mechanical forces^{10, 59, 70, 83}, stress or strain^{20, 53}, and stiffness^{11, 20, 29, 73}, primarily via integrin linkage, focal adhesion and the associated cytoskeleton structures²⁸. In response, mechanical perceptions are converted to biochemical cues, following the common pathways where these cues normally converge. Subsequently, these initiate cellular changes in shape²⁸, spreading⁵⁰, traction force applied to the ECM, , migration behavior⁵⁶ and other cell properties^{28, 77}.

Cell shape has important implications in cellular functioning and growth^{13, 57, 72}. Both projection or spreading area and aspect ratio have been studied previously as indicators of cell adhesion properties and polarity. Cell projection area was strongly influenced by geometric factors^{13, 81} of the substrates, and was found to positively correlate with traction force that cells generate. For instance, in a very recent study using micro-islands of specific geometry and area, Li and co-workers³⁸ reported that decreases in cell-generated traction force correlates with the decreased aspect ratio when cell spreading (or projection area) remains unchanged.

Owing to the mechanically sensitive nature, and their ubiquitousness in the tissues, fibroblasts were chosen as the model cell type for our probe of the cellular responses to the dynamic stiffnesses.

4B.1.2 Dynamic stimuli

The temporal changes or dynamics in cell morphology, adhesion, migration, proliferation and function have been widely investigated^{19, 48, 50, 56, 67}. However, the majority of the substrates employed in these studies and other biological studies were of fixed mechanical stiffness and/or biological features throughout the culture.

Pioneering work on cellular response to dynamically changing substrate cues has been carried out mainly by Whitesides¹ and Mrksich⁸² and their coworkers, and their work was followed by other investigators³⁷. They also supplied these dynamic cues to cells and examined cellular responses. While the findings are interesting, the utility of their strategies is limited, largely due to the reliance of these approaches on the coupling between electrical, chemical (including pH), mechanical, thermal, optical and biochemical (e.g., protein conformation) cues^{37, 45, 52, 66, 75, 79, 80} whose applicability in *in vivo* conditions is problematic. Moreover, the induced changes are either of surface biochemical properties or of the presentation and biological activities of the surface ligands⁴⁵. In a handful of other studies, the substrates were modified, but the modifications were limited to dynamic load or deformation¹⁸. For instance, Petroll et al.⁴⁹ used micro-needles to apply local stress to cells which initiates a quasi-stiffness change in the local cellular environment. They observed cellular contraction when force or tension was applied towards the cells, whereas a bi-phasic behavior, that is, retraction

of the pseudopodia proceeded by elongation, appeared when they pulled on the ECM away from cells. In these experiments with mechanical load or deformation, the rigidity of the substrates did not change significantly. In the system that we devised, mechanical stiffness can be changed with potential strain generation (Chapter 4A).

4B.1.3 Dynamic stiffness of the substrate

Among the myriad of factors that affect cell growth are the mechanical properties of the extracellular matrix (ECM)^{17, 21, 24}. To better understand the mechanical interactions between cells and ECM, various substrates have been utilized to present different stiffness to a number of cell types. These cell culture systems include, bis-crosslinked polyacrylamide hydrogel⁷⁶, two- and three-dimensional collagen gels⁶², fibrin gel²⁵ and other gel systems. The responses to the gels were found to be cell-type specific and depends on the range of the stiffness^{9, 62, 76}.

In actualities, cells reside in a dynamic environment^{7, 15, 43} and are in contact with the extracellular matrix (ECM) and other cells. The ECM undergoes constant synthesis and degradation, which could cause its mechanical rigidity to vary⁴. Its mechanical stiffness can also be significantly altered with ageing, upon external mechanical loading, or via pathological processes (e.g., cancer)^{23, 26, 29, 46, 61}. Moreover, at the tissue-implant interfaces, dynamic processes and changes for both tissues and implant can lead to alteration in the mechanical compliance, and thus, cannot be overlooked^{42, 48, 64}. Particularly in loading-bearing tissues^{14, 35}, ECM mechanical properties can be changed by exposure to changing load conditions through, for example, collagen realignment^{44, 68}.

Recent studies from our group revealed evidence that specific cellular properties respond differently to distinct mechanical stiffness ranges³³. From an engineering viewpoint, it is sometimes beneficial to be able to control the time course of the physical properties of the biomaterials for the implants to provide optimal conditions for a specific desired outcome at different points during time progression. For instance, based on the results from our latest report³³, initial softer substrates foster axonal elongation and stiffening of the substrates at a later stage could encourage outgrowth of more primary dendrites of neurons, thus promoting synaptogenesis. Since cues such as mechanical compliance can direct cell fate determination²², time control of these cues is also likely to be of importance in tissue engineering effort directed towards establishing cell harvesting systems for stem cell therapeutic applications. All of these reasons make it most desirable to have a dynamic cell culture system with controlled temporal property changes. This also contributes to the effort in addressing the static nature of the current bio-artificial materials and the lack of the ability to go through defined temporal remodeling of the current bio-mimetic materials³⁷.

Previous work from our group showed that by supplying DNA crosslinker or its complementary strands, changes in the mechanical stiffnesses, together with de-gelation, are possible with DNA crosslinked hydrogels⁴⁰. In the current work, we set to explore the potential of designing DNA gel system with specific target crosslinking level and examine cellular responses to such changes.

4B.2 Materials and Methods

4B.2.1 DNA sequence design and DNA gel preparation

DNA sequence design was carried out and DNA crosslinked polyacrylamide gels were synthesized following a method previously described^{33,41}. New sequence design of DNA side chains 14 nucleotides (nt) long and crosslinker DNA of 40 nt long was conducted. Optimized DNA sequences obtained from the customized program were queried against the National Center for Biotechnology Information (NCBI) nucleotide database by using a basic local alignment search tool (BLAST) algorithm² for close resemblance to biological sequences. The closeness of the sequences to those of the genome for the rat (GFP fibroblasts) and the mouse (L929 fibroblasts) was checked in the screening.

4B.2.2 DNA and bis gel functionalization

DNA gel immobilization was performed by following a previous method by using an optical adhesive³³. Bis gels were prepared and immobilized used a method detailed in Chapter 3A and previously³⁴. A bifunctional photoactivable crosslinker, Sulfo SANPAH (Pierce, Rockford, IL) in HEPES was used to conjugate ECM molecules onto the gel surface for cell attachment. Type I collagen (USB, Cleveland, OH) was applied at 0.2 mg/mL in acetic acid (0.02 M) and stored at 4°C for overnight, after which excess collagen was removed.

4B.2.3 Mechanical characterization

We followed the procedures outlined in Section 3.2.3 of Chapter 3 on the mechanical characterization of DNA gels. In brief, by applying a calibrated magnetic force to a bead embedded in the gel sample and measuring the resulting displacement of the bead at 14~15°C, one can calculate the stiffness based on a solution formulated before⁴¹. An increment of 5% crosslinker was then added to the gels, and measurements were repeated. After reaching 100% crosslinking, additional crosslinker DNA solution was added, and testing was performed to ensure that stiffness does not increase beyond 100% crosslinking, which demonstrates that the gel was fully crosslinked. All the experiments were performed at RT.

4B.2.4 Fibroblast cell culture and DNA delivery

L9292 and GFP (obtained from skin tissues of the neonates of a transfected rat) fibroblasts were a gift from Margaret Julias and Drs David Shreiber and Helen Buettner from Chemical and Biochemical Engineering Department at Rutgers University. Both types of cells were maintained in Dulbecco's Modified Eagle's Medium (DMEM, 10% fetal bovine serum, 2% L-glutamine supplemented with antibiotics (penicillin/streptomycin)). The medium was changed periodically until confluence when cells were passed. The schemes of DNA delivery and sample group setting used in this study are detailed in Figure 4B-1, and the schematic of the expected alterations in the gel groups is shown in Figure 4B-2. At the time of experiment, L929 cells were on the 13-15th passage and GFP was on 5-7th passage. Cells were plated at 1×10^4 cells/cm² in the aforementioned medium at 37°C and 5% CO₂. The cell seeding density is relatively low

in comparison to normal culture, to reduce cell aggregation, to minimize cell-cell interactions, and to allow for longer time of culture before confluence is reached. With this cell plating density, it was made sure that the culture would not reach confluence until after 4 DIV (days *in vitro*). At 2 DIV, an appropriate amount of crosslinker DNA solution (3 mM in TE buffer) was added to the culture as shown in Table 4B-1. Delivered DNA is expected to diffuse into the DNA gel network and get incorporated as it base-pairs with available SA1 and SA2 side chains. To assess the effect of the foreign DNA on the fibroblast growth, we cultured fibroblast on 24 well plates and for one group of cells we delivered DNA to the medium (DNA+) and none for the other (DNA-). The quantity of the delivered DNA was the same as what we delivered in the studies of cells grown on DNA gels. Comparisons were made between these two groups.

4B.2.5 Cell growth characterization and statistical analysis

At 4 DIV, cells were fixed using paraformaldehyde (4% in PBS) for 20 min and incubated in blocking solution (PBS with 0.1% Triton X-100, 2% normal goat serum, 0.02% sodium azide) for 30 min at RT to eliminate non-specific antibody binding. Subsequently, monoclonal antibody against FAK (1:300, Chemicon) was used for cell incubation for two hours at RT or overnight at 4C, followed by appropriate secondary antibody (raised in goat, 1:200, Jackson ImmunoResearch). For actin staining, cells were permeabilized with 0.5% Triton X-100 incubation of 15 min at RT before rhodamine phalloidin (1:300, Invitrogen) was applied. The cells were kept in rhodamine-conjugated phalloidin for 20 min at RT. DAPI staining was performed to identify intact cells that were marked for morphological characterization. Cells with condensed nuclei as

identified by DAPI were excluded from characterization, and the number of intact cells was counted for each image.

Cells grown on DNA gels were imaged under the same conditions (same exposure time and setting) using fluorescence microscopy in order to quantify FAK intensity and make comparisons between different groups³⁸. Firstly, the fluorescence intensity inside the fibroblast cell body was measured using ImageJ software (NIH, Bethesda, MD), which yielded the mean, maximal and minimal intensity inside each cell body. Care was exercised to ensure that area close to the edge was not included to avoid the potential contribution from the outside background. The ratio between maximum and minimum of intensity is an indicator of the size of the focal adhesion, which is proportional to the quantity of FAK recruited at FA^{3,27}. Secondly, to eliminate the effect of potential non-specific binding of the fluorophore, two gel groups each for both static and dynamic gels were used in which fluorophores were applied without prior treatment with primary antibodies. Cell bodies were imaged, and the fluorescence intensity was assessed. The final fluorescence intensity was calculated by subtracting the fluorescence due to non-specific binding (2nd step) from that obtained in the first step.

Cell spreading area was measured by manually tracing along the boundary of the cell outline in the phase contrast images with the help of ImageJ software (NIH, Bethesda, MD). By fitting the cell outline to an ellipse by using ImageJ, the aspect ratio was calculated by dividing length of the major axis with that of the minor axis. For the case when comparisons are made among three or more groups of DNA gels with same initial gel design (e.g., D50, D50_80, and D50_Non are of the same initial DNA gel design as D50), one way ANOVA was implemented, whereas if only two groups of data

were compared, unpaired two-tailed *t*-test was performed to determine significance. The difference in distribution among distinct groups was assessed by using Chi-square test of goodness of fit. $p < 0.05$ was considered significant.

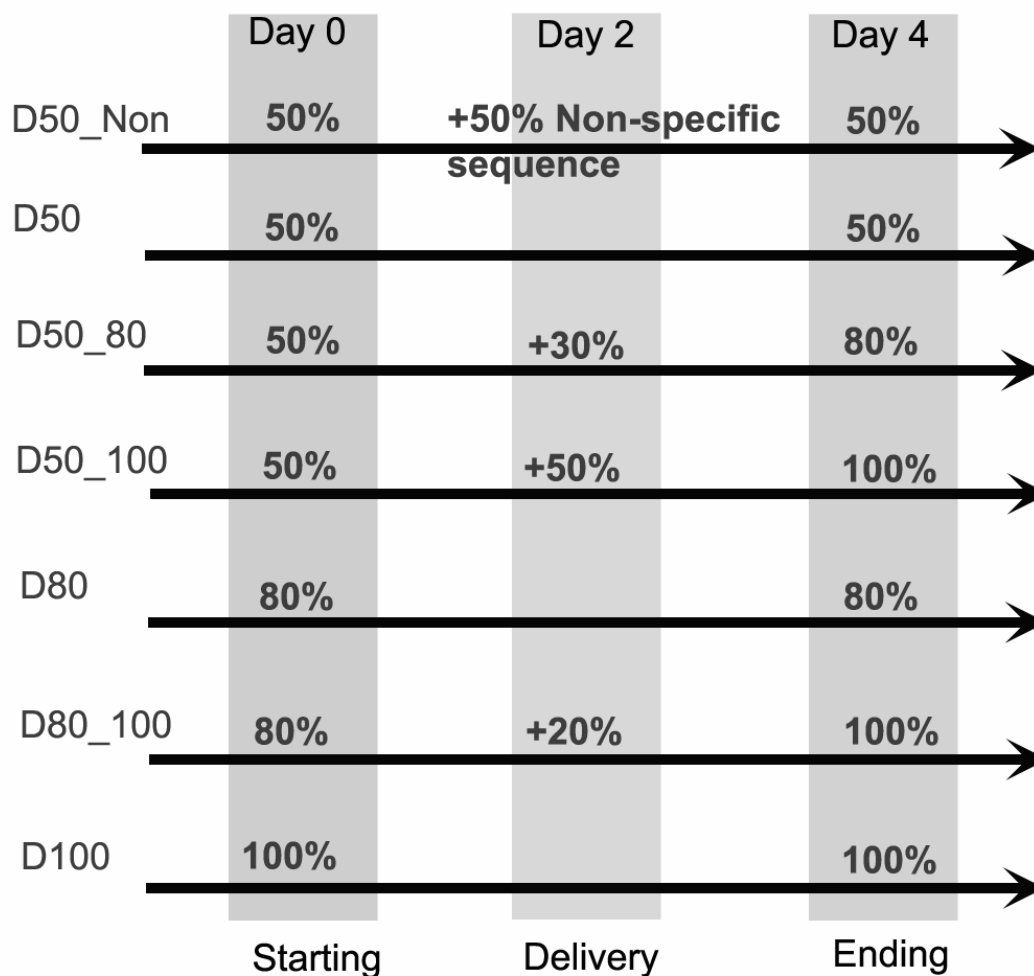


Figure 4B-1 Schemes of DNA delivery to the fibroblast culture on DNA crosslinked hydrogels.

At Day 0, the cells are seeded and allowed to adhere and grow for two days. Different amount of crosslinker DNA is delivered at Day 2. DNA diffusion into gel network is estimated to be within hours and fibroblasts will be exposed to the changing stiffness of the DNA gel. Cells were fixed at Day 4, and analyzed.

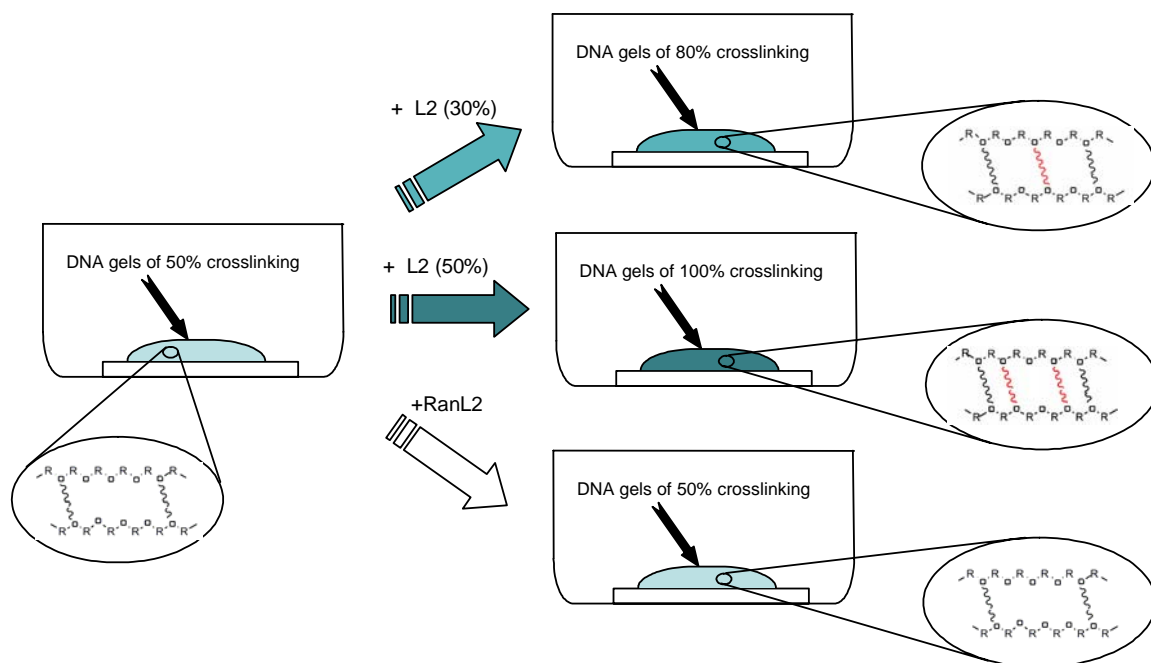


Figure 4B-2 Schematic illustrating the alteration of the mechanical properties of the DNA crosslinked hydrogels via DNA delivery.

Delivered crosslinker DNA diffuses into gel network and gets incorporated, which results in the changes in the crosslinking density. It is noted that delivery of DNA strands with non-specific sequence (indicated as +RanL2) is used as a negative control.

4B.3 Results

4B.3.1 Effect of substrate mechanical stiffness on fibroblast growth

We first confirmed the mechano-sensing capability of the two types of fibroblasts, namely, L929 fibroblasts and GFP fibroblasts to the range of stiffness (300 Pa to 230 kPa) by using a bis-crosslinked polyacrylamide hydrogel. The stiffness range is what is available from DNA crosslinked gels. L929 fibroblasts, for example, exhibited a much better survival on bis-gels with stiffness two orders of magnitude higher than that of the soft gels (Figure 4B-3).

4B.3.2 DNA sequence screening and similarity analysis

The sequences of crosslinker DNA of both designs (Table 4B-2) and their complementary strands were acquired based on the aforementioned method and checked against the rat and mouse genome for similarity with BLAST search. No significant similarity was found for both sequences of the complementary strands of CL2 (Table 4B-2) in Designs A and B (Appendix 4). The likelihood is small that delivered crosslinker DNA could act as anti-sense DNA affecting gene expression, which could potentially alter the phenotype of the cells. Thus, it is unlikely that these DNA strands would cause any significant change in the cellular response, particularly in their morphology and adhesion.

Table 4B-1 The initial and final crosslinking density of different schemes of crosslinker DNA delivery.

Designation	D50	D50_80	D50_Non	D80	D80_100	D100	D50_100
Initial crosslinking density	50%	50%	50%	80%	80%	100%	50%
Final crosslinking density	50%	80%	50%	80%	100%	100%	100%
DNA delivery	—	30%	50%*	—	20%	—	50%

*ssDNA strand of non-specific sequence was delivered.

Table 4B-2 DNA sequence design for the study of fibroblasts on DNA gels with dynamic stiffness.

SA1 and SA2 are single-stranded DNA (ssDNA) side chains. L2 is the crosslinker DNA with part of its sequences complementary to SA1 and SA2. CL2 is the strand complementary to L2. NonL2 is the ssDNA whose sequence is not complementary to SA1, SA2 or L2.

(A)

DNA strand	# of bases	Design A- DNA sequence (5' to 3')
SA1	10	GCA CCT TTG C
SA2	10	GTC AGA ATG A
L2	30	TCA TTC TGA CGC AAA GGT GCG CTA CAC TTG
CL2	30	CAA GTG TAG CGC ACC TTT GCG TCA GAA TGA
NonL2	30	AAA AAA AAA AAA AAA AAA AAA AAA AAA AAA

(B)

DNA strand	# of bases	Design B - DNA sequence (5' to 3')
SA1	14	CGT GGC ATA GGA CT
SA2	14	GTT TCC CAA TCA GA
L2	40	TCT GAT TGG GAA ACA GTC CTA TGC CAC GGT TAC CTT CAT C
CL2	40	GAT GAA GGT AAC CGT GGC ATA GGA CTG TTT CCC AAT CAG A

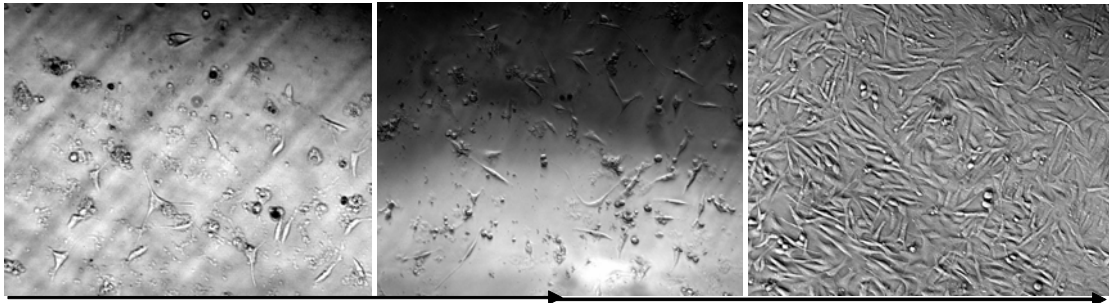
L929 Fibroblasts on Polyacrylamide hydrogels

Figure 4B-3 The survival and proliferation of L929 cells correlate strongly with the substrate mechanical stiffness.

As the stiffness of the bis-crosslinked gels increases from 0.3 kPa (left most) to intermediate one of 5.8 kPa, and to the stiffest substrate (46.6 kPa, right most), survival is greatly improved as indicated by the number of polarized cells.

4B.3.3 Mechanical stiffness of the substrates

The mechanical stiffness of the DNA gels of Design B (14/14/40) at 50%, 80%, and 100% crosslinking, respectively, is shown in Table 4B-3. As crosslinking level rises, the gels get stiffer. The range of mechanical stiffness of the resulting gels is 5.9~22.9 kPa (Table 4B-3), comparable to that of the gels of Design A (10/10/30). We note that the examinations were performed under RT in which gels were not fully swelled, as the first priority was given to probing cellular behavior and activities.

4B.3.4 Effect of DNA delivery on L929 and GFP fibroblast growth

To examine the direct effect of delivered foreign DNA on fibroblast growth, crosslinker DNA was delivered to fibroblasts grown on tissue culture plate (DNA+) with quantity same to that used in the cell culture on gels. Cells in both conditions (with and without DNA delivery, or DNA+ and DNA-, respectively) exhibited similar polarized morphology (Figure 4B-4, upper panel). Most L929 fibroblasts are bipolar while a considerable number of them displayed stellar or multipolar shape. A small percentage of cells remain round. Characterization was performed only on the polarized fibroblasts. There is no significant difference in the primary morphology of the cells, including spreading area, aspect ratio, or cell density between the two groups (DNA+ vs. DNA-, Figure 4B-4, Lower panel). Similar observations were made for GFP fibroblasts (Figure 4B-5). GFP fibroblasts displayed a variety of morphologies, including polygonal and triangular shapes. Their morphology was assessed based on the fluorescent images of GFP expression (Figure 4B-5, upper panel).

Combined with the finding in the BLAST search, these results confirmed that the delivered DNA *per se* does not significantly affect fibroblast cell survival, adhesion or proliferation. Hence, whatever difference shows up between DNA gel groups in the cell growth studies on dynamic gels can be attributed to the stiffness change induced by the introduction of the crosslinker DNA and the incorporation of these strands into the gel network.

4B.3.5 Effect of dynamic stiffness on L929 fibroblasts

Examination of fibroblast growth on 2 day *in vitro* (DIV) on DNA gels of both Designs A and B (Table 4B-2) before DNA delivery reveals little difference in projection area and aspect ratio of gels of two designs at the same crosslinking density (Figure 4B-6). Consequently, we decided to focus on cell growth on DNA gels of Design B (14/14/40), and performed immunofluorescence staining for FAK and staining for F-actin.

To facilitate the understanding of the results, it would be instrumental to consider gels of 50%, 80%, and 100% crosslinking as *soft*, *medium*, and *stiff* gels, respectively; thus groups of D50_80, D80_100, and D50_100 are essentially *Soft_Medium*, *Medium_Stiff*, and *Soft_Stiff* groups, respectively, in terms of crosslinking density and thus stiffness change.

Figure 4B-7 (upper panel) is exemplary of the typical morphologies of L929 fibroblasts grown on six DNA gel groups (the D50_100 group is excluded) on 4 DIV, two days after DNA delivery. Following the aforementioned protocol, these cells were characterized. The results are illustrated in lower panel of Figure 4B-7, and the figures were divided into three sections, with section (I) on the comparison between the negative

control (D50_Non) and D50 gel groups, section (II) on the comparison between gel groups of initial crosslinking density at 50% (D50, D50_80, and D50_100), and section (III) on rest of the three groups (D80, D80_100, and D100). The details of the results are as follows:

(I) No appreciable difference was found in the spreading area or aspect ratio between L929 fibroblasts grown on DNA gels of the two designs D50_Non and D50. This confirms that the exogenous DNA delivered to the cell culture did not give rise to significant modification to the cellular behavior due to potential cellular intake of these short ssDNA (30 or 40 nucleotides). These observations do not change when cells were on the culture plate or on the gels (I in Figure 4B-7, lower panel).

(II) There is a significant cell contraction on D50_80 gels, as indicated in the cell projection area (II in Figure 4B-7), while, interestingly, cells became more polarized (i.e., higher aspect ratio) (II in Figure 4B-7, lower panel). This is almost the same for the comparison between D50 and D50_100 groups, except that on D50_100 gel group, cells maintain their projection area while becoming more polarized.

(III) Delivery of 20% crosslinker DNA to the gel group with 80% initial crosslinking density resulted in a change similar to that seen between D50 and D50_100. In particular, there is no apparent difference in projection area while polarity of the cells strengthens (III in Figure 4B-7, lower panel).

There is no significant difference in cell projection area between the three DNA gel groups of D50, D80 and D100 (Figure 4B-7) although the projection area seems to reach a maximum on D80 gels with intermediate stiffness, and is significantly lower on D100 gels than that on D80 gels. This is also in agreement with the observations on 2

DIV before DNA delivery (Figures 4B-6 and 4B-7). For the trend in cell growth among D50, D80, and D100 groups, the only difference noticed between 4 DIV (Figure 4B-7) and 2 DIV (Figure 4B-6) was that the projection area increased from approximately $500 \mu\text{m}^2$ on 2 DIV to $600 \mu\text{m}^2$ on 4 DIV. In contrast, the aspect ratio increases as the substrate stiffens, and this trend did not change with the mechanical dynamics in DNA gels (Figures 4B-6 and 4B-7). The aspect ratio assessed in the current study is comparable to that reported for B16F10 rat melanoma cells (e.g., $1 \sim 4^{31}$), but lower than that for NIH 3T3 cells (e.g., $1 \sim 14^{74}$, and $1 \sim 68^6$).

After assessment of the average behavior of the total cell population grown on DNA gel groups, we focused on the impact of the mechanical stiffness change on the cellular response in terms of the population distribution. In the comparison in II (Figure 4B-7), it is clear that on D50_80 gels, unlike that on D50 and D50_100 gels, a much greater proportion of the cells have projection area smaller than $600 \mu\text{m}^2$, whereas there is no difference in the projection area of populations between the D50 and D50_100 groups (Figure 4B-8:A1). The difference in cell distribution in projection area is not significant among D80, D80_100 and D100 groups, although there appears that a larger number of cells have a much larger projection area ($>1500 \mu\text{m}^2$) on D80, D80_100, and D100 groups (Figure 4B-8:A2).

Table 4B-3 Mechanical stiffness of the DNA crosslinked polyacrylamide hydrogels used in this study.

	Design B		
DNA crosslinker length	14/14/40		
Monomer Concentration	10%		
DNA crosslinker density	50%	80%	100%
Stiffness (kPa) *	5.85 ± 0.62	12.67 ± 1.33	22.88 ± 2.77
Designation	B50	B80	B100

* Mean ± SEM (Standard Error of Mean)

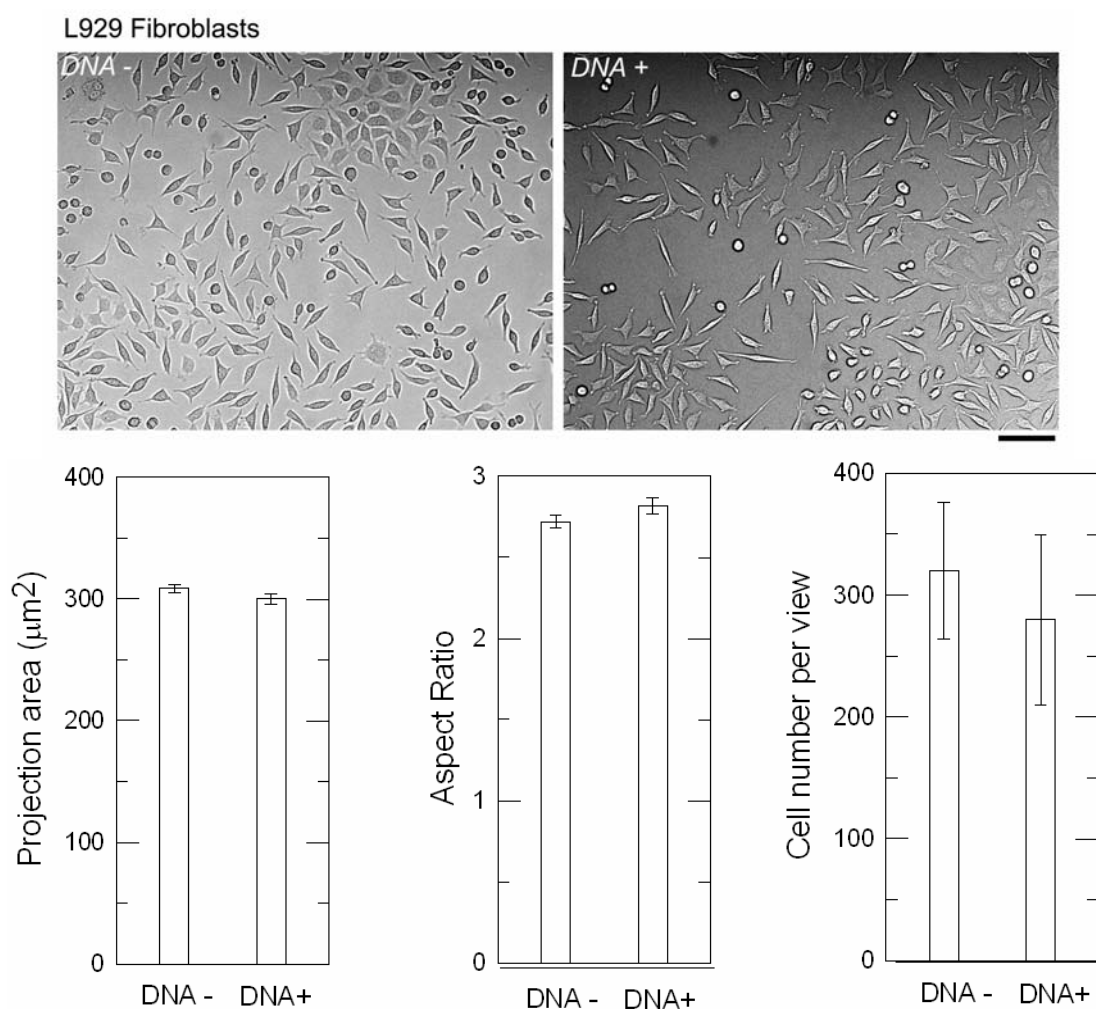


Figure 4B-4 The growth of L929 fibroblasts on tissue culture plates, with (DNA+) and without (DNA-) DNA delivery.

Delivered crosslinker DNA did not significantly alter cellular properties, including spreading area, aspect ratio, or cell number. $n > 100$ for projection area and aspect ratio; $n = 6$ for cell number. Scale bar: 100 μm.

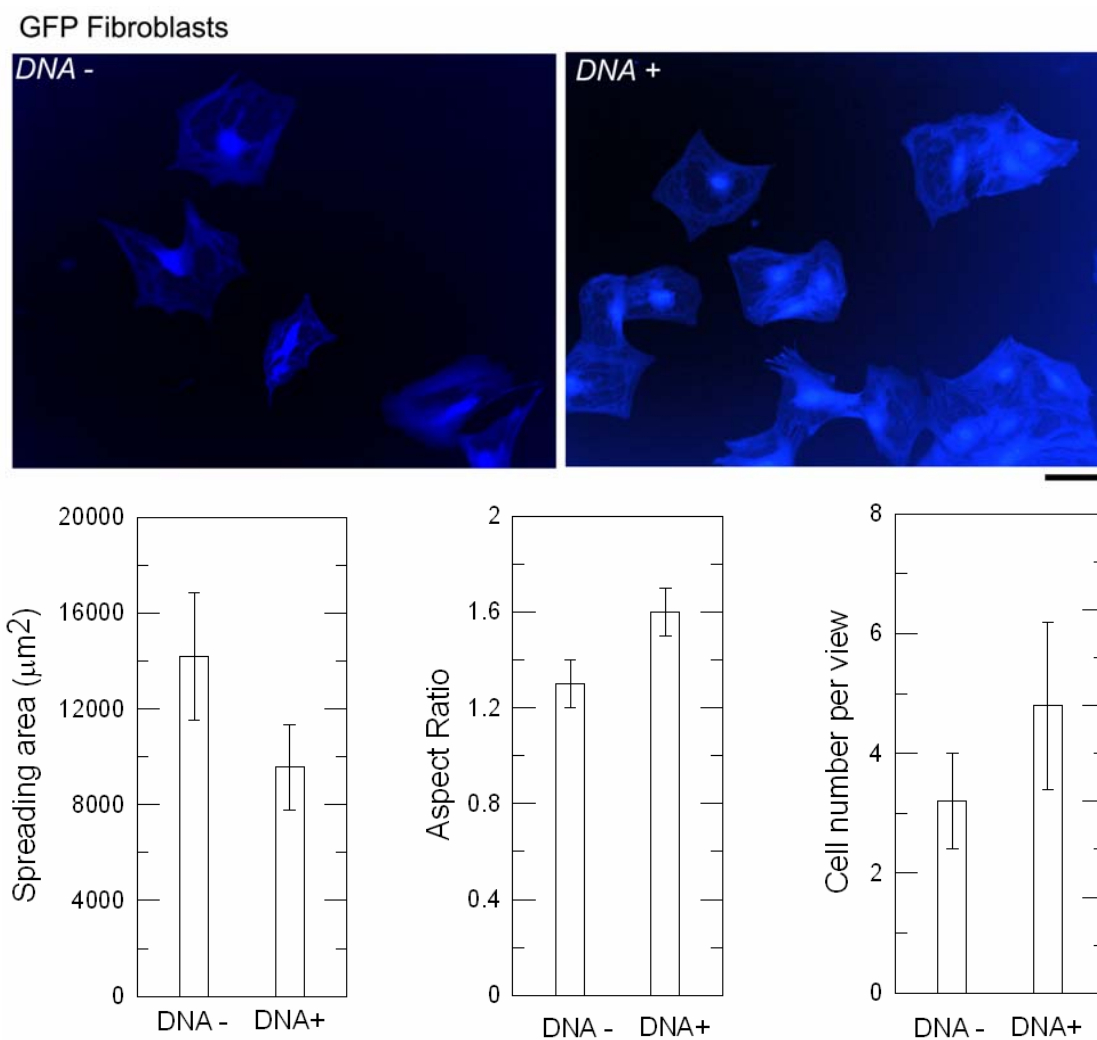


Figure 4B-5 The growth of GFP fibroblasts on tissue culture plates, with (DNA+) and without (DNA-) DNA delivery.

Delivered crosslinker DNA did not significantly ($p > 0.1$) alter cellular properties, including spreading area, aspect ratio, or cell number. $n > 10$ for projection area and aspect ratio; $n = 6$ for cell number per view. Scale bar: 100 μm .

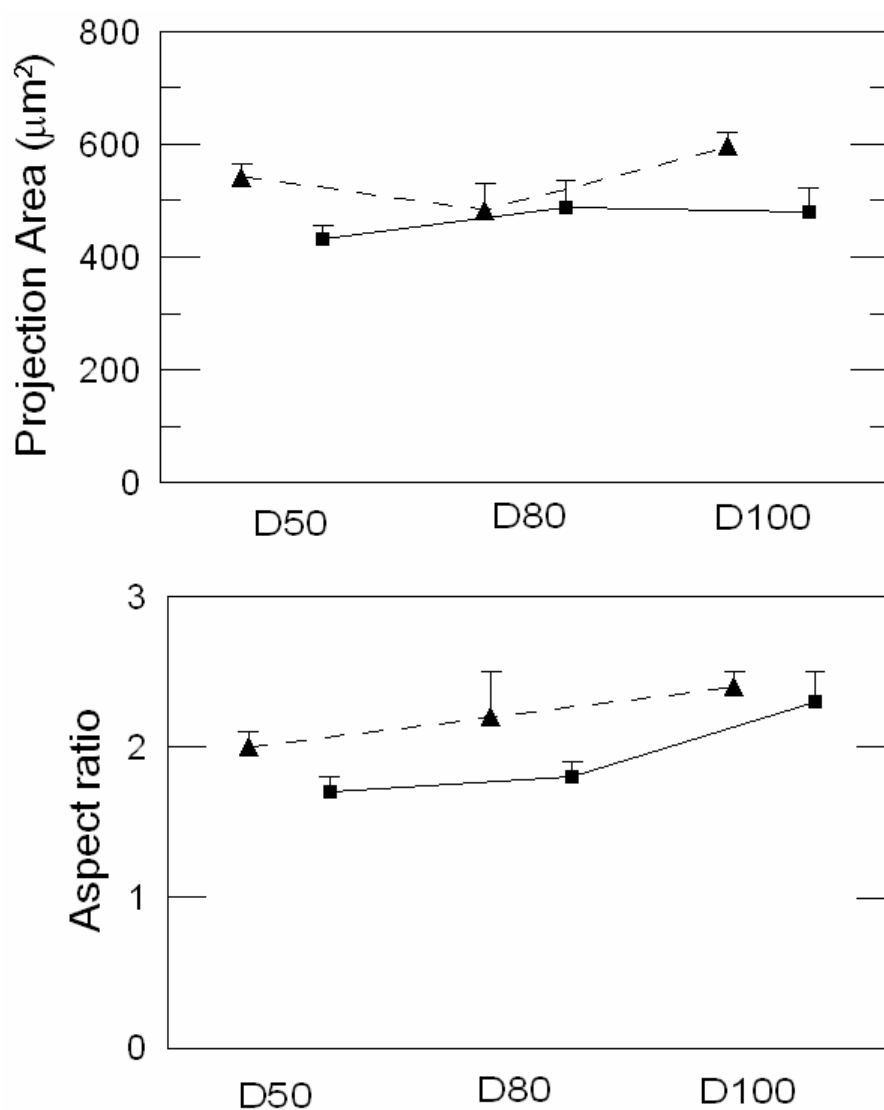


Figure 4B-6 Projection area and aspect ratio of L929 fibroblasts on DNA crosslinked hydrogels of Designs A (▲) and B (■) (Table 4B-2) on Day 2, before DNA delivery. There is no significant difference between gels of two designs at the same crosslinking density. $n \geq 20$.

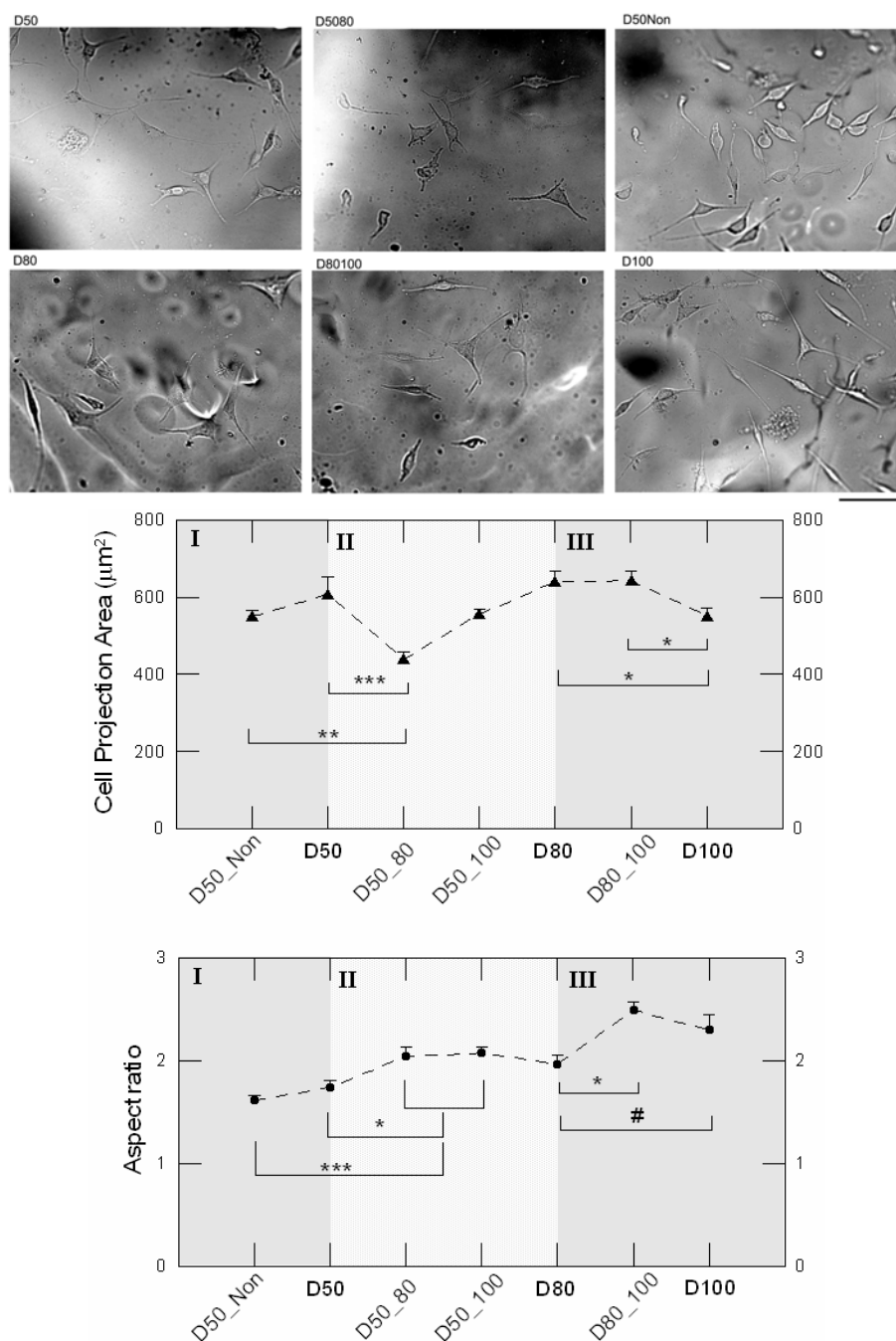


Figure 4B-7 L929 fibroblasts growth on dynamic DNA substrates.

(Upper panel) Typical morphology of L929 fibroblasts grown on DNA crosslinked hydrogels at Day 4, two days following DNA delivery. Scale bar is 100 μm. (Lower panel) Projection area and aspect ratio of L929 fibroblasts on DNA crosslinked hydrogels on Day 4. *** p<0.001, * p<0.05 as determined by one-way ANOVA followed by Tukey's multiple comparisons test. # p<0.05 as determined by two-tailed unpaired *t*-test. No significant difference was found as determined by one-way ANOVA with Tukey's multiple comparisons test. Error bars represent standard error of mean. n>160 for spreading area; n>100 for aspect ratio.

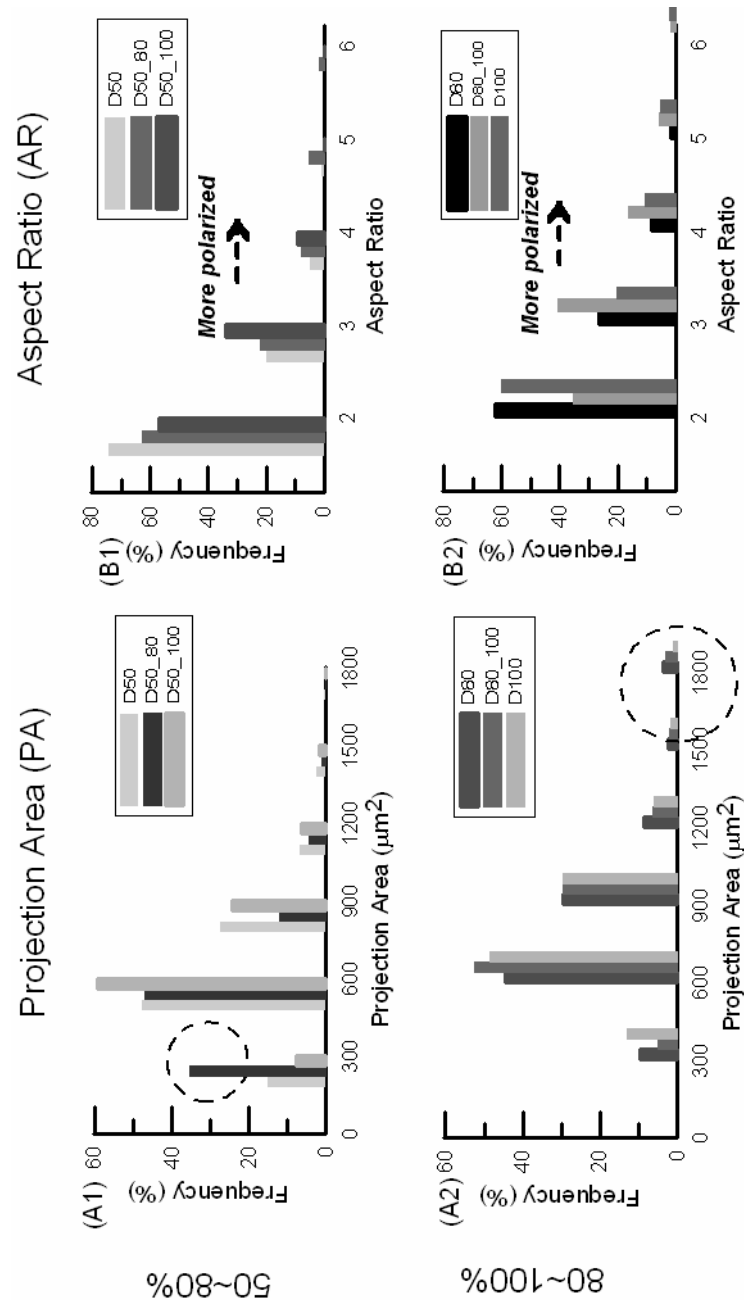


Figure 4B-8 Frequency plots of projection area (A) and aspect ratio (B) of L929 fibroblasts grown on dynamic DNA crosslinked hydrogels.

(A1) Among the three groups of gels with starting crosslinking density at 50%, the proportion of the cells on D50_80 gels having small projection area is greater than that on the other two groups. (A2) Among the three groups of D80, D80_100 and D100, a greater proportion of fibroblasts have large projection area ($> 1200 \mu\text{m}^2$) than that on the other gel groups. (B1) A greater proportion of cells have more polarized or elongated shape on dynamic gels (D50_80 or D50_100) than that on D50 group. (B2) The proportion of cells having more polarized shape on D80 is less than that on the other two groups.

For aspect ratio, the DNA delivery to 50% crosslinked gels resulted in the increase in the degree of elongation of L929 cells (Figure 4B-8:B1), and significant difference was found in between D50 and the other groups (D50_80 or D50_100) where more cells became more polarized after DNA delivery. The impact from dynamic stiffness on cellular polarity is significant by comparing groups of D80, D80_100 and D100, and on gels of D80_100 cells were more elongated (Figure 4B-8:B2).

4B.3.6 Effect of dynamic stiffness on GFP fibroblasts

GFP fibroblasts exhibited typical morphologies as shown by GFP expression (Figure 4B-9, upper panel, D100 group is not shown). Following the same time line in DNA delivery and cell culture, GFP cells adhered to the surface of DNA gels and spread (Figure 4B-9, upper panel). The results are illustrated in lower panel of Figure 4B-9, and the figures were divided into three sections, with section (I) on the comparison between the negative control (D50_Non) and D50 gel groups, section (II) on the comparison between gel groups of initial crosslinking density at 50% (D50, D50_80, and D50_100), and section (III) on rest of the three groups (D80, D80_100, and D100). The details of the results are as follows:

(I) As seen in the case for L929 fibroblasts, there is no significant difference in the projection area or aspect ratio of GFP fibroblasts between D50 and D50_Non groups where ssDNA strands were delivered which are of non-specific DNA sequence (I in Figure 4B-9, lower panel).

(II) Among three DNA gel groups, D50, D50_80, and D50_100, only on D50_80 group, GFP cells displayed significantly smaller projection area and increased polarity (II in Figure 4B-9, lower panel).

(III) Similar to the responses of L929 cells on D80_100 gel group, the projection area of the GFP fibroblasts did not vary greatly; however, the aspect ratio remained the same (III in Figure 4B-9, lower panel) which is different than that of the L292 fibroblast counterpart.

Again, comparisons among GFP fibroblasts on three groups, D50, D80, and D100, show a trend similar to that shown by L929 cells. Cell projection area decreases on D100 gels as compared to two other groups, whereas the aspect ratio is higher on the stiffest gels.

A greater proportion of GFP fibroblasts ‘shrinks’ and reduces the projection area in response to the mechanical stiffness hike from the D50 to D50_80 gels (Figure 4B-10: A1), while this did not occur for cells on D50_100, where the stiffness change is greater. A larger percentage of these cells on D50_80 become more polarized (Figure 4B-10: B1). The proportion of cells with specific projection area and aspect ratio was not significantly altered on other gel groups (D80, D80_100, and D100, Figure 4B-10:A2 & B2).

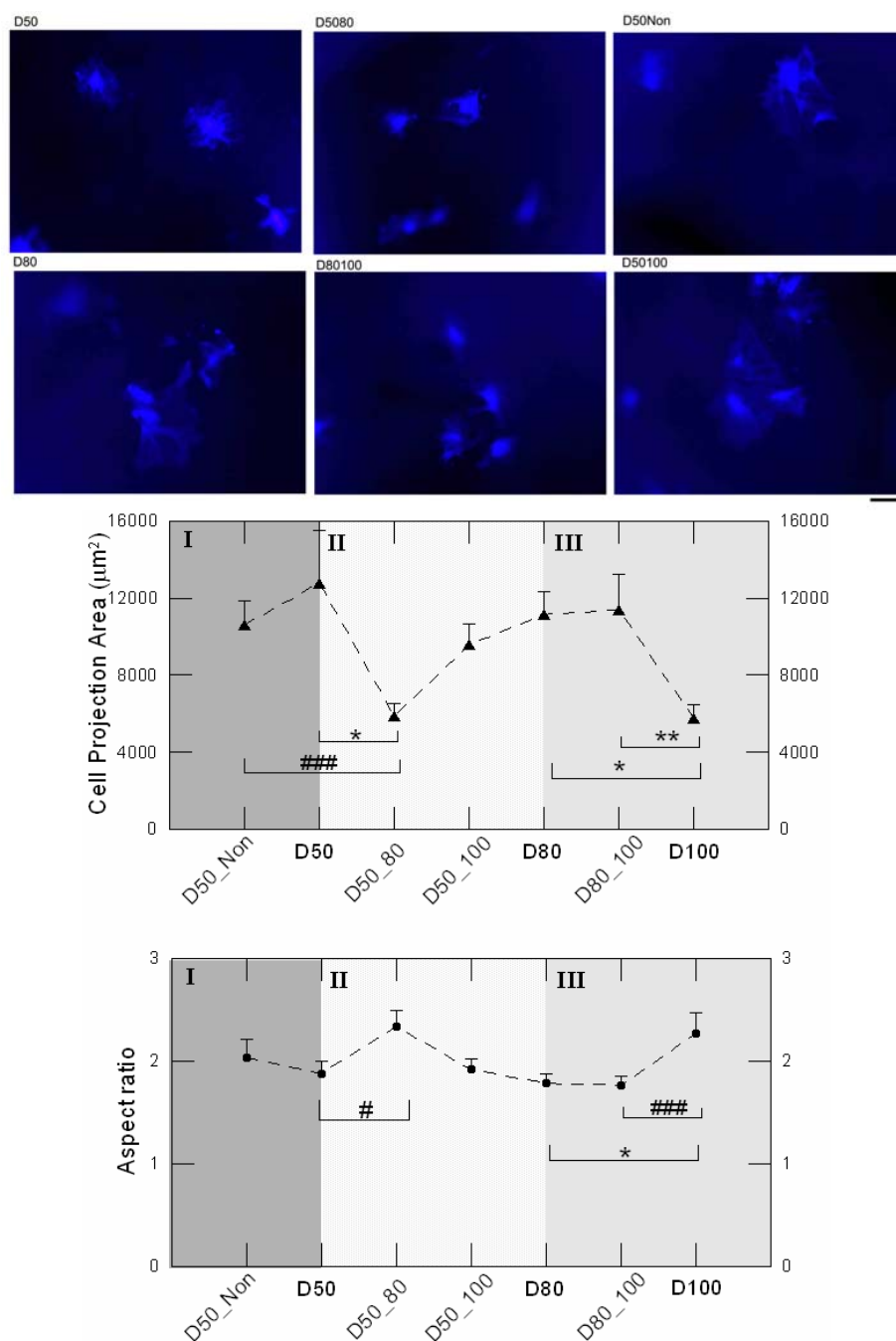
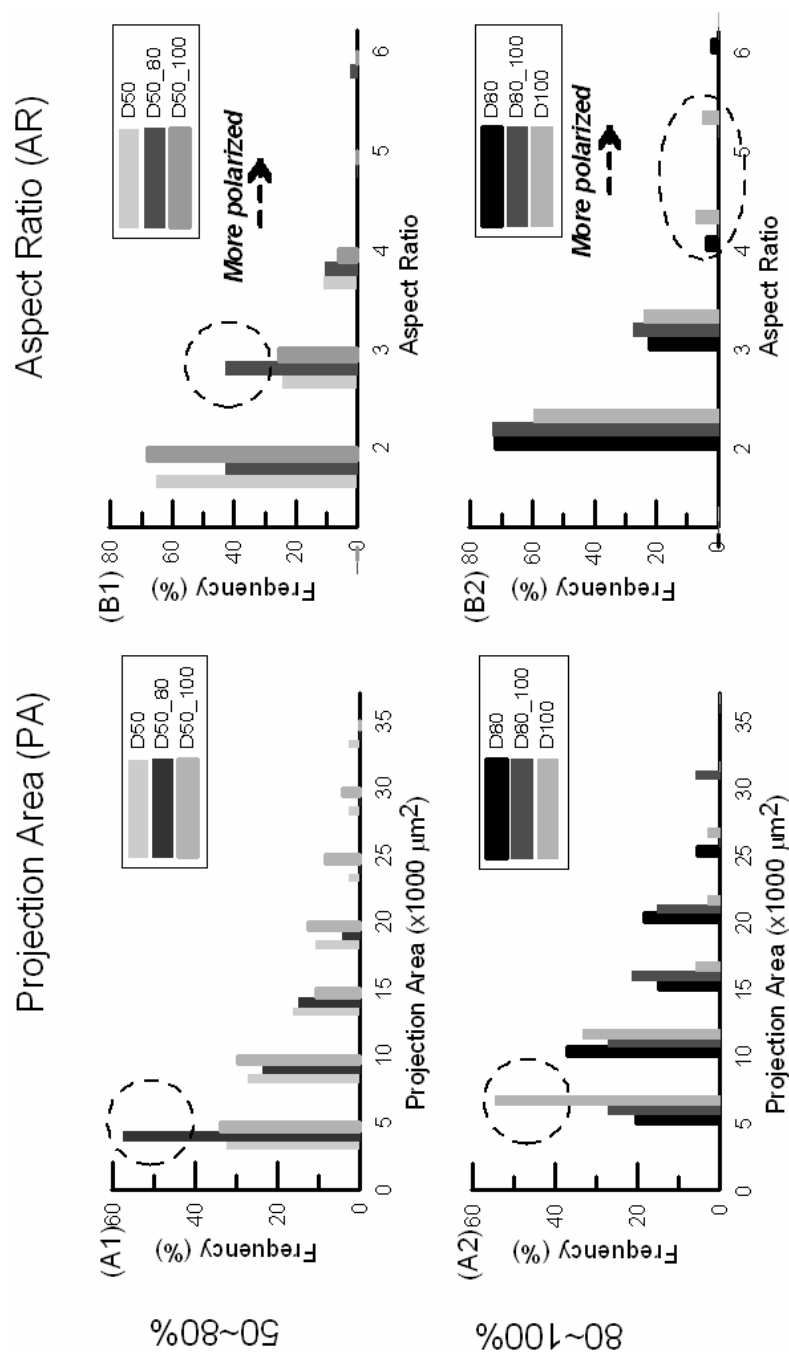


Figure 4B-9 GFP fibroblasts growth on dynamic DNA substrates.

(Upper panel) Typical morphology of GFP fibroblasts grown on DNA crosslinked hydrogels at Day 4, two days following DNA delivery. They have much larger projection area than L929 fibroblasts. Scale bar is 100 μm. (Lower panel) Projection area and aspect ratio of GFP fibroblasts on DNA crosslinked hydrogels on Day 4. ** $p < 0.01$, * $p < 0.05$ as determined by one-way ANOVA followed by Tukey's multiple comparisons test. ### $p < 0.001$, # $p < 0.05$ as determined by two-tailed unpaired t -test. No significant difference was found as determined by one-way ANOVA with Tukey's multiple comparisons test. Error bars represent standard error of mean. $n > 25$.



4B.4 Discussion

4B.4.1 Mechanically dynamic cues applied to fibroblasts

Probing of the mechanical characteristics of the extracellular matrix (ECM) is an integral part of cell decision making process. Most, if not all, of the previous work studying cellular response to mechanical stiffness has focused on the ‘static’ setting of the culture system, where the stiffness of the substrates or scaffold remain unchanged throughout the culture. However, the stiffness of the natural environment of the cells can be, sometimes greatly, altered due to pathological conditions or tissue re-modeling during development, upon dynamic external load, or external assault. With the help of a DNA crosslinking mechanism, we are able to modify the substrate stiffness *in situ* during culture. To our knowledge, it is the first time that fibroblasts’ responses to the changing stiffness of the substrate have been studied and quantified.

Our approach is significantly different than the previous approaches where mechanical load or deformation was applied. Although mechanical load or deformation was relatively easy to compute and implement *in vitro*, the applicability *in vivo* is questionable. In our DNA gel system, the mechanical properties can be adjusted simply through DNA delivery and with carefully designed delivery profiles and experimental conditions, which potentially can be used in clinical setting. In addition, forces can be potentially generated from the DNA gels based on the deformation induced by changes in the crosslinking level. These make DNA gels promising in utilities for tissue engineering applications.

Based on the results from the acellular study outlined in Chapter 4A and the results in the quantification of the local deformation with microbeads (Appendix 1), we attribute the changes in the cellular responses to the alterations in the mechanical compliance induced by DNA delivery and the resulting crosslinking level change. As we discussed in Chapter 3B, DNA incorporation might also cause changes in other physical or chemical properties. From the examination of the neuronal growth and neurite outgrowth in the static studies, it appears that other properties (e.g., surface topography, surface pore size and adhesivity) do not change significantly^{33, 40} or at least not significantly enough to induce alterations in cellular responses.

Our effort in the study of the cellular responses to dynamic cues has been focused on the feasibility of changing the mechanical compliance of the substrate, and in the implementation of the cellular culture and characterization of the cellular behavior. We have the capability of measuring the stiffness of the soft materials at various stiffness ranges and length scales through the use of traditional mechanical testing methodology, magnetic-bead based testing schemes, and a magnetic-microneedle based testing scheme.

4B.4.2 Expression of FAK and F-actin in L929 fibroblasts

To eliminate the possibility of inaccurate interpretation of the immunofluorescent staining due to cross-over in the fluorescence channels, we performed tests on the specificity on secondary antibodies. The results show that there is non-appreciable cross-over between fluorescence channels, thus eliminating its possible contribution to the fluorescence intensity measurement (Figure 4B-11).

The L929 fibroblasts grown on the DNA gel substrate were stained with antibodies against focal adhesion kinase, and the F-actin structures in the cytoskeleton were highlighted with the help of fluorophore-conjugated phalloidin (Figure 4B-12). FAK was expressed in both cell soma and processes. High abundance was seen on the periphery of the soma, whereas relatively low expression was seen in the center of the cell body (Figure 4B-12). Cells appeared to express more FAK on D50 gels, and there is also higher expression of FAK on both D80_100 and D100 gels (Figure 4B-12). It is further observed that the co-expression of the FAK and F-actin in the cells is high, suggesting the close affinity of FAK to the actin of cytoskeleton, which agrees with the previous reports⁵⁸ (Figure 4B-12).

The quantification of the fluorescence is illustrated in Figure 4B-13, and the figures were divided into three sections, with section (I) on the comparisons between the negative control (D50_Non) and D50 gel groups, section (II) on the comparisons between gel groups of initial crosslinking density at 50% (D50, D50_80, and D50_100), and section (III) on rest of the three groups (D80, D80_100, and D100). Quantification of the FAK intensity in the cell soma (Figure 4B-13) reveals the following observations:

(I) There is no appreciable variation in the immuno-staining intensity or maximum/minimum ratio of intensity between D50_Non and D50 gel groups. This further confirms the observations from the preceding sections that the DNA strands themselves do not significantly alter cell behavior. Thus the distinction in the behavior between static and dynamic gel groups can be attributed to the stiffness change induced by DNA strand incorporation and DNA crosslinking density increase (I of Figure 4B-13).

(II) A significant reduction in the FAK expression was seen on dynamic gels of both D50_80 and D50_100 gels (II of Figure 4B-13, upper panel), while no marked difference was found in the ratio of maximum/minimum of intensity in the cell body (II of Figure 4B-13, lower panel).

(III) As to the gel groups of D80, D80_100 and D100, it was found that on the dynamic gels, the mean intensity of the FAK expression was greatly elevated (III of Figure 4B-13, upper panel), whereas the ratio of maximum/minimum of intensity stayed the same (III of Figure 4B-13, lower panel). On D100 gels, both the ratio and the mean intensity of the FAK expression were significantly higher than the other gel groups.

Despite the caution exercised in quantifying the intensity of FAK expression based on immuno-fluorescence, possibilities exist that the practical aspects, including measurement methodology, instrumentation involved, and reagents used, could more or less affect the observations. For instance, it is possible that the choice of focal planes for the fluorescence microscopy adds to the variation between samples.

4B.4.3 Distribution of FAK and F-actin in GFP fibroblasts

For GFP fibroblasts which are much larger in size compared to L929 cells, the F-actin was found aligning the direction of cell elongation and concentrates on the boundary of the cell periphery (Figure 4B-14). Cell nuclei were not all stained by F-actin. Moreover, on D50_80 gels, cells appeared to be smaller in size (i.e., projection area) and more polarized (upper panel, Figure 4B-14). There did not seem to be any significant difference in cell shape between the D80 and D80_100 groups.

All of the cells expressed FAK in the cell body as seen in Figure 4B-15. Most of the cell nuclei appeared to be FAK negative, except for the cases on D80_100 and D100 groups. As seen in L929 cells, GFP fibroblasts displayed a strong correlation between FAK and actin (GFP expressing cytoskeleton) (Figure 4B-15).

4B.4.4 FAK expression and actin structure of cells on dynamic gels

Anchorage-dependent cells largely establish connections with the ECM via focal adhesion or focal contacts⁵¹. Focal adhesion is the focal point of multiple signaling pathways and is essentially the convergence point for the mechanical and biochemical coupling in cell sensing^{51, 55} of the external signals. Focal adhesions kinase (FAK), as we have implicated in the study of neuronal response to mechanical stiffness by using a DNA crosslinked hydrogel (Chapter 3B), has been shown to be heavily involved in the mechano-sensing of external forces or substrate mechanical stiffness changes. Mechanical stiffness has been shown to impact the structures of focal adhesion and its dynamics²¹. For instance, Wang et al.⁶⁹ showed that non-FAK-expressing cells did not show a response to the changes in the substrate, where as FAK-expressing cells demonstrated distinctive responses to the compliance differences in the underlying substrate. Therefore, it is reasonable to hypothesize that FAK is also involved in the cell adjustment to the *changing* external physical conditions. Li et al.³⁹ detected that when endothelial cells are at the state of being stretched, the phosphorylated form of FAK is co-expressed with regular form of FAK, suggesting the recruitment of the regular form of FAK in response to mechanical stimuli.

It is noted that appropriate isotype control can be applied to further study the specificity of the FAK antibodies in assessing the fluorescence intensity. Additional studies can also be conducted to analyze other molecules involved in the cellular adhesion.

DNA crosslinked hydrogels provide a platform for the study of FAK expression in response to mechanical stiffness in the *time* dimension, in contrast to the majority of the previous work which was limited to gels of discrete and static stiffnesses. By using DNA crosslinked polyacrylamide hydrogels, we were able to observe cellular responses to changing mechanical stiffnesses as well as focal adhesion organization. In both GFP and L929 fibroblasts, FAK expression concentrates in the peri-nuclear part of the cells as expected since focal adhesions are closely associated with the termini of actin structures, especially those thick actin fibers³⁶.

The variation in the FAK expression of cells in the same gel group is small enough to be negligible. On the softer gels as well as those with initial 50% crosslinking (D50_80 and D50_100), FAK expression is relatively low in comparison to that on the stiffer gels (D80, D80_100, and D100). This is consistent with previous reports that on softer gels the stress fiber formed by actin and supported by FA is irregular and highly dynamic, whereas on stiffer gels it assumes normal morphology and is relatively stable^{58, 60}.

The size of focal adhesion is indicated by the ratio between the maximal and minimal fluorescence intensity of the expressed FAK. This follows from the fact that the maximal immune-fluorescence intensity is a measure of how much FAK has been recruited to the focal adhesion^{3, 27}. The minimal immune-fluorescence provides a

convenient normalization since it is approximately the same across the sample groups. Therefore, the higher the max./min. ratio, the greater the size of FA. Since the mean intensity of FAK expression in the cell body is positively correlated to both the number and size of FA, we qualitatively estimate the focal adhesion size for comparison, based on the mean intensity (Figure 4B-13, upper) of the FAK expression and the ratio of max./min intensity (Figure 4B-13, lower). We recognized the following relationship:

$$(\text{Mean intensity}) \propto [(\text{FA size}) \times (\text{FA number})], \text{ i.e.,}$$

$$(\text{FA number}) \propto [(\text{Mean intensity}) / (\text{FA size})]$$

Focal adhesion has been shown to be a significant component of the cell mechanosensing machinery and in cell motility⁵⁸, and its organization is strongly dependent on the substrate mechanical stiffness^{47, 81}. It has been established by the previous studies that actin structures and focal adhesion are closely associated since actin structures connect with extracellular matrix mainly through focal adhesions or focal contacts and stability of focal adhesions or focal contacts is dependent on the integrity of the actin structure³⁶. These adhesions are controlled by two major mechanisms, depending on the molecular organization of adhesions at the cell-biomaterial interface, both of which involve both FAK and the cytoskeleton, as summarized by Katz et al³⁶. Contraction of actin fibers has been implicated as important in FA movement. It was reported that the engagement of actin with FA sites occurs in a different fashion for stationary and mobile cells⁵⁸. Potentially, stress fiber formation is sensitive to the

chemical composition on the surface as well. Therefore in our study, we maintain the same adhesiveness for all gel samples as probed and demonstrated by using fluorescent collagen previously^{47, 81} (chapter 3B).

Microtubules, as a primary cytoskeleton component, can potential play a significant role in the mechanosensing. For examples, it was suggested that although only actin is needed for extension of pseudopodia and formation of bipolar shape, interactions between microtubules and microfilament is required to enable elongation of fibroblasts⁶⁵. It is conceivable that intermediate filaments also participate in the stiffening and re-organization of the actin filaments in response to the changing stiffness of ECM at cells' immediate proximity⁷¹. This could be involved in the progression of the decease, and be part of the underlying mechanism of the pathological processes, e.g., cancer.

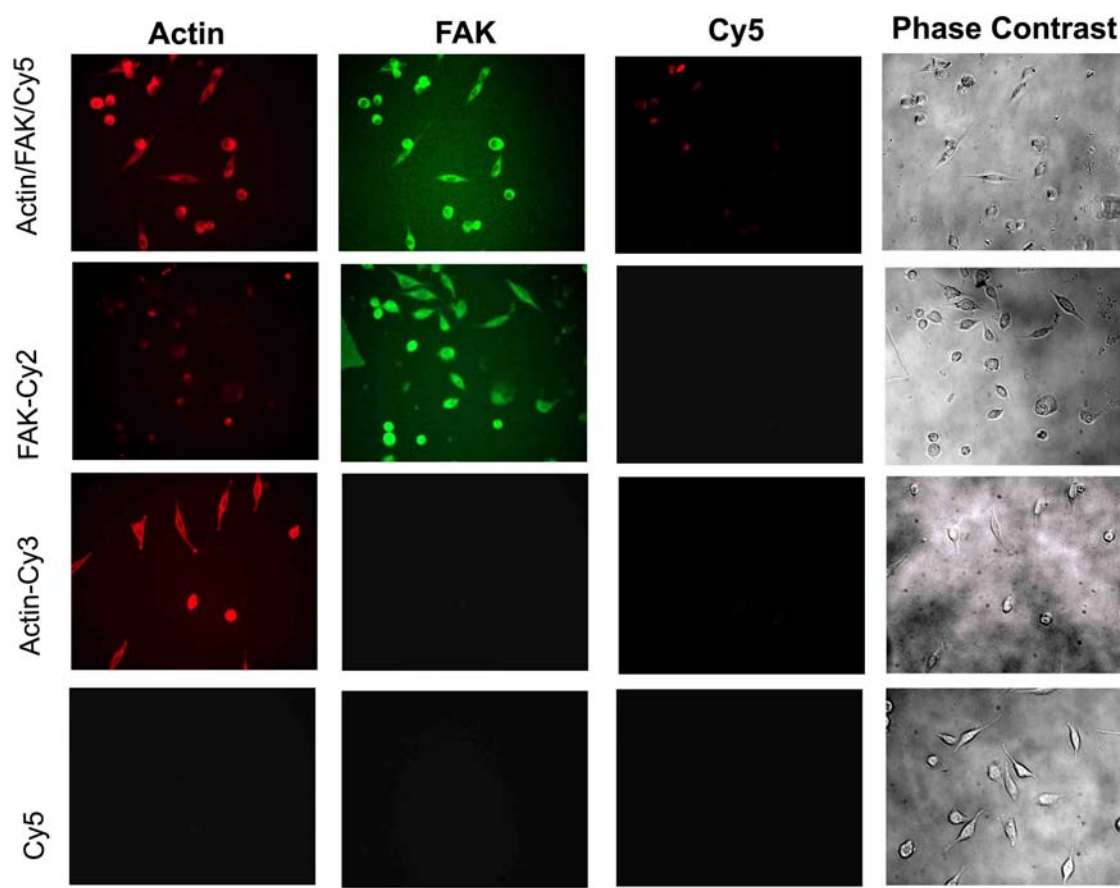


Figure 4B-11 Study of the ‘bleeding-over’ of the fluorescence channels.

In the first sample group (the first row), the primary antibody FAK was used in incubation of fixed cells and permeabilization was performed; in the second sample group, only antibody against FAK was used and in the third group only actin staining was applied. In the last groups, neither FAK nor Actin staining was applied. Secondary antibodies against FAK and Cy5 were applied to all groups. The comparisons between gel groups demonstrate that there is non-appreciable cross-over between fluorescence channels, thus eliminating its possible contribution to the fluorescence intensity measurement. Scale bar: 100 μm .

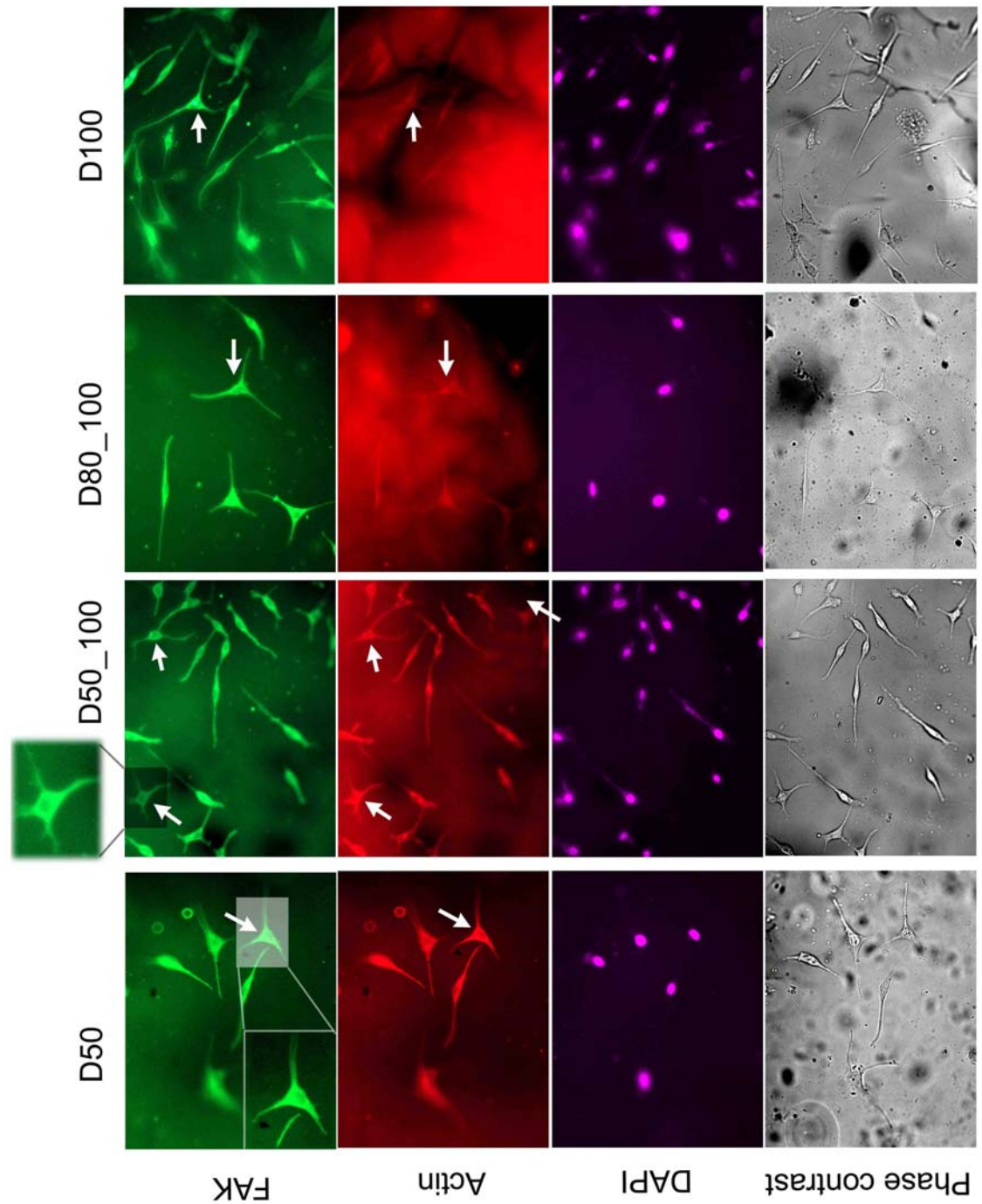


Figure 4B-12 FAK expression and actin staining of L929 fibroblasts on four groups of DNA gel samples: D50, D50_100, D80_100 and D100. Scale bar is 100 μm . FAK concentrates on the peripheral of the cell soma (arrow)

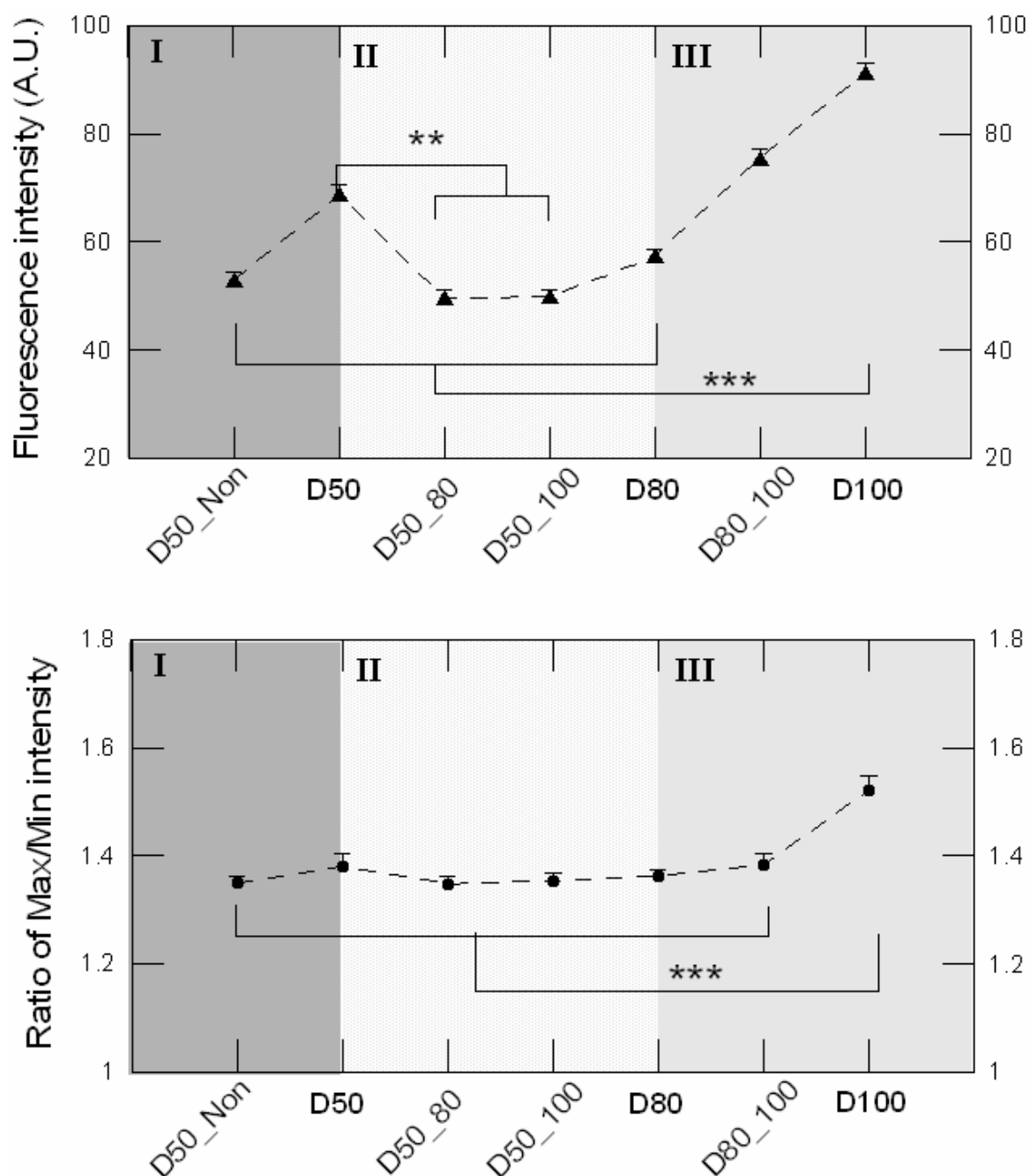


Figure 4B-13 Quantification of the fluorescence intensity (in arbitrary unit, A.U.) of focal adhesion kinase (FAK) of L929 fibroblast grown on DNA gels.

(upper panel) Mean fluorescence intensity. (lower panel) the ratio between maximal and minimal intensity in each cell. *** $p < 0.001$, ** $p < 0.01$, as determined by one-way ANOVA followed by Tukey's multiple comparisons test. $n \geq 27$.

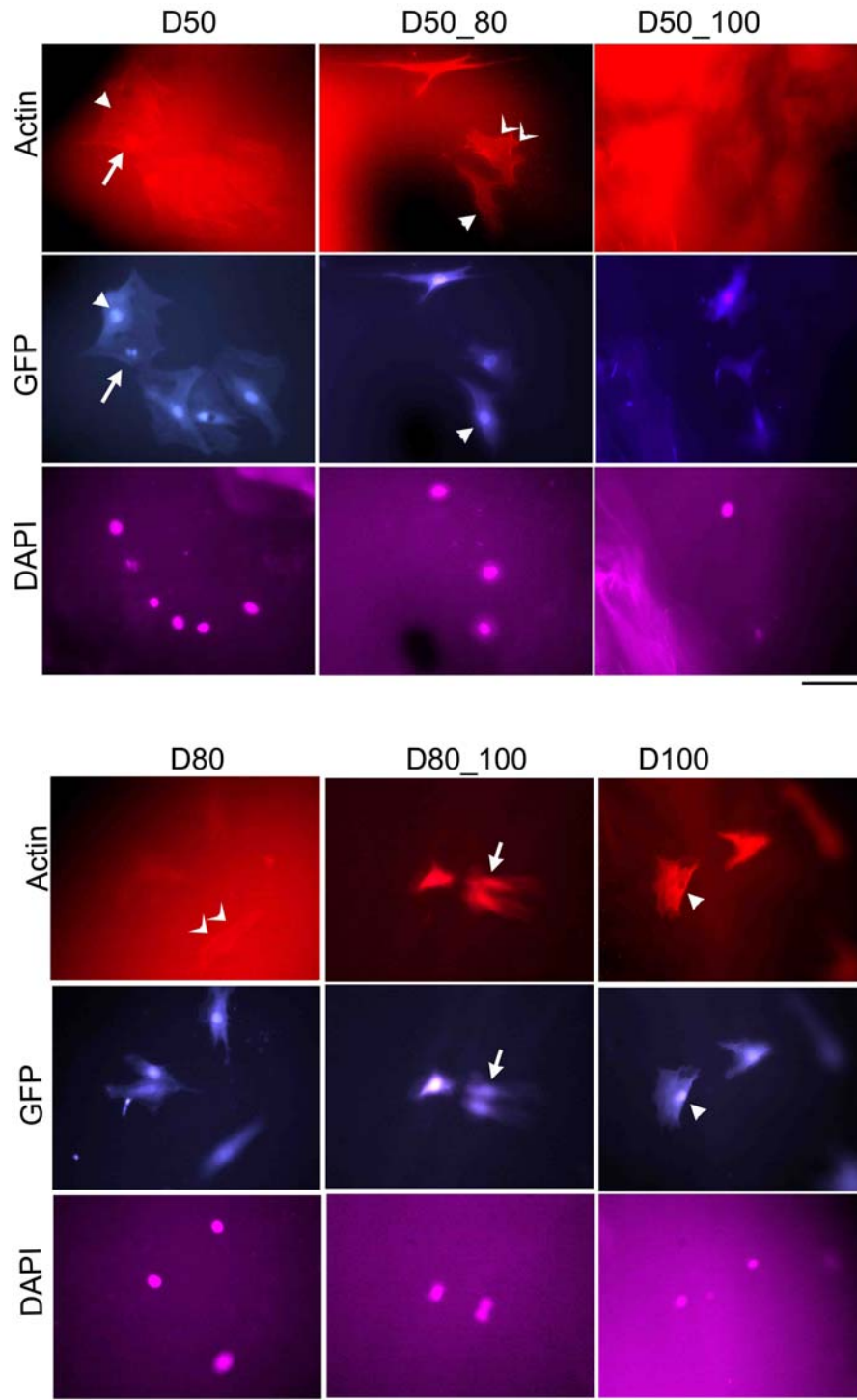


Figure 4B-14 Actin staining of GFP fibroblasts grown on DNA crosslinked gels. Staining of F-actin correlates well with GFP expressed everywhere in the cells and concentrates in the cell nuclei (arrow). A small number of the nuclei were not stained with F-actin (filled arrow head). F-actin expression sometimes concentrates on the edge of the cells (hollow arrow head). Scale bar: 100 μm .

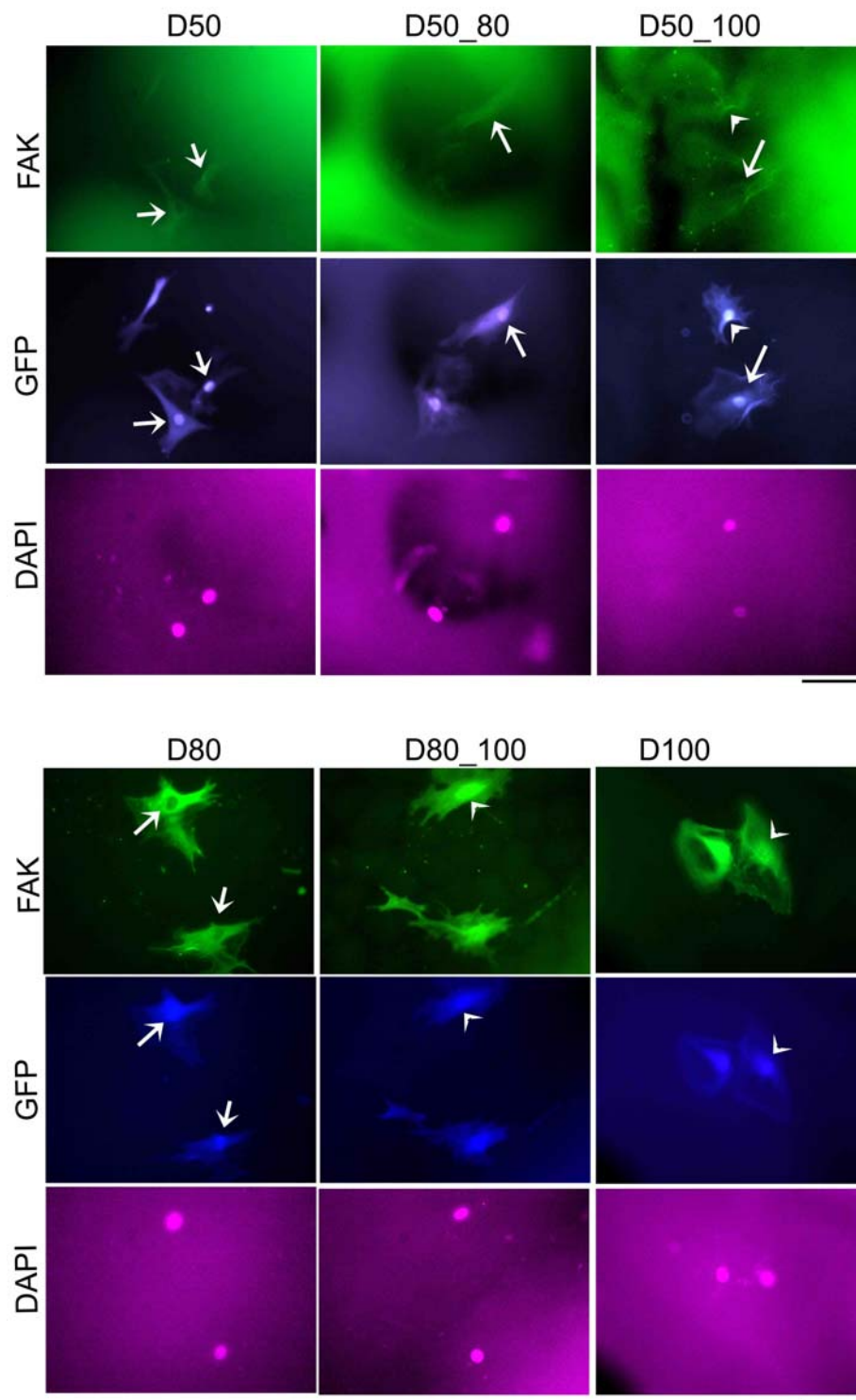


Figure 4B-15 FAK immunostaining of GFP fibroblasts grown on DNA crosslinked gels.

The nuclei of the GFP fibroblast appear to be FAK negative (arrow) for most of the cells, except that on D80_100 and D100 gels, cell nuclei were also stained (arrow head). Scale bar: 100 μ m.

4B.4.5 Cell growth in response to mechanically dynamic cues

Two types of fibroblasts, L929 and GFP fibroblasts, differ in their responses to the changes in the stiffness but also share some common traits in their responses. L292 is a subclone of the parental strain L, derived from normal mouse subcutaneous areolar and adipose tissue. GFP cells were derived from neonatal rat skin after transfection. The consideration of choice of cell types is on the fact that they are from different species and distinct tissue types though both are fibroblasts. When the DNA gel substrate changes from 50% to 80% crosslinking, both L929 and GFP cells significantly contract and reduce their projection area while becoming more polarized. L929 cells also maintain the focal adhesion kinase expression. When the substrate changes from 50% to 100% crosslinking, there is no noticeable change in projection area for either L929 or GFP, while L929 cells become more polarized and GFP cells do not. When the substrate changes from 80% to 100% crosslinking, again, there is no noticeable change in projection area for either L929 or GFP, while L929 cells become more polarized and GFP cells do not. If one compares DNA gels of 100% crosslinking both from static and dynamic (i.e., D80_100) gels, both L929 and GFP cells are more spread on dynamic gels, while GFP cells are more polarized on static gels and L929 cells are not.

Our data show that it is the mechanical property change triggered by external DNA rather than delivered DNA *per se* that is causing the alterations in the cellular responses. This is one of the very first attempts to examine the time-domain for cellular response to mechanical stiffness of the substrate or the ECM. This report offers the evidence that cells do respond to dynamic alternations in the mechanical characteristics of the ECM. Reasonably, the complete picture of the cell-ECM interaction may require

investigation of many more factors than we currently have. These factors include the interactive nature of the cell-ECM relationship, as cells facing the substrate stiffness change can actively modify the close surroundings. They also include the timing of the stiffness change and also that of the time course of cellular responses¹⁵, which necessitates time-lapse studies.

Cell aggregation and subsequent dominant cell-cell interactions could greatly affect the cellular sensing of the substrate's physical and biophysical characteristics. Reports have been made suggesting that cells are able to sense the stiffness of cells adjacent to them⁶⁰. Therefore, the characterization of the cell projection area and aspect ratio was conducted on only 'isolated' fibroblasts and aggregates were not characterized.

The results of the cell shape (projection area and aspect ratio) and FAK expression level are summarized in Table 4B-4. There appears to be a biphasic trend with 80% crosslinked gel as a threshold line. This finding might be explained by a recent study, on the stiffness of fibroblasts themselves⁶⁰, where fibroblasts match their own rigidity with that of the ECM, or adopt a slightly lower stiffness. They can do so below a stiffness threshold of 20 kPa. Beyond this threshold, the cells are not able to increase their own stiffnesses and, instead, form stress fibers and modulate their adhesion to the substrates. In our study of the L929 cells, beyond a stiffness of 80% gels, cells not only change polarity but also alter their adhesion properties, which also depend on the starting stiffness (Figure 4B-7 and Table 4B-4).

On the dynamic gels, uniformly the L929 fibroblasts respond by becoming more polarized (i.e., increase in aspect ratio) (Table 4B-4A), although it is unclear whether this response can be attributed primarily to cell initial responses to changes or cell responses

to the progression of changes. When the ending stiffness is no more than that of the 80% crosslinked gels, cells not only contract but may also reduce the number of focal contacts, for both the total population and the subpopulations investigated (Table 4B-4A). Experiencing the same ending stiffness, cells on gel groups D80_100 and D50_100 maintain their projection area, while exhibiting striking contrasts in the number of focal contacts (Table 4B-4A).

Compared with the static gels with the same ending stiffness, dynamic gels result in a different outcome for the cell projection area, the aspect ratio and the focal adhesion structures (Table 4B-4B). These results show the importance of carrying out studies such as we have performed on the effect of dynamic mechanical cues on the cellular growth. The GFP fibroblasts also show this behavior (Table 4B-5), where comparisons between D50_80 and D80, between D50_100 and D100, and between D80_100 and D100 show the marked disparity in cell projection area and polarity. Additionally, L929 fibroblasts and GFP cells responded in similar fashion for both projection area and aspect ratio to the same ending stiffness of 100% gels (D80_100 and D50_100), and showed reduced projection area and augmented aspect ratio on D50_80 gels (Tables 4B-4 and 4B-5). In contrast to L929 fibroblasts, GFP cells did not become more polarized in response to dynamic stiffnesses (D50_100 and D80_100 gels, Figures 4B-7, 4B-9 and 4B-13).

Table 4B-4 Comparisons between L929 cell behavior on starting stiffness and that on dynamic stiffness (A), and between cell behavior on dynamic stiffness and that on static gels with same ending stiffness (B).

The ellipse represents a typical L929 cell, and the size is proportional to the projection area. The level of elongation indicates the aspect ratio. Black dots represent focal contacts, with their number and size related to those of the focal contacts. (PA = projection area; AR = aspect ratio; FA # = focal adhesion; P1 = proportion of cells with larger projection area; P2 = proportion of cells with greater polarity) (↑ increase; ↓ decrease; → no change)

(A) Starting vs. Dynamic		PA	AR	FA #	FA size	P1	P2
	D50 → D50_80	↓	↑	↓	→	↓	↑
	D80 → D80_100	→	↑	↑	→	→	↑
	D50 → D50_100	→	↑	↓	→	→	↑
(B) Dynamic vs. Static Final		PA	AR	FA #	FA size	P1	P2
	D50_80 ↔ D80	↑	→	→	→	→	→
	D80_100 ↔ D100	↓	→	?	↑	→	↓
	D50_100 ↔ D100	→	→	?	↑	→	→

Table 4B-5 Comparisons between GFP fibroblast behavior on starting stiffness and that on dynamic stiffness, and between cell behavior on dynamic stiffness and that on static gels with same ending stiffness.

The parallelograms schematically indicate the responses exhibited by typical GFP fibroblasts. The size of the parallelograms is proportional to the projection area. The degree of elongation indicates aspect ratio. (PA = Projection Area; AR = Aspect Ratio; P1 = Proportion of cells with larger projection area; P2 = Proportion of cells with greater polarity) (↑ increase; ↓ decrease; → no change)

Starting vs. Dynamic vs. Static Final			PA	AR	P1	P2
D50	D5080	D80	↓↑	↑↓	↓↑	↑↓
D50	D50100	D100	→↓	→↑	→↓	→↑
D80	D 80100	D100	→↓	→↑	→↓	→↑

4B.4.6 Factors in fibroblast mechanosensing of dynamic stiffness

A partial list of the important factors influencing cellular responses to dynamic mechanical stiffness changes is summarized in Table 4B-6. These factors include the range of stiffness, starting and ending stiffness, cellular properties, cell types and rate of changes in mechanical stiffness. A schematic depicting mechanisms in cellular mechanosensing and responses to mechanical stiffness change in the ECM is presented in Figure 4B-16.

Cells actively probe the stiffness of the substrate by applying traction forces largely via integrin linkage in the focal adhesion complex (FAC) where FAK is among the key participants and regulators^{28,30,77}. As the stiffness increases, as is the case in the current study, the resistance to the cell-generated traction forces intensify, and cells receive the feedback, also via integrin linkage. This information, together with other physical cues, dimensionality, biochemical and biological cues (e.g., growth factors), as well as cell-cell interactions (if cell-cell contact occurs) is integrated by cells for decision making. The cells respond by modulating focal adhesion, stress fiber formation, cell shape, and other cellular properties, until a new force or tensional balance is reached (Figure 4B-16).

Our observations suggest that there might be a cut-off point in stiffness between the mechanical stiffness of 80% crosslinked DNA gels and 100% crosslinked DNA gels with regards to fibroblast responses to dynamic stiffnesses. Additionally, there seems to be a distinction between cellular response to acute and progressive change in mechanical stiffness. When cells were plated on stiffer substrates, they were essentially subject to the rather *abrupt* change in mechanical micro-environment, while on dynamic gels, DNA

delivery induced mechanical change is relatively *progressive* and *slower*, and cells might have a different mechanism to cope with the alterations. Thus, it is possible that cells have distinctive ways and kinetics in adapting to the different mechanical compliances.

Cells reside in the microenvironment with a balance in forces before changes in the mechanics of the micro-environment are made³⁰. It is through the linkage between the cytoskeleton and the ECM that cells not only apply tension and forces to actively pull on the ECM (natural or synthetic) or adjacent cells but also receive resistance and other feedback before responding to this feedback²¹. This forms the basis of cell mechanosensing in adhesion-dependent mechano-sensitivity⁷.

The applied forces generated by the interactions between actin and myosin filaments are transmitted to the substrate largely via focal adhesion and are often referred to as traction forces^{7, 12, 21}. The focal adhesion is the mature form of the focal complex. The maturation occurs during the stress fiber formation^{7, 14}. The time scale in cell exerting traction forces, receiving feedback or response from ECM, and the time scale over which cells respond to these feedbacks is likely to be seconds to hours^{5, 21, 78}. This time scale lies within the time duration adopted in the current studies (~48 hrs). The forces applied on these focal adhesions or focal complexes depend on the mechanical characteristics on the substrate. They could be external forces or those generated by cells themselves in their active probing of the microenvironment, which is involved in cellular sensing and in generating responses to the mechanical stiffness. These forces, in turn, modulate the assembly/disassembly and maturation of the focal adhesions¹⁴. On the soft substrate, the force needed to sustain adhesion sites and associated stress fibers is markedly smaller than that on the rigid surfaces, and consequently, the size or the

dimension of the focal adhesion formed is much smaller^{7, 47}. This agrees with our finding that on stiff gels (i.e. D100), the size of the focal adhesion is significantly higher.

Generally, the increase in the mechanical stiffness will translate, at cellular or sub-cellular level, into greater resistance to the forces exerted by the cells, which will engage cells in generating greater traction forces^{32, 84}. The greater forces, subsequently, cause focal adhesion to increase in size (manifested by FAK fluorescence intensity and the max/min fluorescence ratio) and the strength of the coupling to the cytoskeleton¹⁴. Focal adhesion kinase is the earliest marker for FA signaling and demonstrates great sensitivity towards tension, making it a reliable indicator for the cell adhesion properties¹⁴. In this study, we found that comparison among static gels does support this notion, although there appeared to be a threshold, with cut-off point lying somewhere close to the stiffness of 80% gels. This phenomenon may be related to the presence of a set-point, ‘optimal’ strain or stress, that is ‘best’ for cells^{20, 21, 54, 60}, which may also be associated with the existence of pre-stress in cells. In essence, it might be similar to the concept of ‘intrinsic frequency’ of an object in dynamics, where harmonic motion (equilibrium in the forces that cells are experiencing) can be reached if external frequency (ECM mechanical stiffness) matches the intrinsic one (cellular stiffness). If this hypothesis is correct, then the prestress in the cell cytoskeleton may essentially serve as a probe for cell mechano-sensing.

Strikingly, on dynamic gels, and especially with comparisons between dynamic gels and ending stiffness, cells were not able to alter their focal adhesion enough to reach the conditions on the targeting stiffness. However, they altered their shape, and became more elongated or polarized, which is closely related to the stress fiber formation and

traction force generation. Therefore, it is suggested that alteration in the focal adhesion and cell shape (related to stress fiber) might be among the major routes through which cells cope with the dynamics in the mechanical stiffness of the gels.

The end results of the mechano-sensing is the formation of a new equilibrium^{16, 63}, also termed as ‘tensional homeostasis’ in the cellular and tissue level⁴⁶, which is most likely a dynamic one^{16, 63}. The imbalance of the mechanical tension or forces has implications in pathology⁴⁶. Thus, the differential responses to the static and dynamic stiffnesses lie in the way to reach the equilibrium from onset of the imbalance, through modulation of the focal adhesion, stress fiber formation, cell shape control, cell stiffness or their combinations. The cells likely seek the most effective way of establishing the new balance, and, as generally recognized, up-regulating focal adhesion might be the choice when facing the large stiffness since force generation is more efficient⁸. If the static stiffness case can be categorized as much greater rate of stiffness change (Figure 4B-17), then the efficient way of force generation maybe modified if the rate of the change is slower, as suggested by the current study.

Although we have tried to minimize the possible cell-cell interactions in the fibroblast culture by restricting the cell plating density, there is still a possibility that interactions between fibroblasts, for example, via soluble factors, could affect their growth as well as their responses to the mechanical dynamics. It is worthwhile pointing out that we have not investigated proliferation and the effect of mechanically dynamic stimuli on proliferation. It would be also interesting to see if cells would further alter their shape and behavior, in general, with longer time in culture (e.g. on 6 or 8 DIV). Also worthwhile noting is that the response of fibroblast cells to the dynamic mechanical

characteristics also depends on the nature of the ECM that they are subjected to³⁶. Thus, by using other ECM molecules such as fibronectin, fibrin, or laminin, the cellular responses to the mechanical dynamics might vary. Lastly, only stiffness increase has been presented in this work, and cellular responses to the decrease in the mechanical rigidity might also be substantial, and could be distinct from those on stiffening gels (Figure 4B-18).

Summary

The current work further underscores the importance of the understanding of the dynamic aspect of cell-ECM interactions, outlines a feasible approach to mimic the mechanical variations in the physiological conditions, and provides guidelines for three-dimensional bio-scaffold design for tissue engineering applications. The strategy developed in this work will ultimately lead to the design and synthesis of a bio-scaffold with controlled mechanical stiffness changes whereby to construct a more physiologically relevant environment and to engineer cellular morphogenesis and functions.

Table 4B-6 Important factors influencing the cellular responses to mechanically dynamic cues.

Parameters	Examples of comparisons
Rate of change	Abrupt (static) vs. progressive, e.g., D50_100 vs. D100
Stiffness range	50%→80% vs. 80%→100%
Starting stiffness	50%→100% vs. 80%→100%
Ending stiffness	50%→100% vs. 50%→80%
Cellular property	Projection Area vs. Aspect Ratio vs. FAK expression
Cell type	L929 vs. GFP

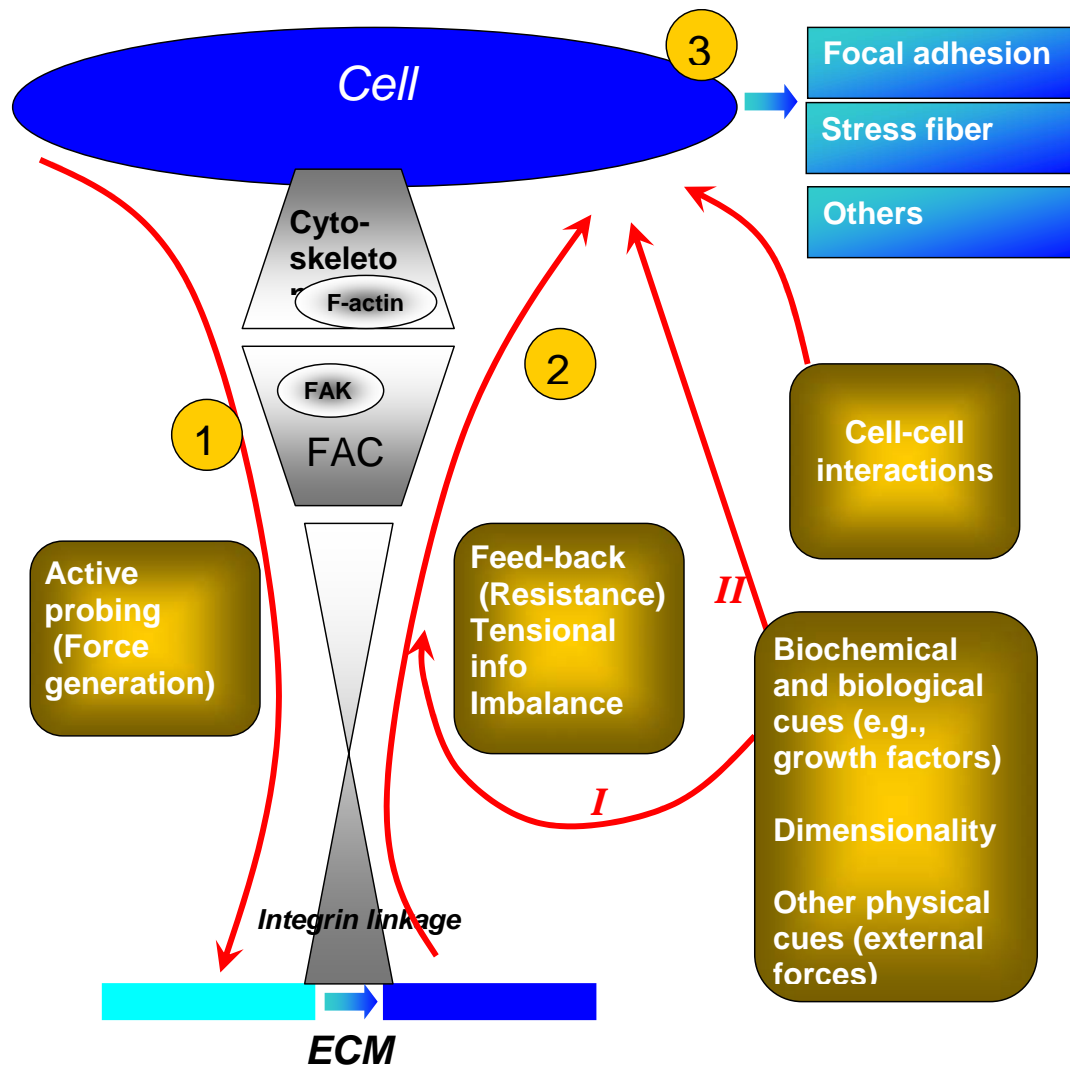


Figure 4B-16 Schematic for the cell-ECM interface with the emphasis on cell mechanosensing and responses to the stiffness change in the ECM or gel substrate.

(1) Cells actively probe the stiffness of the substrate by applying traction forces largely through integrin linkage in the focal adhesion complex (FAC) where FAK is among the key factors. (2) As the stiffness increases, the resistance to the cell-generated traction forces intensifies, and cell receives the feedback also via integrin linkage. This information, together with other physical cues, dimensionality, biochemical and biological cues (e.g., growth factors), as well as cell-cell interactions if cell-cell contact occurs, is received by the cell via integrin linkage (I) or other pathways (II) and is integrated by cells for decision making. (3) Cells respond by modulating focal adhesion, stress fiber structure, cell shape, and other cellular properties.

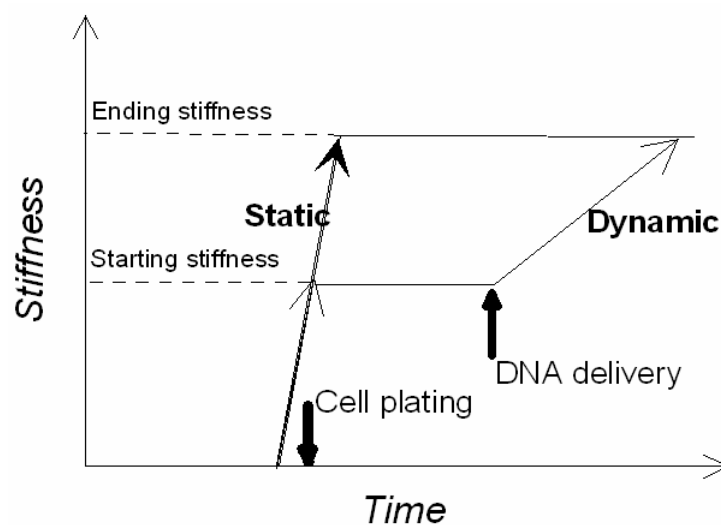


Figure 4B-17 Illustration showing that on the gels with static stiffness, the cells are subjected to much greater rate of change in the mechanical stiffness upon plating than that on the gels of dynamic stiffnesses.

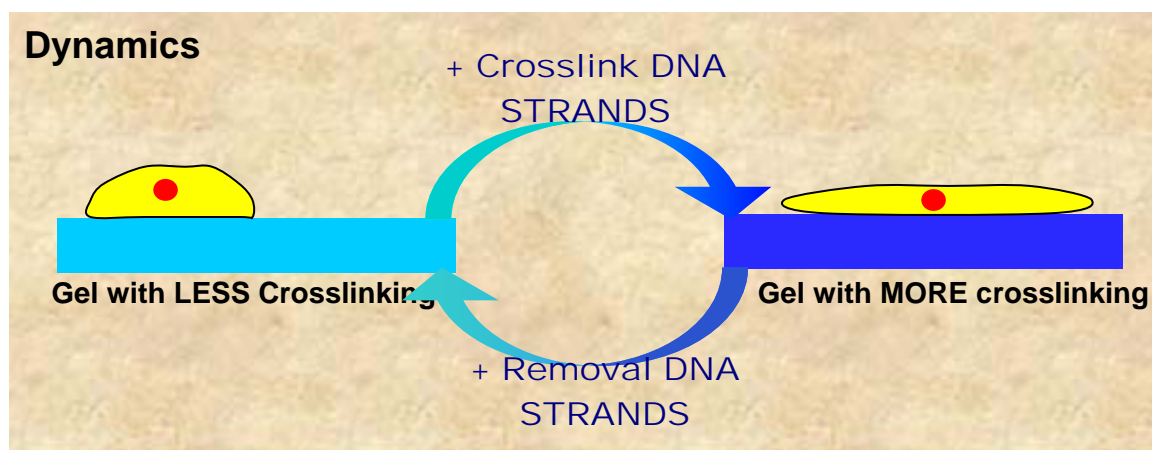


Figure 4B-18 Schematic of the modifications of the mechanical compliance of the substrate upon the delivery of crosslinker DNA or its complements ('Removal DNA'). Both increase and decrease in the mechanical stiffness can be made available.

References

1. Abbott, N. L., C. B. Gorman, and G. M. Whitesides. Active control of wetting using applied electrical potentials and self-assembled monolayers. *Langmuir*. 11:16-18, 1995.
2. Altschul, S. F., W. Gish, W. Miller, E. W. Myers, and D. J. Lipman. Basic local alignment search tool. *J Mol Biol*. 215:403-410, 1990.
3. Angers-Loustau, A., J. F. Cote, A. Charest, D. Dowbenko, S. Spencer, L. A. Lasky, and M. L. Tremblay. Protein tyrosine phosphatase- η regulates focal adhesion disassembly, migration, and cytokinesis in fibroblasts. *J Cell Biol*. 144:1019-1031, 1999.
4. Badylak, S. F. The extracellular matrix as a biologic scaffold material. *Biomaterials*. 28:3587-3593, 2007.
5. Bao, G., and S. Suresh. Cell and molecular mechanics of biological materials. *Nat Mater*. 2:715-725, 2003.
6. Beningo, K. A., M. Dembo, and Y. L. Wang. Responses of fibroblasts to anchorage of dorsal extracellular matrix receptors. *Proc Natl Acad Sci U S A*. 101:18024-18029, 2004.
7. Bershadsky, A. D., N. Q. Balaban, and B. Geiger. Adhesion-dependent cell mechanosensitivity. *Annu Rev Cell Dev Biol*. 19:677-695, 2003.
8. Bischofs, I. B., and U. S. Schwarz. Cell organization in soft media due to active mechanosensing. *Proc Natl Acad Sci U S A*. 100:9274-9279, 2003.
9. Bischofs, I. B., S. A. Safran, and U. S. Schwarz. Elastic interactions of active cells with soft materials. *Phys Rev E Stat Nonlin Soft Matter Phys*. 69:021911, 2004.
10. Bray, D. Axonal growth in response to experimentally applied mechanical tension. *Dev Biol*. 102:379-389, 1984.
11. Brown, R. A., R. Prajapati, D. A. McGrouther, I. V. Yannas, and M. Eastwood. Tensional homeostasis in dermal fibroblasts: Mechanical responses to mechanical loading in three-dimensional substrates. *J Cell Physiol*. 175:323-332, 1998.
12. Butler, J. P., I. M. Tolic-Norrelykke, B. Fabry, and J. J. Fredberg. Traction fields, moments, and strain energy that cells exert on their surroundings. *Am J Physiol Cell Physiol*. 282:C595-605, 2002.
13. Chen, C. S., M. Mrksich, S. Huang, G. M. Whitesides, and D. E. Ingber. Geometric control of cell life and death. *Science*. 276:1425-1428, 1997.
14. Chen, C. S., J. Tan, and J. Tien. Mechanotransduction at cell-matrix and cell-cell contacts. *Annu Rev Biomed Eng*. 6:275-302, 2004.
15. Chen, C. S., X. Jiang, and G. M. Whitesides. Microengineering the environment of mammalian cells in culture. *MRS BULLETIN*. 30:2005.
16. Chicurel, M. E., C. S. Chen, and D. E. Ingber. Cellular control lies in the balance of forces. *Curr Opin Cell Biol*. 10:232-239, 1998.
17. Cukierman, E., R. Pankov, D. R. Stevens, and K. M. Yamada. Taking cell-matrix adhesions to the third dimension. *Science*. 294:1708-1712, 2001.
18. Cullen, D. K., M. C. Lessing, and M. C. LaPlaca. Collagen-dependent neurite outgrowth and response to dynamic deformation in three-dimensional neuronal cultures. *Ann Biomed Eng*. 35:835-846, 2007.

19. De, R., A. Zemel, and S. A. Safran. Dynamics of cell orientation. *Nat Phys.* 3:655-659, 2007.
20. De, R., A. Zemel, and S. A. Safran. Do cells sense stress or strain? Measurement of cellular orientation can provide a clue. *Biophys J.* 94:L29-31, 2008.
21. Discher, D. E., P. Janmey, and Y. L. Wang. Tissue cells feel and respond to the stiffness of their substrate. *Science.* 310:1139-1143, 2005.
22. Engler, A. J., S. Sen, H. L. Sweeney, and D. E. Discher. Matrix elasticity directs stem cell lineage specification. *Cell.* 126:677-689, 2006.
23. Freed, L. E., R. Langer, I. Martin, N. R. Pellis, and G. Vunjak-Novakovic. Tissue engineering of cartilage in space. *Proc Natl Acad Sci U S A.* 94:13885-13890, 1997.
24. Geiger, B. Cell biology. Encounters in space. *Science.* 294:1661-1663, 2001.
25. Georges, P. C., W. J. Miller, D. F. Meaney, E. S. Sawyer, and P. A. Janmey. Matrices with compliance comparable to that of brain tissue select neuronal over glial growth in mixed cortical cultures. *Biophys J.* 90:3012-3018, 2006.
26. Georges, P. C., J. J. Hui, Z. Gombos, M. E. McCormick, A. Y. Wang, M. Uemura, R. Mick, P. A. Janmey, E. E. Furth, and R. G. Wells. Increased stiffness of the rat liver precedes matrix deposition: Implications for fibrosis. *Am J Physiol Gastrointest Liver Physiol.* 293:G1147-1154, 2007.
27. Goffin, J. M., P. Pittet, G. Csucs, J. W. Lussi, J. J. Meister, and B. Hinz. Focal adhesion size controls tension-dependent recruitment of alpha-smooth muscle actin to stress fibers. *J Cell Biol.* 172:259-268, 2006.
28. Goldmann, W. H. Mechanical aspects of cell shape regulation and signaling. *Cell Biol Int.* 26:313-317, 2002.
29. Huang, S., and D. E. Ingber. Cell tension, matrix mechanics, and cancer development. *Cancer Cell.* 8:175-176, 2005.
30. Ingber, D. E. Mechanical signaling and the cellular response to extracellular matrix in angiogenesis and cardiovascular physiology. *Circ Res.* 91:877-887, 2002.
31. James, J., E. D. Goluch, H. Hu, C. Liu, and M. Mrksich. Subcellular curvature at the perimeter of micropatterned cells influences lamellipodial distribution and cell polarity. *Cell Motil Cytoskeleton.* 65:841-852, 2008.
32. Janmey, P. A., and D. A. Weitz. Dealing with mechanics: Mechanisms of force transduction in cells. *Trends Biochem Sci.* 29:364-370, 2004.
33. Jiang, F. X., B. Yurke, B. L. Firestein, and N. A. Langrana. Neurite outgrowth on a DNA crosslinked hydrogel with tunable stiffnesses. *Ann Biomed Eng.* 36:1565-1579, 2008.
34. Jiang, X., P. C. Georges, B. Li, Y. Du, M. K. Kutzin, M. L. Previtiera, N. A. Langrana, and B. L. Firestein. Cell growth in response to mechanical stiffness is affected by neuron-astroglia interactions. *Open Neuroscience Journal.* 1:7-14, 2007.
35. Jungbauer, S., H. Gao, J. P. Spatz, and R. Kemkemer. Two characteristic regimes in frequency dependent dynamic reorientation of fibroblasts on cyclically stretched substrates. *Biophys J.* 2008.

36. Katz, B. Z., E. Zamir, A. Bershadsky, Z. Kam, K. M. Yamada, and B. Geiger. Physical state of the extracellular matrix regulates the structure and molecular composition of cell-matrix adhesions. *Mol Biol Cell*. 11:1047-1060, 2000.
37. Lahann, J., and R. Langer. Smart materials with dynamically controllable surfaces. *MRS BULLETIN*. 30:185-188, 2005.
38. Li, F., B. Li, Q. M. Wang, and J. H. Wang. Cell shape regulates collagen type i expression in human tendon fibroblasts. *Cell Motil Cytoskeleton*. 65:332-341, 2008.
39. Li, S., P. Butler, Y. Wang, Y. Hu, D. C. Han, S. Usami, J. L. Guan, and S. Chien. The role of the dynamics of focal adhesion kinase in the mechanotaxis of endothelial cells. *Proc Natl Acad Sci U S A*. 99:3546-3551, 2002.
40. Lin, D., N. Langrana, and B. Yurke. Inducing reversible stiffness changes in DNA-crosslinked gels. *Journal of Materials Research*. 20:1456-1464, 2006.
41. Lin, D. C., B. Yurke, and N. A. Langrana. Mechanical properties of a reversible, DNA-crosslinked polyacrylamide hydrogel. *J Biomech Eng*. 126:104-110, 2004.
42. Marquez, J. P., G. M. Genin, K. M. Pryse, and E. L. Elson. Cellular and matrix contributions to tissue construct stiffness increase with cellular concentration. *Ann Biomed Eng*. 34:1475-1482, 2006.
43. McElhaney, J. H., J. W. Melvin, V. L. Roberts, and H. D. Portnoy. Dynamic characteristics of the tissues of the head,. In: R. M. Kenedi, editor. *Perspectives in biomedical engineering*, MacMillan Press: London, 1973; pp 215-222.
44. Meiss, R. A. Dynamic stiffness of rabbit mesotubarium smooth muscle: Effect of isometric length. *Am J Physiol*. 234:C14-26, 1978.
45. Mrksich, M. Dynamic substrates for cell biology. *MRS BULLETIN*. 30:180-184, 2005.
46. Paszek, M. J., and V. M. Weaver. The tension mounts: Mechanics meets morphogenesis and malignancy. *J Mammary Gland Biol Neoplasia*. 9:325-342, 2004.
47. Pelham, R. J., Jr., and Y. Wang. Cell locomotion and focal adhesions are regulated by substrate flexibility. *Proc Natl Acad Sci U S A*. 94:13661-13665, 1997.
48. Petroll, W. M., and L. Ma. Direct, dynamic assessment of cell-matrix interactions inside fibrillar collagen lattices. *Cell Motil Cytoskeleton*. 55:254-264, 2003.
49. Petroll, W. M., M. Vishwanath, and L. Ma. Corneal fibroblasts respond rapidly to changes in local mechanical stress. *Invest Ophthalmol Vis Sci*. 45:3466-3474, 2004.
50. Reinhart-King, C. A., M. Dembo, and D. A. Hammer. The dynamics and mechanics of endothelial cell spreading. *Biophys J*. 89:676-689, 2005.
51. Rivelino, D., E. Zamir, N. Q. Balaban, U. S. Schwarz, T. Ishizaki, S. Narumiya, Z. Kam, B. Geiger, and A. D. Bershadsky. Focal contacts as mechanosensors: Externally applied local mechanical force induces growth of focal contacts by an mdia1-dependent and rock-independent mechanism. *J Cell Biol*. 153:1175-1186, 2001.
52. Roy, I., and M. N. Gupta. Smart polymeric materials: Emerging biochemical applications. *Chem Biol*. 10:1161-1171, 2003.

53. Saez, A., A. Buguin, P. Silberzan, and B. Ladoux. Is the mechanical activity of epithelial cells controlled by deformations or forces? *Biophys J.* 89:L52-54, 2005.
54. Saez, A., M. Ghibaudo, A. Buguin, P. Silberzan, and B. Ladoux. Rigidity-driven growth and migration of epithelial cells on microstructured anisotropic substrates. *Proc Natl Acad Sci U S A.* 104:8281-8286, 2007.
55. Schwarz, U. S., N. Q. Balaban, D. Riveline, L. Addadi, A. Bershadsky, S. A. Safran, and B. Geiger. Measurement of cellular forces at focal adhesions using elastic micro-patterned substrates. *Materials Science & Engineering C-Biomimetic and Supramolecular Systems.* 23:387-394, 2003.
56. Shreiber, D. I., V. H. Barocas, and R. T. Tranquillo. Temporal variations in cell migration and traction during fibroblast-mediated gel compaction. *Biophys J.* 84:4102-4114, 2003.
57. Singhvi, R., A. Kumar, G. P. Lopez, G. N. Stephanopoulos, D. I. Wang, G. M. Whitesides, and D. E. Ingber. Engineering cell shape and function. *Science.* 264:696-698, 1994.
58. Smilenov, L. B., A. Mikhailov, R. J. Pelham, E. E. Marcantonio, and G. G. Gundersen. Focal adhesion motility revealed in stationary fibroblasts. *Science.* 286:1172-1174, 1999.
59. Smith, D. H., J. A. Wolf, and D. F. Meaney. A new strategy to produce sustained growth of central nervous system axons: Continuous mechanical tension. *Tissue Eng.* 7:131-139, 2001.
60. Solon, J., I. Levental, K. Sengupta, P. C. Georges, and P. A. Janmey. Fibroblast adaptation and stiffness matching to soft elastic substrates. *Biophys J.* 93:4453-4461, 2007.
61. Sumura, M., K. Shigeno, T. Hyuga, T. Yoneda, H. Shiina, and M. Igawa. Initial evaluation of prostate cancer with real-time elastography based on step-section pathologic analysis after radical prostatectomy: A preliminary study. *Int J Urol.* 14:811-816, 2007.
62. Sundararaghavan, H. G., G. A. Monteiro, N. A. Lapin, Y. J. Chabal, J. R. Miksan, and D. I. Shreiber. Genipin-induced changes in collagen gels: Correlation of mechanical properties to fluorescence. *J Biomed Mater Res A.* 2008.
63. Thoumine, O. Control of cellular morphology by mechanical factors. *Journal de Physique III.* 6:1555-1566, 1996.
64. Tjia, J. S., and P. V. Moghe. Regulation of cell motility on polymer substrates via "Dynamic," Cell internalizable, ligand microinterfaces. *Tissue Eng.* 8:247-261, 2002.
65. Tomasek, J. J., and E. D. Hay. Analysis of the role of microfilaments and microtubules in acquisition of bipolarity and elongation of fibroblasts in hydrated collagen gels. *J Cell Biol.* 99:536-549, 1984.
66. Trotter, J. A., J. Tipper, G. Lyons-Levy, K. Chino, A. H. Heuer, Z. Liu, M. Mrksich, C. Hodneland, W. S. Dillmore, T. J. Koob, M. M. Koob-Emunds, K. Kadler, and D. Holmes. Towards a fibrous composite with dynamically controlled stiffness: Lessons from echinoderms. *Biochem Soc Trans.* 28:357-362, 2000.
67. Tseng, Y., T. P. Kole, S.-H. J. Lee, and D. Wirtz. Local dynamics and viscoelastic properties of cell biological systems *Current Opinion in Colloid & Interface Science.* 7:210-217 2002.

68. Wakatsuki, T., M. S. Kolodney, G. I. Zahalak, and E. L. Elson. Cell mechanics studied by a reconstituted model tissue. *Biophys J.* 79:2353-2368, 2000.
69. Wang, H. B., M. Dembo, S. K. Hanks, and Y. Wang. Focal adhesion kinase is involved in mechanosensing during fibroblast migration. *Proc Natl Acad Sci U S A.* 98:11295-11300, 2001.
70. Wang, N., and D. E. Ingber. Control of cytoskeletal mechanics by extracellular matrix, cell shape, and mechanical tension. *Biophys J.* 66:2181-2189, 1994.
71. Wang, N., and D. Stamenovic. Contribution of intermediate filaments to cell stiffness, stiffening, and growth. *Am J Physiol Cell Physiol.* 279:C188-194, 2000.
72. Wang, N., E. Ostuni, G. M. Whitesides, and D. E. Ingber. Micropatterning tractional forces in living cells. *Cell Motil Cytoskeleton.* 52:97-106, 2002.
73. Wang, N., I. M. Tolic-Norrelykke, J. Chen, S. M. Mijailovich, J. P. Butler, J. J. Fredberg, and D. Stamenovic. Cell prestress. I. Stiffness and prestress are closely associated in adherent contractile cells. *Am J Physiol Cell Physiol.* 282:C606-616, 2002.
74. Wang, Q., W. Xian, S. Li, C. Liu, and G. W. Padua. Topography and biocompatibility of patterned hydrophobic/hydrophilic zein layers. *Acta Biomater.* 4:844-851, 2008.
75. Wang, X., M. Berggren, and O. Inganäs. Dynamic control of surface energy and topography of microstructured conducting polymer films. *Langmuir.* 24:5942-5948, 2008.
76. Wang, Y. L., and R. J. Pelham, Jr. Preparation of a flexible, porous polyacrylamide substrate for mechanical studies of cultured cells. *Methods Enzymol.* 298:489-496, 1998.
77. Wells, R. G. The role of matrix stiffness in regulating cell behavior. *Hepatology.* 47:1394-1400, 2008.
78. Wottawah, F., S. Schinkinger, B. Lincoln, R. Ananthakrishnan, M. Romeyke, J. Guck, and J. Kas. Optical rheology of biological cells. *Phys Rev Lett.* 94:098103, 2005.
79. Yang, J., M. Yamato, and T. Okano. Cell-sheet engineering using intelligent surfaces. *MRS BULLETIN.* 30:189-193, 2005.
80. Yeo, W.-S., M. N. Yousaf, and M. Mrksich. Dynamic interfaces between cells and surfaces: Electroactive substrates that sequentially release and attach cells. *Journal of the American Chemical Society* 125:14994-14995, 2003.
81. Yeung, T., P. C. Georges, L. A. Flanagan, B. Marg, M. Ortiz, M. Funaki, N. Zahir, W. Ming, V. Weaver, and P. A. Janmey. Effects of substrate stiffness on cell morphology, cytoskeletal structure, and adhesion. *Cell Motil Cytoskeleton.* 60:24-34, 2005.
82. Yousaf, M. N., B. T. Houseman, and M. Mrksich. Using electroactive substrates to pattern the attachment of two different cell populations. *Proc Natl Acad Sci U S A.* 98:5992-5996, 2001.
83. Zheng, J., P. Lamoureux, V. Santiago, T. Dennerll, R. E. Buxbaum, and S. R. Heidemann. Tensile regulation of axonal elongation and initiation. *J Neurosci.* 11:1117-1125, 1991.
84. Zhu, C., G. Bao, and N. Wang. Cell mechanics: Mechanical response, cell adhesion, and molecular deformation. *Annu Rev Biomed Eng.* 2:189-226, 2000.

CHAPTER 4C SPINAL CORD NEURONS ON A DYNAMIC SUBSTRATES

4C.1 Background

4C.1.1 Neuronal mechano-sensing

By using a number of hydrogel-based cell culture systems, previous studies by our group^{28, 29} and others^{17, 20, 47, 54} showed that neurons and other cell types, including fibroblasts, epithelial cells, hepatocytes and embryonic stem cells³⁶, have the capability of sensing and reacting to mechanical stiffnesses. Flanagan and colleagues¹⁷ first introduced a popular bis-acrylamide crosslinked hydrogel based culture system for probing neuronal behavior and found that, indeed, compared to those grown on gels of 550 Pa (shear modulus), mouse spinal cord neurons on much softer gels (50 Pa, shear modulus) have significantly higher dendrite branch number (i.e., secondary dendrite number), and glial cell growth is notably suppressed. Along the same line, cortical neurons were the subject of the study by Georges and co-workers²⁰. They also observed strikingly less spreading of astrocytes and disorganized F-actin structure on approximately 200 Pa (shear modulus) substrates than on 9 kPa (shear modulus) substrates. PC12 cells, a neuron-like cell type, were cultured on a polyethylene glycol (PEG) hydrogel, and their outgrowth was found to be greater on more compliant hydrogels²³. Leach et al.³² further discovered that, on a stiffness range lower than that in the work by Gunn et al.²³, neurites appear to demonstrate preference for more rigid gels,

which suggests an optimal stiffness range and that the preference over stiffness is not monotonic. Contributing factors such as species difference and cell type disparity were noted in these studies and demonstrate the complexity of neuronal mechano-sensing. On the system level, mechanical cues, such as stress, have been implicated in neuro-degenerative disorders²⁴ (for instance, by promoting protein aggregation) and spinal cord injury (SCI).

Recently, by examining neurite outgrowth of rat spinal cord cells on bis gels, our group pointed out that for primary neuronal types including rat spinal cord neurons, neuron-astroglia interactions would be coupled with their respective mechano-responses²⁹. It was further recognized that even for the primary structures, including primary dendrite and axons, for each property, there is a distinctive response to mechanical stiffness depending on the stiffness range²⁸. For instance, on softer gels (around a few kPa), primary dendrite number is lower while axons are significantly longer, whereas the average primary dendrite length remains unchanged over the range of gel stiffnesses.

A partial list of published studies on the mechano-sensing of the neurons to the substrate mechanical stiffness is presented in Table 4C-1.

Table 4C-1 Partial list of the previous reports of neuronal responses to the rigidity of the substrate and ECM.

(Ms = mouse; Rt = rat; Ck = chick; PAM = polyacrylamide; SC = spinal cord; DRG = dorsal root ganglion; PAM = polyacrylamide gels; DNA-PAM = DNA crosslinked polyacrylamide gels; ↓ decrease; ↑ increase)

Neuronal type	Substrate	Major observations	Ref.
Ms SC	PAM	No glia grew on any of the gels (50~550 Pa); Neuron branch points ↑ on soft gels ¹⁷	¹⁷
Ms cortical	PAM	Astrocytes spreading ↓ organized F-actin ↓ on soft gels; Neurons extended long neurites and polymerize actin filaments on both soft and stiff gels ²⁰	²⁰
Ck DRG	Collagen	Duro-taxis	⁴⁷
Ck DRG	PAM	Neurite extension on soft gels	⁵⁴
Ms hippocampal	PAM	Neurite extension inhibited on rigid surfaces	³⁰
PC12*	PAM	Threshold response	³²
Rt SC	PAM	Neuron-glia interactions affect cell mechano-sensing	²⁹
Rt SC	DNA-PAM	Mechanosensing of neurons is cell property specific Axons length ↑ dendrites length does not change; Dendrite number ↓ on soft gels,	²⁸
Ck DRG	Agarose gel	Rate of neurite extension was inversely correlated to the mechanical stiffness	⁴

* These are neuron-like cells.

4C.1.2 Mechanically dynamic stimuli

CNS tissue, like other tissues, constantly undergoes remodeling, and ECM undergoes degradation and synthesis, which forms the basis for potential mechanical stiffness changes. Moreover, under external load, their mechanical compliance may be modified. For instance, there is a significant increase in mechanical stiffness of dura mater upon mechanical load^{37, 46, 53}.

As with the case of fibroblasts, the neurons of the CNS experience constantly changing physiological conditions, in this case due, in part, to the functional roles assumed by the abundant supporting glial cells. These glia work closely with neurons by acting as scaffolds for neuronal migration and axonal elongation, providing structural support to neurons by secreting ECM molecules such as proteoglycans and proteins and scavenging debris generated by neurons³⁵. As a result, neurites extend in an environment which is both complex and dynamic¹². This picture has been established by some early studies including one on the mechanical stiffness of the brain tissues¹⁴ and other reports^{26, 50}. Ageing and pathological conditions could also add to the variation in the mechanical property changes of the CNS¹⁹.

We deployed DNA crosslinked polyacrylamide hydrogel to probe the mechano-responses of the rat spinal cord cells as we did for the fibroblasts in Chapter 4B. Dynamic stiffness changes were introduced and neurite outgrowth was assessed.

4C.2 Materials and methods

4C.2.1 DNA sequence design and DNA gel preparation

Sequences of Design B (10/10/20, Table 3B-1 and Appendix 2) were chosen, and in order to make it possible to decrease the DNA crosslinking density, a toe-hold region was designed and added to the end of the crosslinker L2 used in the study with static stiffness (Chapter 3B) (Figure 2-1 and Table 4C-2). Like the sequences of the strands for Design B, the sequence of the toe-hold was chosen to minimize unwanted hybridization, reduce the possibility of secondary structure formation, and to reach balanced AT/GC content. Delivery of the complement of L2 and its toe-hold will enable reduction in the crosslinking level, owing to DNA strand displacement via branch migration (Figure 2-1). It was assumed that, by attachment of the toe-hold sequence to 3' of the crosslinker DNA, the resulting mechanical stiffness of the gel would not be significantly changed, since the toehold does not participate in crosslinking and is flexible as single stranded DNA. For instance, it is conceivable that 10/10/20 gels (Table 3B-1B) and 10/10/30 gels (Table 4C-2) have the same rigidity under the same level of crosslinking and experimental conditions.

DNA gels were prepared following procedures as described in Chapter 3B, Section 3B.2.1. The gels were crosslinked either at 100% or 50%, which means that the initial quantity (in number of moles) of the crosslinker DNA is either the same or half of that of SA1 and SA2. Prepared DNA gels were then rinsed and allowed to swell to equilibrium for over two days.

4C.2.2 DNA gel functionalization

The procedure used for DNA gel immobilization, functionalization and protein conjugation is outlined in Figure 4C-1. DNA gel immobilization was performed by following a previous method using an optical adhesive²⁸ (Figure 4C-1). A bifunctional photo-activable crosslinker, Sulfo SANPAH (Pierce, Rockford, IL), in HEPES was used to conjugate ECM molecules onto the gel surface for cell attachment. Poly-D-lysine (PDL, Sigma, St. Louis, MO) at 1 mg/mL was applied in all experiments and stored at 4°C for overnight, after which excess PDL was removed.

4C.2.3 Neuronal cell culture and DNA delivery

Procedures for acquisition of rat embryonic spinal cord, spinal cord dissociation, and cell culture were followed as described in Chapter 3B. On DIV 4, an appropriate amount of sterile ssDNA strand was added to the cell culture, and the culture was kept a humidified CO₂ incubator at 37°C for three more days, and on DIV 7, cells were fixed. The details of the DNA delivery to each of the gel groups are provided in Table 4C-3 and Figure 4C-2. The minimal number of experiments performed was three.

Two sample groups were used to study the potential direct effect of the exogenous DNA on neurite outgrowth. One of the groups consisted of PDL coated culture plates without exogenous DNA addition (designated as ‘DNA-’); the other is identical except that CL2 (Table 4C-2) was added to assess the biological effect of the delivered DNA (designated as ‘DNA+’). For dynamic DNA gels, three dynamic gel groups were adopted, including D100_80 (100%→80%), D100_50 (100%→50%), and D100_Non (100%→100%) with the delivery of DNA strands of non-specific sequences, where the

percentages are in terms of crosslink density of DNA gels). A 30-nt long strand of poly-A sequence (NonL2) was used as the non-specific sequence, and D100_Non was introduced to serve as negative control for the other groups.

4C.2.4 Cell growth characterization and statistical analysis

Similar to the studies carried out in Chapter 3B, spinal cord cells were fixed, blocked and immunostained for axon (anti-Tau-1), dendrites and cell body (anti-MAP2), and DAPI stain was performed to identify intact cells. The antibodies used in the current study were also the same as those used in Chapter 3B, with the addition of the polyclonal antibody against neural cell adhesion molecules (N-CAM) (1:1000, Chemicon) for which cells were not permeabilized. In actin staining, cells were permeabilized by 0.5% Triton X-100 incubation for 15 min at RT before rhodamine phalloidin (1:300, Invitrogen) was applied. The cells were kept in rhodamine-conjugated phalloidin for 20 min at RT followed by intensive rinsing.

In quantification of the FAK expression in the neuronal cell body, spinal cord cells grown on DNA gels were imaged under the same conditions (same exposure time and camera setting) using fluorescence microscopy. The fluorescence intensity inside the neuronal cell body (identified by MAP2 immunofluorescence) was measured using ImageJ software (NIH, Bethesda, MD), which yielded the mean, maximal and minimum of intensity inside the cell body. The FAK fluorescence intensity in each neuron was grouped for each gel condition. In quantification of the neurite growth, a blinding procedure was used to eliminate possible operator bias (conscious or unconscious) due to the knowledge of the results from neurons on static gels (Chapter 3B).

When making comparisons among three and more groups of DNA gels with same initial gel design (e.g., D100, D100_80, and D100_50, are of the same initial DNA gel design as D100), one way ANOVA was implemented, followed by Tukey's multiple comparisons test. If only two groups of data were compared, unpaired two-tailed *t*-test was performed to determine significance. The difference in distribution among distinct groups was assessed by using Chi-square test of goodness of fit. $p < 0.05$ was considered significant.

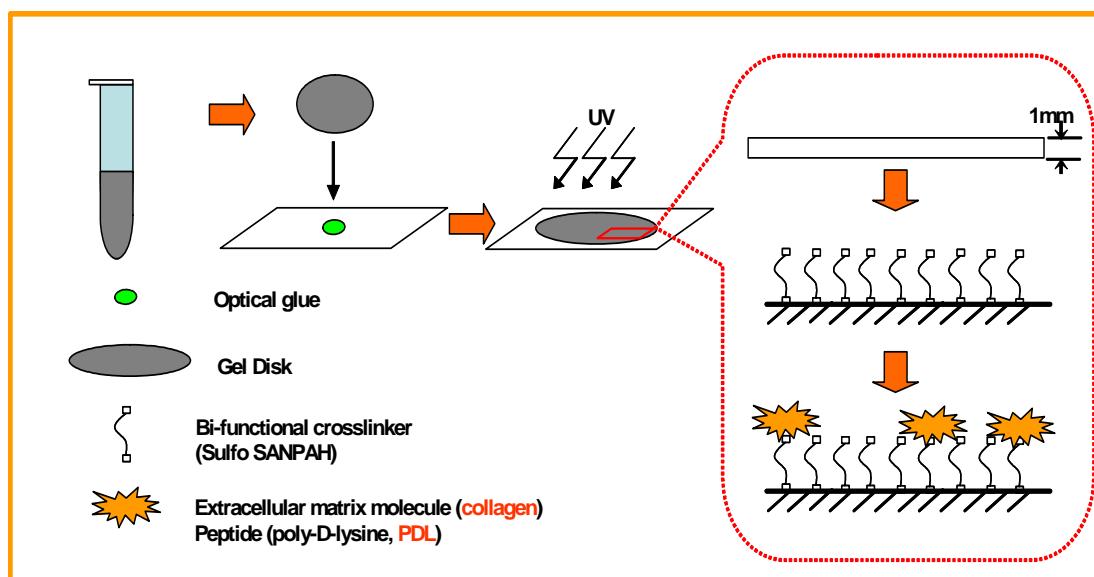


Figure 4C-1 Schematic of procedures in the preparation of DNA crosslinked poly-acrylamide hydrogel.

First, gels were immobilized by using an optical glue under UV exposure. A bifunctional crosslinker, Sulfo SANPAH is used to conjugate protein to the gel surface.

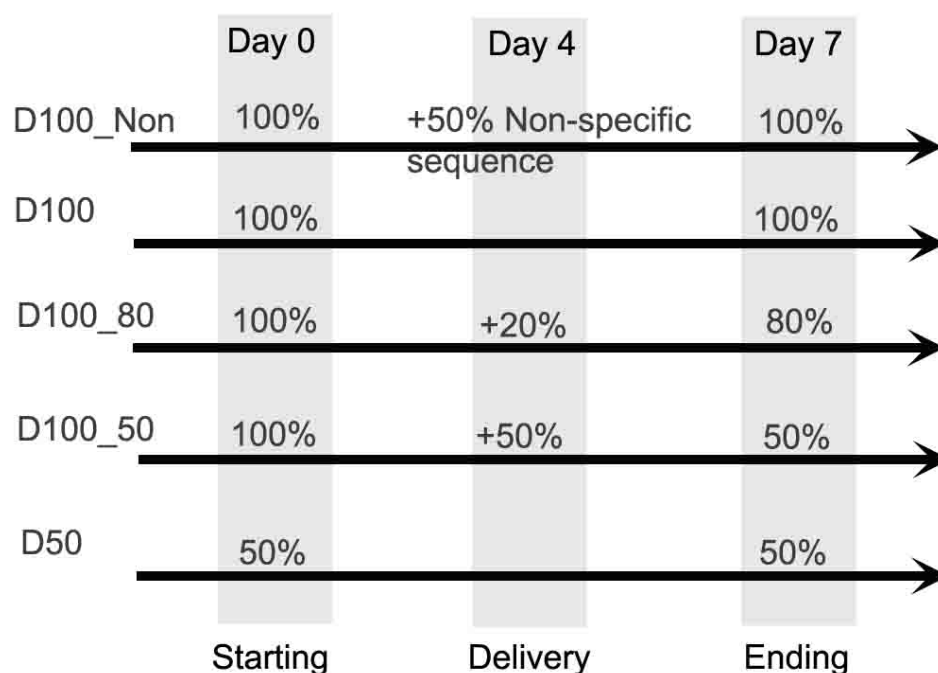


Figure 4C-2 Schematic of the DNA delivery to the DNA gel groups for spinal cord cell culture.

At Day 0, the cells are seeded and allowed to adhere and grow for two days. As indicated, various amounts of crosslinker DNA is delivered at Day 4. DNA diffusion into gel network is estimated to be within hours and spinal cord cells will be exposed to the changing stiffness of the DNA gel. Cells were fixed at Day 7, and analyzed.

4C.3 Results

4C.3.1 DNA sequence screening and similarity analysis

The sequences of the DNA strands used in preparation of DNA gels are similar to that used in Chapter 3B, except that a 10 nt long toe-hold region is attached to the 3' end of the crosslinker DNA to enable de-gelation (Table 4C-2). The sequences of crosslinker DNA (L2, Table 4C-2) and their complementary strands (CL2) were queried against the National Center for Biotechnology Information (NCBI) nucleotide database by using a basic local alignment search tool (BLAST) algorithm² for close resemblance to the biological sequences and particularly in relation to CNS tissues and cells. The genome for rat (rat spinal cord) was checked against in the screening.

No significant similarity was found for the sequences of the complementary strands of CL2 (Table 4C-2) in Design B (Appendix 4). The likelihood is small that delivered crosslinker DNA could act as anti-sense DNA affecting gene expression, which could potentially alter the phenotype of the cells including neurons. Thus, it is unlikely that these DNA strands would cause any significant change in the cell response and behavior as manifested in their morphology and function.

Table 4C-2 DNA sequences used in the study of neurite outgrowth on DNA gels with dynamic stiffness. .

SA1 and SA2 are single-stranded DNA (ssDNA) side chains. L2 is the crosslinker DNA with part of its sequence complementary to SA1 and SA2. CL2 is the strand complementary to L2. L2_Non is the ssDNA whose sequences are not complementary to SA1, SA2 or L2 and here we used poly-A sequence.

DNA strand	# nt	Design A- DNA sequence (5' to 3')
SA1	10	GCA CCT TTG C
SA2	10	GTC AGA ATG A
L2	30	TCA TTC TGA CGC AAA GGT GCG CTA CAC TTG
CL2	30	CAA GTG TAG CGC ACC TTT GCG TCA GAA TGA
L2_Non	30	AAA AAA AAA AAA AAA AAA AAA AAA AAA AAA

Table 4C-3 The initial and final crosslinking density of different schemes of crosslinker DNA delivery.

Designation	D100_Non	D100	D100_80	D100_50	D50
Initial crosslinking density	100%	100%	100%	100%	50%
Final crosslinking disunity	100%	100%	80%	50%	50%
DNA delivery	50% *	—	20%*	50%	—

*ssDNA with non-specific sequence was delivered.

4C.3.2 Effect of DNA delivery on neurite outgrowth

Neurite outgrowth of the spinal cord cells cultured on tissue culture plates with delivery of exogenous ssDNA (DNA+) was compared with that of the normal control group (DNA-) to assess the potential direct effect of the delivered exogenous DNA on neurite outgrowth. The largest quantity of crosslinker DNA delivered for the groups using DNA gels was applied (50%, Table 4C-3). There was no apparent difference in the morphology of neurites (axons identified by Tau-1 immunostaining and dendrites by MAP2 immunostaining) (Figure 4C-3, upper panel). Quantification of the primary dendrite length and number, and axonal length did not reveal notable variation (Figure 4C-3, lower panel).

This, together with the findings from BLAST search, shows that the delivered DNA *per se* does not markedly alter neuronal survival or neurite outgrowth, and that the difference between DNA gel groups, if any, can be attributed to the stiffness change induced by the introduction of the crosslinker DNA or its complementary strand, and also the incorporation of these strands into the gel network.

4C.3.3 Effect of DNA -induced stiffness change on neurite outgrowth

The multi-polar morphology displayed by spinal cord neurons on dynamic DNA gel groups (D100_80 and D100_50) is similar to that on DNA gels with static stiffnesses (Figure 4C-4). GFAP positive mature astroglia were sporadically seen across the gel groups. There is no distinguishable difference in the total cell number or neuronal cell number on different DNA gel groups. Due to the fact that these cells are from embryos, some neurons might not be mature enough to express MAP2, a mature neuronal marker.

To facilitate the understanding of the results, it would be instrumental to consider gels of 50% and 100% crosslinking as *soft* and *stiff* gels, respectively; thus groups of D100_80 and D100_50 are essentially *Stiff_Medium* and *stiff_Soft* groups, respectively, in terms of changes in stiffness and crosslinking density.

Similar to the observations made on gels with static stiffnesses²⁸, there are cells that grew closely in relatively large aggregates. This also takes place on normal tissue culture plates which is reflective of the fact that normal neuronal function involves cell-cell and cell-substrate interactions⁵¹. However, a number of neurons grew relatively far from neighboring neurons and extended long axons (Figure 4C-4). The network formed by axons is sparse in some cases and rather dense in others (Figure 4C-4). For the characterization of dendritic morphology, only those isolated neurons with clear primary dendritic structures were chosen, and for the length measurement of axons, all traceable Tau-1 positive processes with clear starting and ending point were measured. The results are presented in Figure 4C-5, and the figures were divided into three sections, with Section (I) on the comparison between the negative control (D100_Non) and D100 gel group, Section (II) on the comparison between gel groups of initial crosslinking density at 100% (D100, D100_80, and D100_50), and Section (III) on the comparison between gel group of the same final crosslinking density at 50% (D100_50 and D50). Details of the results are as follows:

(I) As a first step, we investigated the potential effect of exogenous DNA on neurite outgrowth of spinal cord neurons on DNA gels if the intake of these short (30 bps) ssDNA or dsDNA does occur and trigger cellular responses. For the three neuronal cell properties, including primary dendrite length, primary dendrite number, and axonal

length, there is no distinguishable differences between two groups of D100 and D100_Non (Tables 4C-2 and 4C-3) where DNA strands were of non-specific sequence but same length as the intended crosslinker DNA (I of Figure 4C-5).

(II) Three groups of DNA gel groups of initial crosslinking of 100% were then compared, two of which received ssDNA (CL2) complementary to the crosslinker DNA (L2) (Table 4C-2) at different amount to reach different final crosslinking density (Table 4C-3). Outgrowth of primary dendrite of a neuron averagely decreases although the decrease is not notable (Section II of Figure 4C-5A), while the number of the primary dendrites was significantly reduced by approximately 20% (Section II of Figure 4C-5B). The length of axons on dynamic substrates (100_80 and 100_50) also increases and the difference is marked by approximately 20% (Section II of Figure 4C-5C).

(III) Except for the mean primary dendrite length (Section III of Figure 4C-5A), the primary neurites behavior on dynamic substrates is the same as that on the static substrate whose crosslinking density is the same as the ending density in dynamic substrates (Section III of Figure 4C-5: B&C).

As a next step, we examined the neuronal population distribution in terms of neurite outgrowth on different groups (Figure 4C-6). On D100_50 gels, as the crosslinking density decreases from 100% to 50%, a larger percentage of neurons have primary dendrites shorter than 40 μm in average while fewer neurons have primary dendrite longer than 100 μm (Figure 4C-6A). As the stiffness of the substrate decreases (D100 to D100_50), a significantly smaller ($p < 0.01$) proportion of neurons exhibits more than three primary dendrites (Figure 4C-6B). A significantly greater proportion of neurons extended longer ($> 240 \mu\text{m}$) axons when the substrate became softer (e.g., D100

vs.D100_50) (Figure 4C-6C). This is in line with the observations made in the study using gels with static stiffnesses²⁸.

4C.3.4 FAK expression in neurons on dynamic DNA gels

Typical images of focal adhesion kinase (FAK) expression in neurons grown on DNA gels with dynamic stiffnesses are shown in Figures 4C-7 and 4C-8. As reported previously, FAK is expressed in the neuronal cell soma, dendrites and axons. In the mixed cell population of spinal cord cells, FAK was expressed mainly in neurons and only occasionally expressed by other cells (Figure 4C-7).

The fluorescence intensity of FAK in the neuronal soma (identified by MAP2 immuno-fluorescence) was quantified, and there is an apparent difference between gel group whose stiffness was changed from that of the 100% to 50% crosslinked gels (D100_50) and gels with 50% crosslinking throughout the process (D50) (Figure 4C-9, upper panel). The comparison between D100 and D50 groups was also in accordance with the previous finding that there is higher expression of FAK on softer gels²⁸. At the same time, the variation in the expression in the neuronal cell body, as indicated by the ratio between maximal and minimal expression of FAK (Figure 4C-9, lower panel) was greatest on stiffest D100 gels ($p < 0.05$).

4C.3.5 N-CAM expression of spinal cord cells on dynamic substrate

Neuronal cell adhesion molecules (N-CAM) were expressed by neurons and other cells as well (Figure 4C-7), though the expression was not homogenous. It was rarely expressed at the neurites, and commonly in a non-continuous and discrete manner (Figure 4C-7).

Abundance of N-CAM expression was seen in the cell aggregates where fluorescence intensity was highest on the periphery of the neuronal soma (Figure 4C-7).

F-actin staining using phallotoxins showed (Figure 4C-8) that the co-expression between FAK and F-actin is dominant and that there appeared to be a reduction in the F-actin expression in D100_50 gel groups (Figure 4C-8). Unlike that of N-CAM, the expression of F-actin was not limited to cell soma, and F-actin was also stained in the neurites (Figure 4C-8). The intensity of F-actin staining appeared to decrease with the softening of the gels (e.g., from D100 to D100_50 or D50) (Figure 4C-8).

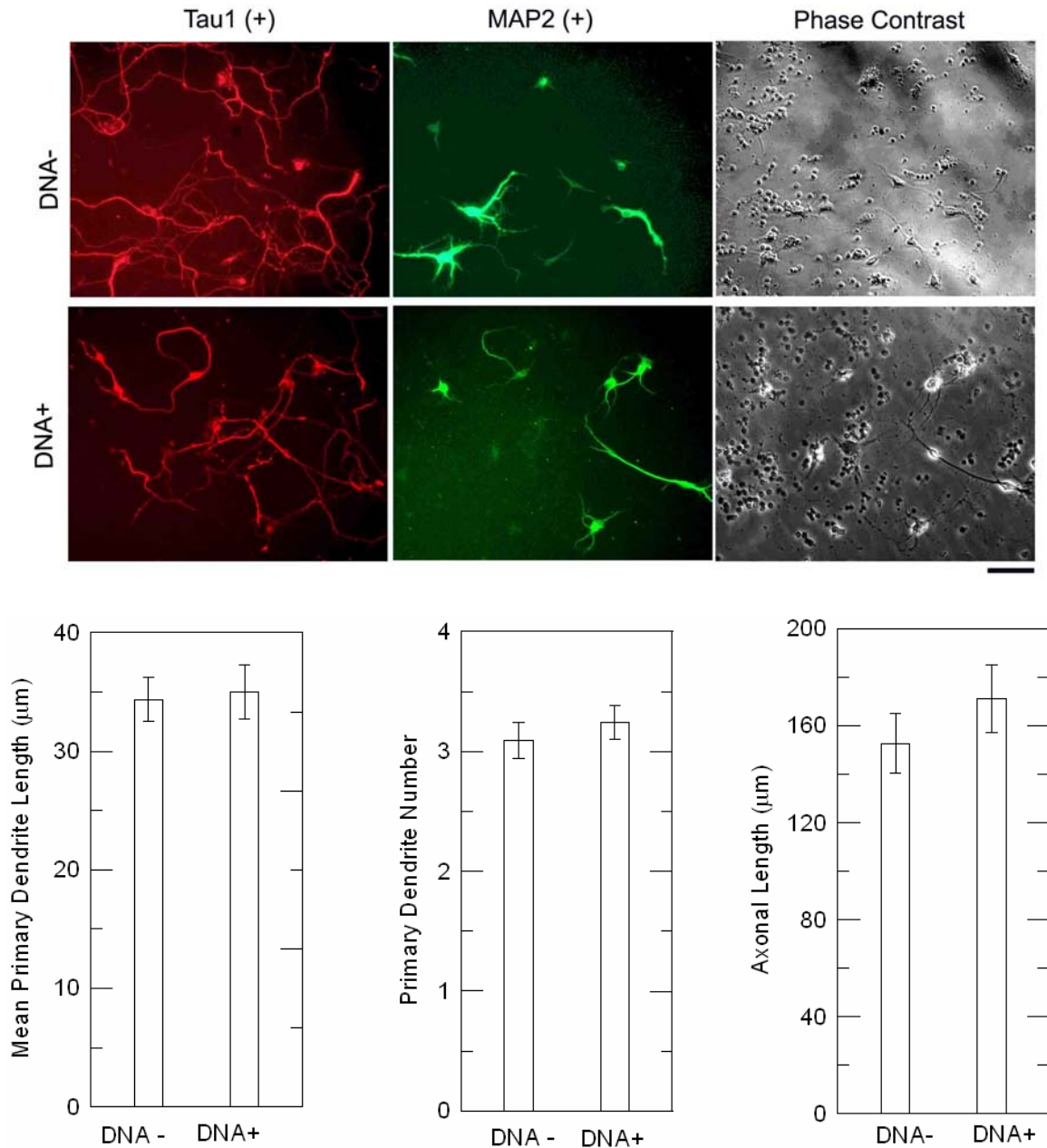


Figure 4C-3 Neurite outgrowth on tissue culture plates with (DNA+) and without (DNA-) DNA delivery.

(Upper panel) Typical morphology of neurons grown on the plates. Scale bar is 30 μm. (Lower panel) Delivered crosslinker DNA did not significantly alter cellular properties, including primary dendrite length, primary dendrite number or axonal length. $n \geq 34$ for mean primary dendrite length; $n \geq 53$ for mean primary dendrite number; $n \geq 25$ for axonal length.

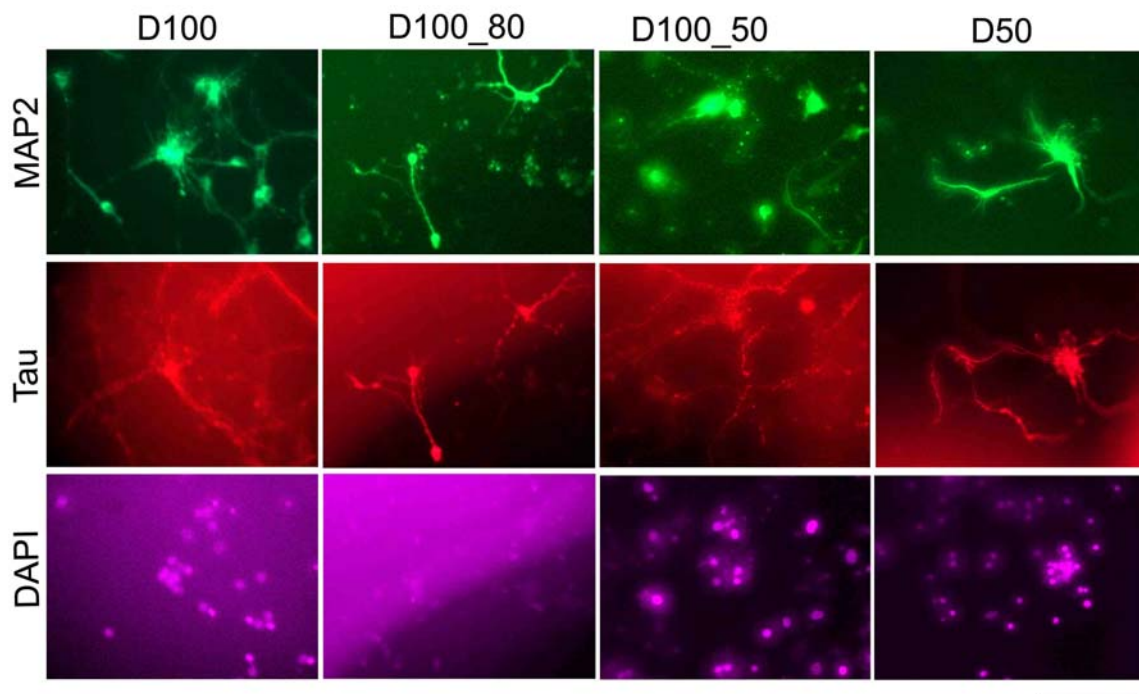


Figure 4C-4 Typical image of spinal cord neurons grown on DNA crosslinked hydrogels with both static (D100 and D50) and dynamic (D100_80 and D100_50) stiffnesses.

Tau-1 immunostaining indicates axons and occasionally neuronal soma, and MAP2 immunostaining shows dendrite and neuronal soma. The blurriness of part of the images is due to the relative unevenness on the gel surface. Scale bar is 100 μm .

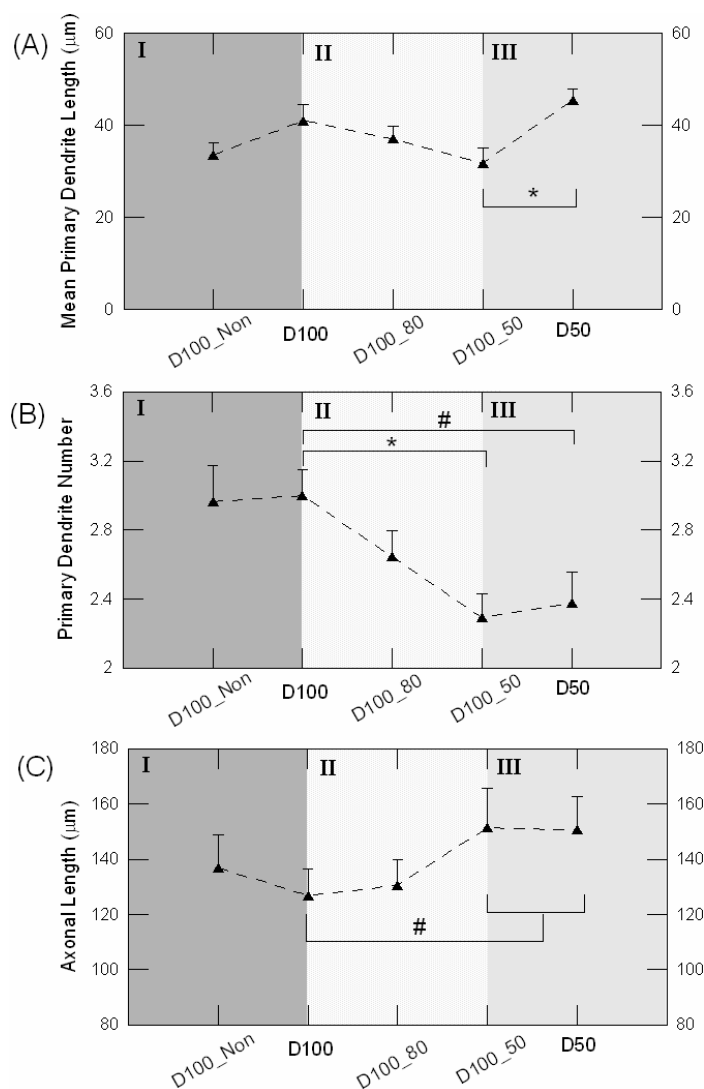


Figure 4C-5 Neurite outgrowth on DNA gels with dynamic stiffnesses.

Comparison of neurite outgrowth, including mean primary dendrite length, primary dendrite number and axonal length per neuron. In section (I), there is no significant difference between D100 and D100_Non, suggesting that delivered DNA does not significantly affect neurite outgrowth. (A) Mean primary dendrite length. No significant difference between groups was observed except that mean primary dendrite length of D100_50 is significantly lower than that on D100 as determined by one-way ANOVA with Tukey's post-test for all three groups. (B) Primary dendrite number. A significant difference was observed between stiffest gels (D100) and D100_50 as determined by one-way ANOVA with Tukey's post-test for all four groups, and also between D100 and D50 as determined by two-tailed unpaired *t*-test. # $p < 0.05$. No significant difference was found as determined by one-way ANOVA with Tukey's post-test for all four groups. (C) Axonal length. Axons on softer gels (D100_50 and D50) are significantly longer than that on stiffer gels as determined by two-tailed unpaired *t*-test. # $p < 0.05$. No significant different was found as determined by one-way ANOVA followed by Tukey's test. Error bars represent standard error of mean. $n > 25$.

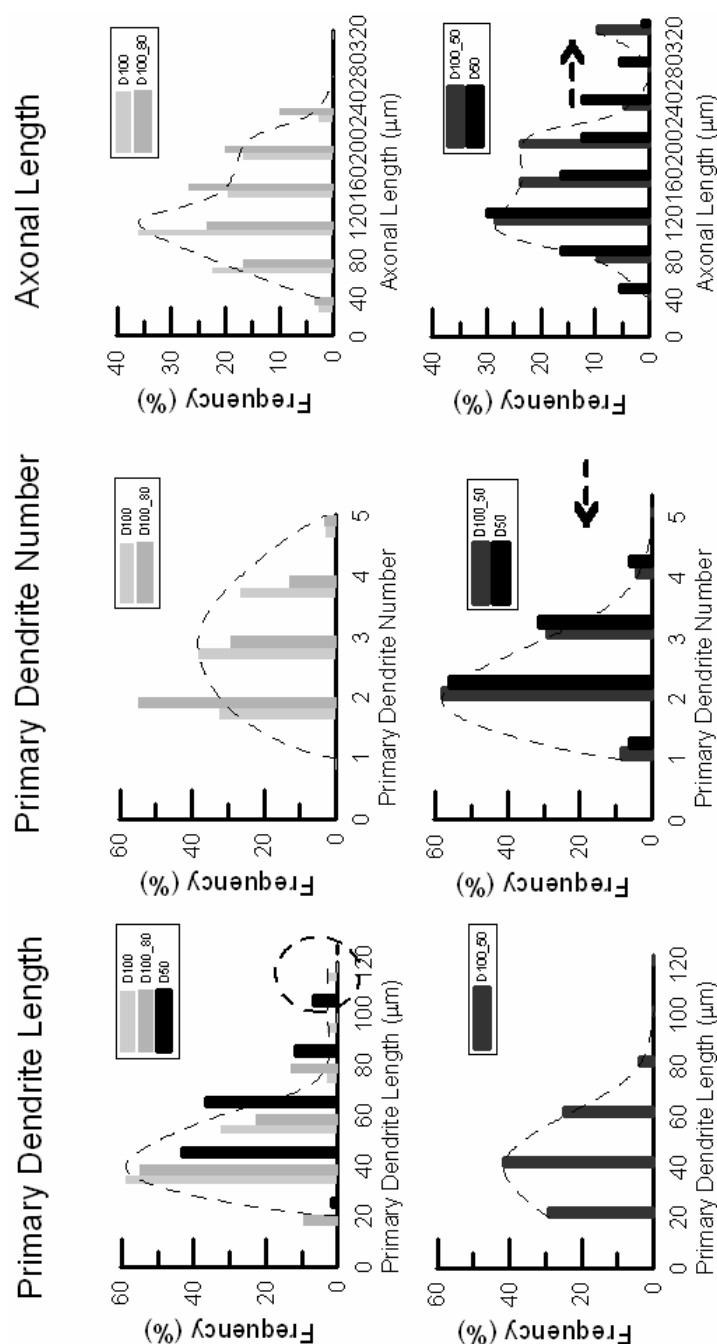


Figure 4C-6 Frequency plots of mean primary dendrite length (A), primary dendrite number (B), and axonal length (C) per neuron on DNA gels with dynamic stiffnesses.

(A) Proportion of neurons having mean primary dendrite length of longer than 80 μm on D100_50 group is much less than D50 as determined by Chi-square test ($p < 0.001$), and slightly lower than the other two groups. (B) A larger proportion of neurons have over 4 primary dendrites on the stiffest gels than the other three groups as determined by Chi-square test ($p < 0.001$). (C) A smaller proportion of neurons have long (over 240 μm) axon on D100 and D100_80 gels than those on B50 and A100 gels as determined by Chi-square test ($p < 0.01$).

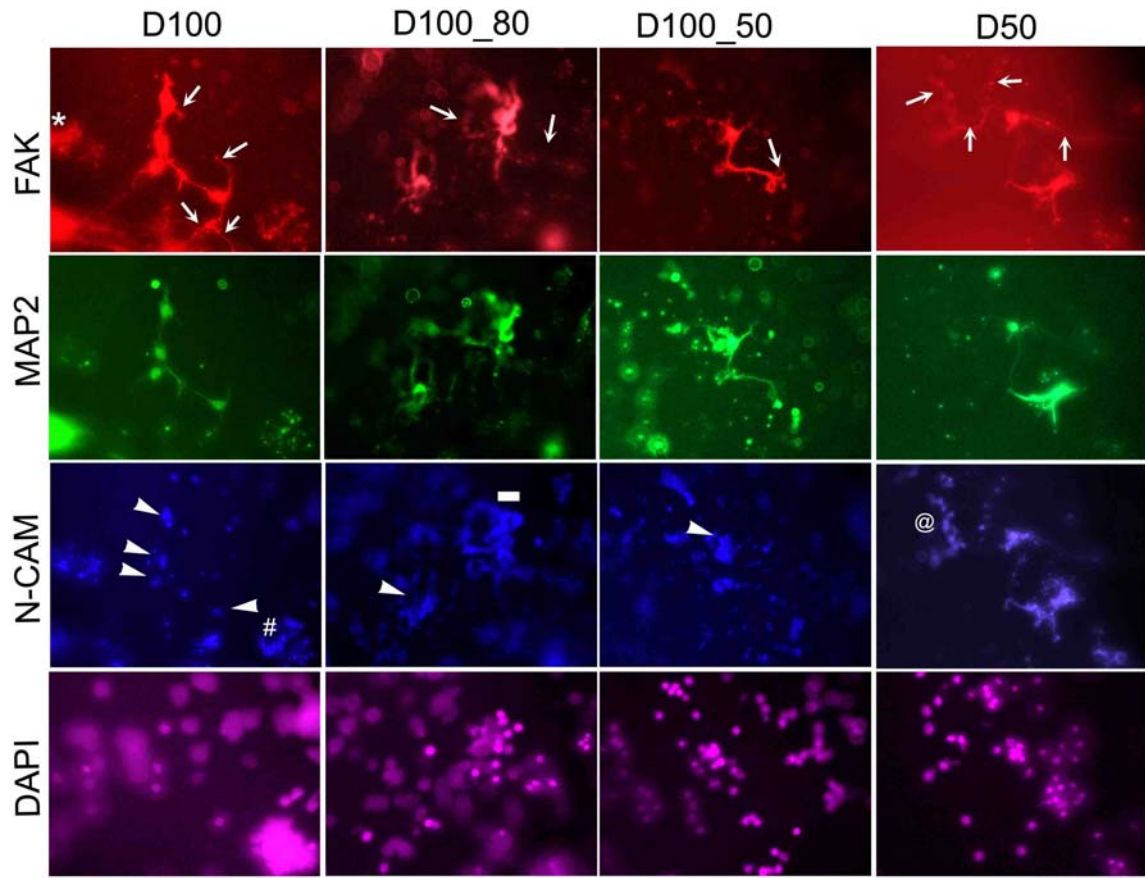


Figure 4C-7 Typical images of focal adhesion kinase (FAK) and neural-cell adhesion molecules (N-CAM) in the spinal cord neurons grown on DNA gels with dynamic stiffnesses.

For each gel group, immunostaining images of FAK (Red), N-CAM (Blue) and MAP2 (Green) are shown for the same spot, along side with DAPI (Purple) nuclei staining. FAK was expressed in both dendrites and axons (arrow), and MAP2 negative cells (*). N-CAN was expressed in the neuronal soma and other cells (#). For isolated neurons, the expression of N-CAM is not uniform (Arrow head). Abundance in N-CAM expression can be seen in the cell aggregates and localized in the periphery of the neuronal soma (white rectangle). N-CAM was also expressed along side the axons with the presence of supporting cells (identified by MAP2 negative with DAPI positive nuclei) (@) on the gels. Scale bar is 100 μm .

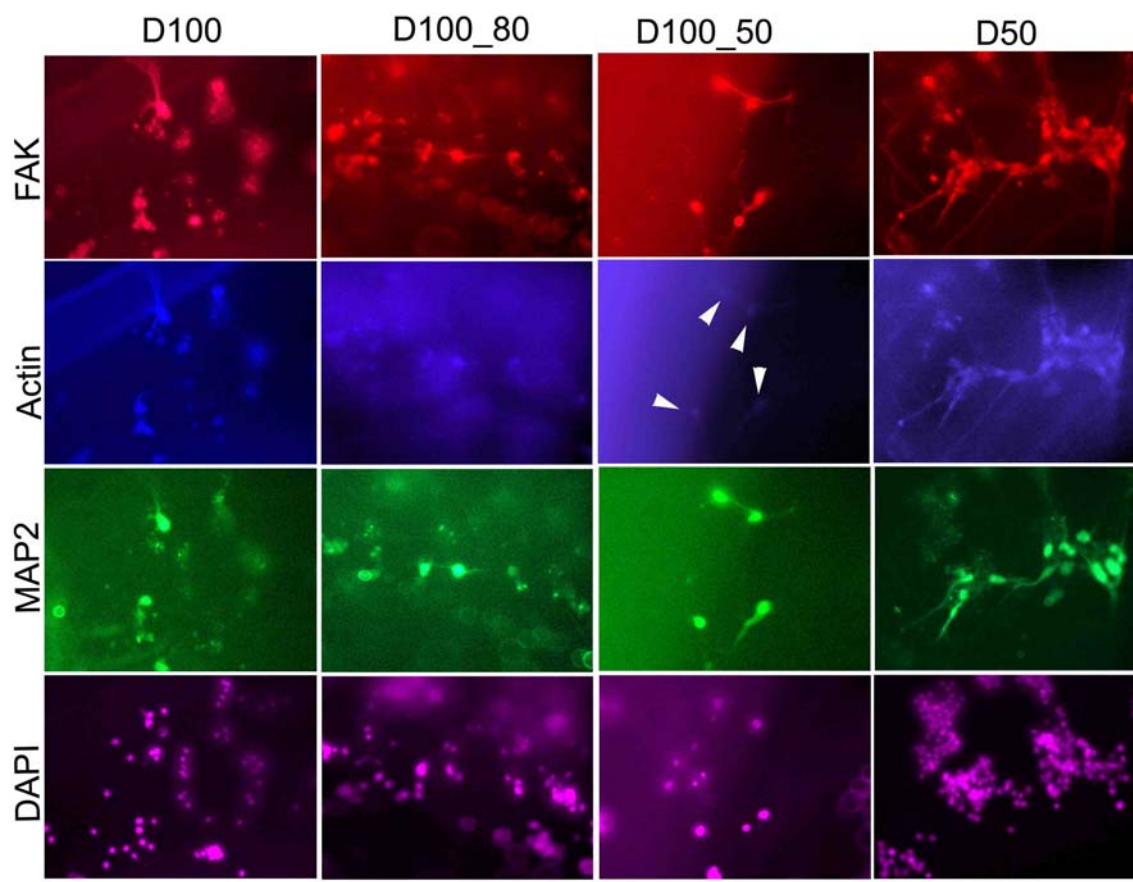


Figure 4C-8 Typical images of focal adhesion kinase (FAK) and actin in the spinal cord neurons grown on DNA gels with dynamic stiffnesses. There appeared to be a decrease in the F-actin expression with the drop in the crosslinking density or substrate rigidity (arrow head). Scale bar is 100 μm .

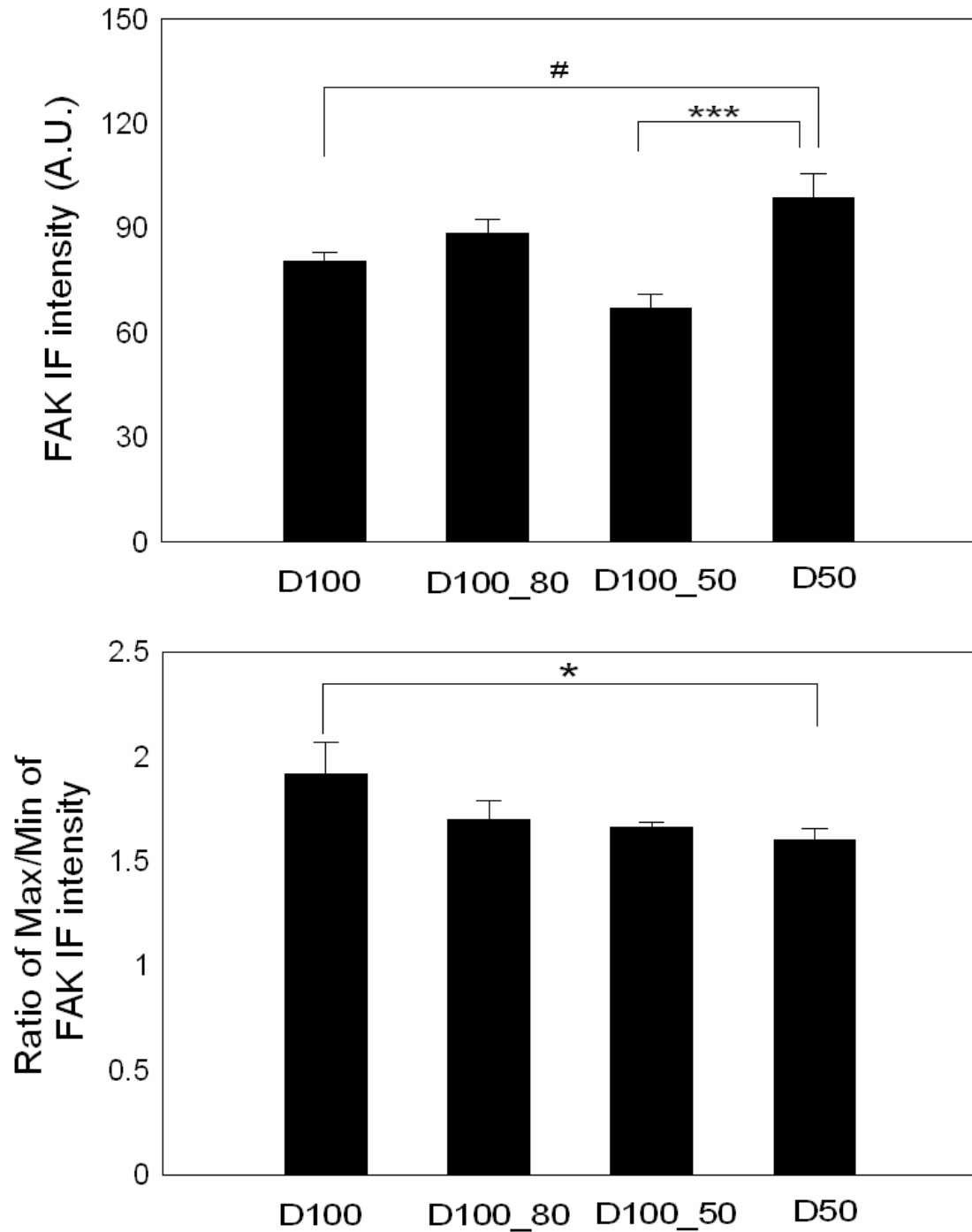


Figure 4C-9 Focal adhesion kinase (FAK) expression in the spinal cord neurons grown on DNA gels with dynamic stiffnesses.

(Upper panel) There is a significant difference between D100 and D50 based on two-tailed unpaired t -test. # $p < 0.05$. A significant difference was found as determined by one-way ANOVA with Tukey's post-test between D100_50 and D50 for all four groups. *** $p < 0.005$. (Lower panel) The disparity is shown by the ratio of maximal/minimal expression intensity in the neuronal cell body. $n \geq 15$.

4C.4 Discussion

4C.4.1 Mechanically dynamic cues applied to neurons

Thanks to the unique opportunities offered by the DNA crosslinked hydrogels, we were able to modify the substrate mechanical stiffness while spinal cord cells were growing on top of the gel substrates. As previous studies imply, by increasing the crosslinking density in the DNA gels, the potential compaction of the gel network would take place, which can be translated into compression rather than traction or tensional forces for the neurons. Inspired by the towed growth demonstrated before^{6, 15} where application of force to the neurite promotes its elongation, we decided to use the reverse of gelation. By including a toe-hold at the end of the crosslinker DNA, one is able to introduce complementary strand to the crosslinkers, and displace the crosslinker DNA out of the gel network, whereby reducing the crosslinking density and hence the mechanical stiffness. This choice was further favored due to the latest finding from our group that longer axons were seen on the softer gels²⁸. In other words, by lowering the DNA gel crosslinking level, we attempted to provide two potential cues, one of which is the decrease in the mechanical stiffnesses, and the other is the possible expansion of the gels. Based on the results from the preliminary study on local deformation of the gels (Appendix 1), it was recognized that the strain rate generated in the specific delivery conditions (initial medium volume, quantity of DNA delivered, time course allowed and surface area of the gels) was most likely not enough to significantly affect neurite growth. As a result, we attribute the changes, if any, in the neurite outgrowth in this study primarily to the variation in the mechanical stiffness of the gels. It is noted that by varying the delivery

conditions, much larger force application and strain generation may be possible, for which investigation is ongoing.

In the work discussed here, there are three dynamic gels groups, with D100_Non (Table 4C-3) serving as a negative control to show that it is the mechanical property change induced by the DNA delivery and incorporation into the gel network that leads to the differential behavior in the neurite outgrowth. D100_80 and D100_50 (Table 4C-3) were chosen due to the availability of the results for comparisons (D100, D80, and D50) from the study on responses of neurite outgrowth to mechanical stiffness outlined in Chapter 3B. The difference between static and dynamic studies lies primarily in the fact that in the static study, the cells were plated on the gels with specific stiffness, and the rate of the stiffness change cells experience is rather *dramatic* or *instantaneous* at the time of cell seeding; whereas in the dynamic stiffness cases, the gel stiffness cells experience is *gradually* or *progressively* modified.

As was argued for the case of the DNA gels we employed in the study presented in Chapter 3B²⁸, it is suggested that the variation in the crosslinking density does not cause pronounced changes in other surface mechanical characteristics (e.g., surface topography, surface pore size, and the level of hydrophilicity). Thus, the differential response between static and dynamic studies is attributed primarily to the cellular response to dramatic or gradual rigidity change of the underlying substrates.

Most of the previous work on the mechanical responses of neuronal growth and neurite outgrowth involves substrates with discrete and pre-determined mechanical stiffnesses^{17, 20, 28, 30, 32, 54} or stiffness gradients⁴⁷. To our knowledge, this is the first time that dynamic mechanical stiffness was applied during the course of in *in vitro* conditions

and that the response of neurite outgrowth to the temporally varying stiffness of the substrate was studied and also quantified.

4C.4.2 Neurite outgrowth in response to mechanically dynamic cues

As a control on the gel and cellular response to the presence of single stranded DNA non-complementary to the crosslinker DNA, we showed that applied poly-A oligomers did not initiate any change in the mechanical stiffnesses of the substrate and did not impact the neurite outgrowth.

When the substrates become softer (initial 100% crosslinking in D100 groups), the primary dendrite number decreases, the mean primary dendrite length drops, and the axonal length markedly increases. This substantiates our hypothesis that neurons, like mechano-sensitive cells such as fibroblasts, are capable of detecting alterations in the mechanical stiffness in the local micro-environment and are capable of responding to that change in a way that is manifested by neurite outgrowth. This provides guidance for neural tissue engineering in cases where promoting axonal regeneration and growth is desired.

Unique in their functional role in the nervous system and assuming processes in their structure, or neurites, including axons and dendrites and further secondary structures (e.g., secondary dendrites), neuronal responses are largely displayed in the modulation of the neurite outgrowth, rather than cell shape or polarity as is the case for fibroblasts. Additionally, in contrast to the mechanical responses of fibroblasts to the dynamic stiffness, the observations of neurons on the dynamic gels are similar to those made on static gels with the same ending crosslinking density (for instance, D100_50 vs. D50)

with the exception of mean primary dendrite length. For fibroblasts, cells on static and dynamic gels of the same ending stiffness differ greatly in projection area, aspect ratio or FA organization, as highlighted in Figure 4B-7 and Chapter 4B. This suggests that the fibroblasts, being more mechanically sensitive, could actively modify and adjust their growth and other behavior (e.g., projection area, polarity, or FA organization) to the changing environment whereas neurons would elect to respond to the environment in different ways.

Primary dendrite length showed no appreciable difference among the cell groups, including both static stiffness (Figure 3B-11) and dynamic stiffness groups (Figure 4C-5), and was measured to be approximately 40 μm . Primary dendrite number on gels of same crosslinking density (e.g., B100 in Figure 3B-11 vs. D100 in Figure 4C-5) is comparable between dynamic and static gels. Axonal length in all the dynamic stiffness gel groups was approximately 20 μm ²⁸ longer than that of the corresponding static gels groups. See for example, B50 in Figure 3B-11C and D50 in Figure 4C-5C, axonal length increase from 130 μm to 150 μm . This is mainly due to the fact that we allowed neurons to extend processes for one more day (DIV 6 vs. DIV 7), in the experiments reported in this section. This extra day was intended to provide sufficient time for DNA incorporation into gel network, and for neurons to sense and respond to the dynamic stiffness. It is also noted that average primary dendrite number (three) for the stiffest gel (D100) is the same as that on the culture plate (Figure 4C-3) which has a stiffness in the gigapascal range. This suggests that there exists a threshold stiffness, or set-point, between that of 80% and 100% DNA gels²⁸ beyond which the average primary dendrite number will be approximately three, assuming that the surface adhesive properties are comparable.

It is also observed that the effect of the substrate mechanical stiffnesses on the average neurite outgrowth is in concert with that on the basis of population distribution. The possible causes for the distinction in the population distributions for all gel groups include the differential responses of the subpopulation in the total neuronal population (e.g., motor, sensory and inter-neurons) to mechanical stiffness, and responses from glial and/or other cell types, particularly immature neurons or neural progenitor cells (e.g., nestin positive cells) and astroglia (e.g., mature GFAP positive cells or immature vimentin positive cells), to alterations in the mechanical stiffness. The responses of the non-neuronal cells could result in biological or biochemical cues (e.g., trophic factors secreted by glia) affecting neurons. If such processes do occur, the neuronal behavior change cannot be attributed, at least entirely, to the change in mechanical stiffness of the substrates. It is noted that by combining the behavior of primary dendrites and axons, one sees that the neurite outgrowth is more pronounced on softer gels, in agreement with most of the previous reports offering no differentiation between dendrites and axons, and instead lumping them as neurites^{17, 20, 28-30, 32, 47, 54}.

As we previously observed²⁸, glial cell survival did not change notably with the stiffness range under study, although there was a biphasic trend in their survival on bis-crosslinked hydrogels²⁹ where glia cell density peaks at an intermediate stiffness of approximately 27 kPa and markedly changed over a small stiffness range. Neurons generally do not proliferate and their survival does not seem to be greatly affected by the mechanical stiffness. Therefore in the work presented in this section, we focused primarily on neurite outgrowth. Additionally, as the previous studies probing the surface ligand density have revealed (Figure 3B-6), delivery of crosslinker DNA does not

significantly alter the surface adhesiveness. PDL, like other ECM molecules including fibronectin, collagen, and proteoglycans^{40, 44}, is sufficient for the probe of neuronal growth and neurite outgrowth responses. We chose PDL for neuronal attachment to the substrates also in consistence with the previous work presented in Chapter 3B.

It is necessary to note that it is possible that secondary structures of the neurites can also respond to the mechanical stiffness change and have implications in the functioning of neurons, which merits investigation.

4C.4.3 FAK and N-CAM expression in response to dynamic substrate

Triple immuno-staining of focal adhesion kinase, N-CAM, and MAP2 was carried out on the neurons on the dynamic DNA gels. FAK expression is primarily from neurons, and both axon and dendrite express FAK, as observed previously²⁸.

As in the analysis conducted in the study using fibroblasts, the following relationship in the FAK expression is use in the interpretation of the FAK expression data,

$$(\text{Mean intensity}) \propto [(\text{FA size}) \times (\text{FA number})].$$

The max./min. ratio of the intensity is proportional to the quantity of FAK recruited at the FA sites^{3, 22} and is an indicator of the size of FA. Thus based on the mean intensity (4C-9, upper panel) and the size of FA, estimated by the ratio of max./min. intensity (4C-9, lower panel), one is able to estimate the relative number of FA for comparisons.

The ratio of max./min. of FAK intensity is significantly higher on stiffer gels (D100), consistent with the general observations that stiffer gels promote up-regulation of focal adhesion, such as recruiting FAK to the FA point. This behavior is similar to that

for fibroblasts (Chapter 4B, Figure 4B-13), where on stiff gels the size of FA is notably greater. Also, the mean fluorescence intensity of FAK on stiffer gels is pronouncedly lower than that on the softer gels²⁸, suggesting that the number of FA on softer gels (D50) is much greater than that on stiffer gels. Considering the dynamic gel groups, however, the level of FAK immuno-reactivity on dynamic gels (D100_50) differs greatly from that on static gels (D50) (Figure 4C-9). There appeared to be significantly lower number of FA on dynamic gels.

N-CAM is a class of trans-membrane proteins, expressed on neurons and a number of other cells³⁴, that plays roles in cell-cell adhesion. Members of this class also contain RGD (Arg-Gly-Asp-) motif in the extracellular domain which is commonly recognized in binding to integrins, again suggesting their involvement in cell-substrate interactions. Thus, N-CAM was shown to be involved in the coupling of cell-cell interplay and cell-substrate interactions^{1, 5}. Not surprisingly, it has been implicated in neuronal migration⁴¹, retina layering⁷ and in neuritogenesis¹³, neurite fasciculation⁴³, synaptogenesis and synaptic plasticity^{11, 39, 42}, during both adulthood and development^{9, 34}, as well as in responses of nervous system to external assault³⁸. Previous reports showed that in mediating cell-substrate interactions by N-CAM, F-actin flow was attenuated and traction force was generated for growth cone movement⁵.

Unlike FAK, which is expressed in both neuronal soma and processes for spinal cord cells on DNA gels, N-CAM was rarely seen expressed on the dendrites or axons (except the growth cone). Double staining of the FAK and actin confirmed the close association of the focal adhesion with microfilaments. The heterogeneity in FAK expression among the neuronal population (Figure 4C-7) was also reported previously⁵².

The abundance of N-CAM expression (Figure 4C-7) in part of the neurons and the co-expression of N-CAM and FAK accords well with the observations made by other investigators that N-CAM clustering recruits FAK^{33,42}. Therefore, the localization of N-CAM correlates with its diversified functional roles in the tissue, especially in neural tissues. The expression of N-CAM appears to be dynamic and mobile along the neurite⁴². In particular, Sytnyk and co-workers^{43,49} observed that N-CAM immunoreactivity in the neuronal soma and growth cone is much higher than that in the center of neurite, which is in agreement with the current study. This phenomenon is mainly due to the fact that N-CAM is mostly synthesized inside the somata and trafficked via axonal transport^{18,43}.

Cell-cell interactions, whether they are neuronal interactions, glial interactions or neuron-astroglia interactions, are necessary for the proper wiring of the neural circuitry and functioning of the nervous system. Their respective mechanical response can be drastically altered by the cell-cell interactions, as reflected by the studies on both fibroblasts⁵⁵ and neurons²⁹. For examples, on soft gels, Yeung et al.⁵⁵ found that with the presence of cell-cell contact, the stress fibers form, whereas in the absence of such interactions no stress fibers appear.

Despite the caution exercised in quantifying the intensity of FAK expression in neurons based on immuno-fluorescence, possibilities exist that the practical aspects, including measurement methodology, instrumentation involved, and reagents used, could more or less affect the observations. For instance, similar to the case for fibroblasts, it is possible that the choice of focal plane with the fluorescence microscopy might add to the variation between samples.

4C.4.4 Factors in neuronal sensing and response to dynamic stiffness

The major changes observed in neuronal properties, including primary dendrite length and number, axonal length, and FAK expression in the neuronal cell body, are summarized in Table 4C-4. A partial list of the important factors in dictating neuronal responses to the dynamic stiffness is summarized in Table 4C-5. A schematic of neuronal cellular mechano-sensing and responses to mechanical stiffness change in the ECM is presented in Figure 4C-10. In general, neurite outgrowth can be determined by three major factors: cell-substrate direct contact; direct cell-cell contact, and cell-cell interactions via soluble factors³⁴.

Due to the embryonic nature of the cell source used in the current study, the cell population consists of a considerable portion of the embryonic stem cell or progenitor cells. Indeed, we detected a large number of nestin positive cells in the cell population on culture plates throughout seven days of culture (Figure 4C-11). Thus the mechanical response of neurons to dynamic stiffness is also coupled with the natural development and growth of the neurons. It was observed that Tau-1 and MAP2 immunostaining showed great abundance after 3 DIV (Figure 4C-12), beyond which the immuno-expression does not appear to change greatly in the level of expression and number of cell expressing Tau-1 or MAP2. This formed the basis of the rationale of delivering crosslinker DNA to the culture on 4 DIV in the current work.

In the last chapter (Chapter 4B), we pointed that it has been suggested that fibroblasts have a threshold, or ‘set point’, in the sensitivity towards mechanical stiffness (e.g., ~20 kPa for NIH 3T3 fibroblasts⁴⁵). Neurons may not be an exception. Probably not coincidentally, many reports shared a common finding that there exists a set-point for

force application (not the strain rate, which is limited by the intracellular transport) to induce neurite elongation^{15, 16, 25, 56}.

It was speculated that the increase in stiffness of ECM in a number of cases (e.g., tumor) could lead to integrin clustering and altered contractility²⁷. This, together with the changes in the focal adhesion, indicates that the changes in ECM stiffness cause loss of dynamic equilibrium in the tension at the cell-ECM interfaces. In order to compensate for the imbalance and to reach a new equilibrium, neurons could either adapt to the new physical status or actively modify the local ECM by secreting ECM molecules. Meanwhile, they can also signal other cell types such as astroglia or oligodendrocytes, which serve supporting roles in the nervous system. Again, essentially, through the effort from neurons and possibly other cells, a new balance can be put in place via the negative feedback loop. However, it was also implicated that cells, in response to the imbalance caused by the stiffening of the ECM, can further increase the ECM stiffness. This positive feedback loop has been implicated in generating un-controlled changes that give rise to pathological conditions²⁷.

The static stiffness used in the current study is effectively a force application with much larger rate (force increase in a unit time) than that on the dynamic counterparts. This is because the instantaneous presentation of the substrate to cells, right after dissection, poses much greater resistance to the active pulling of the neurons in probing the micro-environment. Fass and Odde¹⁵ reported that there is a less chance for neurites to initiate when the ramp rate of force application is high, which might explain why in our study, the decrease in the primary dendrite number is more pronounced on D100_50 gels than that on D100_80 gels (Figure 4C-5), as the former presents steeper ramp in

applied force or resistance. The dependence of neurite initiation on tensile forces has been part of the differential responses of neuronal cells to force application in both long-term or short time scale¹⁵.

The mechanism involved in the cell mechanosensing outlined in Chapter 4B (Figure 4B-16) hold true for neurons. Neurons actively probe the stiffness of the substrate by applying traction forces largely through integrin linkage in the focal adhesion complex (FAC) where FAK is among the key players (Figure 4C-10). As the stiffness increases, the resistance to the cell-generated traction forces (esp. at the growth cone) becomes greater, and the cell receives the feedback, also via integrin linkage, where MAP2 and N-CAM participate in the processes. This information, together with other physical cues, dimensionality, biochemical and biological cues (e.g., trophic factors), as well as cell-cell interactions (e.g., in neuronal aggregates), is integrated by neurons for decision making. During the process, N-CAM serves to couple the cell-cell and cell-substrate interactions. Neurons respond largely by modulating focal adhesion, and/or neurite outgrowth, and other properties (Figure 4C-10).

There are, however, a few distinctions in the mechanosensing mechanism between neurons and fibroblast, which originate from unique functional role and associated structures of neurons:

1. Active probing of the micro-environment has been shown a critical component in growth cone path-finding and axonal elongation, unique to neurons^{6, 15, 25}, as demonstrated in the dynamic protrusion and retraction of membrane structures²¹. The correlation between rate of elongation and mechanical stiffness of ECM might also involve the intrinsic tension in the neurites as well as the adhesion properties⁵⁴.

2. Different primary structures may have different mechanisms in mechano-sensing and different choice of key information. For example, it was hypothesized that axons might rely on compression in the microtubules while dendrites depend on adhesion in elongation³¹ in mechano-sensing.

3. Due to the intrinsic involvement of cell-cell interactions of nervous system, coupling between cell-substrate and cell-cell interactions could play an important role in the neuronal mechano-sensing. N-CAM as one of the handful molecules assuming the ‘coordinator’ role functions in a unique way that is not found in fibroblasts mechano-sensing⁴⁸. A very recent study on the mechanical properties of neuronal processes, somata and glial cells revealed that both neuronal processes and glia are softer than neuronal soma, suggesting that neuronal processes may use glia as substrate, and in doing so, they match their compliance to that of the glia. This extends the stiffness-matching phenomena found in fibroblasts^{10, 45}. Another distinction is that instead of soma, the neuronal processes adjust their stiffnesses, and respond in elongation or retraction⁸.

It remains a question, however, as to where the neuronal mechano-sensor is located. Is it in the cell body, the dendrite or the axon or in all, and if the sensors are in all of three, then how does neuron integrate the information and direct intracellular trafficking for neurite elongation?

Summary

In summary, neuronal mechano-sensing capability is further confirmed and expanded to the case of dynamic stiffnesses of the substrates. It was found that changing mechanical properties might be used as a way to alter neuronal growth and neurite outgrowth, giving rise to a novel way of promoting neurite outgrowth.

Table 4C-4 Comparisons of neurite outgrowth between static and dynamic gels with the same starting stiffness and between dynamic and static gels with the same ending stiffness..

A typical neuron is shown for each condition, and comparisons are made in primary dendrite length and number, axonal length and FA number and size between D100 and D100_50, and between D100_50 and D50. *Estimate based on the mean FAK expression and the max./min. intensity ratio. (↑ increase; ↓ decrease; → no change from the upper group to the lower group)

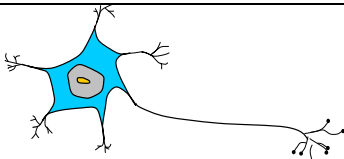
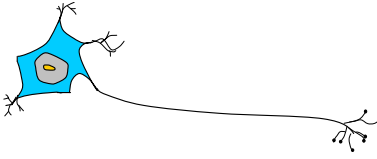
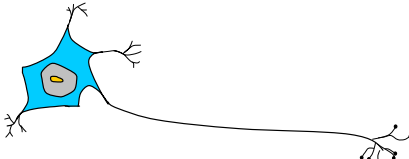
D100	vs.	D100_50	vs.	D50	Primary Dendrite Length	Primary Dendrite Number	Axonal Length	FAK #	FAK size
				<i>D100</i>					
					↓	↓	↑	↑*	↓
				<i>D100_50</i>					
					↑	→	→	↑	→
				<i>D50</i>					

Table 4C-5 Important factors affecting the response in neuronal growth and neurite outgrowth to dynamic stiffnesses.

Parameters	Examples of comparisons
Rate of change	Abrupt (static) vs. progressive (dynamic)
Stiffness range	D100_80 (100%→80%) vs. D100_50 (100%→50%)
Ending stiffness	D100_80 (100%→80%) vs. D100_50 (100%→50%)
Cellular properties	Primary dendrite length vs. axonal length
Cell type	Fibroblast vs. neuron

(1) Neurons actively probe the stiffness of the substrate by applying traction forces, largely through integrin linkage in the focal adhesion complex (FAC) where FAK is among the important factors. (2) As the stiffness increases, the resistance to the cell-generated traction forces intensifies, and cell receives the feedback also via integrin linkage, where MAP2 and N-CAM are involved. This information, together with other physical cues, dimensionality, biochemical and biological cues (e.g., growth factors), as well as cell-cell interactions if cell-cell contact occurs (i.e., in neuronal aggregates), is integrated by neurons for decision making. (3) Neurons respond by modulating focal adhesion, and/or stress fiber, neurite outgrowth, and other cellular properties.

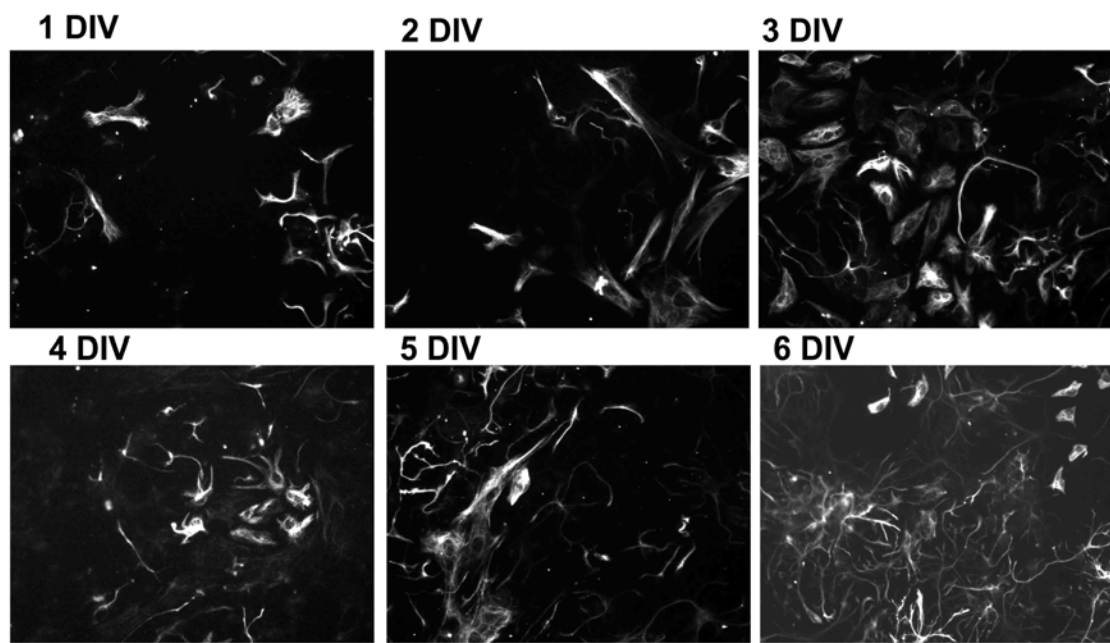


Figure 4C-11 Nestin immunostaining of the spinal cord cells showing neural progenitor cells on culture plates during the course of the culture. Scale bar is 100 μm .

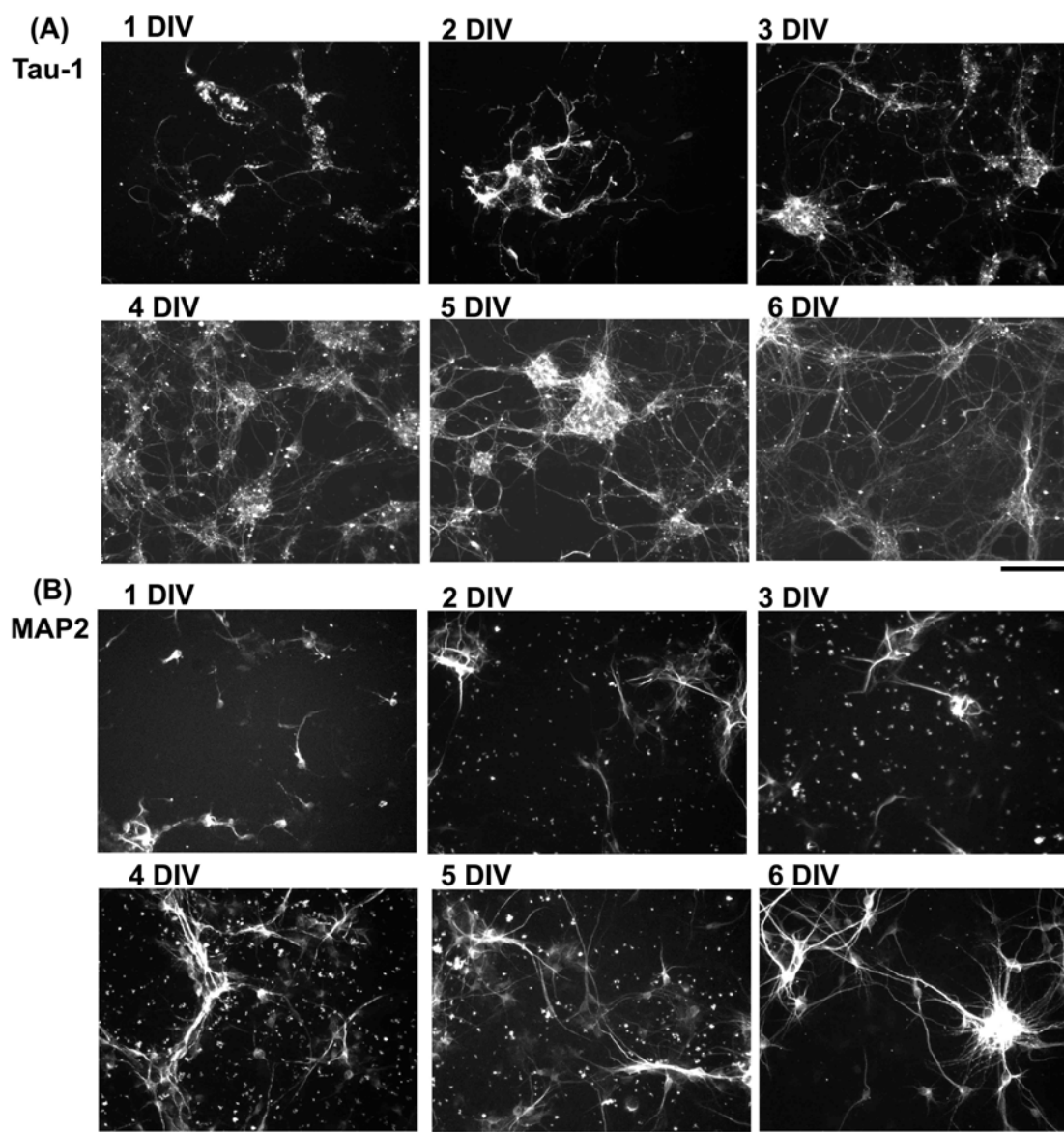


Figure 4C-12 Tau-1 and MAP2 immunostaining of the spinal cord cells showing dendrites and axons, respectively, on culture plates during the course of the culture. Scale bar is 100 μm .

References

1. Acheson, A., J. L. Sunshine, and U. Rutishauser. Ncam polysialic acid can regulate both cell-cell and cell-substrate interactions. *J Cell Biol.* 114:143-153, 1991.
2. Altschul, S. F., W. Gish, W. Miller, E. W. Myers, and D. J. Lipman. Basic local alignment search tool. *J Mol Biol.* 215:403-410, 1990.
3. Angers-Loustau, A., J. F. Cote, A. Charest, D. Dowbenko, S. Spencer, L. A. Lasky, and M. L. Tremblay. Protein tyrosine phosphatase-pest regulates focal adhesion disassembly, migration, and cytokinesis in fibroblasts. *J Cell Biol.* 144:1019-1031, 1999.
4. Balgude, A. P., X. Yu, A. Szymanski, and R. V. Bellamkonda. Agarose gel stiffness determines rate of drg neurite extension in 3d cultures. *Biomaterials.* 22:1077-1084, 2001.
5. Bonanomi, D., and F. Valtorta. Focal adhesion kinase in neuritogenesis In: I. de Curtis, editor. *Intracellular mechanisms for neuritogenesis*, Springer US: New York: NY, 2006; pp 155-179.
6. Bray, D. Axonal growth in response to experimentally applied mechanical tension. *Dev Biol.* 102:379-389, 1984.
7. Buskirk, D. R., J. P. Thiery, U. Rutishauser, and G. M. Edelman. Antibodies to a neural cell adhesion molecule disrupt histogenesis in cultured chick retinae. *Nature.* 285:488-489, 1980.
8. Chicurel, M. E., C. S. Chen, and D. E. Ingber. Cellular control lies in the balance of forces. *Curr Opin Cell Biol.* 10:232-239, 1998.
9. Crossin, K. L. Cell and substrate adhesion molecules in embryonic and neural development. *Clin Chem.* 35:738-747, 1989.
10. Discher, D. E., P. Janmey, and Y. L. Wang. Tissue cells feel and respond to the stiffness of their substrate. *Science.* 310:1139-1143, 2005.
11. Dityatev, A. Synaptic functions of the neural cell adhesion molecule, ncam. In: A. Dityatev; A. El-Husseini, editors. *Molecular mechanisms of synaptogenesis*, Springer, 2006.
12. Escuin, S., and E. Georges-Labouesse. Adhesion-induced intracellular mechanisms of neurite elongation In: I. de Curtis, editor. *Intracellular mechanisms for neuritogenesis*, Springer US: New York: NY, 2006; pp 1-24.
13. Escuin, S., and E. Georges-Labouesse. Adhesion-induced intracellular mechanisms of neurite elongation. In: I. de Curtis, editor. *Intracellular mechanisms for neuritogenesis*, Springer US: New York: NY, 2006; pp 1-24.
14. Fallenstein, G. T., V. D. Hulce, and J. W. Melvin. Dynamic mechanical properties of human brain tissue. *J Biomech.* 2:217-226, 1969.
15. Fass, J. N., and D. J. Odde. Tensile force-dependent neurite elicitation via anti-beta1 integrin antibody-coated magnetic beads. *Biophys J.* 85:623-636, 2003.
16. Fischer, T. M., P. N. Steinmetz, and D. J. Odde. Robust micromechanical neurite elicitation in synapse-competent neurons via magnetic bead force application. *Ann Biomed Eng.* 33:1229-1237, 2005.
17. Flanagan, L. A., Y. E. Ju, B. Marg, M. Osterfield, and P. A. Janmey. Neurite branching on deformable substrates. *Neuroreport.* 13:2411-2415, 2002.

18. Garner, J. A., M. Watanabe, and U. Rutishauser. Rapid axonal transport of the neural cell adhesion molecule. *J Neurosci.* 6:3242-3249, 1986.
19. Gefen, A., N. Gefen, Q. Zhu, R. Raghupathi, and S. S. Margulies. Age-dependent changes in material properties of the brain and braincase of the rat. *J Neurotrauma.* 20:1163-1177, 2003.
20. Georges, P. C., W. J. Miller, D. F. Meaney, E. S. Sawyer, and P. A. Janmey. Matrices with compliance comparable to that of brain tissue select neuronal over glial growth in mixed cortical cultures. *Biophys J.* 90:3012-3018, 2006.
21. Giniger, E. How do rho family gtpases direct axon growth and guidance? A proposal relating signaling pathways to growth cone mechanics. *Differentiation.* 70:385-396, 2002.
22. Goffin, J. M., P. Pittet, G. Csucs, J. W. Lussi, J. J. Meister, and B. Hinz. Focal adhesion size controls tension-dependent recruitment of alpha-smooth muscle actin to stress fibers. *J Cell Biol.* 172:259-268, 2006.
23. Gunn, J. W., S. D. Turner, and B. K. Mann. Adhesive and mechanical properties of hydrogels influence neurite extension. *J Biomed Mater Res A.* 72:91-97, 2005.
24. Hachiya, N. S., Y. Kozuka, and K. Kaneko. Mechanical stress and formation of protein aggregates in neurodegenerative disorders. *Med Hypotheses.* 70:1034-1037, 2008.
25. Heidemann, S. R., and R. E. Buxbaum. Growth cone motility. *Curr Opin Neurobiol.* 1:339-345, 1991.
26. Hrapko, M., J. A. van Dommelen, G. W. Peters, and J. S. Wismans. The mechanical behaviour of brain tissue: Large strain response and constitutive modelling. *Biorheology.* 43:623-636, 2006.
27. Huang, S., and D. E. Ingber. Cell tension, matrix mechanics, and cancer development. *Cancer Cell.* 8:175-176, 2005.
28. Jiang, F. X., B. Yurke, B. L. Firestein, and N. A. Langrana. Neurite outgrowth on a DNA crosslinked hydrogel with tunable stiffnesses. *Ann Biomed Eng.* 36:1565-1579, 2008.
29. Jiang, X., P. C. Georges, B. Li, Y. Du, M. K. Kutzinger, M. L. Previtiera, N. A. Langrana, and B. L. Firestein. Cell growth in response to mechanical stiffness is affected by neuron-astroglia interactions. *Open Neuroscience Journal.* 1:7-14, 2007.
30. Kostic, A., J. Sap, and M. P. Sheetz. Rptalpha is required for rigidity-dependent inhibition of extension and differentiation of hippocampal neurons. *J Cell Sci.* 120:3895-3904, 2007.
31. Lafont, F., M. Rouget, A. Rousselet, C. Valenza, and A. Prochiantz. Specific responses of axons and dendrites to cytoskeleton perturbations: An in vitro study. *J Cell Sci.* 104 (Pt 2):433-443, 1993.
32. Leach, J. B., X. Q. Brown, J. G. Jacot, P. A. Dimilla, and J. Y. Wong. Neurite outgrowth and branching of pc12 cells on very soft substrates sharply decreases below a threshold of substrate rigidity. *J Neural Eng.* 4:26-34, 2007.
33. Lehembre, F., M. Yilmaz, A. Wicki, T. Schomber, K. Strittmatter, D. Ziegler, A. Kren, P. Went, P. W. Derksen, A. Berns, J. Jonkers, and G. Christofori. Ncam-induced focal adhesion assembly: A functional switch upon loss of e-cadherin. *EMBO J.* 27:2603-2615, 2008.

34. Levitan, I. B., and L. K. Kaczmarek. *The neuron: Cell and molecular biology* Oxford University Press: New York, 1997.
35. Levitan, I. B., and L. K. Kaczmarek. *The neuron: Cell and molecular* Oxford University Press: New York, 1997.
36. Li, L., N. Sharma, U. Chippada, X. Jiang, R. Schloss, M. L. Yarmush, and N. A. Langrana. Functional modulation of es-derived hepatocyte lineage cells via substrate compliance alteration. *Ann Biomed Eng.* 36:865-876, 2008.
37. Maikos, J. T., R. A. Elias, and D. I. Shreiber. Mechanical properties of dura mater from the rat brain and spinal cord. *J Neurotrauma.* 25:38-51, 2008.
38. Miller, P. D., S. D. Styren, C. F. Lagenaur, and S. T. DeKosky. Embryonic neural cell adhesion molecule (n-cam) is elevated in the denervated rat dentate gyrus. *J Neurosci.* 14:4217-4225, 1994.
39. Muller, D., P. Mendez, M. De Roo, P. Klauser, S. Steen, and L. Pogli. Role of ncam in spine dynamics and synaptogenesis. *Neurochem Res.* 2008.
40. Poole, A. R. Proteoglycans in health and disease: Structures and functions. *Biochem J.* 236:1-14, 1986.
41. Prag, S., E. A. Lepekhn, K. Kolkova, R. Hartmann-Petersen, A. Kawa, P. S. Walmod, V. Belman, H. C. Gallagher, V. Berezin, E. Bock, and N. Pedersen. Ncam regulates cell motility. *J Cell Sci.* 115:283-292, 2002.
42. Rougon, G., and O. Hobert. New insights into the diversity and function of neuronal immunoglobulin superfamily molecules. *Annu Rev Neurosci.* 26:207-238, 2003.
43. Savtchenko, L. P., N. Kulahin, S. M. Korogod, and D. A. Rusakov. Electric fields of synaptic currents could influence diffusion of charged neurotransmitter molecules. *Synapse.* 51:270-278, 2004.
44. Small, D. H., S. S. Mok, T. G. Williamson, and V. Nurcombe. Role of proteoglycans in neural development, regeneration, and the aging brain. *J Neurochem.* 67:889-899, 1996.
45. Solon, J., I. Levental, K. Sengupta, P. C. Georges, and P. A. Janmey. Fibroblast adaptation and stiffness matching to soft elastic substrates. *Biophys J.* 93:4453-4461, 2007.
46. Sparrey, C. J., A. M. Choo, J. Liu, W. Tetzlaff, and T. R. Oxland. The distribution of tissue damage in the spinal cord is influenced by the contusion velocity. *Spine.* 33:E812-819, 2008.
47. Sundararaghavan, H. G., G. A. Monteiro, B. L. Firestein, and D. I. Shreiber. Neurite growth in 3d collagen gels with gradients of mechanical properties. *Biotechnol Bioeng.* 102:632-643, 2009.
48. Suter, D. M., and P. Forscher. Substrate-cytoskeletal coupling as a mechanism for the regulation of growth cone motility and guidance. *J Neurobiol.* 44:97-113, 2000.
49. Sytnyk, V., I. Leshchyns'ka, A. G. Nikonenko, and M. Schachner. Ncam promotes assembly and activity-dependent remodeling of the postsynaptic signaling complex. *J Cell Biol.* 174:1071-1085, 2006.
50. Toga, A. W., and P. M. Thompson. Temporal dynamics of brain anatomy. *Annu Rev Biomed Eng.* 5:119-145, 2003.

51. Tung, P. S., K. Burdzy, K. Wong, and I. B. Fritz. Competition between cell-substratum interactions and cell-cell interactions. *J Cell Physiol.* 152:410-421, 1992.
52. van den Pol, A. N., U. di Porzio, and U. Rutishauser. Growth cone localization of neural cell adhesion molecule on central nervous system neurons in vitro. *J Cell Biol.* 102:2281-2294, 1986.
53. Viidik, A. A rheological model for uncalcified parallel-fibred collagenous tissue. *J Biomech.* 1:3-11, 1968.
54. Willits, R. K., and S. L. Skornia. Effect of collagen gel stiffness on neurite extension. *J Biomater Sci Polym Ed.* 15:1521-1531, 2004.
55. Yeung, T., P. C. Georges, L. A. Flanagan, B. Marg, M. Ortiz, M. Funaki, N. Zahir, W. Ming, V. Weaver, and P. A. Janmey. Effects of substrate stiffness on cell morphology, cytoskeletal structure, and adhesion. *Cell Motil Cytoskeleton.* 60:24-34, 2005.
56. Zheng, J., P. Lamoureux, V. Santiago, T. Dennerll, R. E. Buxbaum, and S. R. Heidemann. Tensile regulation of axonal elongation and initiation. *J Neurosci.* 11:1117-1125, 1991.

Chapter 5 CONCLUSIONS AND SUMMARY

5.1 Summary of the dissertation work

5.1.1 Summary of motivation and key observations

The detailed objectives and key observations of each research projects involved in this dissertation research are summarized in Table 5-1.

Table 5-1 Summary of motivation and key observations of the dissertation work(SC: spinal cord; *E*: stiffness)

	Cells	Gels	Objectives	Observations
Gels with STATIC stiffnesses	SC cells	Bis gels	<ul style="list-style-type: none"> Apply a popular culture system (bis-gel) to study spinal cord cells; Expand <i>E</i> range; Include intermediate <i>E</i>; 	<ul style="list-style-type: none"> Neuron-astroglia interactions affect a number of cellular properties; Mechano-sensing is <i>E</i> range specific (not necessarily monotonic, but bi- or multi-phasic);
			<ul style="list-style-type: none"> Establish reference line for dynamic study; Expand DNA design; Study cell population distribution; Differentiate axons from dendrites; 	<ul style="list-style-type: none"> Mechano-sensing is neuronal cell property specific; FAK involvement in the neuronal mechano-sensing; Mechano-sensing is <i>E</i> range specific (not necessarily monotonic, but bi- or multi-phasic);
	Acellular	DNA gels	<ul style="list-style-type: none"> Confirm DNA incorporation into gels; Estimate the potential deformation due to DNA incorporation; 	<ul style="list-style-type: none"> Majority of the DNA gets incorporated to the network; DNA incorporation induced deformation is most likely not great enough to affect neurite outgrowth in this specific case, but could be different in other cases;
Gels with DYNAMIC stiffnesses	Two fibroblasts	DNA gels	<ul style="list-style-type: none"> Assess the potential effect of exogenous DNA on the fibroblast growth; BLAST search; Assess effect of dynamic <i>E</i> on mechano-sensitive cells; 	<ul style="list-style-type: none"> BLAST search and morphological examination shows no effect from exogenous DNA on fibroblast growth; Fibroblasts show differential sensitivity to dynamic <i>E</i>, depending on <i>E</i> range, starting/ending <i>E</i>; Sensitivity is also cell-property specific and cell-type specific; Fibroblasts show response also in FAK expression;
	SC cells	DNA gels	<ul style="list-style-type: none"> Assess the potential effect of exogenous DNA on the neurite outgrowth; BLAST search; Assess effect of dynamic <i>E</i> on neurite outgrowth; Assess FAK and NCAM involvement; 	<ul style="list-style-type: none"> BLAST search and morphological examination shows no effect from exogenous DNA on neuron's primary structures; Responses of neurons to dynamic stiffness are in line with the static study except for the primary dendrite length; Neurons show response also in FAK expression;

5.1.2 Significance

The significance of this dissertation research and major contribution to the understanding of basic science, engineering principles and design guidelines include the following:

- 1 *It highlights the importance of the mechanical aspect of the cell-ECM interactions, particularly cellular response to mechanical stiffness.*

With the ever-increasing recognition of the mechanical aspect of the cell-ECM interactions, this work shows that again for neurons and other cell types the responses to the mechanical stiffness need to be addressed and taken into account in the design of tissue engineering scaffolds and constructs.

- 2 *It reveals the complexity of the mechanical aspect highlighting cell-property specificity, cell-type specificity and stiffness-range specificity, which can be further coupled with the cell-cell interactions, and other factors, including dimensionality and biological cues.*

The differential responses among different cell types (neuron vs. glia vs. L929 fibroblast vs. GFP fibroblast), different cell properties (axon vs. dendrite; projection area vs. aspect ratio) that were characterized on different rigidity ranges demonstrate the array of factors that will have to be incorporated in the full description of the cellular responses to mechanical compliances for the design of biomaterials.

- 3 *It adds a new dimension, Time, to the mechanical properties of the substrate in the understanding of the cell-ECM events.*

To our knowledge, there has not been any study demonstrating application of mechanically dynamic substrates, which mimic the natural environment of the cells in the normal and pathological conditions and take advantage of differential behavior among cell properties. We have successfully devised substrates that are mechanically dynamic and we have investigated the effect of the time-dependent changes in the mechanical properties of a substrate on cellular behavior, and provided quantitative data for the responses. The observations make promising the engineered control of cell growth and neurite outgrowth through the use of dynamic mechanical stiffnesses.

- 4 *It provides design guidelines for the choice of the mechanical stiffness of the bio-scaffold in the tissue engineering applications*

The results in this study have direct relevance to the neural and skin tissue engineering, and can be extended to other tissue engineering areas

5.1.3 Novelty

The novelty in this dissertation in the choice of cell types, cell culture platforms, and the design of the experiments include the following:

1. *We based our model system on a DNA crosslinked hydrogel which allows dynamic modification of the mechanical properties of the substrate.*

The use of single-stranded DNA (ssDNA) as external stimuli circumvents the need for environmental changes which are practically problematic in most cases, and delivery of DNA can benefit from the research in gene delivery.

2. *We considered two cell types, one of which is known to be mechanically sensitive and assumes roles in load-bearing tissues, and the other whose mechanical sensing capability has just started being appreciated.*

In this study, both L929 and GFP fibroblasts were cultured on DNA gels, and their responses to the altered mechanical characteristics of the gel induced by delivered crosslinked DNA were assessed. Neurons were cultured on both bis- and DN-A crosslinked gels of static and dynamic rigidity. The results can be used to engineer cell growth, and the properties of the materials can be tailored to specific bioengineering applications.

3. *We differentiated between axons and dendrites.*

The majority of the reports on the neuronal responses to the mechanical cues were focused on neurites. Axons and dendrites assume different functional roles in the neuronal functioning and their difference, at least in the neuronal mechano-responses, has long been overlooked since they are often lumped as neurites. Indeed, we observed differential behavior of axons and dendrites

towards mechanical stimuli, and this difference can facilitate the design of the neural tissue scaffolds.

4. *We confirmed the generation of the mechanical dynamics*

By using an indirect measurement, we discerned DNA strand diffusion as well as DNA incorporation into gel network. Inspired by commonly used traction force assay, we quantified deformation with help of micro-beads.

5. *We proposed and implemented novel ideas in the design of the experiments*

In the experimental design, we introduced DNA strands with non-specific sequence but comparable molecular weight and length as a negative control. In the characterization and analysis of neuronal behavior, we include the analysis of the cell population distribution in addition to the analysis of the aggregate behavior, which offers more insight in the neuronal mechanosensing that can not be obtained by only considering aggregate behavior.

5.2 Limitations and discretion

Although we are excited to report the interesting results, we are aware of the limitations in the interpretation, utility and applicability of the results and wish to exercise discretion.

1. *Possible involvement of other factors in affecting cell responses.*

Complexity in the cellular decision making process makes it necessary to be cautious in interpretation of the results. The potential factors involve in the

cell-ECM event other than mechanical stiffness include dimensionality, biological cues, adhesive cues, and other physical cues.

Dimensionality

We realize three-dimensional (3D) cell culture is more physiologically relevant and one should be very cautious in extending observations and implications from 2D studies to their 3D counterparts. Nevertheless, the information from 2D studies is still important. This is because, on the one hand, in many cases where 3D culture investigation is, at least at this moment, prohibitively costly, 2D research is perhaps the only practically feasible approach; on the other hand, the results from 2D and 3D studies are not always completely different, indicating that 2D research could in a number of cases provide a very similar or approximate image of what happens in *in vivo*¹. In this study, we tend to extract information from 2D culture system and make comparisons to the results from previous studies. Thus, this early study serves as the initial step towards future work using animal models.

Adhesive properties

The coupling between the adhesion properties and cell mechano-sensing has been well documented². We chose poly-D-lysine in the study of neurons and collagen for fibroblast culture, although other ECM molecules can be used such as proteoglycans, fibronectins, and Matrigel (™)^{3, 4}.

2. *Possible cell-cell interactions in affecting cellular responses*

It is possible that glia and other non-neuronal cells in the mixed population can respond to the mechanical stiffness in a manner that is different from that of the neurons, or respond differently on gels of static and dynamic stiffnesses. There is a possibility that they can influence neuronal behavior by, for example, releasing soluble growth factors.

3. *Methodology in studying time-dependent behavior*

All observations and comparisons made in this research were based on statistical analysis of cell properties at particular time points. It would be definitely better to be able to conduct time-lapse study delineating the time progression in the neuronal responses. Current work might be limited due to sample size, sample selection, etc. However, time lapse study is not without concerns. Potential elevated photo-toxicity and photo-bleaching in the fluorescence microscopy pose limits to their utility.

4. *Possibility of the presence of prestress in the gels*

One of the other concerns regarding the utility of the results from this study is the possibility of prestress in the gels. For instance, it was found that there is prestress in collagen gel substrate⁵ from gel formation and cell culturing. The prestress in the DNA gel system, if significant, could make the interpretation of the experimental data questionable.

5.3 Future work

1. *Delivery Profiles*

Different delivery profiles will be presented to cells, including the time point of delivery, the delivery frequency, and quantity of each delivery, which will undoubtedly affect the dynamics of DNA incorporation into the gel network, as well as the dynamics in the mechanical stiffness of the gels. Investigation on the magnitude and rate of the stiffness change together with the stiffness range will provide detailed information regarding the optimization of the implementation of the dynamic compliances. Moreover, it would be meaningful to probe the potential cellular response to both increase and decrease in the mechanical stiffnesses of the substrates for any specific cell type.

2. *Time-lapse study*

It would be interesting to probe the dynamics and time course of the responses of cells to the dynamic cues. The intermediate stage in the cellular responses and neurite outgrowth would provide more information for both basic understanding and engineering designs. In the time-lapse study of neuronal response to dynamic substrates, one may have to deploy either transfected neurons or neuron-specific dye to identify neurons, and trace their growth.

3 *Three dimensional culture system*

Since it is expected that DNA crosslinking mechanism can be applied to the vinyl polymers, it would be highly significant to replace polyacrylamide with other polymers with demonstrated biocompatibilities and benefits for cell and tissue growth.

4. *Local dynamics via local DNA delivery*

The capability of locally modifying mechanical properties holds many-fold promises. It could enable differential cellular responses in a location-specific manner (e.g., inside glia scar, distal or proximal to injury site in SCI). Additionally, it would enable the establishment of gradients in mechanical properties to facilitate directional and guided growth.

5 *Application oriented*

Further study of the effect of mechanical dynamics on stem cell growth and differentiation and the development of stem cell harvesting system could utilize the results from this dissertation research. Scaffold design for neural and skin tissue engineering can reference the results provided herein on neurons and fibroblasts.

References

1. Abbott, A. Cell culture: Biology's new dimension. *Nature*. 424:870-872, 2003.
2. Bershadsky, A. D., N. Q. Balaban, and B. Geiger. Adhesion-dependent cell mechanosensitivity. *Annu Rev Cell Dev Biol*. 19:677-695, 2003.

3. Flanagan, L. A., Y. E. Ju, B. Marg, M. Osterfield, and P. A. Janmey. Neurite branching on deformable substrates. *Neuroreport*. 13:2411-2415, 2002.
4. Georges, P. C., W. J. Miller, D. F. Meaney, E. S. Sawyer, and P. A. Janmey. Matrices with compliance comparable to that of brain tissue select neuronal over glial growth in mixed cortical cultures. *Biophys J*. 90:3012-3018, 2006.
5. Wang, N., I. M. Tolic-Norrelykke, J. Chen, S. M. Mijailovich, J. P. Butler, J. J. Fredberg, and D. Stamenovic. Cell prestress. I. Stiffness and prestress are closely associated in adherent contractile cells. *Am J Physiol Cell Physiol*. 282:C606-616, 2002.

APPENDICES

Appendix 1: Mechanical characterization with microbeads

Appendix 2: DNA sequence design used in this dissertation research

Appendix 3: AFM probe of the neuronal micro-environment

Appendix 4: BLAST search results

Appe 1 Mechanical characterization with microbeads

1.1 Background

1.1.1 Potential neurite elongation induced by gel deformation

Previous studies have shown that the traction force applied on the microenvironment that cells reside also plays a determining role in neuronal morphology and function, including neuronal polarity, and neurite elongation^{5, 8, 12}.

Table App 1-1 shows key observations on stretching induced neurite growth (Figure App1-1) from published studies. Of particular relevance to the current study is the following:

- For chick sensory ganglion neurons, pulling speed up to 100 $\mu\text{m/hr}$ was applied, resulting in elongation of up to 960 μm ¹.
- Stretching rate beyond 84 mm/hr is detrimental, while half that pulling speed is beneficial for neurite outgrowth¹¹.

Taken together, these results demonstrate that tension-mediated axonal growth is a force-dependent phenomenon.

1.1.2 Rationale

The aim of this study is to probe the displacement field by utilizing the location marker to assess the contraction of the DNA hydrogels upon increase in crosslinking density. There are two commonly adopted approaches in acquiring spatial distribution of the traction forces¹⁰. The first is to track the movement of the residing beads inside the deformable substrates and the second to measure the mechanical responses of force-sensing elements. The first approach is chosen in the study owing to its relative ease to work with.

1.2 Materials and method

1.2.1 Choice of micro-bead

Due to the magnification needed to both visualize beads in the gels and capture as many beads as possible in a single view, spherical beads of 4~5 micron (Polysciences Inc., Warrington, PA) were used and a magnification of 200X was applied with each image containing an average of 20 microbeads.

1.2.2 DNA gel preparation and DNA delivery

DNA gels of Design B (Appendix 2, 14/14/40) were prepared according to the protocol outlined before (Chapter 3B), except that 10% of the gel volume was replaced by micro-bead solution (0.18 mg/mL). Initial DNA crosslinking density was 50%. Gels were immobilized to a 12 mm coverglasses by using an optical glue. Each gel is 26 uL in

volume⁷. After swelling in PBS for two nights in the incubator (37°C), crosslinker DNA in the amount needed for 100% crosslinking was delivered to the gel.

1.2.3 Imaging and Image analysis

Images of the same spot in the gels were recorded immediately after DNA deliver and at the end of two days after DNA delivery. The fixed objects on the underlying coverglass were used to register the microbeads embedded in the gels for both images. The focal planes were chosen to be in between 40% and 60% of the depth of the gels, to minimize the edge effect. The coordinates of each identifiable bead were measured with ImageJ software (NIH, Bethesda, MD).

1.3 Results

DNA gel samples were prepared by using DNA Design B of 14/14/40, and a spot on such gel sample was chosen for imaging (Figure App 1-2). The thickness of the gel was 340 μm as determined by using focusing mechanism.

At different time points (0hr, 33hrs, etc.) images of the spatial distribution of the micro-beads were taken (Figure App 1-3(A)&(B)). Then each bead was registered (Figure App 1-3(C)) with the two dimensional displacement vectors being calculated from the change of the coordinate of each bead. Figure App 1-4 illustrates the magnitude and direction of displacement vectors for the local deformation in the DNA, as indicated by the embedded microbeads. There is an apparent trend in deformation towards the center of the gel sample (Figure App1-2), and the magnitude increases away from the center (Figures App1-4&5). A contour map and surface plot of the distribution of the

deformation was generated by using Surfer software (Golden Software, Golden, CO) and is shown in Figures App 1-4&5, where the general trend of deformation as indicated in Figure App 1-6 is clear.

Due to the limited number of the markers that were traced, the contour plot was generated displaying local concentration (foci) of displacement (Figures App 1-4&5). With greater number and density of location markers, one will be able to see the displacement distribution in a graded fashion. It is then estimated that the maximal deformation generated from this area (as seen in Figure App 1-6) is approximately $4 \mu\text{m}/2.5 \text{ mm}$, which is 1.6×10^{-3} .

For neurons, the typical dimension of a neurite is approximately $10\text{-}50 \mu\text{m}$, and in 33 hr time period, the contraction induced elongation rate (Figure App 1-1) is approximately $2 \times 10^{-3} \mu\text{m/hr}$. For axons of length up to 1 mm, the elongation rate is approximately $0.04 \mu\text{m/hr}$. Both of these elongation rates are much lower than those reported in previously published work ($1.5 \mu\text{m/hr}$, Table App1-1)^{6, 12}.

1.4 Discussion

Although the results of the strain distribution in this study are limited due to the number of beads available and the imaging resolution, the method of deriving strain fields proves to be feasible and can provide sufficient quantitative information of gel system and can facilitate the analysis of the mechanical stresses and traction forces.

The density of the beads distributed in the gels together with the relative dimension of beads to cells partly determines the accuracy that can be achieved. For example, Butler et al.² chose $0.2 \mu\text{m}$ beads to study human airway smooth muscle cells that are

much larger than the fibroblasts in our experiments, and constructed traction fields from displacement distribution based on an exact solution involving a Fourier transformation. Other factors affecting the sensitivity and accuracy of this technique include the resolution of the imaging devices utilized and efficacy of the adopted method (e.g., FEA based or Fourier transformation based method). Nevertheless, this method demonstrated the feasibility of probing the local deformation in soft materials.

References

1. Bray, D. Axonal growth in response to experimentally applied mechanical tension. *Dev Biol.* 102:379-389, 1984.
2. Butler, J. P., I. M. Tolic-Norrelykke, B. Fabry, and J. J. Fredberg. Traction fields, moments, and strain energy that cells exert on their surroundings. *Am J Physiol Cell Physiol.* 282:C595-605, 2002.
3. Fass, J. N., and D. J. Odde. Tensile force-dependent neurite elicitation via anti-beta1 integrin antibody-coated magnetic beads. *Biophys J.* 85:623-636, 2003.
4. Fischer, T. M., P. N. Steinmetz, and D. J. Odde. Robust micromechanical neurite elicitation in synapse-competent neurons via magnetic bead force application. *Ann Biomed Eng.* 33:1229-1237, 2005.
5. Georges, P. C., N. M. Hadzimichalis, E. S. Sweet, and B. L. Firestein. The yin-yang of dendrite morphology: Unity of actin and microtubules. *Mol Neurobiol.* 2008.
6. Heidemann, S. R., and R. E. Buxbaum. Growth cone motility. *Curr Opin Neurobiol.* 1:339-345, 1991.
7. Jiang, F. X., B. Yurke, B. L. Firestein, and N. A. Langrana. Neurite outgrowth on a DNA crosslinked hydrogel with tunable stiffnesses. *Ann Biomed Eng.* 36:1565-1579, 2008.
8. Lafont, F., M. Rouget, A. Rousselet, C. Valenza, and A. Prochiantz. Specific responses of axons and dendrites to cytoskeleton perturbations: An in vitro study. *J Cell Sci.* 104 (Pt 2):433-443, 1993.
9. Lamoureux, P., G. Ruthel, R. E. Buxbaum, and S. R. Heidemann. Mechanical tension can specify axonal fate in hippocampal neurons. *J Cell Biol.* 159:499-508, 2002.
10. Roy, P., Z. Rajfur, P. Pomorski, and K. Jacobson. Microscope-based techniques to study cell adhesion and migration. *Nat Cell Biol.* 4:E91-96, 2002.
11. Smith, D. H., J. A. Wolf, and D. F. Meaney. A new strategy to produce sustained growth of central nervous system axons: Continuous mechanical tension. *Tissue Eng.* 7:131-139, 2001.
12. Zheng, J., P. Lamoureux, V. Santiago, T. Dennerll, R. E. Buxbaum, and S. R. Heidemann. Tensile regulation of axonal elongation and initiation. *J Neurosci.* 11:1117-1125, 1991.

Table App 1-1. Key observations in stretching induced neurite growth from published studies.

Key observations	Neuronal cell type	Ref.
<ul style="list-style-type: none"> ▪ Pulling speed up to 100 $\mu\text{m/hr}$ ▪ Elongation of neurite up to 960 μm 	Chick sensory ganglion neuron	¹
<ul style="list-style-type: none"> ▪ Tension threshold required for growth is 250~5600pN ▪ Growth sensitivity of neurite to tension is 10pN (at a elongation rate of 1.5$\mu\text{m/hr}$) 	Chick sensory neuron	^{6, 12}
<ul style="list-style-type: none"> ▪ Tension threshold required for growth is 200~400pN ▪ Growth rate of 100$\mu\text{m/hr}$ at a tensions of less than 1000pN ▪ Increase of 1-3 $\mu\text{m/hr}$ in growth rate for additional 10pN 	Rat hippocampal neuron	⁹
<ul style="list-style-type: none"> ▪ Tension threshold required for growth is 1000~2000pN 	Peripheral neuron	^{4, 12}
<ul style="list-style-type: none"> ▪ Growth rate of bundle of axons is 1mm/day ▪ Stretching rate of 3.5mm/5min is good and 7mm/5 min is detrimental. ▪ Peak forces: 450pN at 3.5mm/5min and 900pN at 7mm/5 min 	Bundles of axons; Primary rat cortical neurons (E18); Differentiated human neurons from the N-tera2 (NT2) cell line	¹¹
<ul style="list-style-type: none"> ▪ Tension threshold for elongation is 15-100 pN ▪ Slow initial force ramps (1.5 and 11 pN/s) more likely to initiate axon than fast ones (450 pN/s) 	Embryonic chick forebrain neurons	³
<ul style="list-style-type: none"> ▪ Tension threshold for elongation is 1500 pN with over 700 pN for E14 neurons ▪ Force application at 10 and 500 pN/s has similar possibility in initiating axonal growth 	Embryonic chick forebrain neurons (between E7 and E22 or equivalent)	⁴

Note: 1 pN= 10^{-12} N

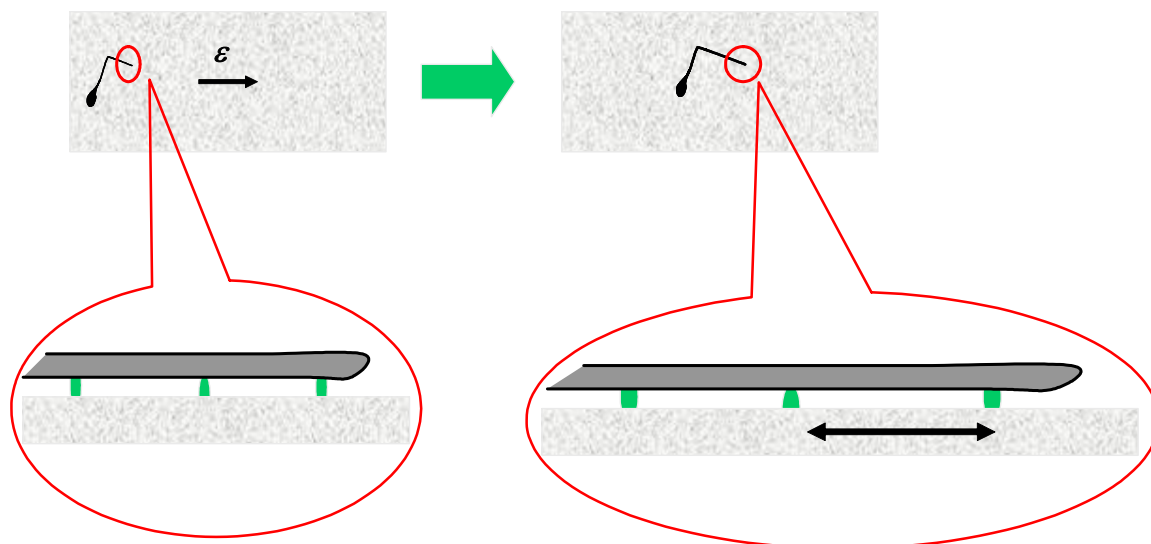


Figure App1-1. Schematic of the concept of potential strain-induced elongation of the neurites. By decreasing the crosslinking level in DNA gels, it is possible to induce reverse of the gel compaction.

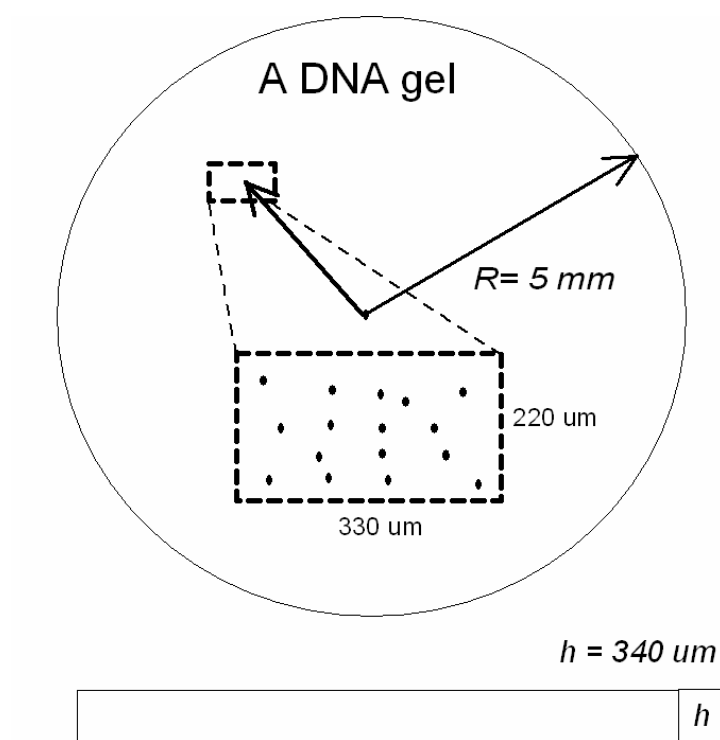


Figure App 1-2. Schematic of experiments using microbeads to probe the deformation of the DNA crosslinked hydrogels. A rectangular area approximately 2.5 mm away from the center was probed on a circular DNA gel sample (5mm in diameter and 340 μm in height).

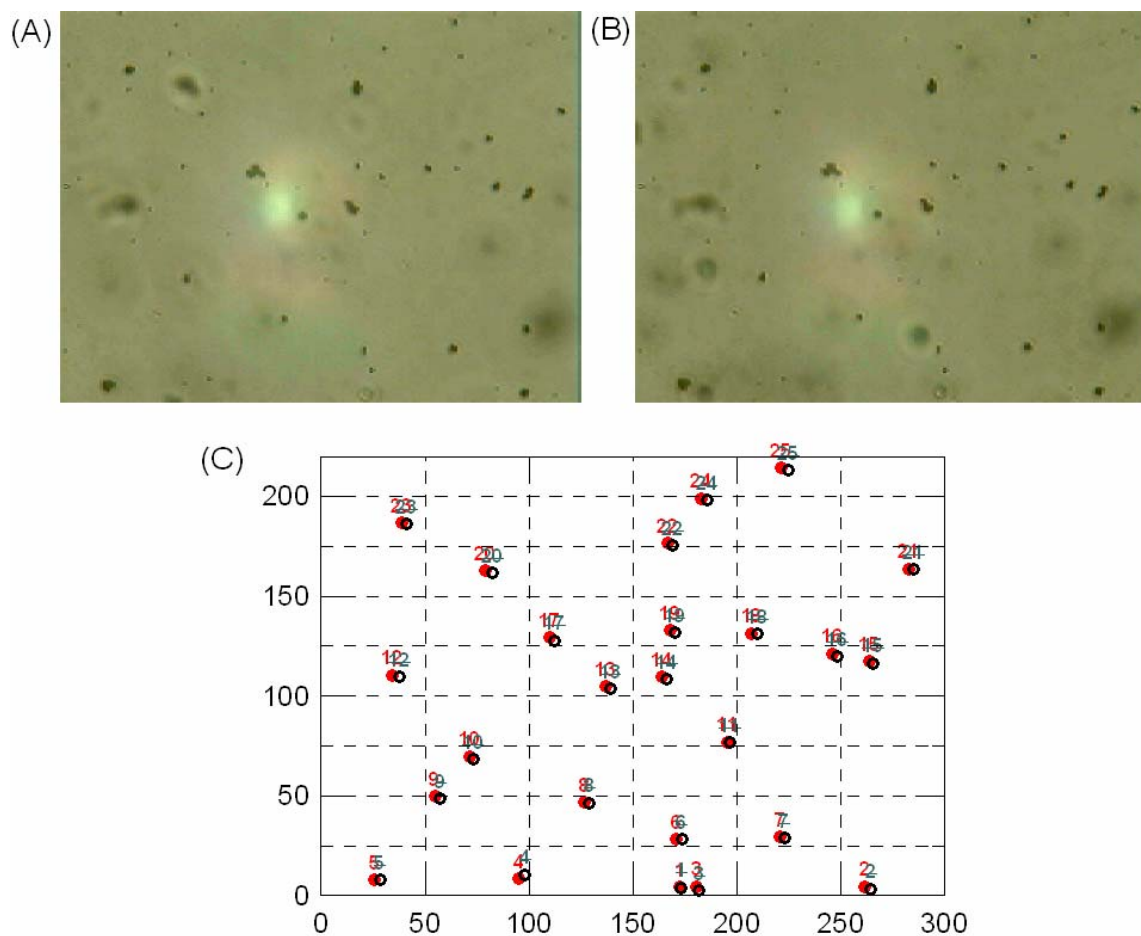


Figure App 1-3. Distribution of the fluorescent beads in the area of interest. (A) Distribution of the beads at $t = 0$ hrs; (B) Distribution of the beads at $t = 33$ hrs; (C) Superposed bead distribution at $t = 0$ hrs (red and solid circle) and $t = 33$ hrs (dark blue and open circle) after registration.

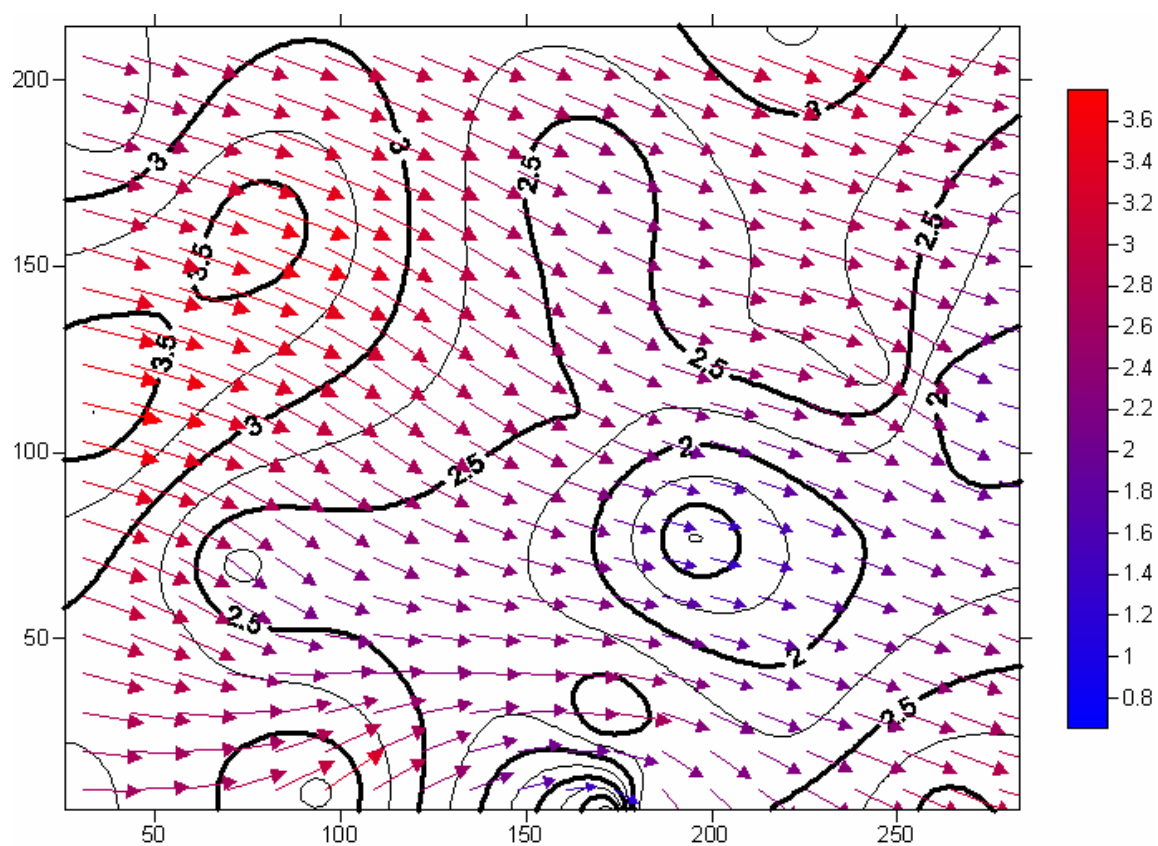


Figure App 1-4. Vector and contour map indicating the distribution of the deformation in the DNA gels based on the displacement of the embedded beads. The general trend of deformation towards the center of the gel is apparent, and the magnitude increases away from the center. Coordinates and magnitude of the deformation are in μm .

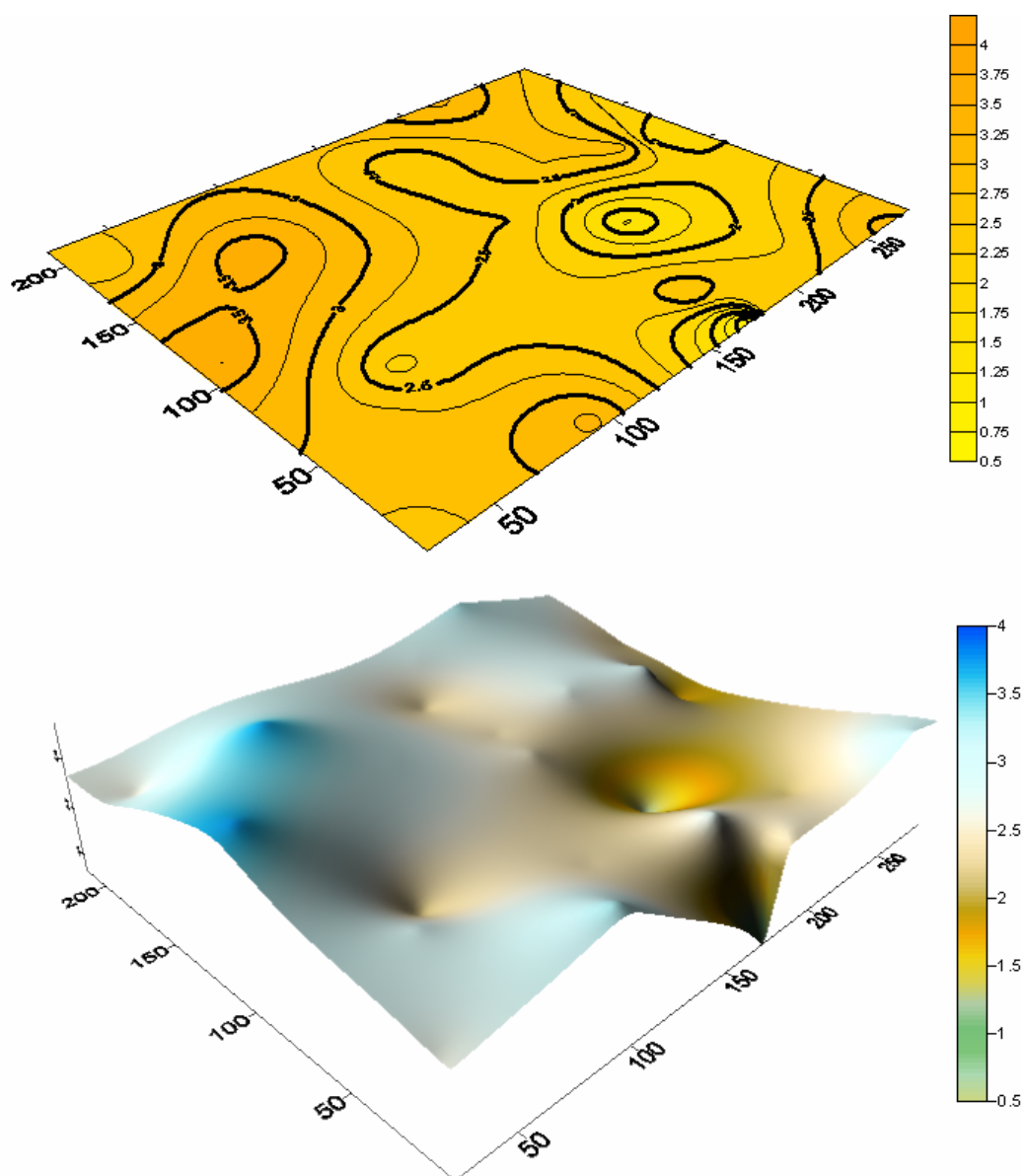


Figure App 1-5. Contour map and surface plot of the deformation as shown in Figure App 1-4. The contour map (upper) shows the loci of deformation, which appear mainly due to the spacing between the beads and bead density in the gels. Coordinates and magnitude of the deformation are in μm .

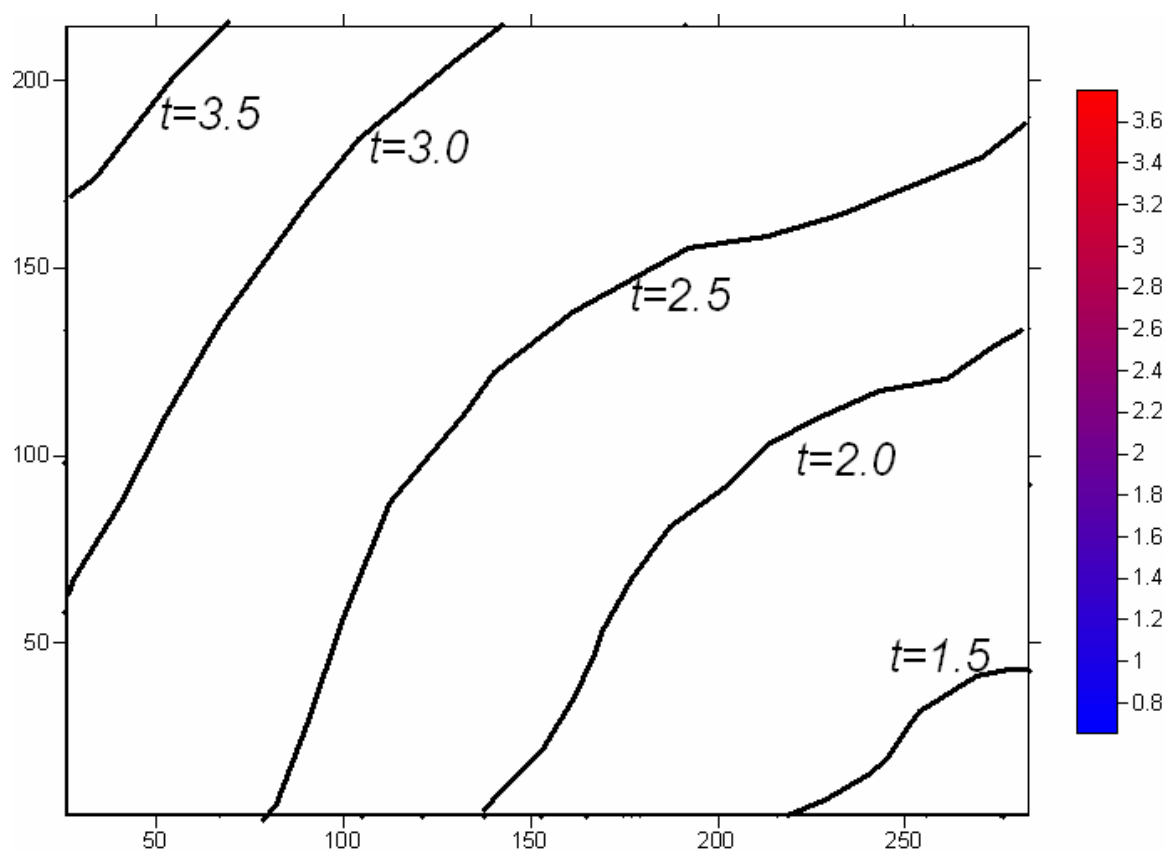


Figure App 1-6. The trend line showing the strain distribution in the DNA gel samples as showing in Figure App 1-4. The loci showing in Figure App 1-4 were attributed to the artifacts due to the limit on the number of beads, the spacing, and the smoothing algorithm used in generating contour. If one ignores the loci and general distribution can be mapped as shown above. The highest deformation one can find is approximately 3.8 μm .

Appe 2 DNA sequence design used in this dissertation research (bp = base pairs)

The DNA sequence designs used in this dissertation research are summarized in Table App 2-1.

Table App 2-1 Sequence design used in this dissertation work.

(A)

Name	# of bps	DNA sequence (5' to 3')	MW	Tm (C)
SSA1	10	5'-Acrydite-GCA CCT TTG C-3'	3226.2	34.9
SSA2	10	5'-Acrydite-GTC AGA ATG A-3'	3323.3	23.6
SL2	20	5'-TCA TTC TGA CGC AAA GGT GC-3'	6117.0	56.0
SL2-D	30	5'-TCA TTC TGA CGC AAA GGT GC -- GCT ACA CTT G	9182.0	63.9
SL2-R	30	5'-CAA GTG TAG C -- GC ACC TTT GCG TCA GAA TGA	9231.0	63.9
L2_Non	30	5'-AAA AAA AAA AAA AAA AAA AAA AAA AAA AAA -3'	9334.3	46.7

Note: This design is used in the study described in Chapters 3B and 4C.

(B)

Name	# of bps	DNA sequence (5' to 3')	MW	Tm (C)
SMA1	14	5'-Acrydite- CGT GGC ATA GGA CT-3'	4551.1	46.9
SMA2	14	5'-Acrydite- GTT TCC CAA TCA GA-3'	4470.0	40.2
ML2	40	5'-TCT GAT TGG GAA ACA GTC CTA TGC CAC GGT TAC CTT CAT C-3'	12222.0	65.9
MR1	40	5'-GAT GAA GGT AAC CGT GGC ATA GGA CTG TTT CCC AAT CAG A-3'	12369.1	65.9

Note: This design is used in the study described in Chapter 4B.

(C)

Name	# of bps	DNA sequence (5' to 3')	MW	Tm (C)
SA1	20	5'-Acrydite-ACG GAG GTG TAT GCA ATG TC-3'	6444.3	55.0
SA2	20	5'-Acrydite-CAT GCT TAG GGA CGA CTG GA-3'	6429.3	56.6
L2	40	5'-TCC AGT CGT CCC TAA GCA TGG ACA TTG CAT ACA CCT CCG T-3'	12151.9	68.8

Note: This design is used in the study described in Chapter 3B.

Apppe 3 AFM testing of spinal cord neurons on hydrogels

(Performed by Dr. David Lin from NIH and Frank Xue Jiang)

This study is aimed to provide insight into mechano-response of neurons to the substrate mechanical stiffness and potential remodeling of the extracellular matrix (ECM) by the neurons or astroglia. We will approach this goal by focusing on the micro-environment (tens to hundreds of micron area surrounding neurons) as well as the mechanical properties of the soma and neurites, including axons and dendrites, in contrast to those of the substrates.

The information obtained will facilitate biomaterial and bio-scaffold design for neural tissue engineering. The AFM has emerged as a powerful tool for characterizing surface properties and analyzing nano scale structures. Its prevalence in many fields, notably neuroscience and biomedical engineering, stems from unique features not found in other imaging and probing techniques. These features (e.g., concurrent imaging and mechanical probing, availability of different tips, and the ability to probe samples submerged in liquid) make it an ideal tool for probing the mechanical properties of sub-cellular structures under near native conditions.

Micro- and nanoindentation of samples was performed using a Bioscope SZ AFM with the latest NanoScope V controller (maximal image resolutions of 5120×5120 pixels) and integrated optical microscopy capabilities. A scan resolution of 32×32 indentations was employed. To prevent damage to the cells, maximal indentation depths were kept below 100 nm. Under such conditions, it is expected that linear elasticity theory can be applied with minimal loss of accuracy in the data analysis.

Cell population was maintained under normal culture conditions in culture dishes prior to testing. To minimize the potential of contamination, AFM tips and tip holders were sterilized with alcohol solution and subjected to UV-ozone cleaning protocols. A typical view of phase contrast micrograph of neurons on 8% bis-crosslinked gels and an AFM scan image is shown in Figure App 3-1.

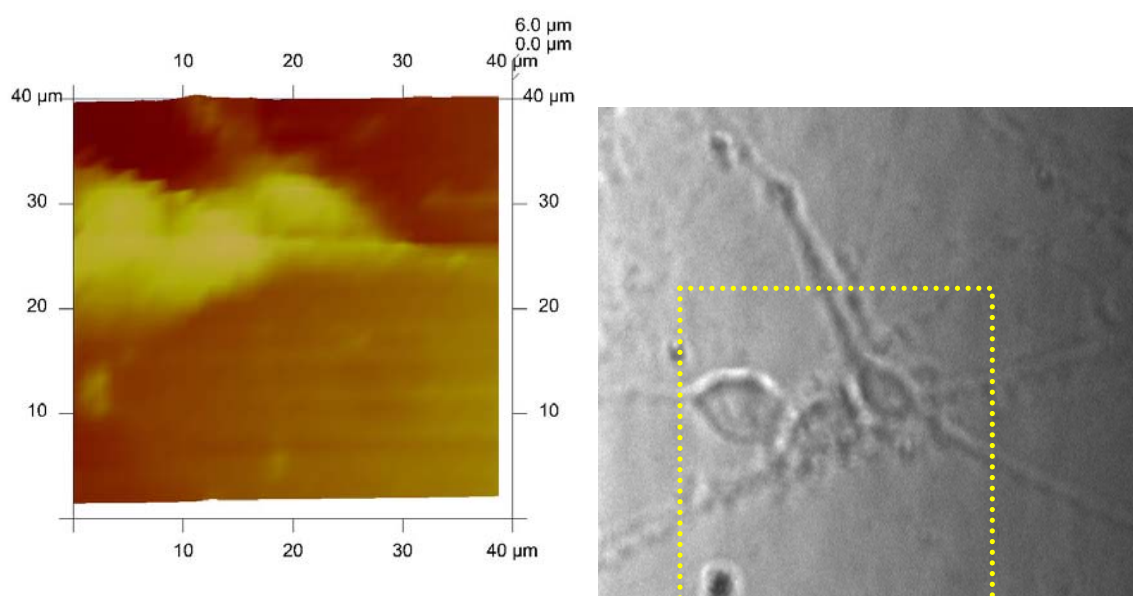


Figure App 3-1. (Right) Rat spinal cord cells cultured on 8% Bis-crosslinked polyacrylamide gels. (Left) An AFM scanning image indicates the topography of the circled area in the right-hand image.

App 4 BLAST search results

4.1 Purpose

The delivered DNA strands, in most cases, in the single-stranded form, can potentially alter the biological activities of the cells, including fibroblasts and spinal cord cells. One of the possible ways for this to happen is that these short ssDNA strands can be taken up by cells and act as anti-sense DNAs to modify gene expression. For instance, these DNA strands could pair with target messenger RNA (mRNA) and prevent the translation of the mRNA.

It is, therefore, necessary to conduct a search of the sequence of the delivered DNA against the genome of the specific species to examine the probability of sequence matching. The survey can be conducted by comparing the sequence of the DNA strands against the National Center for Biotechnology Information (NCBI) nucleotide database by using a basic local alignment search tool (BLAST) algorithm for close resemblance to biological sequences.

4.2 Procedure

We first identify the complement of the delivered ssDNA strand and the target biological tissue types to compare with (Table App 4-1). All surveys were conducted on NCBI website (<http://blast.ncbi.nlm.nih.gov/Blast.cgi>). First, the appropriate specie was chosen according to Table App 4-1. Second, the corresponding sequence was entered, and ‘genome (all assemblies)’ database and ‘megaBLAST’ program’ were opted. The search program yielded reports with the assessment of the level of resemblance.

238699 bp at 5' side: cadherin 10
257928 bp at 3' side: hypothetical protein

4.3 Summary

The likelihood is small that delivered crosslinker DNA could act as anti-sense DNA affecting gene expression, which could potentially alter the phenotype of the cells. Thus, it is unlikely that these DNA strands *per se* would cause any significant change in the cellular response, particularly in their morphology and adhesion.

Table App 4-1. The key information used for conducting BLAST searches for close resemblance to biological sequences.

Study conducted	Crosslinker L2	Specie	Tissue type
L929 fibroblasts (Chapter 4B)	Design B (14/14/40)	Mouse	Subcutaneous areolar and adipose tissue
GFP fibroblasts (Chapter 4B)	Design B (14/14/40)	Rat	Skin tissues
Spinal cord neurons (Chapter 4C)	Design A (10/10/30)	Rat	CNS, Spinal cord

Table App 4-2. Results for BLAST search for close resemblance to biological sequences.

DNA gel	Length/ maximal length of matching	Database Name	Query ID	Program	Conclusion
Design A	30/16	gpipe/10116/all_contig rat build 4 genome database (reference and alternate assemblies)	lcl 5243	BLASTN 2.2.18+	No significant similarity found.
Design B	40/20	dbindex/10090/allcontig_and_rna mouse build 37 RNA, reference and alternate assemblies	lcl 13815	BLASTN 2.2.18+	No significant similarity found.
Design B	40/20	gpipe/10116/all_contig rat build 4 genome database (reference and alternate assemblies)	lcl 22858	BLASTN 2.2.18+	No significant similarity found.

CURRICULUM VITA

Xue (Frank) Jiang

2002 B.S., Naval Architecture and Ocean Engineering
Shanghai Jiaotong University, Shanghai, China

Journal articles

Jiang, FX, Wang, L and Lu, B. (2002) Digital Wave Simulation Based on OpenGL. J. Laboratory Res. Exploration (in Chinese). 21, 60

2002 Associate (full time), Reuters Consulting, Reuters (now Thomson Reuters) Group
Shanghai, China

2004 M.S., Civil Engineering
The University of Akron, Akron, OH

Journal articles

Jiang, FX and Pan, E. (2004) Exact Solution for 2D Polygonal Inclusion Problem in Anisotropic MEE Planes. Int. J. Solids Struct. 41, 4361.

Pan, E and Jiang, FX. (2004) Effect of QWR Shape on the Induced Elastic and Piezoelectric Fields. J. Comp. Model. Eng. Sci. (CMES). 6,77.

Pan, E and Jiang, FX. (2006) Singularity Analysis at the Vertex of Polygonal Quantum Wire Inclusions. Mech. Res. Commun. 33, 1.

Conference Proceedings

Pan, E. and Jiang, FX. (2004) QWR induced surface field of semiconductor substrate. Int'l Conf. Comp. Exp. Eng. Sci. (ICES), Greece.

2004 Graduate Fellow, Biomedical Engineering
The University of Medicine and Dentistry, Piscataway, NJ

2005 Graduate Assistant, Biomedical Engineering
Rutgers, the State University of New Jersey, New Brunswick, NJ

2009 Ph.D., Biomedical Engineering
Rutgers, the State University of New Jersey, New Brunswick, NJ, and
The University of Medicine and Dentistry, Piscataway, NJ

Journal articles (first-authored only)

- Jiang, FX, Georges, PC, Li, B, Du, Y, Kutzing, MK, Previtera, ML, Langrana, NA and Firestein, BL. (2007) Cell growth in response to mechanical stiffness is affected by neuron-astroglia interactions. *Open Neuroscience*. 1, 7-14. (First three with equal contribution)
- Jiang, FX, Yurke, B, Firestein, BL, Langrana, NA. (2008) Neurite outgrowth on a DNA crosslinked hydrogel with tunable stiffnesses. *Annals of Biomedical Engineering*. 36, 1565-1579.
- Jiang, FX, Yurke, B, Schloss, R, Firestein, BL, Langrana, NA. (2008) Fibroblast growth in response to dynamic stiffnesses of a DNA crosslinked hydrogel (In preparation)
- Jiang, FX, Yurke, B, Schloss, R, Firestein, BL, Langrana, NA. (2008) Effect of mechanically dynamic cues on neurite outgrowth by using a DNA-crosslinked hydrogel (In preparation)

Presentations

- Jiang, FX, et al. Neural cell engineering using a polyacrylamide hydrogel: a preliminary study. in ASME Summer Bioengineering Conference. 2006. Amelia Island, FL. (Podium Talk)

Conference Proceedings

- Jiang, FX, et al. The Effect of Dynamic Alterations in Stiffness of The Substrate on Cell Growth. ASME Annual Summer Bioengineering Conference. 2009. Lake Tahoe, CA.
- Jiang, FX, et al. Spinal Cord Neuronal cell properties respond differentially to the stiffness of DNA crosslinked hydrogels. ASME Annual Summer Bioengineering Conference. 2008. Marco Island, FL.
- Jiang, FX. et al. Study on Effect of Substrate Stiffness On Neural Cell Growth Using DNA Crosslinked Hydrogels. BMES Annual Meeting. 2007. Los Angeles, CA.
- Jiang, FX., et al. Neurite Elongation And Branching on DNA Crosslinked Polyacrylamide Hydrogels. ASME Annual Summer Bioengineering Conference. 2007, Keystone, CO.
- Jiang, FX., et al Design of DNA-crosslinked hydrogels for neural cell study. BMES Annual Meeting. 2006. Chicago, IL.